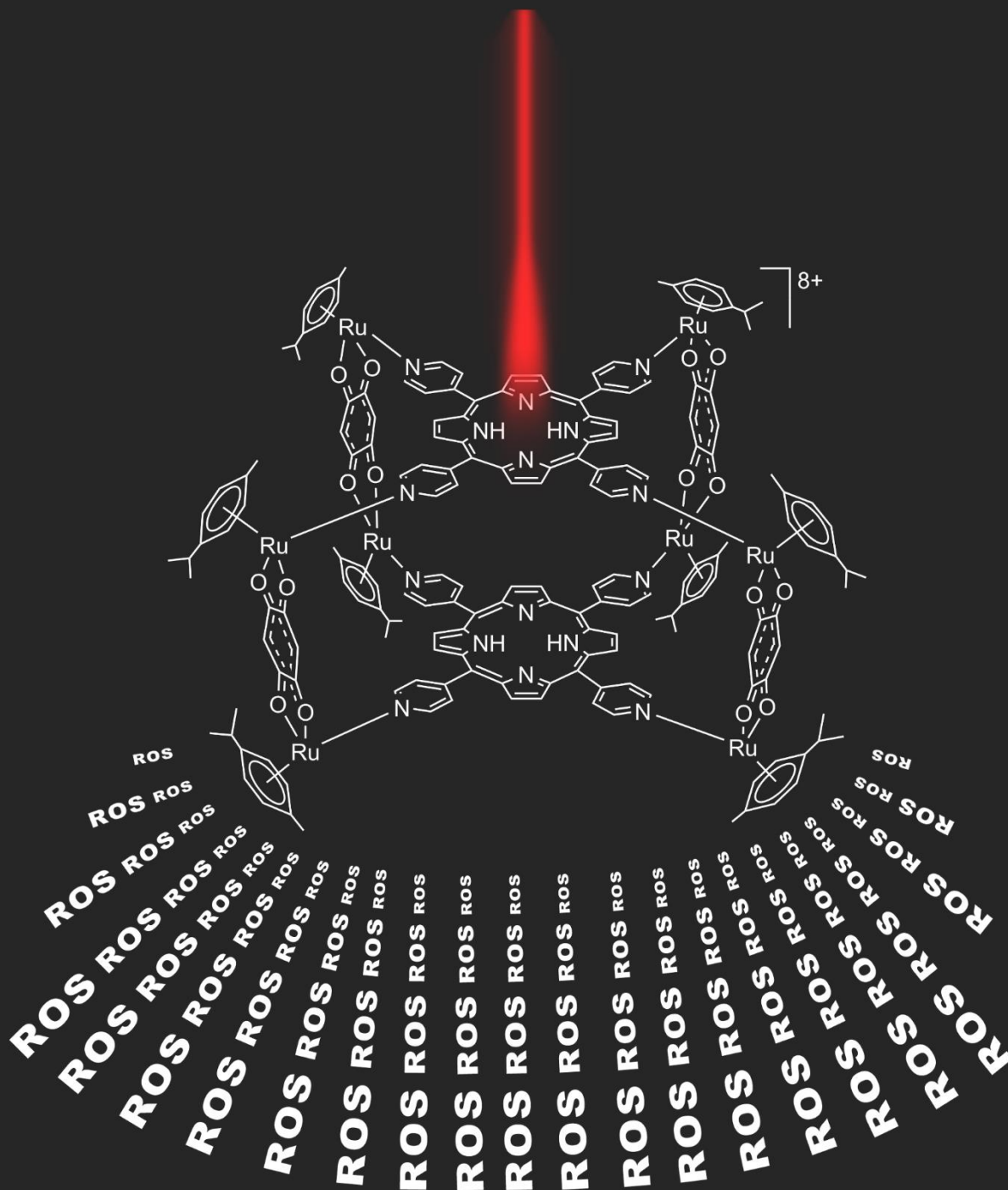# New anti-inflammatory and pro-apoptotic photosensitizers against arthritis and synovial sarcoma

Thèse de Manuel Ángel Gallardo Villagrán

Directeurs: Pr Bertrand Liagre et Pr Bruno Therrien, Co-directeur: Dr David Leger

Membres du jury: Pr Maité Sylla et Pr Robert Deschenaux

POLYTHEA   unine UNIVERSITÉ DE NEUCHÂTEL   Université de Limoges   le cnam

Thesis

New anti-inflammatory and pro-apoptotic photosensitizers against arthritis and synovial sarcoma

by

Manuel Ángel Gallardo-Villagrán

Supervisors:

Pr Bertrand Liagre (University of Limoges, France)

Pr Bruno Therrien (University of Neuchâtel, Switzerland)

Co-supervisor:

Dr David Leger (University of Limoges, France)

Members of the jury:

Pr Maité Sylla (Conservatoire National des Arts et Métiers de Paris, France)

Pr Robert Deschenaux (University of Neuchâtel, Switzerland)

Thesis defended on May 10th, 2022

Résumé

En 1993, un premier médicament a été approuvé pour une utilisation en thérapie photodynamique (PDT). Près de trente ans plus tard, ce traitement peu invasif, activé de manière localisée et précise par la lumière, a été utilisé pour traiter diverses pathologies. Son utilisation pour le cancer de la peau est la plus répandue, mais elle a également été utilisée pour d'autres types de cancer et pour l'acné. D'autres pathologies, telle que la polyarthrite rhumatoïde (PR), méritent encore une exploration en termes de solution thérapeutique. L'objectif de cette thèse était de proposer une nouvelle technologie adjuvante avec l'utilisation de systèmes de transport de substances actives par thérapie photodynamique sur un modèle in vitro de cellules synoviales provenant de patients atteints de PR.

L'un des principaux inconvénients de la PDT est la solubilité faible ou nulle des substances photoactives utilisées. Les systèmes que nous présentons dans cette thèse sont constitués d'assemblages d'arène ruthénium qui contiennent une cavité interne dans laquelle la substance photoactive est logée. Il est également possible d'incorporer les substances actives dans la structure même de l'assemblage arène ruthénium.

Les résultats que nous avons obtenus sont prometteurs et constituent une avancée dans l'utilisation de la PDT dans le traitement de la PR.

Keywords

INDEX OF CONTENTS

INTRODUCTION

Light is part of the radiation field known as the electromagnetic spectrum, which is a combination of oscillating electric and magnetic fields that propagates through space carrying energy, the photon being the elemental unit. Part of this energy is the basis of most living organisms on earth since it can be absorbed and used to transform inorganic matter into organic. The process by which this transformation takes place is called photosynthesis and the base substance that absorbs light energy in the first instance is chlorophyll. Like chlorophyll, other substances are capable of absorbing part of the light energy and transferring it to other nearby molecules or compounds. This group of substances is known as chromophores, photoactive substances, or photosensitizers (PS). The PhotoDynamic Therapy (PDT) uses this process to generate radical oxygen species (ROS) by adding a PS and irradiating a certain wavelength in the target tissue. ROS initiate localized cell death processes in the irradiated area, being able to eliminate or reduce a desired amount of tissue without the need for invasive surgery. Therefore, PDT is considered a non-invasive treatment that can serve to improve the life quality of patients with certain diseases. Undoubtedly, the disease where PDT has developed the most has been cancer, but other diseases such as rheumatoid arthritis (RA) have also been studied and there is still a long way to walk and explore. Recently, we have developed several groups of ruthenium organometallic compounds that serve well as PS transporters as PS themselves. The *in vitro* evaluation in RA and cancer human cells shows the great potential of this compounds in PDT. In this work, we gather our most important and significant results, doing our bit for the tower to the development of this therapy.

The treatment of a disease by inducing cell death processes through light activation of a photoactive substance is known as photodynamic therapy (PDT). The photoactive substance is known as the photosensitizer (PS) and cell death processes are initiated by the production of radical oxygen species (ROS).

1.1 Mechanism of PDT

When a photon interacts with a PS, one of its electrons is promoted to a higher energy state, known as the excited singlet state (S). The excited electron can return to its ground state, giving rise to fluorescence (Figure 1), or could take an intersystem crossing, reaching an intermediate energy state known as excited triplet state (T). From this intermediate excited state, the electron can return to the ground state of the PS, giving rise to phosphorescence (Figure 1), or it could be transferred to another nearby molecule by quenching. When this transfer involves an oxygen molecule (O_2), the PS returns to its base energy state and the O_2 reaches an excited state of energy known as singlet oxygen ($^1O_2$). The extremely unstable $^1O_2$ reacts with other oxygen molecules or oxygen-containing species giving rise to ROS. The lifetime of ROS is on the order 0.04 µs and the radius of action is approximately 0.02 µm, so they can lead to oxidative stress in cells, initiating specifically and locally cell death processes [1].
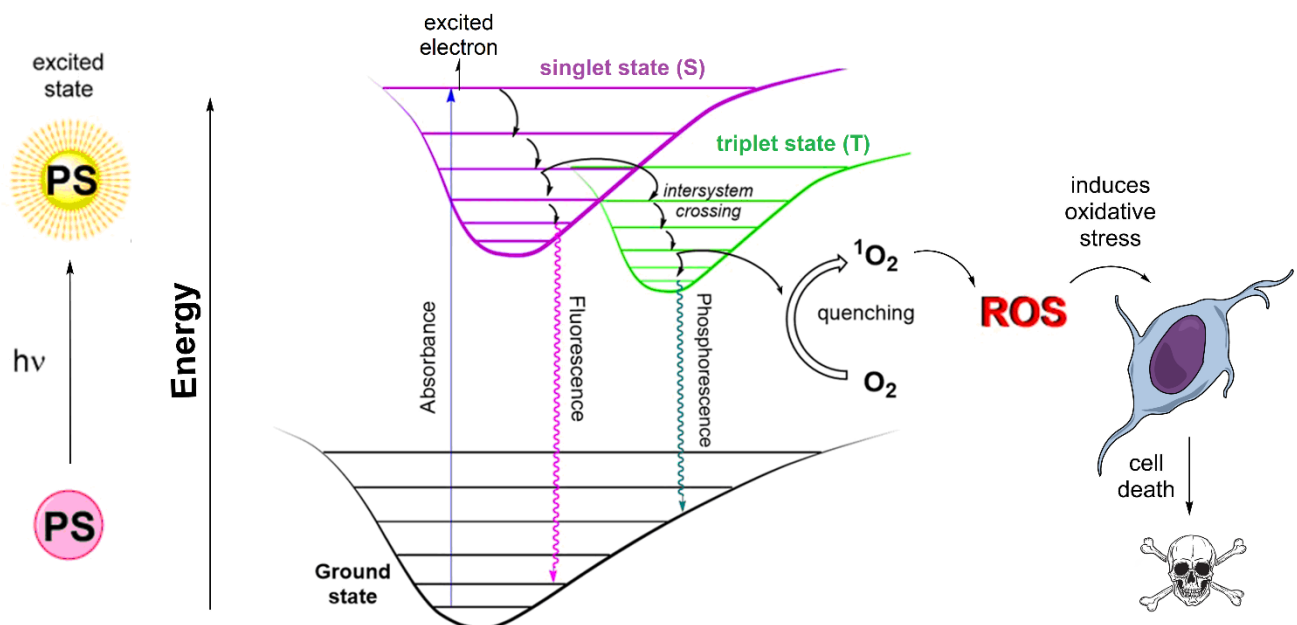
Figure 1. Excitation of PS to reach the singlet state. The electron can return to the ground state (fluorescence) or pass to the intermediate triplet state (phosphorescence), where it can quench with O_2, giving rise to ROS. The ROS cause the cell death by oxidative stress.

Two types of mechanisms are described in PDT (Figure 2): if the energy transfer occurs directly from the excited PS to O_2 is known as type II mechanism. On the contrary, if the energy transfer occurs from the excited PS to another biomolecule or substrate and subsequently to O_2, is known as the type I mechanism [2]. Both types of mechanism can occur simultaneously, and the ratio between both processes depends on the type of PS and the concentration of O_2 and substrate [3].
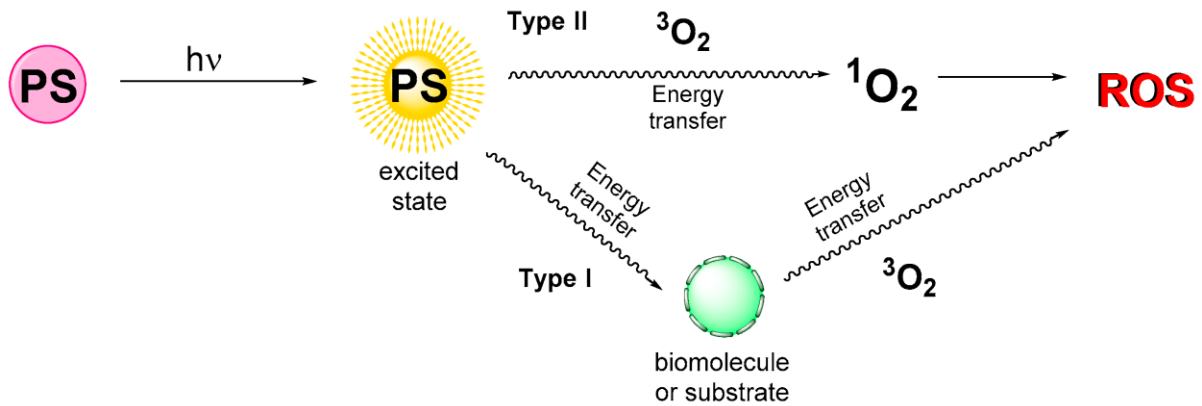
Figure 2. Type I mechanism: transfer of energy to a substrate and from this to oxygen. Type II mechanism: direct transfer of energy to oxygen.

1.2 Historical background of PDT

The first time PDT was approved for use in people was in 1993 in Canada, using a commercial porphyrin, Photofrin, as PS (Figure 3). A few years later it was also approved in the European Union (later withdrawn for commercial reasons), the United States and Japan, along with other commercial porphyrins as PS such as Foscan and Protoporphyrin IX. Nowadays, many more drugs have been approved as PS, temoporfin, talaporfin and verteporfin among others [4]. However, light has been used as a treatment for diseases such as skin cancer or psoriasis since ancient civilizations [5]. During the 20th century, the greatest contribution to the development of PDT was made. The term "Photodynamic" was introduced in 1907 by Jodlbauer and von Tappeiner. The latter, in previous years, had been working on the use of topical eosin and white light to treat skin tumors. In 1913, the German scientist Friedrich Meyer-Betz used hematoporphyrin and light on his own skin, describing swelling and pain in the irradiated areas. After, in 1978 Dougherty and co-workers, conducted a controlled clinical trial on 113 skin tumors in 25 patients, using HPD (hematoporphyrin derivative) and red light. They observed a complete response in 98 tumors, a partial response in 13 and only 2 tumors showed resistance to the treatment by PDT [6]. Nowadays, PDT is used to treat cancer [5, 7-9], acne [10,11], psoriasis [12], age-related macular degeneration [13], or to treat infections [14].
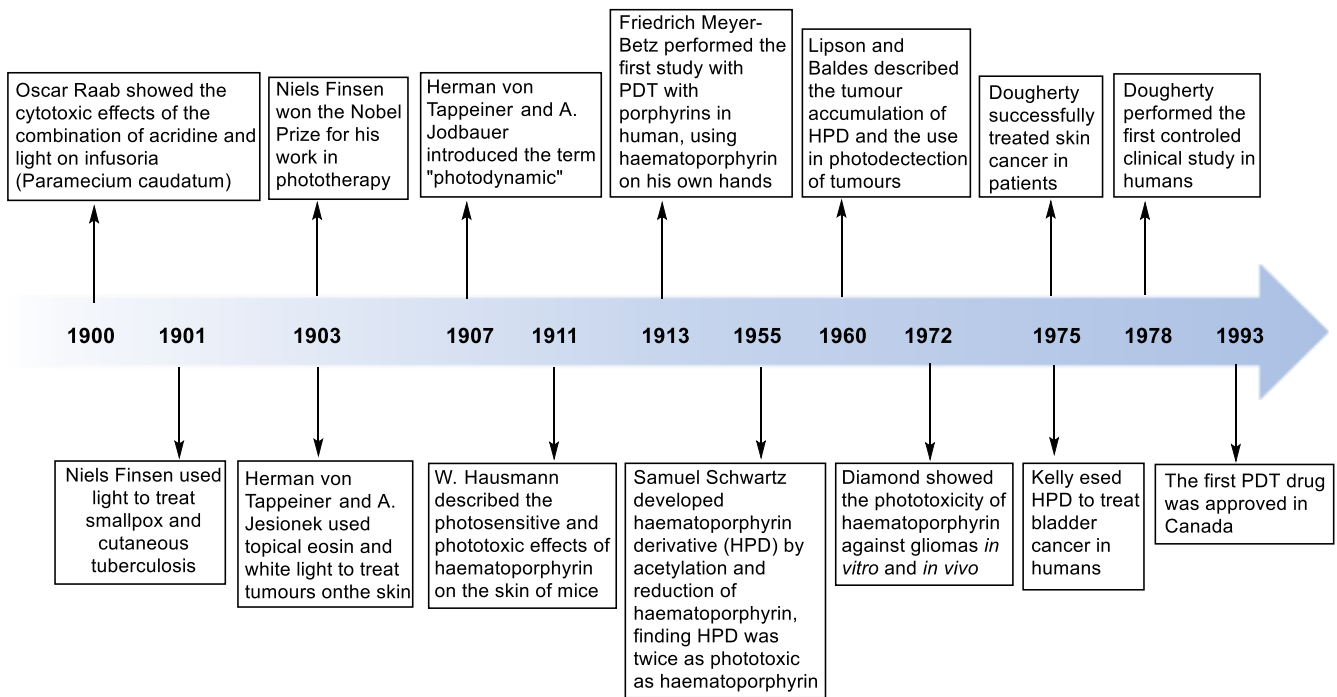
Figure 3. Development of PDT from 1900 until approval of the first drug in 1993 [5].

1.3 The ideal photosensitizer

As already described above, the main elements that act in the PDT process are the PS, light and O_2. The light is defined by the wavelength and the dose (J/cm^2). Oxygen is commonly found in tissues to a greater or lesser extent. As regards the PS, it should have as many of the following characteristics as possible:

- Its synthesis should be simple and in high yield.
- It should be soluble and stable in biological media.
- It should accumulate in target tissue in high concentration.
- It should not lead to toxicity in the dark. The toxicity must be only in the irradiated area.
- It should produce a high amount of singlet oxygen, giving rise to ROS.
- It should be eliminated from the body within a few hours, to avoid post-treatment side effects such as skin photosensitivity.
- It should not generate aggregates.
- It should be able to be activated by red light between 600 – 800 nm, which is known as therapeutic window. This is due to the fact that there are compounds in the blood and tissues that also absorb part of the light energy provided during irradiation, reducing the light that reaches to the PS. Among these compounds, the most abundant are hemoglobin, oxyhemoglobin and melanin (Figure 4), whose lowest absorbance is found from 600 nm [15]. Above 800 nm, the intensity of the irradiation is not usually sufficient

to excite the PS and produce enough ROS. Furthermore, when approaching 900 nm, the absorption bands of water [16], also abundant in tissues, begin to appear. Moreover, the therapeutic window corresponds mainly to red light, being this, among the visible wavelengths, the most penetrating in the tissues (Figure 5).
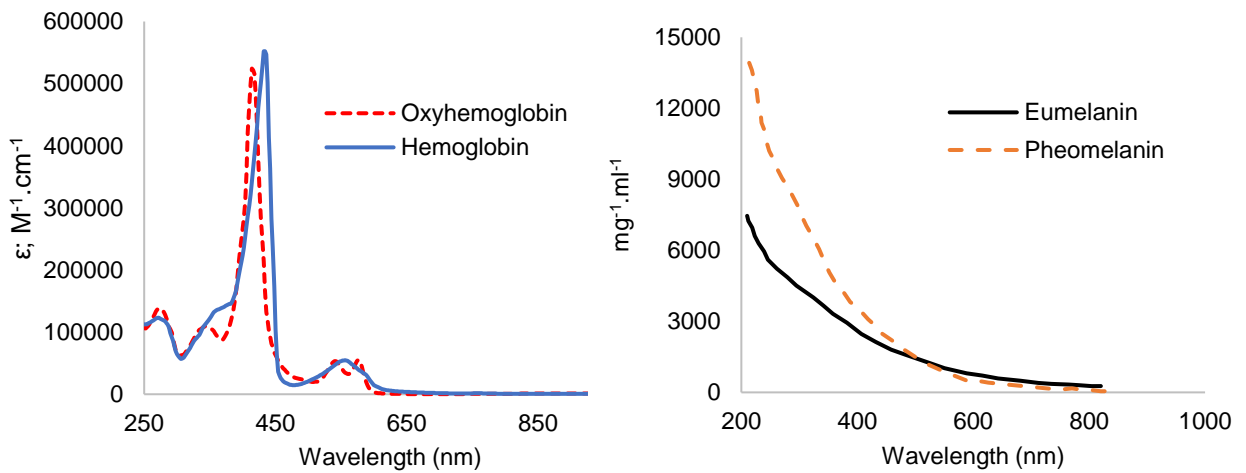
Figure 4. Left; absorption of oxyhemoglobin (red) and hemoglobin (red) in the visible spectrum. The molar extinction coefficients were compiled by Scott Prahl using data from W. B. Gratzer, Med. Res. Council Labs, Holly Hill, London and N. Kollias, Wellman Laboratories, Harvard Medical School, Boston. Right; absorption of Eumelanin (black) and Pheomelanin (orange), two types of melanin in human [15].
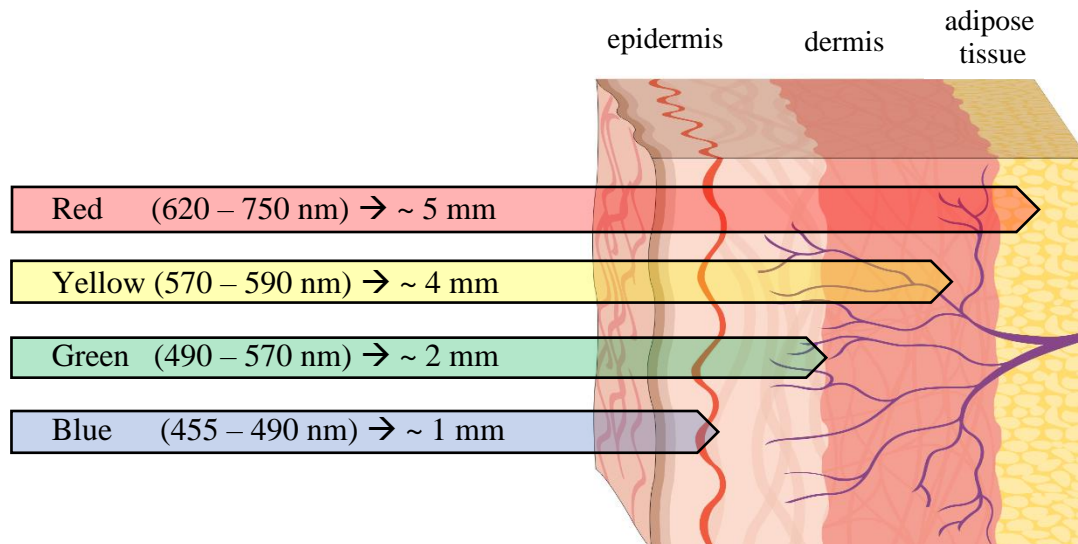
Figure 5. Approximate penetration of different visible wavelengths in the skin.

Rheumatoid arthritis (RA) is considered a chronic inflammatory disorder of immune origin. It should not be confused with osteoarthritis, which is caused by wear and tear of cartilage in the joints. RA mainly affects the regular function of synovial tissue, which is to coat and lubricate the joints (Figure 6). A disorder in synovial tissues gives rise to chronic inflammation that could cause bone and cartilage destruction and finally joint deformation, making movement difficult and causing pain. RA can even cause systemic disorders beyond the joints, such as cardiovascular, pulmonary and skeletal disorders among others [17]. This pathology is more common in women than in men and is usually diagnosed between the age of 30 to 50 years old. It is commonly detected in a bilateral and symmetrical pattern and is infrequently diagnosed in a single joint [18]. The etiology of RA is still unknown; however, it is thought that is due to a combination of triggers and genetic background. Furthermore, some factors can increase the propensity to develop this pathology, such as environmental factors, dust exposure, and particularly the effect of the microbiome [19], as well as obesity and smoking, mostly if there is a genetic predisposition (histocompatibility complex, cytokines, chemokines, and growth factor genes) to autoimmune responses [17,20-22].
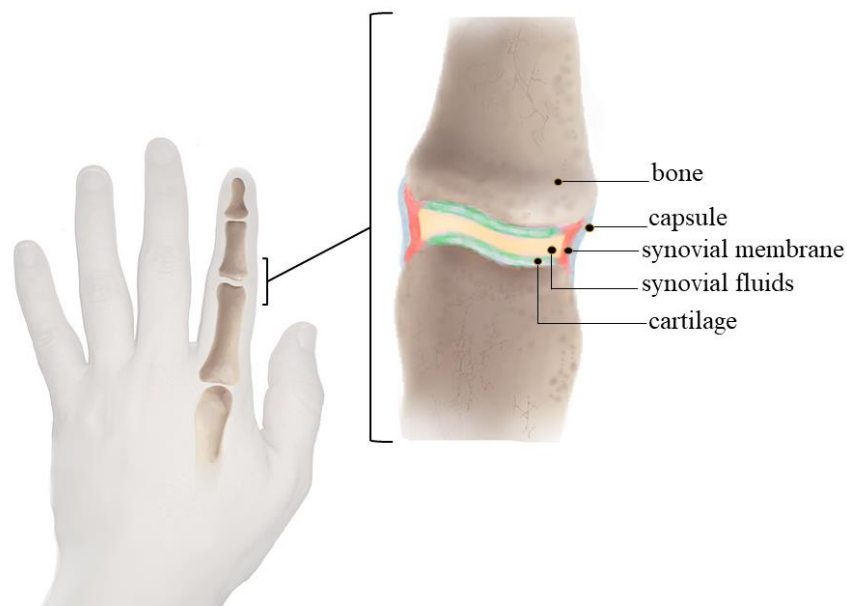
Figure 6. Representation of the major tissues in the synovial tissue connecting the bones in the joints.

The synovial lining generally consists of 1–3 cell layers, however with RA becomes extremely thickened. This is known to be due to an invasion of macrophage-like cells and the proliferation of resident synovial fibroblasts. The degree of synovial hyperplasia connects with the gravity of cartilage erosion, resulting in inflammatory pannus formation that attaches to, and occupies

joint cartilage (Figure 7) [17,24]. Moreover, osteoclast (cell that degrades, reabsorbs, and remodels bone) activation leads to parallel bone destruction [17]. The interaction between synovial resident cells and cells of the inherent and adaptative immune system gives rise to the production of numerous pro-inflammatory cytokines (TNF-α, IL-1 and IL-6, among others), proteolytic enzymes, and inflammatory molecules [23].
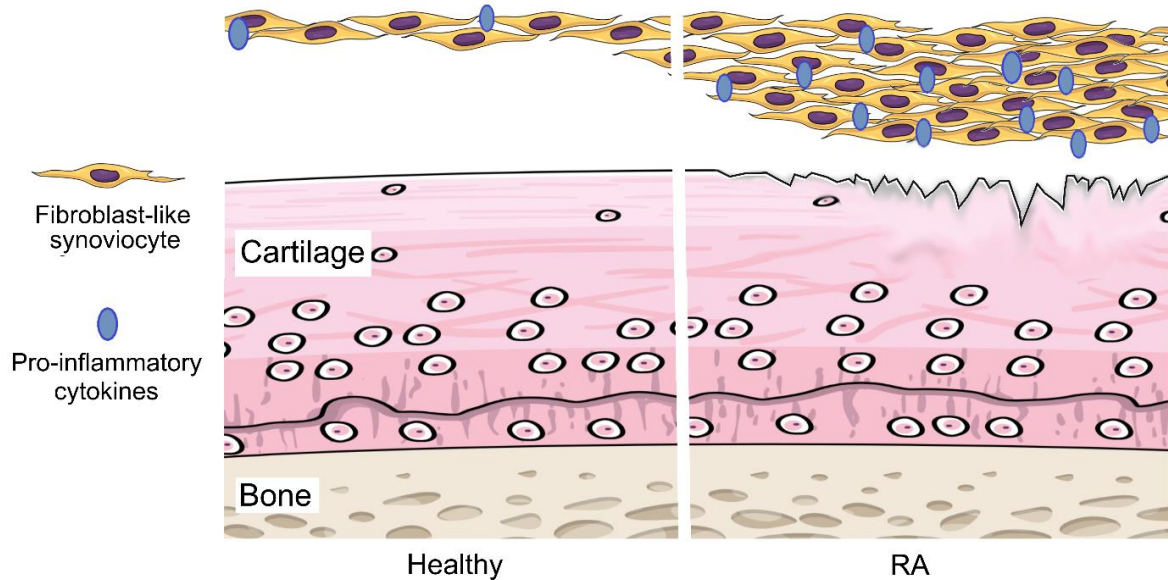
Figure 7. Health FLSs (left) and pro-inflammatory environment with damaged cartilage in RA (right).

Many of the newly developed treatments and drugs for RA have focused on reducing inflammation and cytokine production by fibroblast-like synoviocytes (FLS) and immune cells. Since old standard treatments against RA, such as synovectomy, were invasive, destructive, and involve long rehabilitation periods, in recent decades, less invasive treatments have been investigated [25-27]. Nowadays, the current treatment strategy is to initiate aggressive therapy by applying antirheumatic drugs (DMARDs) and to escalate the therapy, guided by an evaluation of the clinical disease activity and structural damage [25]. Conventional synthetic (csDMARDs) and biological (bDMARDs) antirheumatic drugs maintain rigid remission or at any rate low disease activity, reducing pain, disability and joint destruction [28,29]. However, these therapies sometimes fail or produce only partial response and, consequently, clinical remission is not completed. In this perspective, alternative or complementary therapies could be of benefit, such as Janus kinase inhibitors and PDT, however, Janus kinase inhibitors are currently on European Medicines Agency revaluation for severe adverse effects. The purpose of PDT in RA is to reduce persistent synovitis and it could be even use simultaneously with csDMARDs and bDMARDs [30,31].

The RA FLS used for the evaluation of our compounds were isolated from synovial tissue extracted in arthroplasty surgery from patients with RA (Figure 8). The isolation process was carried out under strict aseptic conditions and subsequently cultured for all the tests carried out (see experimental part).

During synovectomy some of the inflamed tissue is removed

Under aseptic conditions, we discard fatty tissue and select small pieces of synovial tissue.

Washing with PBS we manage to isolate the FLS, cultivate them and multiply them

By enzymatic digestion we separate the individual cells

Finally, used the FLS to test the effectiveness of PSs by PDT
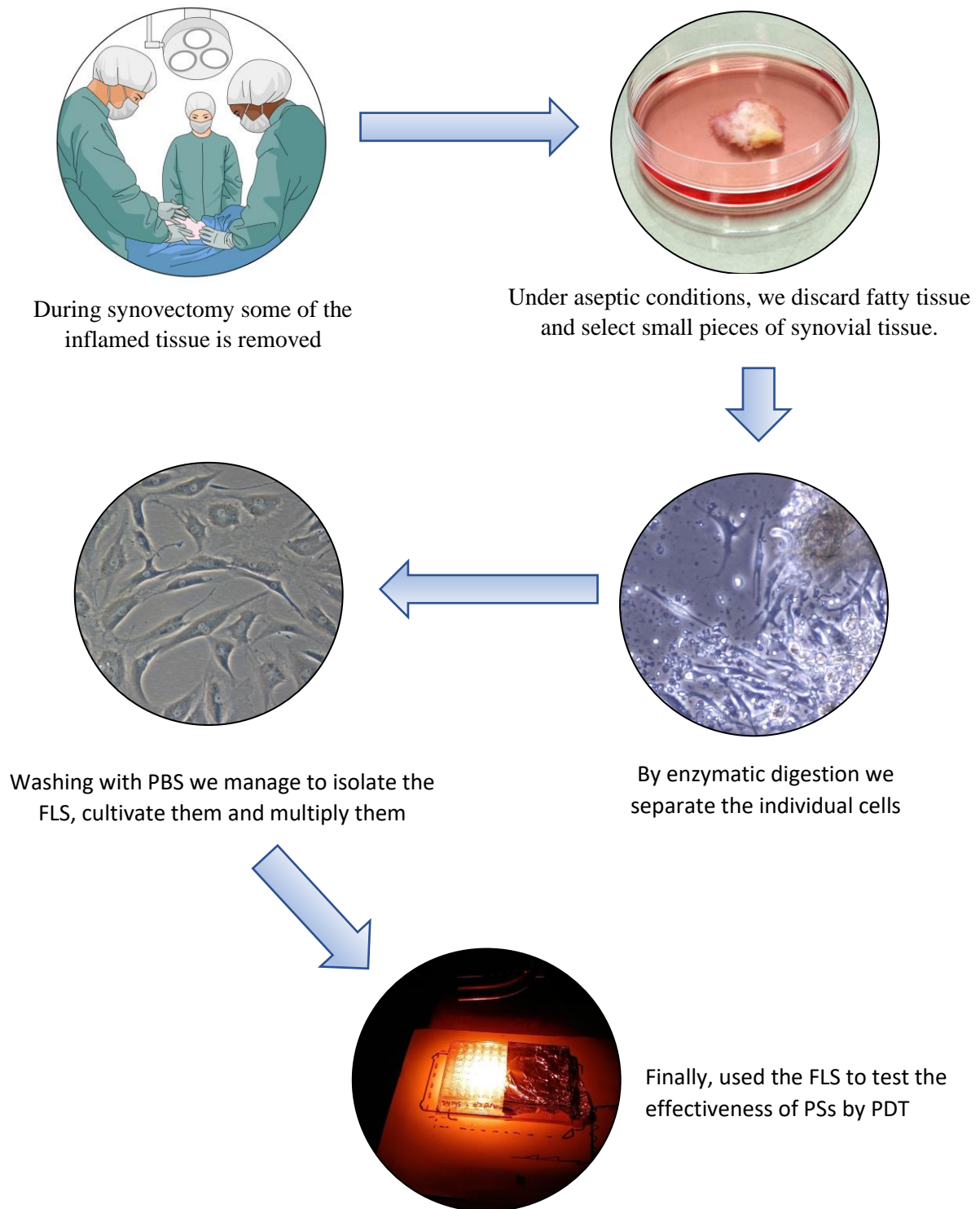
Figure 8. Extraction, digestion and isolation of FLS to be use in the *in vitro* evaluation.

On the other hand, dimethyl sulfoxide (DMSO) is the solvent used to dissolve the compounds evaluated in this work. The literature shows results of DMSO toxicity in cancer cells at certain concentrations, but there are not reported results about RA FLS. Since the growth and multiplication of FLS in primary culture is much lower than that observed in cancer cells, the results in the latter cannot be extrapolated and could lead to error. Therefore, we decided to evaluate the toxicity of this solvent in RA FLS by antiproliferative activity (MTT assays). The tests were performed on all available RA FLSs, that is, RA FLSs from the finger joint of three women aged 60, 71 and 72 years, from the hand joint of a 65 years woman and from the joint of the hip of a 69 years woman. The results show concordance between the different samples of RA FLS and significant toxicity is observed from 0.1 % of DMSO after 24 h of exposure. No significant toxicity observed between 0.01 and 0.05% DMSO (Figure 9). In the evaluation of the compounds studied in this work, the maximum concentration of DMSO used was 0.05 %.
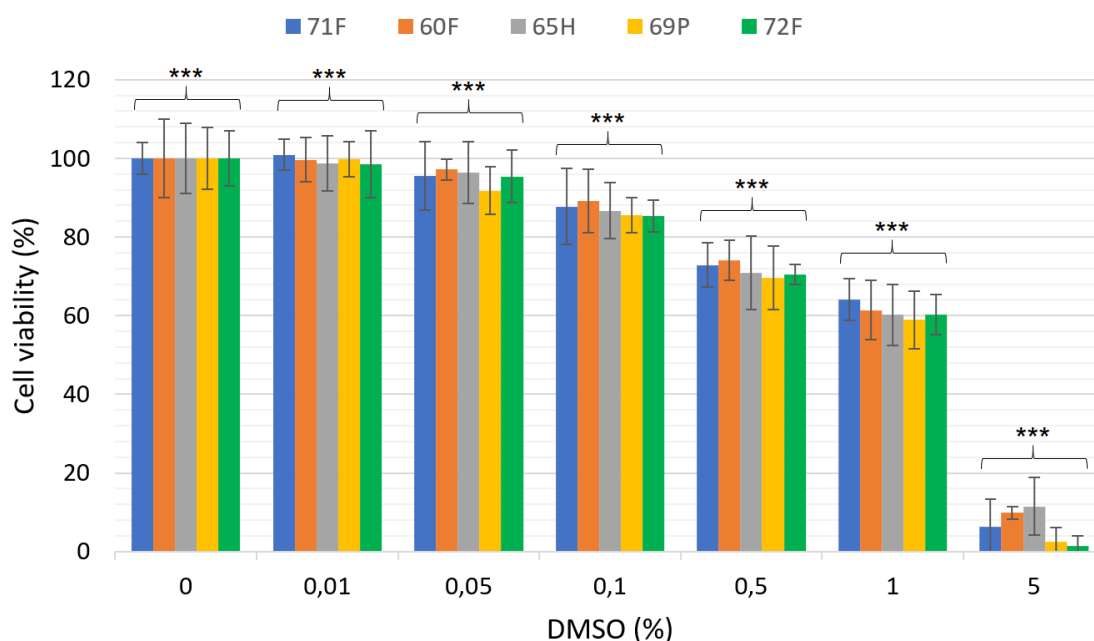
Figure 9. Toxicity of DMSO in the FLS from the five patients after 24 h of exposure. Finger 71 years woman (71F), 60 years (60F), 72 years (72F), hip 69 years woman (69P) and hand 65 years woman (65H) Antiproliferative assays were performed by MTT assays. Statistical significance by two-tailed unpaired Student's t-test, P-value < 0.001 (***).

CHAPTER 3 – PHOTOSENSITIZERS USED AGAINST RHEUMATOID ARTHRITIS

The design and development of new PS for use in PDT to treat RA began three decades ago, and new compounds and strategies have grown rapidly in recent years (see Figure 10 in pages 19, 20 and 21). The design of PS requires considering multiple factors, such as physiological solubility, excitation wavelength, biological stability, reactivity, toxicity or retention time. The first-generation of photosensitizers were mainly based on porphyrin derivatives. Porphyrins have a structure built on four pyrrole units linked by another atom or group forming a ring. This structure is considerably rigid and has conjugated double bonds, which permits some electrons to be delocalized rather than fixed in a single bond. This electronical delocalization promotes the excitation of the system after irradiation, and then energy transmission, justifying its vast use as PS [32-35].

In 1994 Ratkay and co-workers demonstrate that it was possible to alleviate the symptoms associated with RA in mice by PDT, using benzoporphyrin derivative monoacid ring A (BPD-MA, structure *(1)* in Figure 10) as PS [36]. After the treatment with BPD-MA and PDT, they observed a reduction in pannus formation and a reduction in bone and cartilage destruction, maintaining the normal survival rate. They used irradiation at 690 nm, which made possible the excitation of BPD-MA by transcutaneous application, demonstrating the non-invasiveness potential of the treatment. After this promising result, the same research group proved that the efficacy of the treatment is influenced by both the type of administration of the drug and the method of irradiation. To do this, using BPD-MA again, they compared intravenous and intra-articular administration, and transcutaneous and intra-articular irradiation in rabbits [37]. Both intravenous and intra-articular administration achieved rapid adsorption in vascularized and inflamed tissues, however, after intravenous administration, uptake in cartilage and tendons was much lower, which reduces the destruction of these tissues, concentrating photocytotoxicity in the synovial membrane. However, after intravenous administration, clearance was fast, shortening the useful time for irradiation. In contrast, using intra-articular administration, clearance was slower, allowing greater control of drug concentration in the tissue and more flexibility to apply irradiation. On the other hand, it was shown that intra-articular administration ensures that transcutaneous irradiation could be as effective as intra-articular irradiation. In 1998, Trauner and co-workers. published complementary results to the previous ones with BPD-MA and went even deeper into the uptake of the drug in different tissues [38]. These results aroused interest in the use of PDT in RA, and two years later, in 2000, Hendrich and co-workers carried out their study in rabbits

using BPD-MA again [39]. By intravenous administration and intra-articular irradiation, they demonstrated that cartilage, menisci, tendons and ligaments were not affected after PDT. In addition, they demonstrated that in the absence of light, no adverse effects occur one week after drug administration.

Another porphyrin derivative used in early PDT studies in RA was Photofrin *(2)*. It is a porphyrin oligomer that shows poor solubility in physiological media. In parallel to their work with BPD-MA in 1998, Trauner and co-workers tested the use of Photofrin in PDT, through intravenous administration and irradiation by bare cleaved fiber irradiation [40]. Due to the required high concentrations of PS (2 mg/kg) as a consequence of its low solubility, they found that the treated animals had a high concentration of the drug in the skin, which caused cutaneous hypersensitivity to light for at least one month after treatment. In addition, PS absorption into synovial tissue was slow (maximum concentration after 48 h), which made treatment impractical. However, despite the drawbacks described, they showed that only the synovial tissue was necrotic and managed to reduce inflammation one week after PDT treatment.

Photosan-3 *(3)* is another porphyrin derivative oligomer. Like Photofrin, Photosan-3 had already been used in the treatment of cancer by PDT. In this first stage of PDT study in RA it was also tested by Hendrich's group in 1995 [41]. In this case, the study was carried out *in vitro* in fibroblast-like synoviocytes (FLS) and *in vivo* in rabbits two years after [42]. The *in vitro* study showed the effectiveness of the therapy depended on the concentration of PS. They also demonstrated the lack of toxicity of Photosan-3 by itself, and also when irradiation is applied without drug. The *in vivo* study showed complete destruction of the inflamed synovial tissue and no changes in cartilage and meniscus.

The next PS that was brought to PDT in RA was Protoporphyrin IX (PpIX) *(8)*. This porphyrin is synthesized intracellularly from 5-aminolevulinic acid (ALA) [43,44]. So and co-workers were the first to test the capacity of PpIX in PDT to treat RA (2002) [45]. They examined the formation, accumulation and cytotoxicity of PpIX using ALA as a precursor, both *in vitro* in human cells and *in vivo* in mice. The *in vivo* protocol consisted of intra-articular administration and transcutaneous irradiation. The accumulation of PpIX formed from ALA occurred mainly in animals with RA and not significantly in healthy animals. While *in vitro* assays showed accumulation of PpIX in synovial lyning layer, vascular endothelium and macrophages mainly. In 2005, Bagdonas and coworkers carried out an *in vivo* study in rabbits with rheumatoid mono-arthritis (opposite joint remains healthy) using ALA as a PpIX precursor again [46]. No differences were found between intravenous or intra-articular injection. The accumulation of PpIX in the inflamed joint was more than double that in the healthy joint, after

3 h post injection. In addition, in the affected joint it was detected by fluorescence that PpIX accumulated in the skin, tendons and cartilage, while in the healthy joint PpIX was only detected in the cartilage.

Some porphyrins like meso-tetraphenylporphyrin sulfonate (TPPS$_{2a}$) *(9)* tend to accumulate in membranes of lysosomes and endosomes. On the other hand, cells can survive partial destruction of lysosomes, thus reducing the effectiveness of PDT. In 2005, Dietze and co-workers took these two concepts into account and used TPPS$_{2a}$ in combination with Gelonin, a ribosome inactivator that cannot cross cell membranes due to its structural characteristics. In this way, the TPPS$_{2a}$ accumulated in the lysosome membranes can be activated by irradiation in a specific zone. This breaks these membranes and release the Gelonin trapped in the lysosome inside the cell, increasing the cytotoxic effect during the PDT in the treatment of RA [47].

Being the low solubility of compounds derived from porphyrins a problem, in later years many groups tried to include structural modifications to increase physiological affinity of these tetrapyrroles. In 2006, Nishida and co-workers conducted an interesting study on the use of ATX-S10.Na(II) *(10)*, a porphyrin that includes sodium carboxylates as substituents, making it a salt and increasing its hydrophilic character [48]. The study covered both *in vitro* assays in FLS and *in vivo* assays in mice. The *in vitro* study showed that photocytotoxicity was proportional to the concentration of the drug, and also that ATX-S10.Na(II) accumulated mainly in lysosomes. *In vivo* tests confirmed the direct relationship between concentration and photocytotoxicity (using transcutaneous irradiation). On the other hand, it was found that this PS was completely eliminated from the body in less than 48 hours, which reduced side effects such as light photosensitization of the skin.

In 2008 and following the same strategy, Talaporfin *(11)*, another porphyrin with sodium carboxylates, was tested [49]. It was again found that PS was located mainly in lysosomes in the *in vitro* assays. In the *in vivo* tests in mice, they used intra-articular administration of Talaporfin, and it was found that the concentration in the synovial membrane was higher than in the rest of the surrounding tissues, such as skin and cartilage, 4 hours after injection. The authors suggest that it is because the synovial capsule acts as a compartmentalized system, and the synovium shows greater affinity for Talaporfin. After transcutaneous irradiation, only necrosis was observed at the irradiated point. Almost two months after PDT, no inflammation of the synovial membrane and no damage in cartilage or bone was observed in histological analysis.

Also in 2008, Hansch and co-workers used a different strategy, which consisted of increasing the retention time of PS in order to carry out several irradiations without having to inject the drug again [50]. For this, they used Temoporfin *(12)* as PS, a tetrapyrrole that has phenol substituents, which serve as an anchor point for polyethylene glycol (PEG) chains. This study compared the drug itself and its PEGylated form, carrying out *in vivo* tests in mice. Temoporfin alone did not show good distribution in arthritic joints, according to the authors because of the low physiological solubility of this tetrapyrrole. In contrast, Temoporfin-PEG showed greater solubility and accumulation in inflamed tissue. The author suggested that the coating the liposomes with PEG results in protection against liposome destruction and weaker recognition by cells of the mononuclear phagocyte system, preventing the Temoporfin-PEG system from being destroyed prior to cellular internalization. Photosensitivity was observed up to 96 h after administration of Temoporfin-PEG, which allowed repeating the irradiation dose for several days without requiring another injection.

In 2012, Pheophorbide A *(16)* was tested as PS to treat RA by PDT. This porphyrin derived from the breakdown of chlorophyll had been tested as an imaging and anticancer agent. Gabriel and co-workers tested in mice Pheophorbide A alone and Pheophorbide A bound to a polymerized lysine [51]. The purpose of using this porphyrin was to visualize the location of the PS and at the same time generate photocytotoxicity. The main differences found were that while the maximum accumulation occurred 5 h after putting the injection of PS alone, with PS-lysine it was 24 h after the injection. Furthermore, a linear relationship between concentration and photocytotoxicity was achieved using PS-lysine and not with PS alone. The healthy joints did not show photocytotoxicity since PS visualization showed that accumulation in these tissues was minimal. Finally, without irradiation, no cytotoxicity was observed.

However, the use of porphyrin derivatives as PS is not the only strategy followed in the treatment of RA by PDT. There have also been notable studies that have used different compounds as PS. In 1997, after Hendrich and co-workers tested Photosan 3, they carried out the same assays but using chloroquine *(4)*, methotrexate *(5)*, piroxicam *(6)*, and sodium morrhuate *(7)* as PSs [52]. After *in vitro* PDT, piroxicam and sodium morrhuate did not show photocytotoxicity in FLS. Nevertheless, the photocytotoxic activity of chloroquine and methotrexate was significant and potentially useful in PDT. Methotrexate was used as PS in 2010, using light-emitting diodes (LEDs) as irradiation source [53]. The main purpose of this study was to demonstrate the applicability of LEDs as an irradiation source *in vivo*. The results concluded that infrared irradiation achieved a better PDT effect than red, yellow and white irradiation using methotrexate as PS. After, this was transferred to *in vitro* assays in human

cells from patients with RA, achieving similar results. Photocytotoxicity was lower in cells from healthy patients.Another non-porphyrin related compound tested as PS in PDT to treat RA was Hypericin *(19)*. This derivative of anthraquinone had already been used as an antimicrobial agent [54] and as an anticancer agent [55], since it accumulates preferentially in cancerous tissue, and can be used as an indicator of tumor cells. In 2018, Guo and co-workers tested *in vitro* Hypericin as PS in RA FLS from human patients [56]. The results showed that after PDT, the production of ROS increases, which was directly related to the PS concentration.

Other strategies used to improve the solubility and retention of PSs was encapsulation. In 2010, Juillerat-Jeanneret and co-workers demonstrated the efficacy of this methodology in PDT by encapsulating tetra(4-sulfonatophenyl)porphine (TSPP) *(13)*, tetra(4-carboxyphenyl)chlorin (TPCC) *(14)* and chlorin e6 (Ce6) *(15)* in chitosan-based nanogel [57]. The study was tested both *in vitro* (human THP-1 macrophages and murine RAW 264.7 macrophages) and *in vivo* (mice with antigen-induced arthritis). *In vitro* tests showed that the maximum concentration was achieved between 3-4 hours after administration with all PSs. In addition, the three encapsulated PSs showed significant photocytotoxicity, each of them varying in the dose of irradiation. Only Ce6 showed some toxicity in the absence of light. *In vivo* tests showed how PS-nanogels were retained for a longer time in joints affected by RA. The retention time was also much longer than for the PS alone.

Another example of porphyrin encapsulation to improve its performance in PDT of RA was carried out in 2016. In this case, Wang and co-workers used TiO_2 nanoparticles to contain tetra(4-sulfonatophenyl)porphine (TSPP) *(17)* molecules [58]. This study was done *in vitro* (in human RA FLS) and *in vivo* in murine with RA. The TiO_2-TSPP tandem showed by fluorescence that it can successfully accumulate in FLS, something that TSPP alone was unable to do. The *in vivo* assays showed that TiO_2-TSPP accumulates mainly in inflamed tissue. That same year, in another publication, Wang and co-workers also showed that this TiO_2-TSPP tandem can reduce the presence of biomarkers indicative of RA, such as TNF-α and IL-17 [59].

In 2017, Zhu and co-workers followed the same encapsulation strategy, using indocyanine green (ICG) *(18)* as PS. The PS encapsulation was carried out using poly[DL-lactide-co-glycolic acid] (PLGA), a biodegradable/biocompatible globular polymer. In addition, perfluoro-n-pentane (PFP) was used as O_2 carrier [60]. A combination of PDT and sonodynamic therapy was used. The function of the latter was to break the polymer structure allowing the release of ICG and PFP. Assays were done *in vitro* on human FLS. ICG by itself has good solubility in physiological medium, however, using it encapsulated in this form, a

three times higher concentration was detected than when ICG is used alone. As a consequence of this, the photocytotoxicity was also triple. Encapsulation with/without PFP was also compared, being the PDT effect better with PFP although without significant differences.

Some nanoparticles can be photoactive and used as PS. This is the case of $Cu_{7.2}S_4$ nanoparticles, which can be use in PDT as photoactive compound. At the same time, it can increase the temperature when excited, giving rise to apoptosis processes, which is known as photothermal therapy (PTT). Xia *et al*. in 2018 tested these nanoparticles *in vitro* in mouse FLS and *in vivo* in a murine collagen-induced arthritis model, using NIR (near-infrared) irradiation [61]. *In vitro* it was shown that after NIR irradiation the temperature of the cells reached 51 °C, while the cells that did not contain nanoparticles remained at 32 °C. Furthermore, ROS production increased with the presence of $Cu_{7.2}S_4$. The *in vivo* study showed that pro-inflammatory cytokines production can be reduced. Additionally, the treated joints did not show damage in bone and cartilage, being similar in appearance to healthy joints.

Based on the multiple publications and promising results, the great potential of PDT in RA is unquestionable. However, it is still necessary to overcome some drawbacks such as the solubility of the system. As discussed above, many of the latest studies on the use of PDT in RA have focused on improving the physiological solubility of PSs using soluble carriers such as nanoparticles or adding functional groups that improve the solubility (among various strategies). We reported that this poor solubility of some PSs could be solved by using ruthenium-based metallacages as carriers in two different ways (Figure 1, page 21):

- The solubility in biological media of these organometallic complexes is good and they can be the host to PS as guest in their inner cavity, transporting and releasing them into target cells (page 28).

- We can include the PS as part of the structure of the metallacage, which maintain excellent physiological solubility and keep the PS available to be irradiated at all times (page 36).

BPD-MA *(1)*

1994

Ratkay *et al*. Benzoporphyrin derivative monoacid ring A (**BPD-MA**) tested *in vivo* (mice).Transcutaneous irradiation. Reduction in pannus formation and reduction in bone and cartilage destruction

1995

Hendrich *et al*. **Photosan-3** tested *in vitro* (FLS). Transcutaneous irradiation. Photocytotoxicity depends on concentration.

Photosan-3 *(3)*

R = and/or OH
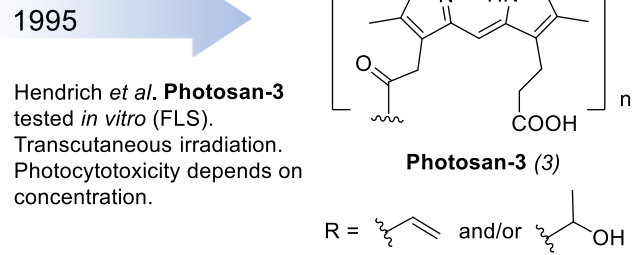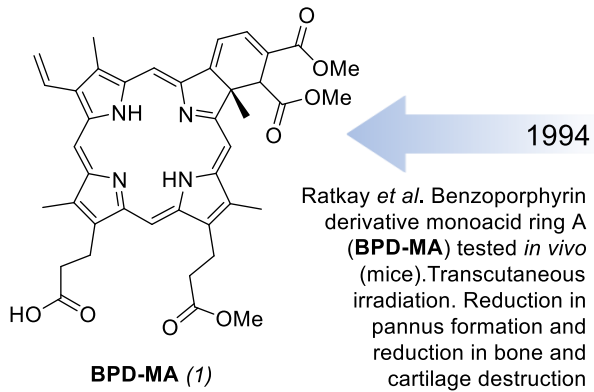
BPD-MA. Ratkay *et al*. Comparation intravenous and intra-articular administration, and transcutaneous and intra-articular irradiation (in rabbits). Significant differences are found
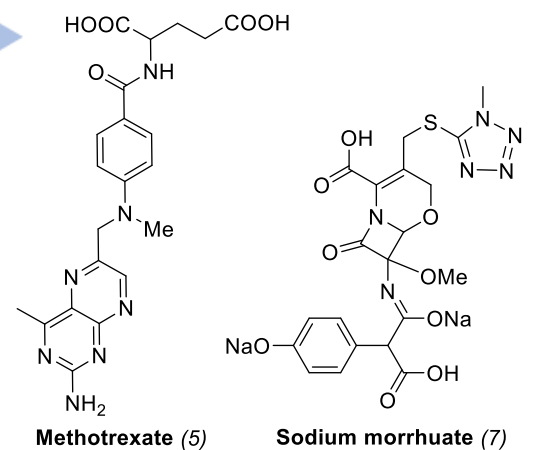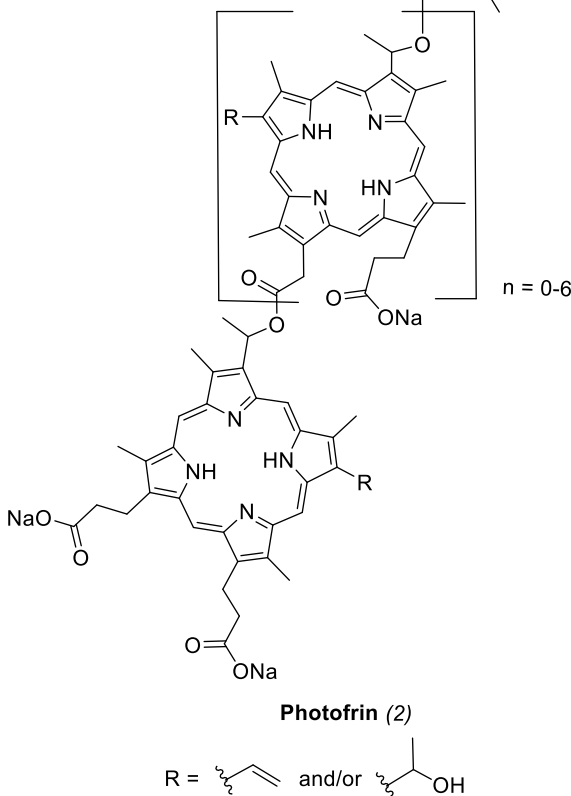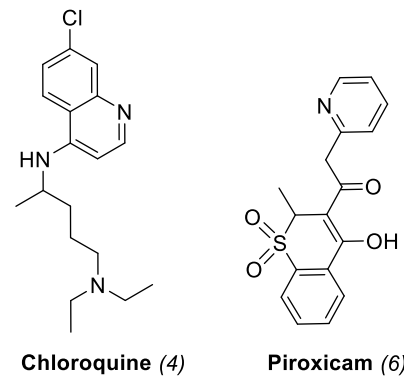
1997

Hendrich *et al*. **Photosan 3** tested *in vivo* (rabbits).
No toxicity by PS without irradiation and no toxicity by irradiation alone.Complete destruction of inflamed synovial tissue and no changes in cartilage and meniscus

1998

BPD-MA. Trauner *et al*. Uptake in different tissues after administration. Concentration peak in the synovium after 15 min

Hendrich *et al*. tested *in vitro* (FLS) **Chloroquine**, **Piroxicam**, **Sodium morrhuate** and **Methotrexate** to treat RA by PDT. Only **Chloroquine** and **Methotrexate** showed significant results.

Trauner *et al*. **Photofrin** tested *in vitro* (FLS). Intravenous administration and irradiation by bare cleaved fiber irradiation. Skin hypersensitivity for at least one month after treatment due to the required high concentrations (poor solubility). PS absorption into synovial tissue was slow (48 h), which make the treatment impractical

Chloroquine *(4)*   **Piroxicam** *(6)*

Methotrexate *(5)*   **Sodium morrhuate** *(7)*
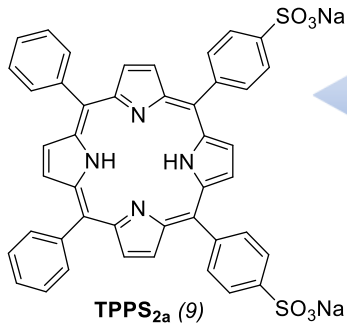

Photofrin *(2)*
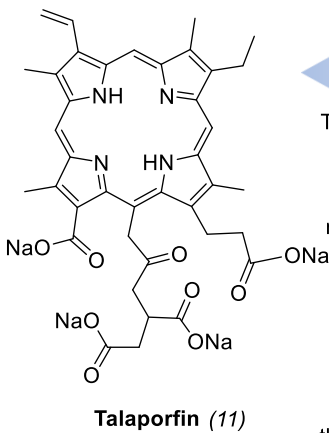
R = and/or OH

2000

Hendrich *et al*. **BPD-MA** tested in rabbits using intravenous injection and intra-articular irradiation. Cartilage, menisci, tendons and ligaments were not affected after therapy. In absence of light, no adverse effects occur after 1 week

19

Bagdonas *et al*. **PpIX** tested in rabbits with rheumatoid mono-arthritis. Accumulation mainly in the affected joint.

2005

2002

So *et al*. Protoporphyrin IX (**PpIX**) tested as PS in PDT of RA *in vitro* (human cells from patient with RA) and *in vivo* (mice). Using 5-aminolevulinic acid (ALA) as precursor. Accumulation in synovial lyning layer, vascular endothelium and macrophages mainly. Accumulation *in vivo* only in RA animals and not in healthy animals.

COOR   COOR

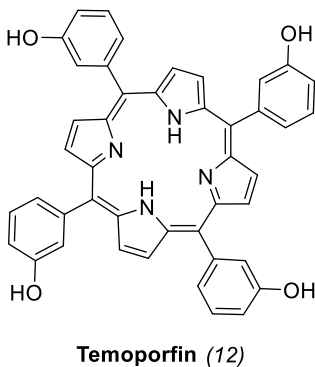**PpIX** *(8)*

R = H, alkyl

SO₃Na

TPPS₂ₐ *(9)*

SO₃Na

Dietze *et al*. tested meso-tetraphenylporphyrin sulfonate (**TPPS₂ₐ**) in combination with Gelonin to treat RA by PDT. The PS breaks the lysosomal membrane and helps the release of Gelonin in the cytoplasm improving the cytotoxicity

2006

Nishida *et al*. tested **ATX-S10.Na(II)** as PS in PDT to treat RA *in vitro* (FLS) and *in vivo* (mice). In both assays, direct relationship between concentration and phototoxicity is demonstrated.

NaO   ONa

HN   NH

OH

NOH

ATX-S10.Na(II) *(10)*

2008

Torikai *et al*. **Talaporfin** tested as PS in PDT of RA. *In vitro* assays show that it is located mainly in lysosomes. *In vivo* assays (intra-articular administration and transcutaneous irradiation) show accumulation in the synovial tissue much greater than the rest of the surrounding tissues.
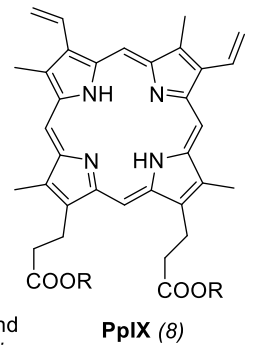
NaO   ONa

NaO   ONa

Talaporfin *(11)*

2010

Hendrich *et al*. **Methotrexate** tested *in vivo* using LEDs as irradiation source. Infrared get better photocytotoxicity than red, yellow and whited light. In vitro assays showed the same results.

Juillerat-Jeanneret *et al*. Encapsulation of tetra(4-sulfonatophenyl)porphine (TSPP), tetra(4-carboxyphenyl)chlorin (**TPCC**) and chlorin e6 (**Ce6**) in chitosan-based nanogel. Tested both in vitro (human THP-1 macrophages and murine RAW 264.7 macrophages) and in vivo (mice with antigen-induced arthritis). Maximum concentration after 3-4 *in vitro*. **Ce6** showed toxicity in dark. PS-nanogels were retained longer time in joints affected by RA.

HO   OH

HO   OH

Temoporfin *(12)*

Hansch *et al*. **Temoporfin** added to PEGylated form tested as PS in PDT of RA *in vivo* (mice). Temoporfin-PEG shows gretaer solubility and accumulation in inflamed tissue than PS alone
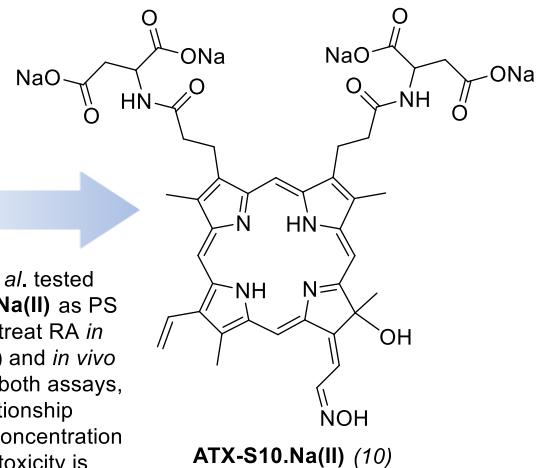
CO₂⁻

CO₂⁻   CO₂⁻

Ce6 *(15)*

R   R

R   R

TSPP, R= SO₃⁻ *(13)*
TPCC, R= CO₂⁻ *(14)*

2012

Pheophorbide A *(16)*

modified lysine polymer

Gabriel *et al.* tested **Pheophorbide A** linked to modified lysine polimer *in vivo*. Goals: to visualize the location of PS and give rise to photocytotoxicity.Maximum concentration with PS-lysine 24 h after injection (5 h with PS alone). Linear correlation concentration/death cells with PS-lysine (not with PS alone). No toxicity in health joints and no toxicity in dark.

Guo *et al.* tested *in vitro* (FLS) **Hypericin** as PS to treat RA by PDT. ROS production increases after PDT proportional to the concentration used.

Hypericin *(19)*

Xia, Li *et al.* tested i*n vitro* (FLS) and *in vivo* (murine) Cu-S nanoparticules to treat RA by PDT. *In vitro* after NIR irradiation the temperature was 51 °C giving rise to apoptosis. *In vivo* pro-inflammatory cytokines can be reduced and no damage in bone and cartilage.

Cu$_{7.2}$S$_4$

Cu-S nanoparticules

2018

TSPP *(17)*

TiO$_2$

TiO$_2$ nanoparticule

2016

Wang *et al.* tested **TiO$_2$** nanoparticules containing tetra(4-sulfonatophenyl)porphine (**TSPP**) *in vitro* (FLS) and *in vivo* (murine). *In vitro* assays show tandem **TiO$_2$-TSPP** accumulated in FLS. I vivo assays showed accumulation mainly in inflamed tissue and can reduce the presence of biomarkers of RA (TNF-alpha and IL-17).

2017

ICG *(18)*

Zhu *et al.* tested Indocyanine green (**ICG**) encapsulated in poly[DL-lactide-co-glycolic acid] (PLGA) as PS in PDT of RA *in vitro* (FLS). Combination of sonodynamic therapy (break the structure of the PLGA and release **ICG**) and PDT. Concentration in FLS three time higher with ICG-PLGA than **ICG** alone. **ICG**-PLGA triple photocytotoxicity.

2022 our work

Evaluation of ruthenium-based assemblies as carriers of photosensitizers to treat rheumatoid arthritis by photodynamic therapy.

Ruthenium-based assemblies incorporating tetrapyridylporphyrin panels: A photosensitizers delivery strategy for the treatment of rheumatoid arthritis by photodynamic therapy.

PS

PS = porphine, Mg-porphine, phthalocyanine and Zn-phthalocyanine

PS = H$_2$-TPyP, Zn-TPyP and Co-TPyP

Figure 10. PS used in the treatment of RA by PDT from the first results reported until our work.

CHAPTER 4 - ARENE RUTHENIUM METALLA-ASSEMBLIES

Although our work is the first to demonstrate the applications of arene ruthenium metallacages in the PDT of RA, the synthesis and some applications for these organometallic complexes have been studied and reported for more than two decades. We can establish the starting point 25 years ago, when Süss-Fink and co-worker reported the synthesis of the first tetranuclear arene ruthenium assembly (Scheme 1) [62]. Starting from the Zelonka and Baird dimer [63], they formed a di-ruthenium clip complex with oxalate salt and then, by adding the bidentate ligand 4,4'-bipyridine, they obtained a rectangular metallacage. During subsequent years, the design and development of arene ruthenium metallacages has continued in progress, giving rise to different structures, more complex and with greater functionalities, and also different synthesis strategies. However, the basic steps and methodology introduced by Süss-Fink remain today.
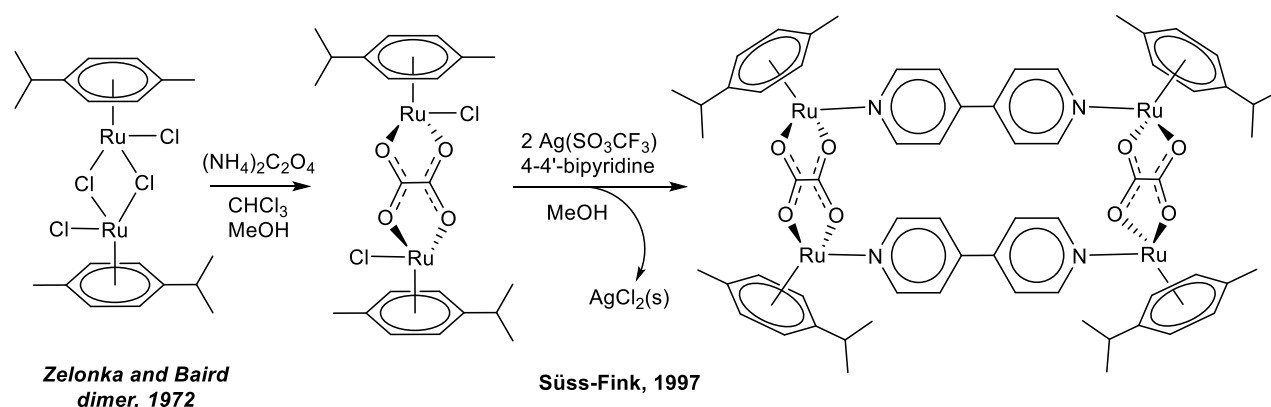

Scheme 1. Synthesis of rectangle metallacage by Süss-Fink and co-workers in 1997.

The shape and size of metallacages are determined by the nature of the ligands coordinating to the metals. In the arene ruthenium dimer reported by Zelonka and Baird, the metal atoms present an octahedral hexacoordination, in which the arene occupies three ligand positions and three chloride ligands the remaining three. Even though the dimer is inert and stable at room temperature and in air, the chlorides are labile ligands easily removable or interchangeable with other ligands through substitution reactions. This versatility has been used by many groups to build various structures with different functionalities starting from this ruthenium arene dimer [64-71].

The metallacages are built from two main building blocks:

a) The arene ruthenium bimetallic complex (**clip**), which can be considered the edges of the metallacage. The tetradentate spacer ligand (Figure 11) separates the two ruthenium atoms and establishes the distance between them and therefore the size of the metallacage.
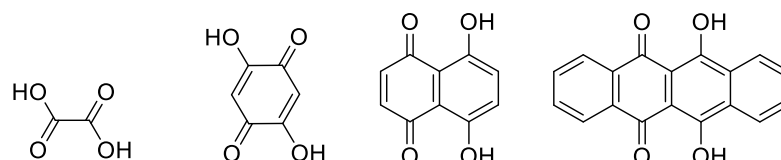

Figure 11. Protic ligands used as spacer in the arene ruthenium bimetallic complex. Form left to right: oxalic acid, 2,5-dioxydo-1,4-benzoquinona, 5,8-dioxydo-1,4-naphthoquinona and 6,11-dioxydo-5,12-naphthacenediona.

b) The **panel ligand** (Figure 12), which shapes the metallacage. In our work we use triangular or square panel ligands, giving rise to prismatic or cubic metallacages, respectively.
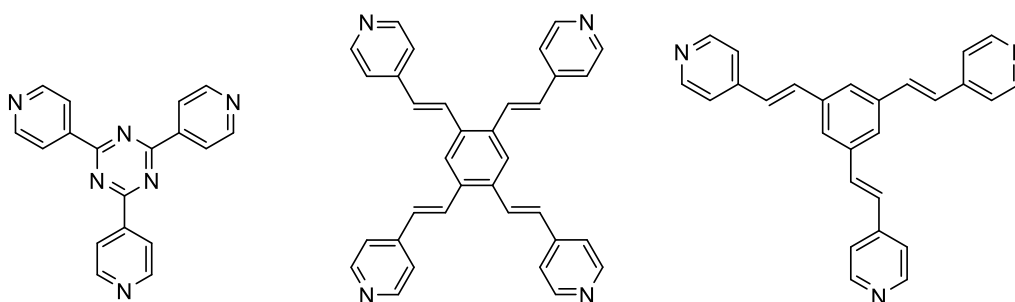

Figure 12. Panel ligands used to give rise to prismatic o cubic metallacages. From left to right: 2,4,6-tri(pyridin-4-yl)-1,3,5-triazine, 1,2,4,5-tetrakis{2-(pyridine-4-yl)vinyl}benzene and 1,3,5-tris{2-(pyridin-4-yl)vinyl}benzene.

The first step of the synthesis begins with $RuCl_3 \cdot nH_2O$ and a cyclohexadiene (1-isopropyl-4-methyl-1,3-cyclohexadiene in our work) which will give rise to the arene ligand. Therefore, in this first reaction, it is decided the arene that will contain the final metallacage. An excess of the cyclohexadiene is used and the reaction is refluxed for 4 h (Scheme 2), giving rise to the arene ruthenium dimer as an orange solid, by a substitution reaction that releases HCl.
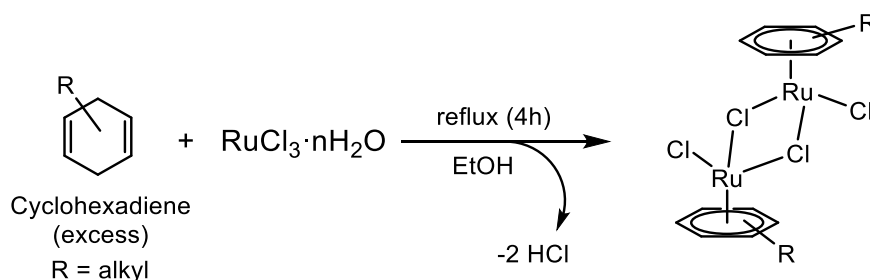

Scheme 2. Synthesis of arene ruthenium dimer.

The arene ruthenium dimer is the starting point for the second step of the synthesis (Scheme 3). This is reacted in stoichiometric amounts with a protic ligand in methanol at room temperature. This mixture gives rise to a substitution reaction between the ligand and the bridging chlorides of the two ruthenium atoms. In this way, a bimetallic complex is formed in which the new ligand acts as a spacer determining the distance between two metal atoms.
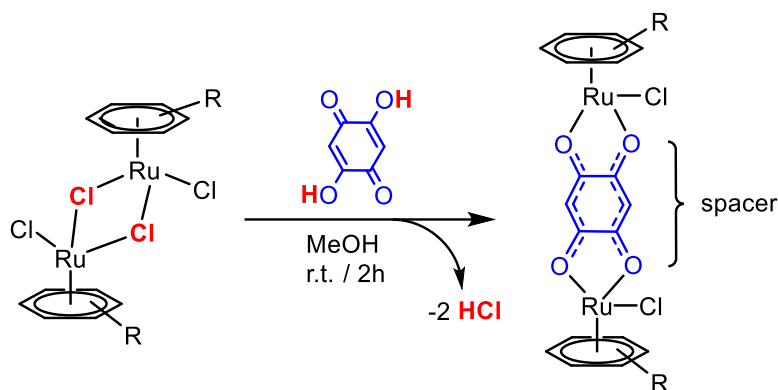

Scheme 3. Synthesis of arene ruthenium clip.

The last step of the synthesis consists of adding the panel ligand which, together with the ruthenium clip complex, will give rise to the metallacage (Scheme 4). First, the complex is mixed with silver triflate (AgSO$_3$CF$_3$), which removes the chloride ligands, giving rise to silver chloride (AgCl) as precipitate, and an intermediate cationic complex. Without isolating this intermediate, the panel ligand is added in solution in the appropriate stoichiometric amounts and the mixture is kept stirring for 48 h at room temperature. The metallacage is formed as a cationic complex (whose counterion is the triflate anion). The metallacage is soluble in biological media, as well as in other common solvents.
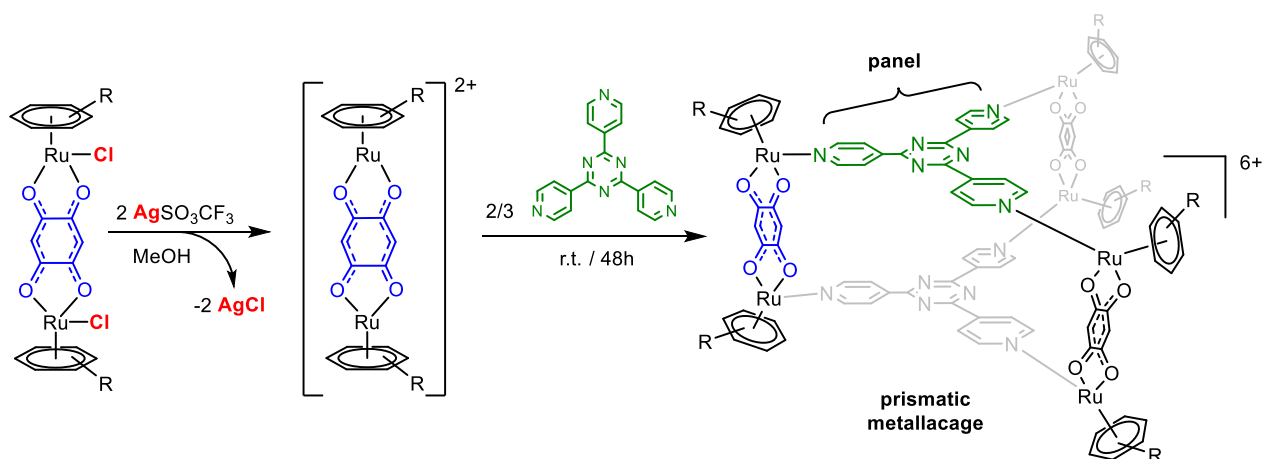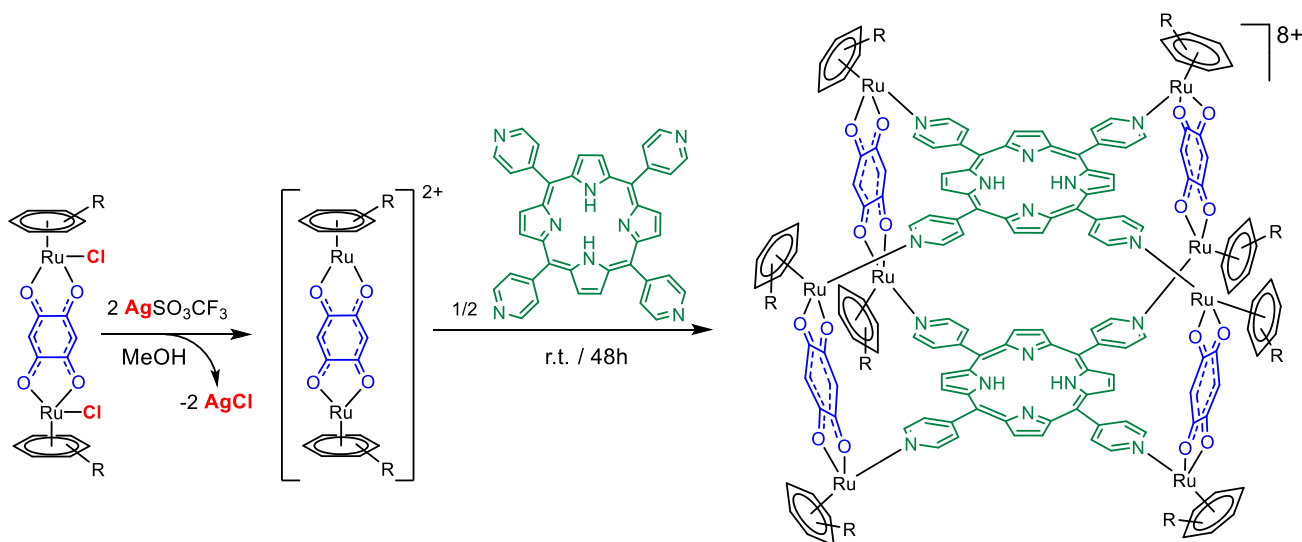

Scheme 4. Synthesis of metallacage.

The structure of these metallacages contains an inner cavity with hydrophobic nature. When a planar compound with a hydrophobic character is added to the reaction mixture at the same time as the panel ligand, this guest (as long as its structure and size allow it) ends up by affinity in the cavity (Scheme 5). This is the strategy used to host PSs of poor water solubility within metallacages, in order to be transported in biological media.
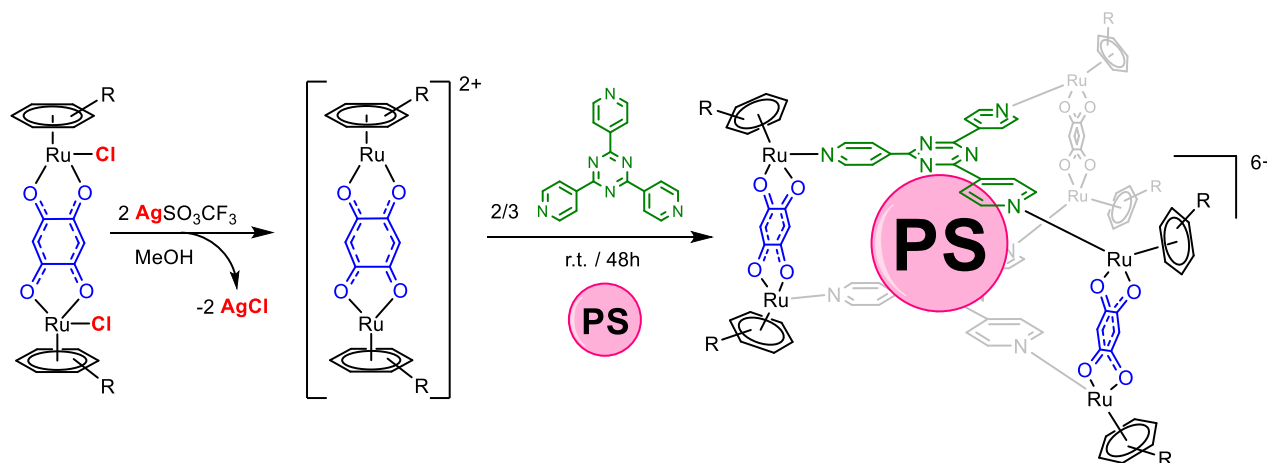

Scheme 5. Synthesis of the metallacage with PS in the inner cavity.

On the other hand, it is possible to build metallacages in which the PS forms part of the structure, using the PS itself as a ligand panel (Scheme 6). The methodology coincides with the one discussed before. The PS containing pyridine substituents can be coordinated to the ruthenium atoms in the same way as the triangular and square panels described above.

Scheme 6. Synthesis of metallacages using the PS (5,10,15,20-tetra(4-pyridyl)-21*H*,23*H*-porphine) as panel ligands.

To identify and confirm that the PS is located in the interior cavity of the metallacage, we used Diffusion-Ordered Spectroscopy (DOSY). This NMR technique identifies the different species in the sample according to their diffusion coefficients. Therefore, since PS and metallacage are different species, if their signals show the same diffusion coefficient, it means that they are together (Figure 13). It is also possible to use other techniques such as mass spectrometry (MS), but the host-guest system does not always resist the experimental conditions of MS.
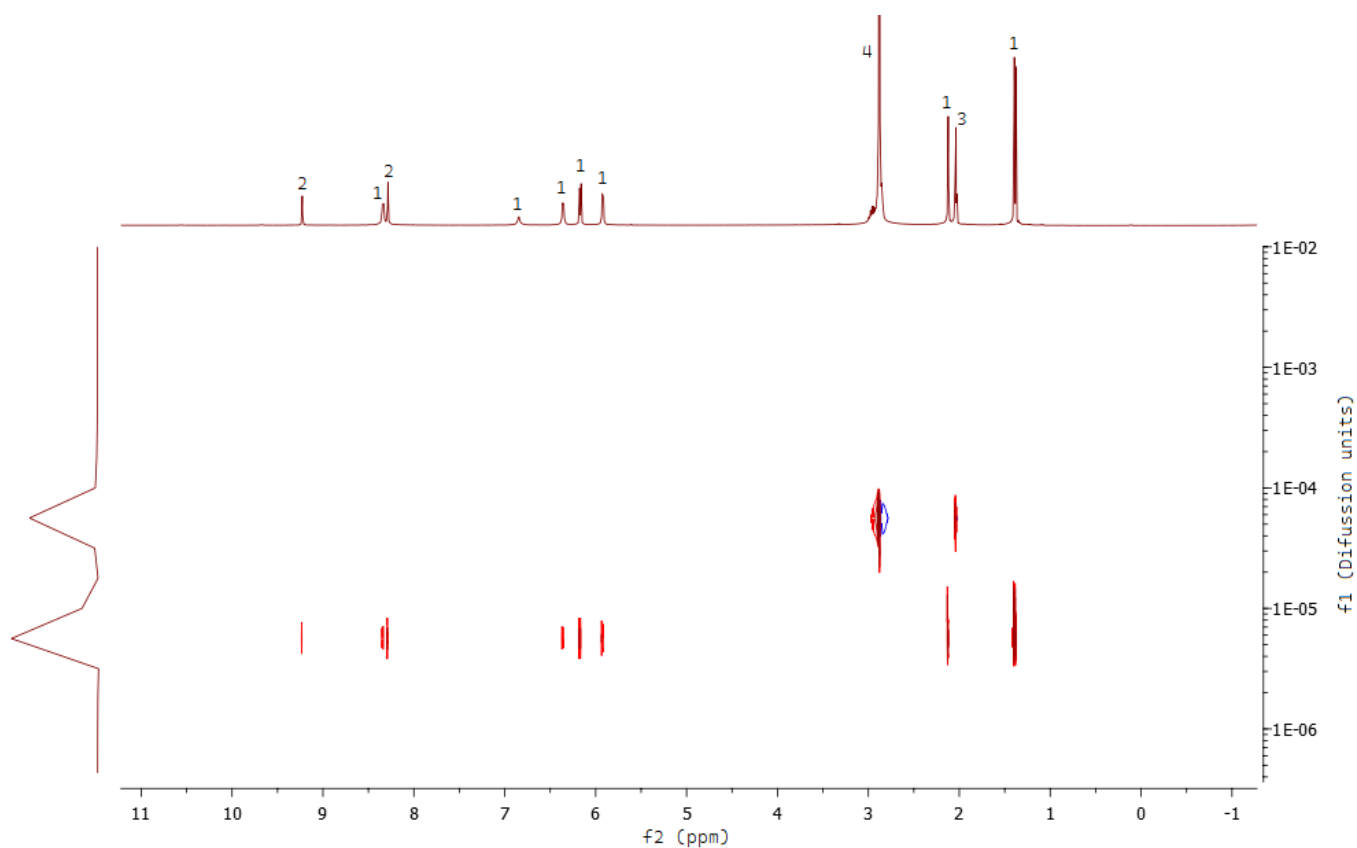
Figure 13. DOSY NMR spectrum of metallacage with PS (porphine) in the inner cavity. ^{1}H signals of metallacage (1), PS (2), acetone (3) and water (4).

CHAPTER 5 – OBJECTIVES

1. Synthesis of arene ruthenium metalla-assemblies.

   a) Study of different structural characteristics applicable to metallacages:

   -Volume of the ruthenium edge complex.

   -Shape of the ligand panel (cubic and prismatic cages).

   -Size of the ligand panel.

   b) Study of the photoactive organic compounds that can be host in the internal cavity of the metallacages.

   c) Isolation and characterization of the systems Cage-PS.

   d) Study, synthesis and characterization of tetra- and bi-pyridylporphyrins with arene ruthenium complexes to improve the solubility in biological media.

2. *In vitro* evaluation of the compounds as PS for PDT in human RA FLS and in SW982 synovial sarcoma cells.

   a) Isolation of FLS from RA patients.

   b) Evaluation of the antiproliferative activity after PDT in human RA FLS.

   c) Evaluation of anti-inflammatory activity:

   -Quantification in cultured supernatants of pro-inflammatory cytokine IL-1β.

   -Expression of cyclooxygenase-2 (COX-2), enzyme responsible for the formation of pathological prostaglandins. Quantification in cultured supernatants of PGE_2 (pro-inflammatory mediator of arachidonic acid metabolism).

   d) Evaluation of antiproliferative activity and apoptosis in SW982 synovial sarcoma cells using the tetra- and bi-pyridylporphyrins with arene ruthenium complexes.

6.1 Evaluation of ruthenium-based assemblies as carriers of PS to treat RA by PDT.

In this work [72], we reported, for the first time in RA, that these ruthenium metallacages (**M1**-**M6**) can be applied as PDT agents, fulfilling the role of carriers of PSs to the target cells (FLS from RA patients). The compounds evaluated as PS were 21*H*,23*H*-porphine (**G1**), magnesium(II)-porphine (**G2**), 29*H*,31*H*-phthalocyanine (**G3**), and zinc(II)-phthalocyanine (**G4**) (Figure 14). These photoactive compounds had never before been evaluated as PS by themselves in the PDT of RA due to their low or null physiological solubility. They can be hosted in the cavity of the metallacages and transported in biological media. Moreover, we have synthesized cages with structural modifications to evaluate how the different elements of the metallacage change the PDT effect (Figure 15). These metallacages can be distinguished by their two main blocks: the panel ligand, on the top and bottom of the metallacage, and the dinuclear ruthenium clips complex in every edge of the structure. The panel ligand is a flat organic compound with three or four pyridine substituents, giving the shape of a prism or a cube to the metallacages, respectively. We used 2,4,6-tri(pyridin-4-yl)-1,3,5-triazine or 1,3,5-tris{2-(pyridin-4-yl)vinyl}benzene for the prismatic structures (**M1**, **M2**, **M3**, **M5** and **M6**), and 1,2,4,5-tetrakis{2-(pyridine-4-yl)vinyl}benzene for the cube (**M4**). In the dinuclear arene Ru(II) complexes, the two metal atoms are linked by 2,5-dioxydo-1,4-benzoquinonato, 5,8-dioxydo-1,4-naphthoquinonato, or 6,11-dioxydo-5,12-naphthacenedionato ligands (Figure 15). These three heterocycles differ primarily in the number of aromatic rings, varying the volume of the complex and directly influencing the deformation of the structure in solution, and being able to change the stability of the **G⊂M** system.
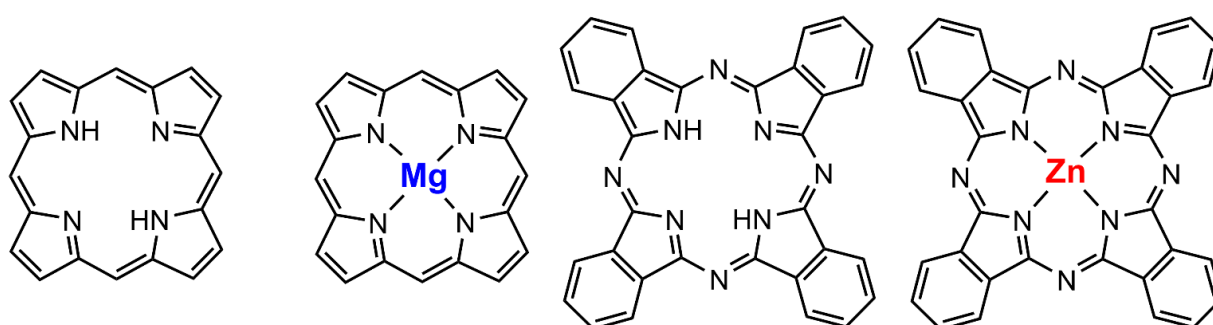
Figure 14. Photosensitizers used in this work. From left to right: 21*H*,23*H*-porphine (**G1**), Mg(II)-porphine (**G2**), 29*H*,31*H*-phthalocyanine (**G3**) and Zn(II)-phthalocyanine (**G4**).
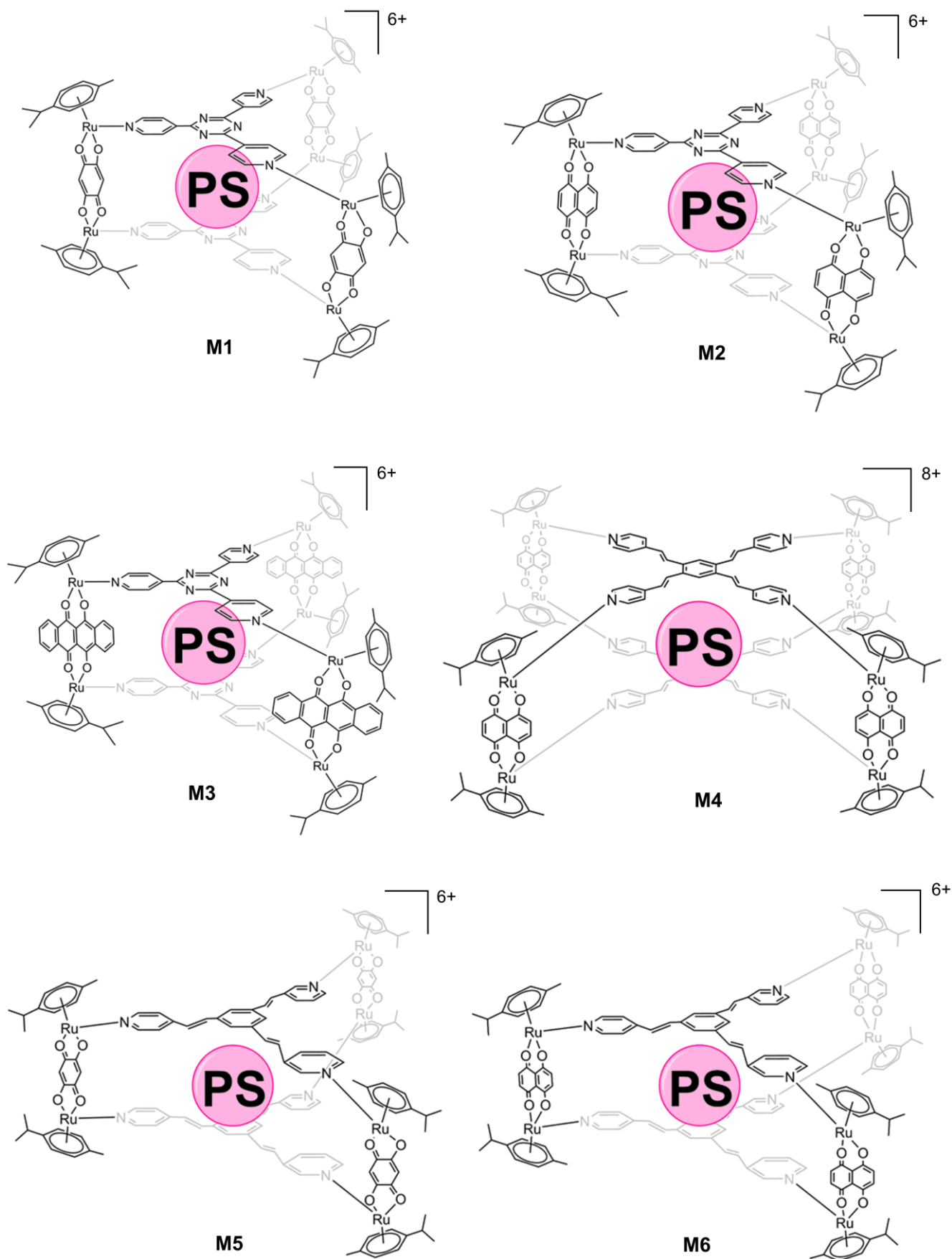
Figure 15. Structures of ruthenium(II) metallacages used in this work. The photosensitizer is represented by a sphere (**PS**), 21*H*,23*H*-porphine (**G1**) was hosted in **M1**–**M6**, Mg(II)-porphine (**G2**) in **M1**, **M4**, and **M6**, 29*H*,31*H*-phthalocyanine (**G3**) and Zn(II)-phthalocyanine (**G4**) in **M4**–**M6**.

6.1.1 Antiproliferative evaluation

We evaluated the PDT effect of these systems analyzing the photocytotoxicity after irradiation in RA FLS. For that, we carried out MTT assays, calculating the 50 % inhibition concentrations (IC_{50}). The results of the PDT treatment were excellent (Table 1). The IC_{50} with these compounds were lower than those seen in cancer cells [73]. However, such higher antiproliferative effect was expected, since RA FLS are primary cells and their growth is not accelerated, unlike cancer cells. On the other hand, as anticipated, the structural differences in the metallacages resulted in significant changes in the PDT effect.

First, we have noticed that when the size of the panel ligand is bigger, the photocytotoxicity is higher. For instance, in the structures of cages **M2**, **M4**, and **M6** only the panel ligand differ, 2,4,6-tri(pyridin-4-yl)-1,3,5-triazine, 1,2,4,5-tetrakis{2-(pyridine-4-yl)vinyl}benzene and 1,3,5-tris{2-(pyridin-4-yl)vinyl}benzene, respectively. If we compare the IC_{50} values obtained with **G1** as PS inside the metallacages (entries 2, 4, and 6 in Table 1), we observed that the metallacage **M2**, with the smallest panel, required a higher concentration than **M4** and **M6** (triple when compared to **M6**). This variation is more obvious if we compare the metallacages **M1** and **M5**, involving the panels 2,4,6-tri(pyridin-4-yl)-1,3,5-triazine and 1,3,5-tris{2-(pyridin-4-yl)vinyl}benzene, respectively; With **G1** as PS, the IC_{50} of **M1** is six times higher than the one observed with **M5** (entries 1 and 5 in Table 1). This matches with the results described in cancer cells [73]. Larger panel ligands provide larger apertures that facilitate the release of the PS, resulting in higher ROS production and, consequently, more photocytotoxicity. This conclusion is in harmony also with the other three PSs tested, **G2**, **G3** and **G4** (Table 1).

Regarding the second of the structural features of the metallacages that we have modified, the dinuclear clip, similar variations in the photoactivity are observed, as we estimated. When the volume of the Ru(II) clip complex is bulkier (more aromatic rings in the spacer ligand), we noticed that the IC_{50} is lower, which means a better PDT effect. For instance, cages **M1**, **M2**, and **M3** contain the same panel ligand (2,4,6-tri(pyridin-4-yl)-1,3,5-triazine) and vary only in the spacer ligand, being 2,5-dioxydo-1,4-benzoquinonato, 5,8-dioxydo-1,4-naphthoquinonato, and 6,11-dioxydo-5,12-naphthacenedionato respectively. With the same PS (**G1**), the IC_{50} found with **M3** was four times lower than the IC_{50} found with **M1** (entries 1 and 3 in Table 1), while the IC_{50} of **M2** (entry **2** in Table 1) shows an intermediate value. These results are consistent with the structure of metallacages suggesting PS release through an aperture of the metallacage [74]. This is, when the metallacage is smaller, the host-guest system is stabilized, making more difficult the releasing of the PS, which translates into lower ROS production and

reduced PDT effect. The same result, although to a lesser proportion, was observed with the other PSs, **G2**, **G3** and **G4** (Table 1).

Table 1. Results of the MTT assays. Irradiation after 24 h of incubation with **G⊂M** systems. $\lambda = 630$ nm, 72 J/cm^2 for 30 min. IC$_{50}$ values were determined fitting the curve to a second-degree polynomial $\pm$ 3 sigma deviations. The maximum concentration analyzed was 1500 nM. Quantum yield (ϕ_F) was determined using TPP as an internal standard in DMSO at 25 °C. Phototoxic index (PI) is ratio dark/light IC$_{50}$. Empty metallacages (without PS in the inner cavity) were tested using the same procedure without any signal of toxicity, even at concentrations five times higher than the maximum concentration tested for the compounds.

| Entry	G ⊂ M	IC$_{50}$ (nM) Light	IC$_{50}$ (nM) Dark	Φ_F (%)	PI
1	**G1 ⊂ M1**	211.7 ± 5.8	>1500	-	>7
2	**G1 ⊂ M2**	95.0 ± 5.9	>1500	-	>16
3	**G1 ⊂ M3**	53.6 ± 4.3	>1500	-	>28
4	**G1 ⊂ M4**	48.1 ± 9.7	>1500	-	>31
5	**G1 ⊂ M5**	35.4 ± 4.7	>1500	0.8	>42
6	**G1 ⊂ M6**	31.7 ± 6.6	>1500	1.1	>47
7	**G2 ⊂ M1**	302.6 ± 5.2	>1500	-	>5
8	**G2 ⊂ M4**	100.7 ± 5.8	>1500	-	>15
9	**G2 ⊂ M6**	91.8 ± 8.3	>1500	2.0	>16
10	**G3 ⊂ M4**	>1500	>1500	-	-
11	**G3 ⊂ M5**	53.4 ± 4.5	>1500	0.11	>28
12	**G3 ⊂ M6**	47.4 ± 6.3	>1500	-	>32
13	**G4 ⊂ M4**	>1500	>1500	-	-
14	**G4 ⊂ M5**	66.0 ± 2.6	103.8 ± 2.9	1.6	2
15	**G4 ⊂ M6**	64.4 ± 4.4	163.8 ± 17.1	-	3

The last difference between the systems evaluated was the PS itself that they transport, and significant differences were also observed. First, it is worth mentioning the absence/presence of a metal (Mg, Zn) in the center of the PS. In all cases, employing the same metallacage, the PSs without metal showed greater photocytotoxicity (Table 1). This result can be directly attributed to the higher fluorescence of the PSs with a metal center. This occurs because when the PS is irradiated it causes its excitation, that is, it absorbs part of the irradiation energy and reaches a higher energy state (excited singlet state). When the PS relaxes, it can release that extra energy in the form of fluorescence and the PS returns to its ground state. However, as explained in Chapter 1 (page 5), an intermediate excited state (excited triplet state) can be involved, and the PS can relax and return to the ground state by releasing the extra energy in the form of phosphorescence, or it can also interact with other molecules or substrates, such as O$_2$, transmitting the extra energy to the latter that will give rise to ROS [75-77]. Consequently, since the Zn(II) and Mg(II) produce higher fluorescence (Figure 16), reduced ROS production would be expected, compared their metal-free analogues. The fluorescence quantum yields (Φ_F), support these results (Table 1), that is, greater Φ_F equates to less PDT effectivity.
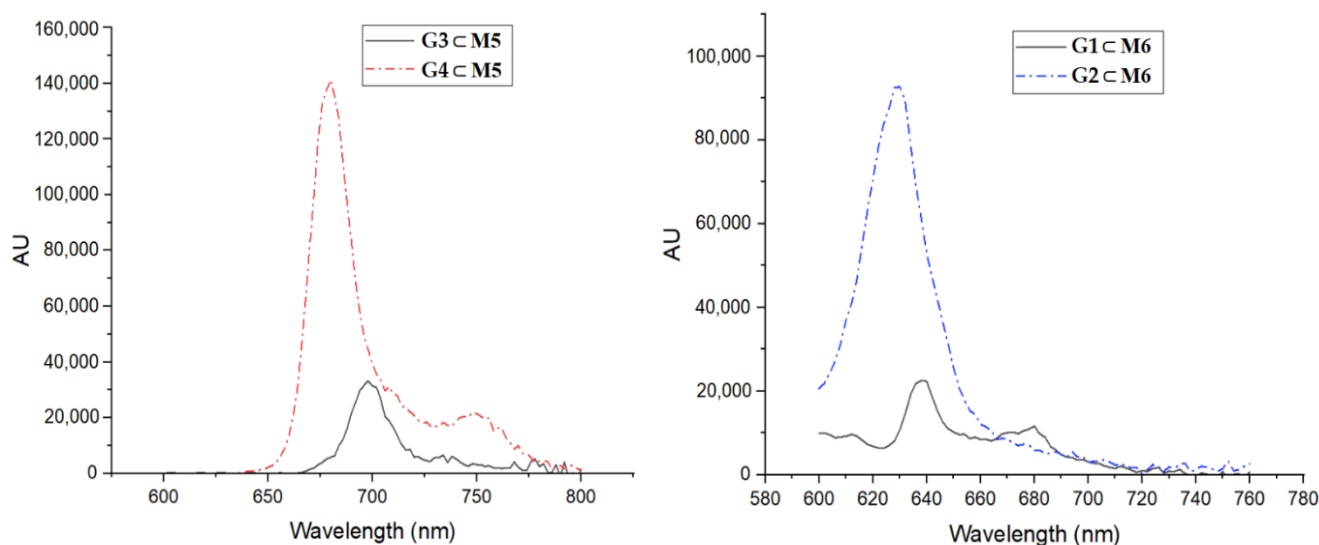
Figure 16. Emission spectra of **M5** with **G3** or **G4** (left) and **M6** with **G1** or **G2** (right). 10 nM concentration in DMSO at 25 °C.

The high fluorescence of the metal-based tetrapyrrole can be explained through electronic orbitals. When the PS is excited, an electron is promoted from the Highest Occupied Molecular Orbital (HOMO) to the Lowest Unoccupied Molecular Orbital (LUMO), and later when the PS relaxes that electron returns to the HOMO giving rise to fluorescence. However, if there is not a metal center in the tetrapyrrole (Figure 17, Case 1), the lone electron pairs of the N atoms of the tetrapyrrole are free and can occupy this electronic vacancy in the HOMO, making it difficult for the electron in the LUMO to return to the HOMO, resulting in less fluorescence. This does not happen when there is a metal in the center of the tetrapyrrole (Figure 17, Case 2), since it is bonding to the N atoms through their lone pairs of electrons, so these cannot occupy the vacancy in the HOMO and the electron in the LUMO can return to the HOMO easily, resulting in higher fluorescence [78].

We observed also differences between the PSs **G1** (porphine) and **G3** (phthalocyanine). The results showed that **G1** functions better than **G3** when the carrier is the same metallacage for both (Table 1). However, the IC_{50} for **G3** is still brilliant. On the other hand, surprisingly, when **G3** or **G4** are transported by the cubic metallacage (**M4**), we did not observed effect on RA FLS (Table 1), even at the maximum concentration tested (1500 nM). This suggests a robust binding host-guest affinity, thus supporting that the PS is released through an aperture of the metallacage, rather than having a breakage of the metallacage [74].
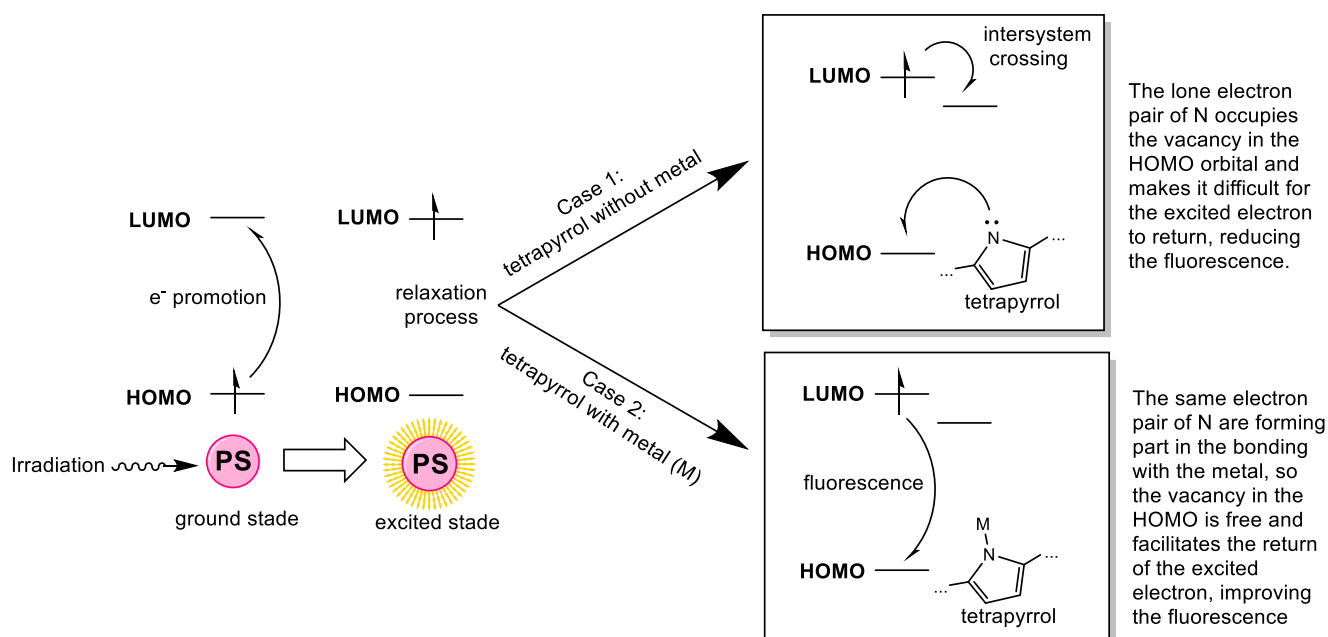
Figure 17. Differences in the relaxation process with or without metal in the tetrapyrrole. The presence of the metal favors fluorescence, while its absence decreases fluorescence in favor of intersystem crossing.

One exceptional result is also the total absence of cytotoxicity in the dark. However, two of the fifteen compounds evaluated, specifically the two with **G4** as PS (entries 14 and 15 in Table 1), showed toxicity in the dark (Figure 18). This observation suggests that **G4** cannot be a good PS. This result agrees with other reported zinc tetrapyrrole derivatives that showed toxicity in the dark [79,80].
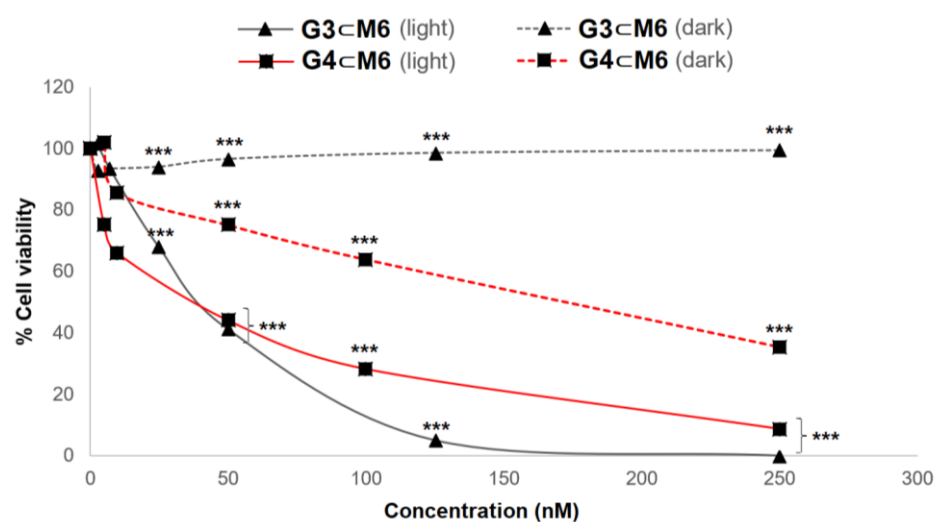

Figure 18. Results of the MTT assays using **G3⊂M6** (black) or **G4⊂M6** (red), in absence of light (dashed line) and after irradiation (solid line). Statistical significance determined by the two-tailed unpaired Student's t-test, p-value < 0.001 (***).

6.1.2 Inflammatory evaluation

The joint is surrounded by the synovial membrane, providing structural support, lubrication, and supplying nutrients to the cartilage. FLS are part of the inner lining layer of the synovial membrane (see page 10). The production of cytokines is one of the main functions of FLS [81], and many of the cytokines implicated in the inflammatory response are these of the interleukin (IL) family. IL-1 induces cyclooxygenase-2 (COX-2) expression, an enzyme involved in the production of prostaglandin E2 (PGE_2) [82-85]. PGE_2 could give rise to vasodilation in the synovial tissue, causing inflammation in the region [86]. We evaluated in RA FLS the *in vitro* inflammatory activity after PDT by measuring the production of PGE_2 and IL-1β in the supernatant. In addition, we also analysed the expression of COX-2 in irradiated and non-irradiated cells. COX-2 expression results show that RA FLS treated with the **G⊂M** systems by PDT causes an overexpression of this enzyme (Figure 19). This result agrees with the literature since many examples of this overexpression after PDT have been reported. For instance, more porphyrin-based PSs such as PpIX-polyamine [87] or Photofrin [88] increased COX-2 expression after PDT. Moreover, this not only occurs with porphyrins, but also with other PSs used in PDT [89,90]. We noticed that most of the **G⊂M** systems with low IC_{50} (Table 1) showed lower COX-2 expression (Figure 19): this is the case for the compounds listed in entries 4, 5, 6, 11 and 12 in Table 1. Overexpression of COX-2 leads to an increased production of PGE_2 [87], which could increase inflammation after treatment. This higher production of PGE_2 was indeed observed under our experimental conditions (Table 2). However, as observed for COX-2 expression, PGE_2 production is also lower when the IC_{50} of the compound is low. This shows that by reducing the required concentration of PS, the adverse effects of PDT on the induction of the COX-2/PGE_2 signaling pathway could be reduced/eliminated. However, as reported in the literature, using a COX-2 specific inhibitor, such as NS-398 during PDT treatment, it could be possible to minimize the overexpression of COX-2 and, therefore, the production of PGE_2 [87,91].

On the other hand, as mentioned above, IL-1β is a pro-inflammatory cytokine which, among other functions, induces COX-2 expression [92]. In view of the overexpression of COX-2 correlated with an increase in PGE_2 production, we expected a proportional presence of IL-1β. Surprisingly, it was not the case, since after PDT in all cases studied, the presence of this cytokine increased (Table 2). This result agrees with other studies in which IL-1β was not involved in the overexpression of COX-2 in synovial tissues [93-95], indicating that other cytokines such as IL-6 or IL-8 are responsible [95].
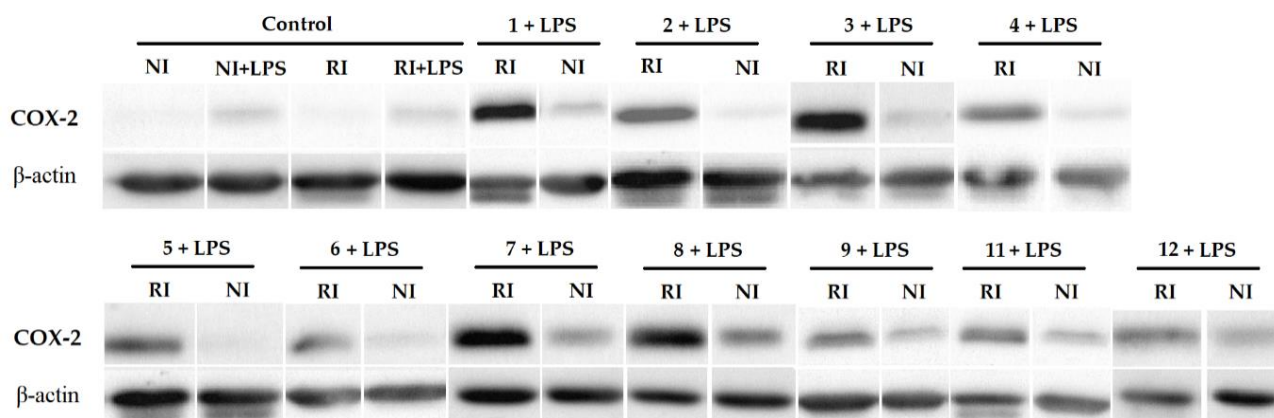
Figure 19. COX-2 expression by Western blot after PDT. The numbers correspond to the entries in Table 1. $2 \cdot 10^6$ FLSs were cultured in DMEM complete medium (FBS 10%, L-glutamine 1%, penicillin 100 U/mL, streptomycin 100 µg/mL) for 24 h and treated with the corresponding system **G⊂M**. After 24 h, the medium was replaced by a DMEM complete medium without red phenol, and then irradiated (RI) or not (NI) using red light (630 nm and 72 J/cm^2 for 30 min). After 18 h, LPS (1 µg/mL) was added to the medium to stimulate the expression of COX-2, and 4 h later the trypsinization was carried out. β-actin was used as a protein loading control. All experiments were done in triplicate. Control samples were treated as treated cells (see Experimental section).

Table 2. PGE$_2$ and IL-1β quantification. The assays were performed using the protocol provided by the ELISA kit in triplicate. The data were treated as explained in this protocol. The cells were treated as described in the experimental section. 18 h after the irradiation dose (without PS), the control sample was treated with 1 µg/mL LPS in the culture medium, the cells were incubated for 4 h, trypsinised and the supernatant was recovered. Results are expressed as the average of three independent experiments.

Entry	G ⊂ M	PGE$_2$ (pg/mL)	IL-1β (pg/mL)
Ctrl	-	286.6 ± 0.1	1.8 ± 0.7
1	**G1 ⊂ M1**	460.8 ± 4.3	2.3 ± 1.2
2	**G1 ⊂ M2**	471.2 ± 3.4	1.9 ± 1.0
3	**G1 ⊂ M3**	445.1 ± 4.7	2.8 ± 0.1
4	**G1 ⊂ M4**	378.3 ± 14.2	3.2 ± 0.4
5	**G1 ⊂ M5**	407.4 ± 14.5	2.1 ± 0.2
6	**G1 ⊂ M6**	439.2 ± 10.1	1.6 ± 0.1
7	**G2 ⊂ M1**	476.8 ± 3.4	1.9 ± 0.6
8	**G2 ⊂ M4**	473.6 ± 7.5	1.4 ± 0.2
9	**G2 ⊂ M6**	430.6 ± 1.4	2.2 ± 0.2
10	**G3 ⊂ M5**	368.2 ± 26.5	2.4 ± 0.4
11	**G3 ⊂ M6**	425.2 ± 2.7	0.1 ± 0.1

6.2 Ruthenium-based assemblies incorporating tetrapyridylporphyrin panels: A PS delivery strategy for the treatment of RA by PDT.

In this work, a different strategy was used, which instead of carrying the PS in the inner cavity of the metallacage as a guest, the PS itself is part of the ruthenium assemblies' structure (Figure 20) [96]. Then, the PS is always available for irradiation since we eliminate the need of liberating the PS from the metallacage once inside the cells [74]. Also, since these systems contain two PS units as panel ligands per metallacages, we though they can reduce the dose necessary for PDT activity [97,98].
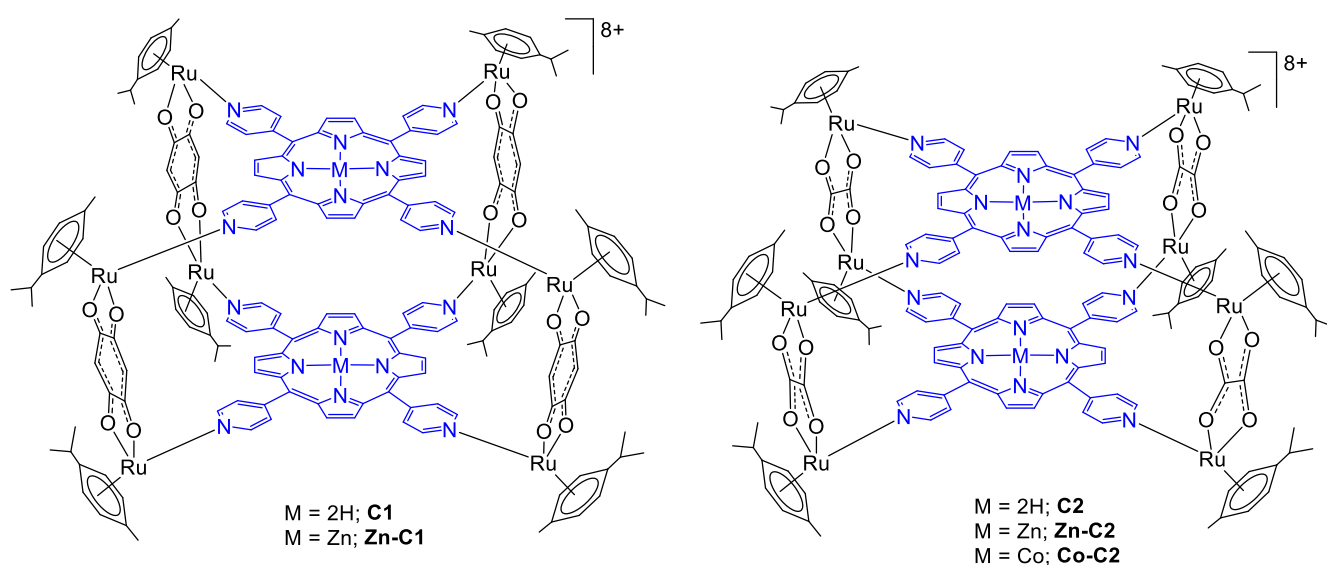
Figure 20. Arene ruthenium metallacages used in this work. All octa-cationic assemblies were isolated as their triflate salts. In blue is showed the tetrapyridylporphyrins, forming part of the metallacage structure as the ligand panels.

As commented previously (page 13), several porphyrin derivatives have already been evaluated in PDT to treat RA with numerous conclusions [38,40,49,50,57]. We decided to use tetra-pyridylporphine (TPyP) as PS because it can be coordinated directly to dinuclear arene ruthenium (II) complexes, such as $[Ru_2(\eta^6\text{-}p\text{-}^iPrC_6H_4Me)_2Cl_2(\mu\text{-}C_6H_2O_4\text{-}\kappa O)]$ and $[Ru_2(\eta^6\text{-}p\text{-}^iPrC_6H_4Me)_2Cl_2(\mu\text{-}C_2O_4\text{-}\kappa O)]$, via Ru-$N_{Py}$ bonding, giving rise to cubic cages (**C**) with porphyrin panels. To evaluate the efficiency of these arene ruthenium tetrapyridylporphyrin-based assemblies, we have tested five compounds with different structural characteristics, including three TPyP derivatives as PSs (H$_2$-TPyP, Zn-TPyP and Co-TPyP) and two dinuclear arene ruthenium clips (Figure 21).

The benzoquinonato and oxalato dinuclear arene ruthenium clips allow to vary the distance between the two PSs units in the structure of the cube, therefore, we can modulate the PS

separation and determine how the distance between the two PS influences their PDT efficiency (Figure 21).

It is known that other tetrapyrroles can give rise to aggregation phenomena, which reduces the production of singlet oxygen and then limits the production of ROS [99,100], reducing the PDT effects. This is due to tetrapyrroles like porphyrin which shows strong π-π interaction, because of their planar structure. It was proved that similar cubic metalla-assemblies with TPyP competently inhibit the intramolecular stacking of porphyrin blocks [101]. Moreover, the electronic repulsion between these cationic assemblies should avoid the formation of aggregates. These two features might have a positive influence in the PDT efficacy.

In addition, we have prepared analogues zinc and cobalt-based tetrapyridylporphyrin (Zn-TPyP and Co-TPyP) assemblies (**Zn-C1**, **Zn-C2** and **Co-C2**). In this way, we can evaluate the impact of the presence of diamagnetic and paramagnetic metals on the PS. It has been reported that diamagnetic metals such as Zn^{2+} can benefit fluorescence and consequently decrease the ROS production, worsening the efficacy of PDT [75]. Furthermore, paramagnetic metals such as Co^{2+} quench fluorescence because of electron transfer between the excited compound and the metal cation [102]. Consequently, no PDT effect should be observed for the **Co-C2** metallacage if such quenching phenomenon is also observed in our systems.
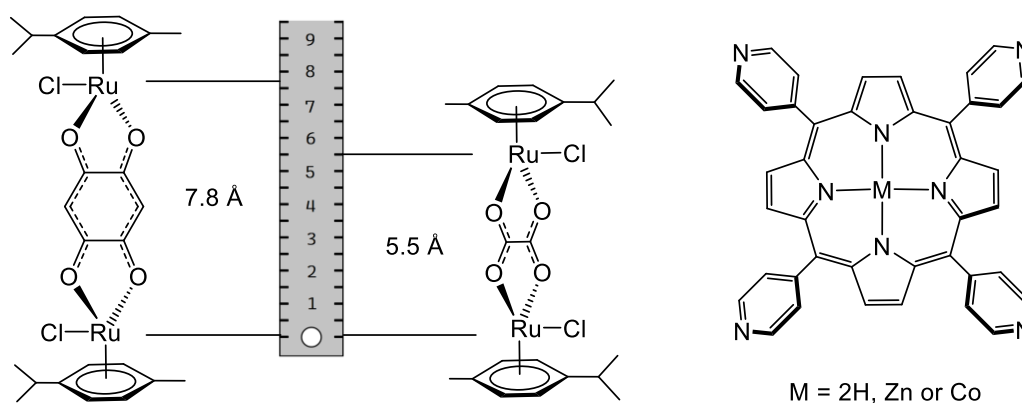
Figure 21. The benzoquinonato and oxalato dinuclear arene ruthenium clips with the distances between the metallic atoms, as well as the structures of the TPyP derivatives: 5,10,15,20-tetra(pyridyl-4-yl)-21H,23H-porphine (H$_2$-TPyP), Zn(II)-5,10,15,20-tetra(pyridyl-4-yl)porphine (Zn-TPyP) and Co(II)-5,10,15,20-tetra(pyridyl-4-yl)porphine (Co-TPyP).

6.2.1 Antiproliferative evaluation

As we did previously, we have evaluated the antiproliferative activity and inflammatory response in FLS extracted and isolated from patients with RA.

In Table 3 we show the results of the antiproliferative assays. Based on the results obtained, we can confirm that the different characteristics in the metallacages significantly condition the PDT efficiency. Among all the results, the one that stands out the most for its excellent photocytotoxicity is **C1**, reaching the lowest IC_{50} (8 nM) (Figure 22). As far as we know, no compound published in the literature showed such a low IC_{50} in PDT on RA FLS. Furthermore, the phototoxic index (PI), which is the IC_{50} ratio between non-irradiated and irradiated cells, is more than 125 (Table 3). These results suggest that **C1** possesses a remarkable potential for PDT. Moreover, the IC_{50} of **Zn-C1**, **C2** and **Zn-C2** are also remarkable, although they are outshined by the excellent performance shown by **C1**. On the other hand, **Co-C2** did not show any photocytotoxic activity, as expected [102]. The Zn(II) derivatives showed higher fluorescence (Figure 23), which brings to lower production of ROS [75], as we already saw with the Zn and Mg compounds inside metallacages (page 32). **C1** and **C2** showed higher photocytotoxicity than their zinc analogues (**Zn-C1** and **Zn-C2**), the IC_{50} concentrations being more than eleven times lower for **C1** and more than eight times lower for **C2** when compared to **Zn-C1** and **Zn-C2**, respectively. It is worth noting that **C1** shows a lower fluorescence quantum yield (ϕ_F) than **C2** and the zinc derivatives (Table 3), confirming that high ϕ_F does not necessarily imply high photocytotoxicity.

Table 3. Results of the MTT assays. Irradiation after 24 h of incubation with PS, λ = 630 nm, 40 mW/cm^2 for 30 min. IC_{50} values were calculated fitting the curve to a second-degree polynomial ± 3 sigma deviations. The maximum concentration tested was 1000 nM. Quantum yield (ϕ_F) was calculated using TPP as an internal standard at 25 °C. Phototoxic index (PI) is the ratio between cell viability in the dark and after irradiation. * Not determined (n.d.).

PS	IC_{50} (nM) light	IC_{50} (nM) dark	ϕ_F (%)	PI
C1	8 ± 3	> 1000	0.9	> 125
Zn-C1	91 ± 7	> 1000	2.7	> 11
C2	22 ± 7	> 1000	1.7	> 46
Zn-C2	185 ± 8	> 1000	2.8	> 5
Co-C2	> 1000	> 1000	0	n.d.*
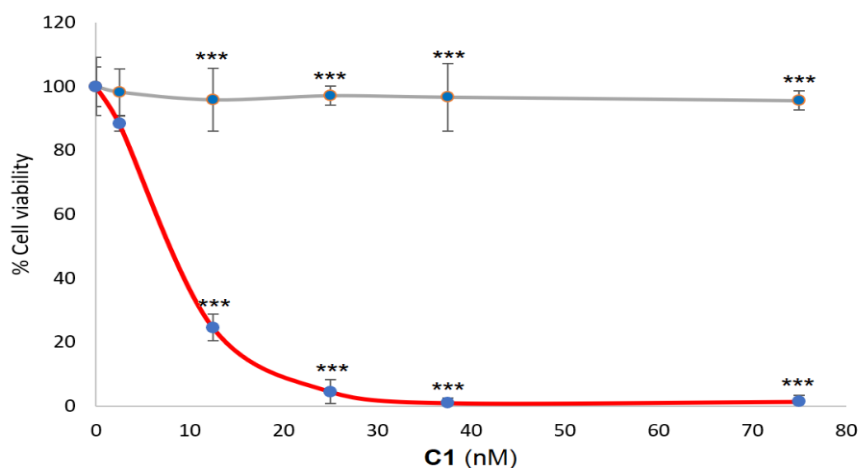
Figure 22. MTT assays of **C1** in the dark (grey line) and after irradiation (630 nm, 72 J/cm^2 for 30 min) (red line) in RA FLS. Statistical significance determined by the two-tailed unpaired Student's t-test, p-value < 0.001 (***).
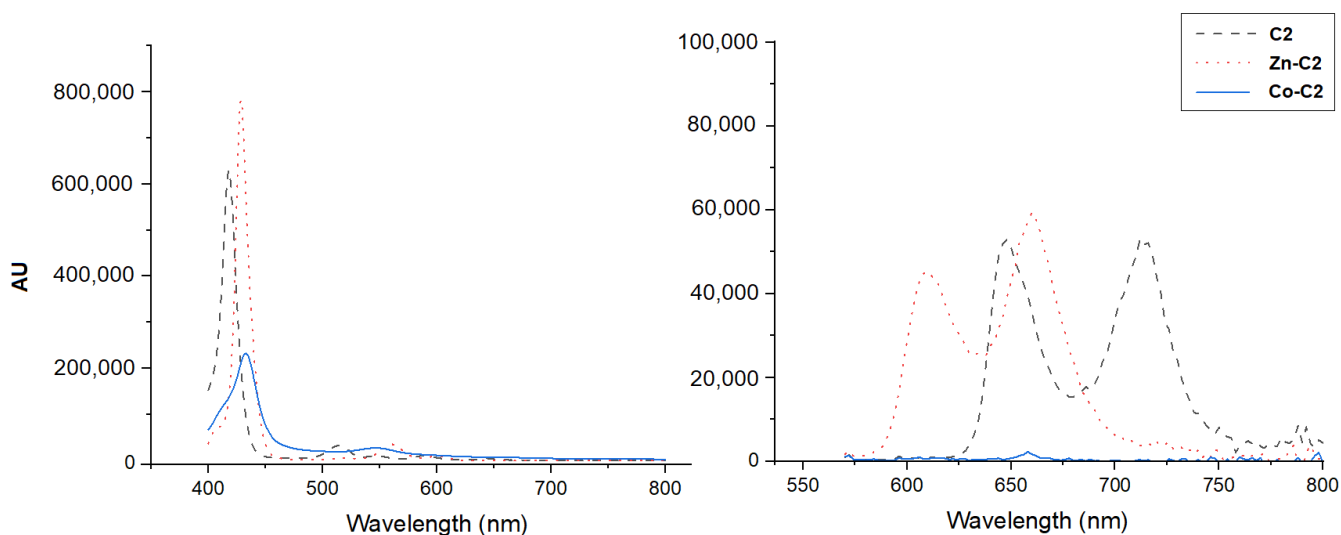
Figure 23. Comparison between UV-vis absorption (left) and fluorescence emission (right) spectra of **C2**, **Zn-C2** and **Co-C2**.

The main structural difference between **C1** and **C2** is the distance that separate the two porphyrin units in the metallacages. According to the results obtained, the PDT effect decreases when the distance is shorter. The IC$_{50}$ of **C1** and **Zn-C1**, which are built from 2,5-dioxydo-1,4-benzoquinonato spacers, are less than half the IC$_{50}$ values of the smaller oxalato analogues, **C2** and **Zn-C2** respectively. This can be explained by an intramolecular energy transfer phenomena between the two porphyrin panels, resulting in quenching and reduction of the ROS production. It is known that quenching and energy transfer phenomena between excited photoactive molecules can occur without collision or direct contact. This phenomenon is known as Resonance Energy Transfer (RET) [103]. The energy transfer could be expressed by the equation formulated by Foster (equation *1*), which is directly related to the distance (*r*) between

the photoactive molecules, and it is susceptible to small changes [104]. It is established that when two PS are at short distance from each other the possibility of quenching increases significantly.

$$RET = \frac{1}{1 + \left(\frac{r}{R_0}\right)^6} \qquad (1)$$

The distance between the two TPyP panels is not fixed since the structure can be deformed in solution [105-107]. However, an approximate distance can be determined from the dinuclear arene ruthenium clip complex (Figure 21). In **C2** and **Zn-C2**, the ruthenium atoms linked to the oxalato ligand are separated from each other by ≈ 5.5 Å [107]. In **C1** and **Zn-C1** the distance is related to the benzoquinonato ligand, and it is ≈ 7.8 Å [108]. Therefore, a larger spacer suggests less quenching, which leads to greater PDT effectiveness, in agreement with the results obtained.

Finally, we further emphasize that none of the evaluated compounds showed toxicity in the dark at the maximum concentration tested (Table 3), which is an essential characteristic for a good PS. We show in Figure 24 the comparison between the irradiated and not irradiated RA FLS containing **C2** (22 nM). Cellular damage is clearly observed in the irradiated RA FLS and not apparent in the non-irradiated cells.
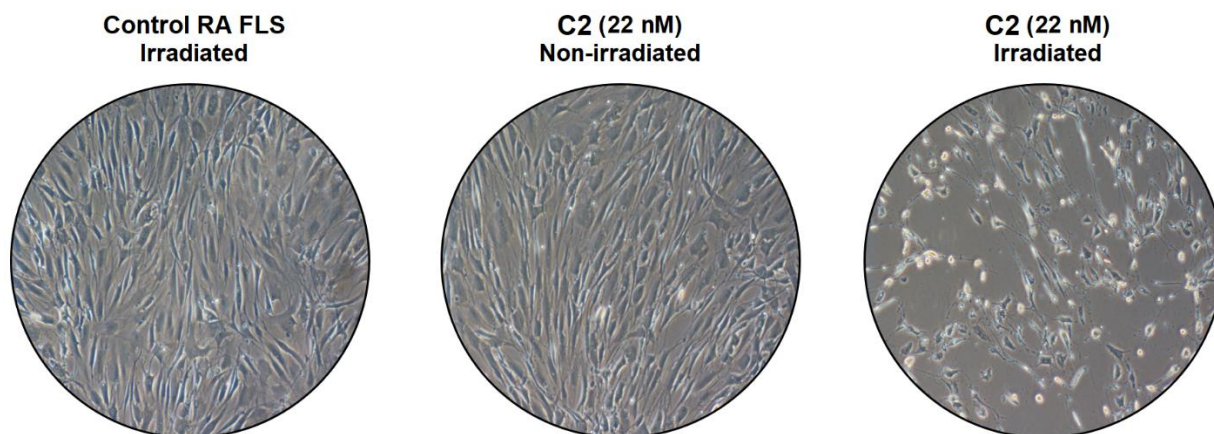

Figure 24. Comparation of the effects of PDT on RA FLS using **C2** at 22 nM (IC$_{50}$) after 24 h. Control cells 24 h after irradiation (left), cells with **C2** but not irradiated (center), and cells with **C2** and irradiation (right) (red-light 630 nm, 72 J /cm^2 for 30 min) after 24 h.

6.2.2 Inflammatory study

Like previously, we decided to assess COX-2 expression, PGE$_2$ production and the presence of IL-1β in RA FLS after PDT with these compounds. However, since the cobalt compound did not show PDT activity in the MTT assays, we decided not to include it in this evaluation, focusing on the four most promising compounds (**C1**, **C2**, **Zn-C1** and **Zn-C2**).

In Figure 25, the expression of COX-2 is presented, showing that these porphyrin-based compounds induce COX-2 overexpression after PDT, as we saw previously with the **G⊂M** systems (page 34). However, **C1** shows remarkable results as the expression of COX-2 is not significantly different from the controls experiments. Also, the overexpression of COX-2 is greater in the irradiated samples than in the non-irradiated ones (as with the **G⊂M** systems). We observed that the expression of COX-2 is directly associated to the results seen in the antiproliferative evaluation. The results stablish that when a lower concentration is used, that is, when the IC$_{50}$ is lower, the overexpression of COX-2 is as well lower. This implies that by reducing the dose of the drug, it should be possible reduce inflammatory adverse effects, while maintaining a good photoactivity.
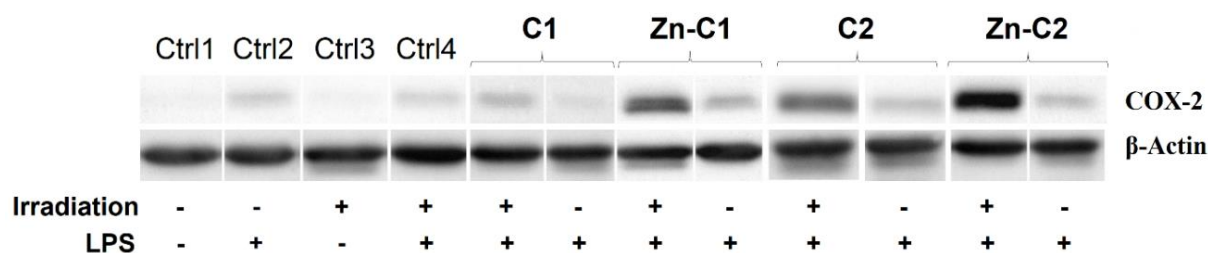
Figure 25. COX-2 expression after PDT determinated by Western blot. Cells ($2 \cdot 10^6$) were cultured in DMEM (FBS 10%, L-glutamine 1%, Penicillin 100 U/mL, Streptomycin 100 µg/mL) during 18 h and treated with the corresponding PS. After 24 h, the medium was replaced by DMEM without red phenol and irradiated at 630 nm (72 J/cm^2 for 30 min). After 18 h, LPS (1 µg/mL) was added in the medium to stimulate the expression of COX-2 during 4 h. Finally, trypsinization and isolation of cells was performed. β-Actin was used as a protein loading control in Western blot. All experiments were done in triplicate. Non-irradiated cells were treated as irradiated cells (see Experimentation section). Control samples were treated as treated cells.

Due to this overexpression of COX-2, overproduction of PGE$_2$ was expected (Table 4) as we saw previously (page 34). As discussed with metallacages with PS in the internal cavity, this overproduction of PGE$_2$ can increase inflammation after PDT and can be reduced or eliminated by the simultaneous use of selective COX-2 inhibitors. Again, it is worth noting the result with **C1**, that the production of PGE$_2$ after treatment with **C1** is significantly close to that observed in the control. This again points to the fact that a lower dose of the PS could produce less adverse effects in PDT.

Regarding the analysis of IL-1β production in the supernatant after PDT, we observe similar results as with the **G⊂M** compounds. Again, IL-1β does not seem to be directly involved to the overexpression of COX-2 and overproduction of PGE$_2$ observed (Table 4) [109]. The results suggest that the concentration of IL-1β after PDT does not differ from the control experiments. This points to other implicated cytokines, which has also been observed in other studies [95].

Table 4. Quantification of PGE$_2$ and IL-1β. The assays were performed according to the protocol provided by the ELISA kit in triplicate. Data were processed as explained in this protocol. Cells were treated with PDT with each of the indicated compounds as described in the experimental section. At 18 h after the irradiation dose (without PS), the control sample was treated with 1 µg/mL LPS in the culture medium, the cells were incubated for 4 h, trypsinised and the supernatant was recovered. Results are expressed as the average of three independent experiments. * Not determined (n.d.).

PS	PGE$_2$ (pg/ml)	IL-1β (pg/ml)
Ctrl	286.6 ± 0.1	1.8 ± 0.7
C1	352.2 ± 21.0	2.1 ± 0.7
Zn-C1	444.4 ± 7.4	1.8 ± 1.4
C2	390.0 ± 11.8	2.0 ± 1.2
Zn-C2	457.1 ± 1.9	1.6 ± 0.4
Co-C2	n.d.*	n.d.*

6.3 Combination of tetrapyridylporphyrins and arene ruthenium (II) complexes to treat synovial sarcoma by PDT.

The use of PDT to treat certain types of cancer is much more widespread and studied than in the case of RA. During the last decades, PDT in cancer has been one of the most fast-growing therapies against skin cancer [110,111], acne [112,113] and other skin diseases [114,115]. The FDA have approved the use of PDT in numerous pathologies like advanced cutaneous T-cell lymphoma, actinic keratosis, basal cell skin cancer, Barrett esophagus, esophageal cancer, non-small cell lung cancer and squamous cell skin cancer. Moreover, other types of cancer and more pathologies such as bacterial infections [116,117] and the cancer studied in this work, synovial sarcoma [118,119], are also under PDT investigations, in addition to the one already described in this thesis, the RA [32,120].

About 10% of soft tissue cancers that are diagnosed are synovial sarcoma. It is the fourth most common soft tissue cancer [121]. Synovial sarcoma usually develops in the adjacent area of large joints such as the synovial membrane, bursae, tendons and joint capsules, without affecting the fluid inside the joints. The incidence in man is higher than in woman and commonly develops between 15 and 40 years old. [122]. It is a slow-growing cancer, and often detected late, since its benign appearance and slow progression are confused by pain from trauma or injury. The causes of synovial sarcoma are not yet completely understood [118]. The common treatment requires invasive surgery where tumoral tissues are removed [123]. Frequently, this surgery is complemented with radiotherapy and/or chemotherapy [124]. This invasive treatment implies a significant loss of soft tissue that could give rise to loss of mobility or add rigidity to the joint. Consequently, by minimizing the impact on healthy tissue, better mobility in the joint should be preserved, and therefore PDT could play an important role. Parallel to the evaluation of the compounds described so far in this thesis to treat RA by PDT, and with the intention of expanding our field of study to another pathology that affects synovial tissue, we decided to design and evaluate a series of compounds *in vitro* to treat synovial sarcoma by PDT.

As described previously for RA, the use of PDT in the treatment of cancers also carries some limitations. The poor solubility of PSs, low concentration of oxygen in the target tissue and skin photosensitivity after treatment are the most common [125]. PDT in RA and cancer share most of the drawbacks, so as in RA many PSs used in PDT to treat cancer have low physiological solubility and this could lead to increase doses of the drug, giving rise to side effects such as skin photosensitivity [125]. However, as we explain in this thesis for RA, this skin photosensitivity after PDT can be solved using PSs that need very low concentrations to

be efficient and being totally inactive in the absence of light. One of the solutions used in the treatment of cancer by PDT to enhance the drug solubility without increasing the dose is the encapsulation of the PS in nanoparticles [126], coordination to peptides [127] or entrapment in lysosomes [128]. Another reported method to improve the solubility of the drug is the design of PSs incorporating hydrophilic substituents like sulfonate ($-SO_3H$) [129] or phosphonate ($-PO(OR)_2$) [130]. In some cases, a solvent (other than water) can be used in which the PS is soluble. However, it is necessary to consider the toxicity of that solvent and the stability of the PS, since some of these solvents are not innocent and could degrade the drug before activation [131], impairing their effectiveness.

As regards the lack of O_2 in the target tissue, the accelerated growth of cancer cells generally leads to diminishing concentrations of O_2 [132,133], which reduces the possibilities of an efficient production of ROS. To solve this problem, some research groups have proposed to oxygenate the tumor tissue by hyperbaric oxygen therapy (HBO_2), prior to PDT [134].

In this work, we used TPyP as base of the PS, bonding to mononuclear arene ruthenium (II) complexes to improve the poor solubility of this tetrapyrrole in biological media (Figure 26). Additionally, some of these ruthenium complexes contain substituents in the arene ligands such as hydroxide groups (OH), that could potentially contribute to the presence of oxygen species, which can give rise to more $^1O_2$ and increase ROS production [135].
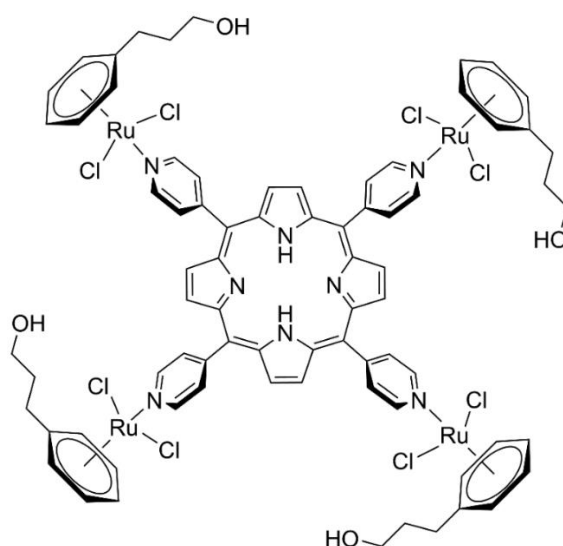
Figure 26. Structure of functionalized tetrapyridylporphyrin arene ruthenium complex.

Contrary to RA, the use of ruthenium organometallic complexes is not new to PDT in cancer [73,136-141], since it has been in extensive use for years. The main raisons to choose ruthenium as metal is its stable oxidation state, being nearly unreactive to air, water or O_2, unlike other

metal-based compounds. Also, it has been reported the capability of arene ruthenium complexes to improve the physiological solubility [142]. Furthermore, the toxicity of ruthenium is minimal and much lower than other metals such as platinum, or metal widely used in metal-based drugs in cancer treatments [138,143].

Our new PSs, for the treatment of synovial sarcoma by PDT, involve arene ruthenium complexes, incorporated on tetrapyridylporphyrin or dipyridylporphyrin. Also, we compared other analogue derivatives, with or without a metal (zinc) in the center of the tetrapyrrole. In addition, we have evaluated two different types of arenes, with or without hydroxyl groups substituent.

6.3.1 Synthesis of compounds

We synthesized these compounds by a one-step reaction (Scheme 7). The dinuclear arene ruthenium dimers (**d1** or **d2**), synthesized as reported in the literature [63,144], are dissolve in methanol, mixing and reacting with the corresponding porphyrin. The dimer **d1** is extensively used [145-148] and, as described previously (page 24), its synthesis was reported by Zelonka and Baird [63] in 1972. The dimer **d2** is a more recent analogue [144] and its reactivity remained unexplored. Our group had already reported the synthesis of **P1** ([Ru$_4$(p-cymene)$_4$(TPyP)Cl$_8$]) [141]. In this work we report the synthesis of new derivatives (with TPyP and Zn-TPyP) involving the dimer **d2**, giving rise to the photosensitizer **P2** ([Ru$_4$(PhPrOH)$_4$(TPyP)Cl$_8$]) and **P4** ([Ru$_4$(PhPrOH)$_4$(Zn-TPyP)Cl$_8$]. Also, we use in this work the dimer **d1** to give rise to the new compound **P3** ([Ru$_4$(p-cymene)$_4$(Zn-TPyP)Cl$_8$]), using the same methodology (see Experimental section). **P1-P4** remain stable and unchanged at 4 °C for at least six months in the solid state. These compounds are soluble in DMSO, but they have poor solubility in other solvents such as water, dichloromethane, chloroform, benzene, acetonitrile, acetone and ethanol. Also, we noted that **P2** easily precipitates after a few minutes in DMSO.

In addition, we report the synthesis and characterization of four new derivatives (**P5-P8**), based on the tetrapyrrole 5,15-diphenyl-10,20-di(pyridin-4-yl)porphyrin (DPhDPyP), using the same method described to **P1-P4** (Scheme 8) but with 1:1 molar ratio. The reason to consider the synthesis with this porphyrin is to study the influence of the number of arene ruthenium complexes coordinated to the porphyrin in terms of its efficacy in PDT. The reactions with the dimers **d1** and **d2** produce the compounds **P5** ([Ru$_2$(p-cymene)$_2$(DPhPyP)Cl$_4$]) and **P6** ([Ru$_2$(PhPrOH)$_2$(DPhPyP)Cl$_4$]) respectively. Their Zn analogues are synthesized from the Zn-DPhDPyP porphyrin, giving rise to **P7** ([Ru$_2$(p-cymene)$_2$(Zn-DPhDPyP)Cl$_4$]) and **P8**

([Ru$_2$(PhPrOH)$_2$(Zn-DPhDPyP)Cl$_4$]). We noted that the yields of **P5-P8** are a little bit lower (51-67 %) than those of **P1-P4**. Even so, no secondary products are observed. Moreover, unlike **P1**, **P2**, **P3** and **P4**, whose solubility was low in water and good in DMSO, **P5**-**P8** showed higher solubility. Like **P1-P4**, they remain unaltered at 4 °C for at least 6 months in the solid state. We observed by NMR that **P1-P8** are stable in DMSO for at least 1 h. After that period, we observed new signals (^{1}H-NMR) in the spectra (< 1%), which can be attributed to the degradation of the compounds by ligand exchange with DMSO [131].
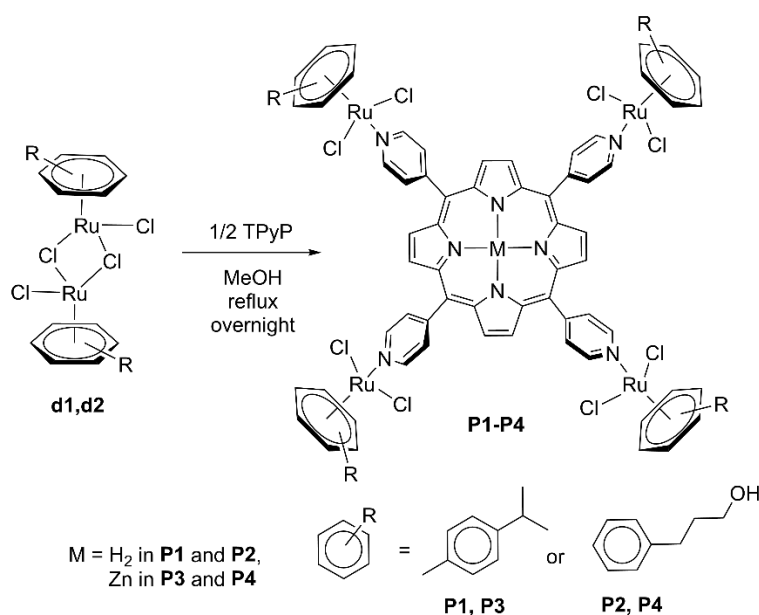
Scheme 7. Reactions between dimers **d1** or **d2** with TPyP or Zn-TPyP giving rise to **P1-P4**.
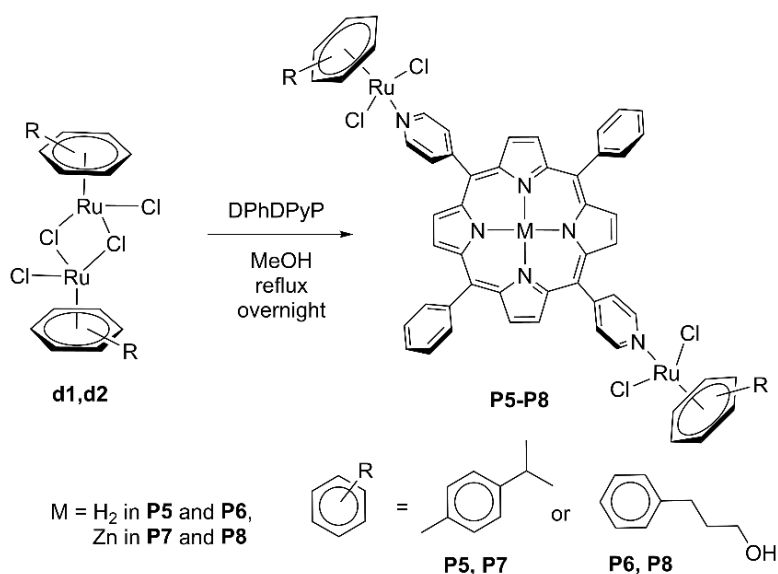

Scheme 8. Reactions between dimers **d1** or **d2** with DPhDPyP or Zn-DPhDPyP giving rise to **P5-P8**.

6.3.2 Antiproliferative evaluation

We evaluated the photocytotoxicity of **P1**-**P8** *in vitro* in SW982 synovial sarcoma cells after PDT (irradiation dose = 630 nm, 72 J/cm^2 for 30 min). Cell viability was examined by MTT assays in irradiated and non-irradiated SW982 cells. The results are presented in Table 5. The irradiated cells curve was fitted to the second order polynomial, from whose equation we calculate the IC$_{50}$ (Figure 27). **P1-P8** showed good photocytotoxicity after PDT, but some of the results are much more significant. The PSs present three structural differences. One of them is the arene ligand, which is *p*-cymene or phenylpropanol (PhPrOH). Remarkably, the four PSs with PhPrOH (**P2**, **P4**, **P6** and **P8**) as the arene, showed a better photocytotoxicity than their *p*-cymene analogues (**P1**, **P3**, **P5** and **P7**) (Table 5). Since the only structural difference is the substituent on the arene, we think that the main reason for this improvement is the OH group. This oxygenated functional group could help to increase the production of ROS after PDT, either by direct interaction with another excited PSs molecules or with other reactive species. Some alcohols have been reported as initiators in the production of ROS by metabolism [149]. In addition, porphyrins with phenol substituents have demonstrated their effectiveness in PDT [150], like 5,10,15,20-tetra(*m*-hydroxyphenyl)chlorin (FOSCAN) [151-153]. Thus, addition of aliphatic alcohol at the periphery of a photosensitizer seems to be positive in our systems, improving the PDT effect.
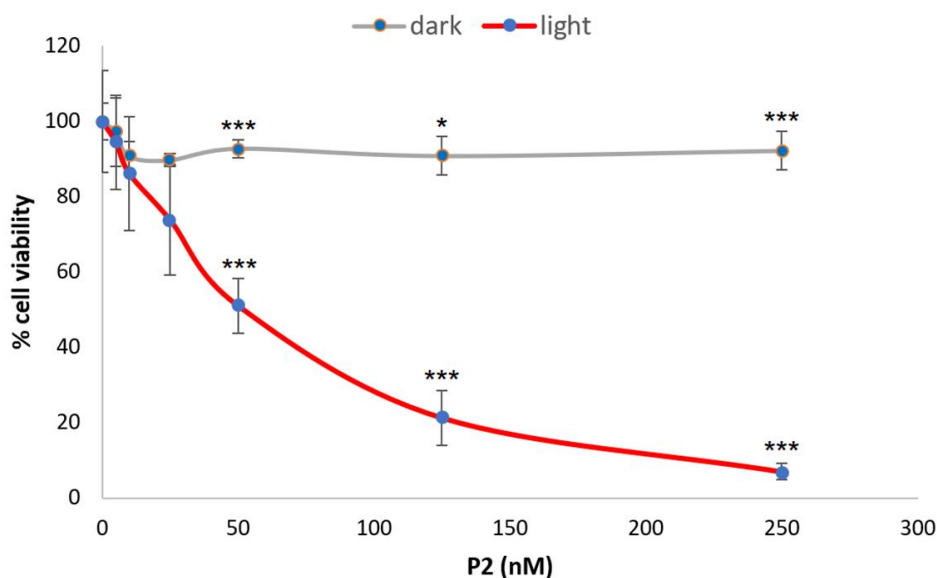

Figure 27. MTT assays in PDT on SW982 synovial sarcoma cells using **P2** as PS. Irradiation 24 h after addition of PS (630 nm, 72 J/cm^2 for 30 min). Two-tailed Student's t-test significance, P<0.05 (*) and P<0.001 (***).

Table 5. MTT results on SW982 synovial sarcoma cells after PDT (spectra in the supporting information). Irradiation 24 h after addition of PS, $\lambda = 630$ nm, 72 J/cm^2 for 30 min irradiation. IC$_{50}$ was calculated fitting the curve to the second-degree polynomial $\pm$ 3 sigma deviation. The maximum concentration tested was 5 µM. Phototoxic index (PI) is the ratio between cell viability in the dark and after irradiation.

PS	Arene	Porphyrin	IC$_{50}$ (µM) light	IC$_{50}$ (µM) dark	PI
P1	p-cymene	TPyP	0.170 ± 0.008	> 5	>29
P2	PhPrOH	TPyP	0.060 ± 0.012	> 5	>83
P3	p-cymene	Zn-TPyP	0.341 ± 0.008	1.092 ± 0.004	3
P4	PhPrOH	Zn-TPyP	0.256 ± 0.010	0.729 ± 0.005	3
P5	p-cymene	DPhDPyP	0.307 ± 0.014	> 5	>16
P6	PhPrOH	DPhDPyP	0.212 ± 0.008	2.341 ± 0.005	11
P7	p-cymene	Zn-DPhDPyP	0.387 ± 0.010	1.096 ± 0.003	3
P8	PhPrOH	Zn-DPhDPyP	0.312 ± 0.010	0.689 ± 0.007	2

One more structural difference in all our systems is the presence or absence of zinc in the center of the tetrapyrrole. The results (Table 5) suggest that when zinc is in the PS the PDT effect is reduced. In all cases, the metal-free systems showed a higher photocytotoxicity than their zinc analogues. The reason, as we have described in the RA FLS works (see page 31 and 38), is due to the increase in fluorescence when the metal is part of the system (Figure 28).
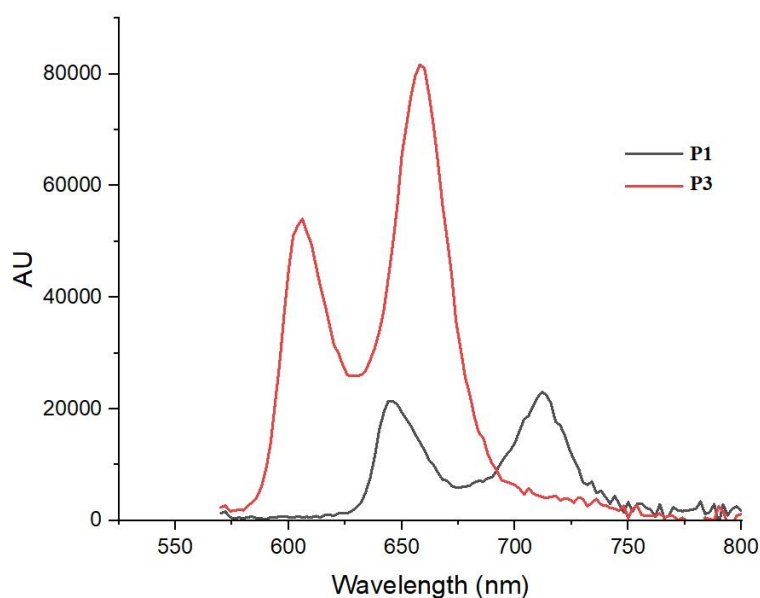
Figure 28. Fluorescence spectra of **P1** and **P3** (10 nM in DMSO).

The last structural difference in our systems is the base porphyrin used (DPhDPyP or TPyP). DPhDPyP contains two pyridyl substituents and as a consequence, the presence of two coordinated arene ruthenium units (**P5-P8**). While TPyP, with four pyridine units, makes the system contain four arene ruthenium units (**P1-P4**). The results showed that **P5-P8**, with DPhDPyP, give rise to a reduced PDT effect than their tetranuclear counterparts. The reason seems due to the lower number of coordinated ruthenium arenes. As described before, Ru (II) arenes have been reported as solubility improvers in biological media for organic compounds [138].

It is worth noting the absence or not significant toxicity of the compounds without zinc (**P1**, **P2**, **P5** and **P6**) in the dark, even at the highest concentrations evaluated, contrary to the zinc compounds, which showed significant toxicity in the dark (Table 5). Analogous results have been reported with other zinc porphyrins, indicating that can generate toxicity by themselves [79,80].

Finally, when the PI (phototoxic index) of the compounds (Table 5) are compared, the difference between zinc compounds and those that do not contain metal is noted, highlighting the latter as potentially more efficient PSs in the treatment of synovial sarcoma by PDT.

CHAPTER 7 – CONCLUSIONS AND PERSPECTIVES

7.1 Conclusions

A series of photosensitizers (**G**) encapsulated in arene ruthenium metallacages (**M**) have been synthesized and characterized. The PDT efficacy of these host–guest systems (**G⊂M**) as PDT agents has been evaluated on RA FLS. In parallel, five physiological soluble metallacages incorporation the PS in their structures as ligand panels (**C1**, **C2**, **Zn-C1**, **Zn-C2**, **Co-C2**) have been tested also as PDT agents in RA FLS.

The compound **C1** shows the best potential as a PDT agent to treat RA synovitis, having a remarkable phototoxicity (IC_{50} = 8 nM). The most promising **G⊂M** compounds seem to be those with the largest cavity, suggesting that the release of the photosensitizers from the host occurs without any breakage of the metallacage. All compounds showed no toxicity in the dark at the highest concentration tested, except for the zinc phthalocyanine derivatives (**G4⊂M5** and **G4⊂M6**) which rules them out as good PSs in PDT. When the phthalocyanines (**G3** and **G4**) are encapsulated in the cubic metallacage (**M4**), no phototoxicity is detected, suggesting a high affinity (or steric hindrance) between the host and guest, which prevents the release the PS from the metallacage. The systems without metals (Mg or Zn) showed better PDT effect because of the lower fluorescence. In the metallacages with the PS as ligand panels, the distance between the two porphyrin blocks in each metallacage significantly influences the PDT efficacy, with a shorter distance being detrimental, possibly as a consequence of quenching phenomena.

Regarding the *in vitro* evaluation, in all systems, PDT gives rise to the overexpression of COX-2, and consequently production of PGE_2. When a lower concentration of the drug is used, the overexpression of COX-2 and production of PGE_2 are substantially reduced. IL-1β does not appear to be participating in this COX-2 overexpression, which could indicate that other cytokines are responsible for this overexpression.

In addition, eight systems (**P1**-**P8**) forming by a porphyrin-based center and arene ruthenium substituent have been synthesized and tested *in vitro*, to treat synovial sarcoma by PDT. The compound **P2** showed the best light/dark photocytotoxicity ratio (0.06 μM / 5 μM), being around two orders of magnitude. The presence of zinc (II) in the core of the photosensitizers have a double negative effect, increasing toxicity in dark and reducing PDT efficacy (because of increasing fluorescence). The alkyl alcohols added on the arene ligands can improve the PDT efficacy in SW982 sarcoma cells.

7.2 Perspectives

In view of the results obtained in the *in vitro* tests, the great potential of the compounds can seem glimpsed. The applications of such ruthenium-based compounds, which have already shown their potential in cancer, has been extended to another pathology. This research has led to the first reported results of ruthenium assemblies compounds in the treatment of RA by PDT. About twenty different compounds had been reported by several methodologies in the PDT of RA, so by adding our 20 systems evaluated, we have doubled the number of compounds studied, which highlights the results presented here.

However, there is still a long way to confirm that the compounds evaluated in this thesis can play an important role in RA treatment. In the future, it will be necessary to study and determine the full mechanism by which the systems $G \subset M$ transport the PS in their internal cavity and carry out the release. In addition, despite that the intracellular localization of both the metallacages and the PS in cancer cells was already known, a similar study in human RA FLS remain to be done. Also, it is necessary to find out which cytokine is responsible for the COX-2 overexpression observed, by testing other cytokines such as TNFα. Another future step is to perform *in vivo* assays, which histologic results can be compared with the *in vitro* photocytotoxicity results reported here. For example, a collagen-induced arthritis model in the Wistar rat would make it possible to analyze the bioavailability of our molecules, to analyze *ex vivo* COX-2 expression and to quantify both pro-inflammatory cytokines (IL-1β, IL-6, TNFα) and PGE_2 in the serum. Regarding the design of our compounds, there are other photoactive compounds with suitable structures to be hosted and transported by metallacages, such as chlorin, bacteriochlorin, porphycene or corrphycene, among others. On the other hand, with metallacages with tetrapyridineporphine as panel ligands, they could be built using larger clip complexes, which can increase the distance between the two porphyrin blocks that form the ligand panels and then, decrease the quenching phenomena observed in this research.

8.1 Synthesis and characterization of compounds

Some of the host–guest systems are new (**G1⊂M2**, **G1⊂M3**, **G2⊂M1**, **G2⊂M4**, **G2⊂M6** and **P2**-**P8**). However, **G1⊂M1**, **G1⊂M4**, **G1⊂M5**, **G1⊂M6**, **G3⊂M4**, **G3⊂M5** **G3⊂M6**, **G4⊂M4**, **G4⊂M5**, **G4⊂M6**, **C1**, **C2**, **Zn-C1**, **Zn-C2**, **Co-C2** and **P1** were known. The dimer complexes [Ru$_2$(*p*-cymene)$_2$(2,5-dioxydo-1,4-benzoquinonato)Cl$_2$], [Ru$_2$(*p*-cymene)$_2$(5,8-dioxydo-1,4-naphthoquinonato)Cl$_2$], [Ru$_2$(*p*-cymene)$_2$(6,11-dioxydo-5,12-naphthacenedionato)Cl$_2$] [154], and the ligands 2,4,6-tris(pyridin-4-yl)-1,3,5-triazine [155], 1,3,5-tris{2-(pyridin-4-yl)vinyl}benzene [156] and 1,2,4,5-tetrakis{2-(pyridine-4-yl)vinyl} benzene [157] were prepared following reported methods. The metallacages **M1** and **M4** with **G1** inside [73], **M4** with **G3** and **G4**, **M5** and **M6** with **G1**, **G3**, and **G4** [158] were synthesized according to the literature. The photosensitizers **G1** and **G2** were synthesized as reported in the literature [159], while **G3** and **G4** were purchased from Sigma-Aldrich. Porphyrin H$_2$-TPyP was purchased from Sigma-Aldrich, while Zn-TPyP and Co-TPyP were obtained from Porphychem (Dijon, France). The metallacages [Ru$_8$(η^6-*p*-^{i}PrC$_6$H$_4$Me)$_8$(μ^4-H$_2$-TPyP-κN)$_2$(μ-C$_6$H$_2$O$_4$-κO)$_4$][CF$_3$SO$_3$]$_8$ (**C1**), [Ru$_8$(η^6-*p*-^{i}PrC$_6$H$_4$Me)$_8$(μ^4-Zn-TPyP-κN)$_2$(μ-C$_6$H$_2$O$_4$-κO)$_4$][CF$_3$SO$_3$]$_8$ (**Zn-C1**), [Ru$_8$(η^6-*p*-^{i}PrC$_6$H$_4$Me)$_8$(μ^4-H$_2$-TPyP-κN)$_2$(μ-C$_2$O$_4$-κO)$_4$][CF$_3$SO$_3$]$_8$ (**C2**), [Ru$_8$(η^6-*p*-^{i}PrC$_6$H$_4$Me)$_8$(μ^4-Zn-TPyP-κN)$_2$(μ-C$_2$O$_4$-κO)$_4$][CF$_3$SO$_3$]$_8$ (**Zn-C2**) and [Ru$_8$(η^6-*p*-^{i}PrC$_6$H$_4$Me)$_8$(μ^4-Co-TPyP-κN)$_2$(μ-C$_2$O$_4$-κO)$_4$][CF$_3$SO$_3$]$_8$ (**Co-C2**) were synthesized as reported in the literature [105,106]. Compounds **d1**, **d2** and **P1** were also prepared as described in the literature [63,141,144]. The solvents dichloromethane, diethyl ether, methanol, *d$_3$*-acetonitrile, and *d$_6$*-DMSO were purchased from Sigma-Aldrich. NMR spectra were measured on a Bruker Avance Neo Ascend 600 MHz spectrometer. The acquired spectra were processed using the Mnova NMR software package (v.14.2.0, MestReLab Research). The ^{1}H and ^{13}C resonances of the deuterated solvents were used as internal references. The following abbreviations are used for describing the signals in the NMR spectra: s (singlet), d (doublet), m (multiplet), br (broad), q (quaternary). IR spectra of the compounds were performed on a Frontier PerkinElmer spectrometer (600–4000 cm^{-1}). Fluorescence spectra were performed on a FLS980 spectrometer from Edinburgh Instruments (550–800 nm) using 5,10,15,20-tetraphenylporphin (TPP) as an internal reference in toluene and the compounds were dissolved in DMSO (10 nM concentration). UV-vis spectra were acquired on a SI Analytics model

UvLine 9400 (Xenon lamp) spectrophotometer, using 1.5 mL polystyrene cuvettes (wavelength range 280–800 nm) and diluting the compounds in DMSO (10 nM).

Synthesis of G1⊂M2. 50.0 mg (0.069 mmol) of [Ru$_2$(p-cymene)$_2$(5,8-dioxydo-1,4-naphthoquinonato)Cl$_2$] and 35.5 mg (0.138 mmol) of AgCF$_3$SO$_3$ were dissolved in 20 ml of methanol and stirred for 2 h at r.t. After that, silver chloride was filtered off. In the remaining solution, 14.6 mg (0.046 mmol) of 2,4,6-tri(pyridin-4-yl)-1,3,5-triazine and 7.1 mg (0.023 mmol) of **G1** were added, and the solution was refluxed and stirred for 18 h. The solvent was then removed by vaccum and the resulting oily dark green solid was dissolved in 20 mL of CH$_2$Cl$_2$. The solution was concentrated to approximately 3 ml, and 5 mL of Et$_2$O were added dropwise. The resulting precipitate was filtered and dried under vacuum. Yield 52% (45 mg). ^{1}H NMR (CD$_3$CN, 25 °C, 600 MHz): δ 9.17 (d, $^3J_{HH}$ = 6.0 Hz, 12H, CH_{naphce}), 8.44 (d, $^3J_{HH}$ = 4.1 Hz, 12H, CH_{naphce}), 8.24 (d, $^3J_{HH}$ = 6.3 Hz, 12H, CH_{py}), 8.00 (s, 4H, CH_{porphine}), 6.89 (s, 8H, CH_{porphine}), 5.91 (d, $^3J_{HH}$ = 6.4 Hz, 12H, CH_{py}), 5.87 (d, $^3J_{HH}$ = 5.9 Hz, 12H, CH_{cym}), 5.57 (d, $^3J_{HH}$ = 5.8 Hz, 12H, CH_{cym}), 2.95 (m, 6H, CH_{iPr}), 1.97 (overlapped singlet, 18H, CH_3), 1.32 (d, $^3J_{HH}$ = 7.0 Hz, 36H, CH$_{3\text{ iPr}}$). ^{13}C NMR (CD$_3$CN, 25 °C, 150 MHz): δ 170.4 (C-O), 164.3 (C_q), 152.1 (CH_{py}), 140.7 (C_q), 134.6 (CH_{naphce}), 130.1 (CH_{porph}), 128.4 (CH_{naphce}), 122.8 (C_q), 122.3 (CH_{py}), 120.7 (C_q), 107.9 (C_q), 104.4 (C_{cym}), 103.3 (CH_{porph}), 100.3 (C_{cym}), 84.9 (CH_{cym}), 83.0 (CH_{cym}), 31.0 (CH_{iPr}), 22.0 (CH$_{3\text{ iPr}}$), 17.3 (CH_3). ESI-MS, m/z, 1120 [**M2**+**G1**-3OTf]$^{3+}$. UV/vis (DMSO), λ, nm (ε, M^{-1}.cm^{-1}): 454 (132400), 488 (117700), 567 (54300), 648 (62900). FT-IR (ATR, solid, cm^{-1}): ν; br s (3700-3100), s (2995), s (1524), s (1516).

Synthesis of G1⊂M3. 50.0 mg (0.060 mmol) of [Ru$_2$(p-cymene)$_2$(6,11-dioxydo-5,12-naphthacenedionato)Cl$_2$] and 31.0 mg (0.120 mmol) of AgCF$_3$SO$_3$ were dissolved in 20 ml of methanol and stirred for 2 h at r.t. Then, silver chloride was filtered off. To the remaining solution, 12.5 mg (0.040 mmol) of 2,4,6-tri(pyridin-4-yl)-1,3,5-triazine and 6.2 mg (0.020 mmol) of **G1** were added, and the solution was refluxed and stirred for 18 h. The solvent was removed by vacuum and the resulting oily dark green solid was dissolved in 20 mL of CH$_2$Cl$_2$. The solution was concentrated to approximately 3 ml, and 5 mL of Et$_2$O were added dropwise. The precipitate was filtered and dried by vacuum. Yield 76% (62 mg). ^{1}H NMR (CD$_3$CN, 25 °C, 600 MHz): δ 8.68 (s, 4H, CH_{porphine}), 8.21 (d, $^3J_{HH}$ = 6.3 Hz, 12H, CH_{py}), 7.92 (s, 12H, CH_{naph}), 7.71 (s, 8H, CH_{porphine}), 6.12 (d, $^3J_{HH}$ = 5.7 Hz, 12H, CH_{py}), 5.68 (d, $^3J_{HH}$ = 5.8 Hz, 12H, CH_{cym}), 5.43 (d, $^3J_{HH}$ = 5.9 Hz, 12H, CH_{cym}), 2.84 (m, $^3J_{HH}$ = 6.8 Hz, 6H, CH_{iPr}), 1.99 (s, 18H, CH_3), 1.33 (d, $^3J_{HH}$ = 6.9 Hz, 36H, CH$_{3\text{ iPr}}$). ^{13}C NMR (CD$_3$CN, 25 °C, 150 MHz): δ 171.9 (C-O), 164.5 (C_q), 152.3 (CH_{py}), 140.9 (C_q), 138.9 (CH_{naph}), 130.9 (CH_{porph}), 124.9 (C_q), 122.8 (CH_{py}), 122.5 (CH_{py}), 120.7 (C_q), 112.5 (C_q), 104.4 (C_{cym}), 103.9 (CH_{porph}), 100.3 (C_{cym}), 85.0

(CH_{cym}), 83.7 (CH_{cym}), 31.0 (CH_{iPr}), 21.9 ($CH_{3\ iPr}$), 16.8 (CH_3). UV/vis (DMSO), λ, nm (ε, $M^{-1}.cm^{-1}$): 489 (53700), 573 (40200), 623 (62900). FT-IR (ATR, solid, cm^{-1}): ν; br s (3700-3100), br s (3092), s (2992), s (2915), s (1531), s (1502).

Synthesis of G2⊂M1. 50 mg (0.074 mmol) of [Ru$_2$(*p*-cymene)$_2$(2,5-dioxydo-1,4-benzoquinonato)Cl$_2$] and 37.8 mg (0.148 mmol) of AgCF$_3$SO$_3$ were dissolved in 20 ml of methanol and stirred for 2 h at r.t. Then, precipitated silver chloride was filtered off. To the remaining solution, 15.4 mg (0.049 mmol) of 2,4,6-tri(pyridin-4-yl)-1,3,5-triazine and 8.1 mg (0.025 mmol) of **G2** were added, and the solution was refluxed and stirred for 18 h. The solvent was then removed by vaccum and the resulting oily dark green solid was dissolved in 20 mL of CH_2Cl_2. The solution was concentrated to 3 ml, and 5 mL of Et$_2$O were added dropwise. Then, the precipitate was filtered and dried under vacuum. Yield 64 % (59 mg). ^{1}H NMR (DMSO-d6, 25 °C, 600 MHz): δ 10.42 (s, 4H, $CH_{Mg-porphine}$), 9.61 (s, 8H, $CH_{Mg-porphine}$), 8.57 (m, 24H, CH_{py}), 5.62 (d, $^3J_{HH}$ = 6.1 Hz, 12H, CH_{cym}), 5.98 (d, $^3J_{HH}$ = 6.1 Hz, 12H, CH_{cym}), 5.91 (s, 6H, CH_{bz}), 2.82 (m, 6H, CH_{iPr}), 2.08 (s, 18H, CH_3), 1.28 (d, $^3J_{HH}$ = 6.9 Hz, 36H, $CH_{3\ iPr}$). ^{13}C NMR (DMSO-d6, 25 °C, 150 MHz): δ 184.1 (*C*-O), 169.4 (C_q), 154.5 (CH_{py}), 149.3 (C_q), 144.6 (C_q), 132.7 ($CH_{Mg-porphine}$), 129.2 (C_q), 126.5 (C_q), 124.8 (CH_{py}), 122.2 (C_q), 120.0 (C_q), 105.9 ($CH_{Mg-porphine}$), 103.8 (C_{cym}), 101.8 (CH_{bz}), 99.7 (C_{cym}), 84.1 (CH_{cym}), 81.9 (CH_{cym}), 31.1 (CH_{iPr}), 22.4 ($CH_{3\ iPr}$), 17.9 (CH_3). Elemental analysis: Calcd. For $C_{140}H_{126}F_{18}MgN_{16}O_{30}Ru_6S_6$ + 6H$_2$O: C, 44.42; H, 3.67; N, 5.92. Found: C, 45.23; H, 4.08; N, 6.09. ESI-MS, m/z, 770 [**M1**+**G2**-4OTf]$^{4+}$. UV/vis (DMSO), λ, nm (ε, $M^{-1}.cm^{-1}$): 500 (140700), 535 (130400). FT-IR (ATR, solid, cm^{-1}): ν; s (3093), s (2977), s (2911), s (2804), s (1508).

Synthesis of G2⊂M4. 50 mg (0.069 mmol) of [Ru$_2$(p-cymene)$_2$(5,8-dioxydo-1,4-naphthoquinonato)Cl$_2$] and 35.5 mg (0.138 mmol) of AgCF$_3$SO$_3$ were dissolved in 20 ml of methanol and stirred for 2 h at r.t. Then, silver chloride was filtered off. To the remaining solution, 16.81 mg (0.034 mmol) of 1,2,4,5-tetrakis{2-(pyridine-4-yl)vinyl} benzene and 5.7 mg (0.017 mmol) of **G2** were added, and the solution was refluxed and stirred for 18 h. The solvent was then removed by vacuum and the resulting oily dark green solid was dissolved in 20 mL of CH_2Cl_2. The solution was concentrated to 3 ml, and 5 mL of Et$_2$O were added dropwise. The precipitate was filtered and dried under vacuum. Yield 59 % (52 mg). ^{1}H NMR (CD$_3$CN, 25 °C, 600 MHz): δ 10.02 (s, 4H, $CH_{Mg-porphine}$), 9.13 (s, 8H, $CH_{Mg-porphine}$), 8.18 (d, $^3J_{HH}$ = 5.1 Hz, 16H, CH_{py}), 7.49 (d, $^3J_{HH}$ = 15.1 Hz, 8H, CH=C), 7.20 (m, 40H, CH_{naph}, CH_{py}, CH=C), 6.90 (s, 4H, CH_{ar}), 5.60 (d, $^3J_{HH}$ = 4.46 Hz, 16H, CH_{cym}), 5.41 (d, $^3J_{HH}$ = 3.1 Hz, 16H, CH_{cym}), 2.76 (m, $^3J_{HH}$ = 6.9 Hz, 8H, CH_{iPr}), 2.03 (overlapped singlet, 24H, CH_3), 1.25 (d, $^3J_{HH}$ = 6.9 Hz, 48H, $CH_{3\ iPr}$). ^{13}C NMR (CD$_3$CN, 25 °C, 150 MHz): δ 171.4 (*C*-O), 152.3 (CH_{py}),

149.9 (C_q), 147.7 (C_q), 138.1 (CH_{py}), 128.6 ($CH=C$), 127.6 ($CH=C$), 123.6 (CH_{naph}), 122.8 (C_q), 112.1 (C_q), 104.1 (C_{cym}), 99.7 (C_{cym}), 84.7 (CH_{cym}), 83.7 (CH_{cym}), 31.0 (CH_{iPr}), 21.9 ($CH_{3\ iPr}$), 16.9 (CH_3). ESI-MS, m/z, 880 [**M4**+**G2**-5OTf]$^{5+}$. UV/vis (DMSO), λ, nm (ε, $M^{-1}.cm^{-1}$): 536 (137900), 572 (80300), 610 (64600). FT-IR (ATR, solid, cm^{-1}): ν; s (3089), s (2947), s (2911), s (2861), s (1619), (1554).

Synthesis of G2⊂M6. 50 mg (0.069 mmol) of [Ru$_2$(*p*-cymene)$_2$(5,8-dioxydo-1,4-naphthoquinonato)Cl$_2$] and 35.5 mg (0.138) of AgCF$_3$SO$_3$ were dissolved in 20 ml of methanol and stirred for 2 h at r.t. Then, precipitated silver chloride was filtered off. To the remaining solution, 17.8 mg (0.046 mmol) of panel ligand 1,3,5-tris{2-(pyridin-4-yl)vinyl}benzene and 7.6 mg (0.023 mmol) of **G2** were added, and the solution was refluxed and stirred for 18 h. The solvent was then removed by vacuum and the resulting oily dark green solid was dissolved in 20 mL of CH$_2$Cl$_2$. The solution was concentrated to approximately 3 ml, and 5 mL of Et$_2$O were added dropwise. The resulting precipitate was filtered and dried under vacuum. Yield 61 % (56 mg). ^{1}H NMR (CD$_3$CN, 25 °C, 600 MHz): δ 10.29 (s, 4H, C$H_{Mg\text{-}porphine}$), 9.41 (s, 8H, C$H_{Mg\text{-}porphine}$), 8.57 (d, $^3J_{HH}$ = 5.7 Hz, 12H, CH_{py}), 7.50 (s, 6H, CH_{ar}), 7.33 (d, $^3J_{HH}$ = 5.7 Hz, 12H, CH_{py}), 7.26 (s, 12H, CH_{naph}), 7.22 (overlapped doublet, 6H, C$H=C$), 6.98 (d, $^3J_{HH}$ = 16.1 Hz, 6H, C$H=C$), 5.69 (d, $^3J_{HH}$ = 5.9 Hz, 12H, CH_{cym}), 5.48 (d, $^3J_{HH}$ = 4.2 Hz, 12H, CH_{cym}), 2.84 (m, $^3J_{HH}$ = 7.0 Hz, 6H, CH_{iPr}), 2.10 (s, 18H, CH_3), 1.33 (d, $^3J_{HH}$ = 7.0 Hz, 36H, CH$_{3\ iPr}$). ^{13}C NMR (CD$_3$CN, 25 °C, 150 MHz): δ 171.3 (*C*-O), 152.3 (CH_{py}), 147.9 (C_q), 138.0 (CH_{py}), 137.0 (CH_{naph}), 135.1 (CH_{naph}), 132.5 ($CH_{Mg\text{-}Porphine}$), 127.4 ($CH=C$), 125.2 ($CH=C$), 123.1 (CH_{ar}), 120.6 (C_q), 112.0 (C_q), 105.9 ($CH_{Mg\text{-}porphine}$), 104.0 (C_{cym}), 99.7 (C_{cym}), 84.6 (CH_{cym}), 83.5 (CH_{cym}), 31.0 (CH_{iPr}), 21.9 ($CH_{3\ iPr}$), 16.9 (CH_3). Elemental analysis: Calcd. For C$_{170}$H$_{150}$F$_{18}$MgN$_{10}$O$_{30}$Ru$_6$S$_6$ + 6CH$_2$Cl$_2$: C, 46.49; H, 3.62; N, 3.06. Found: C, 45.47; H, 3.51; N, 3.88. ESI-MS, m/z, 1177 [**M6**+**G2**-3OTf]$^{3+}$. UV/vis (DMSO), λ, nm (ε, $M^{-1}.cm^{-1}$): 446 (150800), 536 (110500), 573 (53500), 610 (47100). FT-IR (ATR, solid, cm-1): ν; s (3101), s (2979), s (2914), s (1604), s (1522).

Synthesis of P2. In a 100 mL round bottom flask, a solution containing 60.0 mg (0,098 mml) of **d2** and 30.1 mg (0,049 mmol) of TPyP in 30 mL of methanol, was prepared. The solution was heated at reflux for 12 h, then cooled to room temperature. The solution is filtered off, the resulting brown solid was washed with Et$_2$O (5 x 10 mL) and dried by vacuum.

P2. Yield 86 % (78 mg). ^{1}H NMR (DMSO-d$_6$, 25 °C, 500 MHz): δ 9.08 (m, 8H, CH_{py}), 8.92 (br s, 8H, CH_{porph}), 8,28 (m, 8H, CH_{py}), 5.98 (m, 8H, *m*-CH_{ar}), 5.76 (overlapping doublets, 8H, *o*-CH_{ar}), 5.75 (overlapping triplets, 4H, *p*-CH_{ar}), 4.59 (s, 4H, OH), 3.45 (m, 8H, CH_2), 2.47 (m, 8H, CH_2), 1.73 (m, 8H, CH_2), -3.06 (s, 2H, NH). ^{13}C NMR (DMSO-d$_6$, 25 °C, 125 MHz): δ

142.06 (C_{py}), 128.16 (C_{py}), 128.10 (C_{porph}), 125.46 (C_{py}), 107.83 ($C_{propanol}$), 88.79 (m-C_{ar}), 84.80 (o-C_{ar}), 82.91 (p-C_{ar}), 59.89 (CH_2), 32.04 (CH_2), 29.42 (CH_2). UV/vis (DMSO), λ, nm (ε, $M^{-1}.cm^{-1}$): 445 (262300), 523 (197400), 588 (152500), 638 (125300). FT-IR (ATR, solid, cm^{-1}): ν; br s (3700-3200), s (3108), s (2916), s (2824), s (1614), s (1418).

In synthesis of **P3** and **P4** we used the same protocol and molar ratio as in **P2**, but using the corresponding dimer (**d1**, **d2**) and porphyrin. **P5-P8** were synthesize in the same manner but using 1:1 molar ratio dimer:porphyrin (**DPhDPyP** or **Zn-DPhDPyP**).

P3. Yield 81 % (234 mg). ^{1}H NMR (DMSO-d$_6$, 25 °C, 400 MHz): δ 9.03 (d, $^3J_{HH}$ = 5.55 Hz, 8H, CH_{py}), 8.85 (s, 8H, CH_{porph}), 8,23 (d, $^3J_{HH}$ = 5.72 Hz, 8H, CH_{py}), 5.83 (d, $^3J_{HH}$ = 6.14 Hz, 8H, CH_{ar}), 5.78 (d, $^3J_{HH}$ = 6.15 Hz, 8H, CH_{ar}), 2.84 (m, $^3J_{HH}$ = 6.91 Hz, 4H, CH iPr), 4.58 (bs, 4H, OH), 2.09 (s, 12H, CH_3), 1.20 (m, $^3J_{HH}$ = 5.55 Hz, 24H, C$H_{3\ iPr}$). ^{13}C NMR (DMSO-d$_6$, 25 °C, 101 MHz): δ 149.12 (C_{ar}), 148.50 (C_{py}), 132.48 (C_{porph}), 129.72 (C_{py}), 118.57 (C_{py}), 106.83 (C_{porph}), 100.56 (C_{ar}), 86.83 (CH_{ar}), 85.99 (CH_{ar}), 30.44 (CH iPr), 21.97 ($CH_{3\ iPr}$), 18.34 (CH_3). Elemental analysis: Calcd. for C$_{80}$H$_{80}$Cl$_8$N$_8$O$_4$Ru$_4$Zn + 4 H$_2$O: C, 48.56; H, 4.48; N 5.66. Found: C, 48.46; H, 4.63; N, 5.90. UV/vis (DMSO), λ, nm (ε, $M^{-1}.cm^{-1}$): 472 (59400), 518 (138300), 558 (55000), 599 (53300). FT-IR (ATR, solid, cm^{-1}): ν; br s (3600-3250), s (3091), s (2944), s (2881), s (1609).

P4. Yield 88 % (82 mg). ^{1}H NMR (DMSO-d$_6$, 25 °C, 400 MHz): δ 9.02 (br s, 8H, CH_{py}), 8.65 (br s, 8H, CH_{porph}), 8,22 (br s, 8H, CH_{py}), 5.98 (m, 8H, m-CH_{ar}), 5.75 (overlapping doublet, 8H, o-CH_{ar}), 5.73 (overlapping triplet, 4H, p-CH_{ar}), 4.58 (br s, 4H, OH), 3.45 (m, 8H, CH_2), 2.48 (m, 8H, CH_2), 1.73 (m, 8H, CH_2). ^{13}C NMR (DMSO-d$_6$, 25 °C, 101 MHz): δ 149.11 (C_{ar}), 148.47 (C_{py}), 132.48 (C_{porph}), 129.72 (C_{py}), 108.44 ($C_{propanol}$), 89.40 (m-C_{ar}), 85.33 (o-C_{ar}), 83.43 (p-C_{ar}), 60.46 (CH_2), 32.64 (CH_2), 30.00 (CH_2). Elemental analysis: Calcd. for C$_{76}$H$_{72}$Cl$_8$N$_8$O$_4$Ru$_4$Zn: C, 47.67; H, 3.79; N 5.85. Found: C, 47.67; H 3.79; N 6.09. ESI-MS, m/z, 954.8 [M – [Ru(PhPrOH)Cl$_2$]$_3$ – Cl]$^{+1}$. UV/vis (DMSO), λ, nm (ε, $M^{-1}.cm^{-1}$): 522 (95300), 561 (45200), 598 (49800). FT-IR (ATR, solid, cm^{-1}): ν; br s (3500-3200), s (3067), s (2910), s (2881), s (1619), s (1408).

P5. Yield 51 % (51 mg). ^{1}H NMR (CDCl$_3$, 25 °C, 400 MHz): δ 9.47 (m, 4H, CH_{py}), 8.87 (m, 10H, CH_{Ph}), 8.21 (m, 8H, CH_{porph} and CH_{py}), 7.78 (br s, 4H, CH_{porph}), 5.69 (d, $^3J_{HH}$ = 5.72 Hz, 4H, CH_{ar}), 5.47 (d, $^3J_{HH}$ = 5.48 Hz, 4H, CH_{ar}), 3.20 (m, 2H, CH iPr), 2.23 (s, 6H, CH_3), 1.47 (d, $^3J_{HH}$ = 6.86 Hz, 12H, C$H_{3\ iPr}$), -2.81 (s, 1H, NH), -2.87 (s, 1H, NH). ^{13}C NMR (CDCl$_3$, 25 °C, 101 MHz): δ 153.04 (C_{py}), 141.76 (C_{ph}), 134.54 (C_{py}), 130.20 (C_{ph}), 127.97 (C_{py}), 126.77 (C_{porph}), 121.55 (C_{porph}), 120.93 (C_{porph}), 83.23 (CH_{ar}), 82.55 (CH_{ar}), 30.92 (CH iPr), 22.50 ($CH_{3\ iPr}$), 18.42 (CH_3). Elemental analysis: Calcd. for C$_{62}$H$_{56}$Cl$_4$N$_6$Ru$_2$: C, 60.99; H, 4.59; N 6.84.

Found: C, 62.76; H 4.81; N 7.09. UV/vis (DMSO), λ, nm (ε, $M^{-1}.cm^{-1}$): 513 (143500), 549 (319100), 590 (134400), 648 (29000). FT-IR (ATR, solid, cm^{-1}): ν; br s (3550-3400), s (3080), s (2968), s (1638), s (1491).

P6. Yield 61 % (60 mg). ^{1}H NMR (CDCl$_3$, 25 °C, 400 MHz): δ 9.50 (d, $^{3}J_{HH}$ = 5.96 Hz, 4H, C*H*$_{py}$), 8.89 (m, 10H, C*H*$_{Ph}$), 8.23 (m, 8H, C*H*$_{porph}$ and C*H*$_{py}$), 7.80 (m, 4H, C*H*$_{porph}$), 5.93 (t, $^{3}J_{HH}$ = 5.64 Hz, 4H, *m*-C*H*$_{ar}$), 5.81 (t, $^{3}J_{HH}$ = 5.58 Hz, 2H, *p*-C*H*$_{ar}$), 5.62 (d, $^{3}J_{HH}$ = 5.72 Hz, 4H, *o*-C*H*$_{ar}$), 3.88 (q, $^{3}J_{HH}$ = 5.83 Hz, 4H, C*H*$_2$), 2.84 (t, $^{3}J_{HH}$ = 7.71 Hz, 4H, C*H*$_2$), 2.07 (m, 4H, C*H*$_2$), 1.69 (overlapping multiplet, 2H, O*H*), -2.80 (s, 2H, N*H*). Elemental analysis: Calcd. for C$_{60}$H$_{52}$Cl$_4$N$_6$O$_2$Ru$_2$: C, 58.45; H, 4.25; N 6.82. Found: C, 59.85; H 4.56; N 6.88. UV/vis (DMSO), λ, nm (ε, $M^{-1}.cm^{-1}$): 509 (43400), 550 (154700), 589 (48200), 648 (4000). FT-IR (ATR, solid, cm^{-1}): ν; br s (3600-3200), s (3102), s (2892), s (1641).

P7. Yield 54 % (68 mg). ^{1}H NMR (DMSO-d6, 25 °C, 400 MHz): δ 9.00 (m, 4H, C*H*$_{py}$), 8.82 (m, 10H, C*H*$_{Ph}$), 8.20 (m, 8H, C*H*$_{porph}$ and C*H*$_{py}$), 7.81 (m, 4H, C*H*$_{porph}$), 5.83 (d, $^{3}J_{HH}$ = 5.39 Hz, 4H, C*H*$_{ar}$), 5.78 (d, $^{3}J_{HH}$ = 6.18 Hz, 4H, C*H*$_{ar}$), 2.84 (m, 2H, C*H* $_{iPr}$), 2.09 (s, 6H, C*H*$_3$), 1.20 (d, $^{3}J_{HH}$ = 6.94 Hz, 12H, C*H*$_{3 iPr}$). Elemental analysis: Calcd. for C$_{62}$H$_{54}$Cl$_4$N$_6$Ru$_2$Zn: C, 57.62; H, 4.21; N 6.50. Found: C, 58.51; H 4.32; N 6.59. ESI-MS, m/z, 950.9 [M – [Ru(*p*-cymene)Cl$_2$] – Cl]$^{+1}$, 680.8 [Zn-DPhDPyP + H]$^{+1}$. UV/vis (DMSO), λ, nm (ε, $M^{-1}.cm^{-1}$): 493 (55600), 524 (99900), 562 (349500), 600 (221100), 626 (81300) (. FT-IR (ATR, solid, cm^{-1}): ν; br s (3650-3200), s (3080), s (2988), s (1639).

P8. Yield 67 % (84 mg). ^{1}H NMR (DMSO-d*6*, 25 °C, 400 MHz): δ 9.01 (m, 4H, C*H*$_{py}$), 8.82 (m, 10H, C*H*$_{Ph}$), 8.20 (m, 8H, C*H*$_{porph}$ and C*H*$_{py}$), 7.82 (m, 4H, C*H*$_{porph}$), 5.99 (m, 4H, *m*-C*H*$_{ar}$), 5.75 (m, 6H, *p*-C*H*$_{ar}$ and *o*-C*H*$_{ar}$), 4.59 (m, 2H, O*H*), 3.46 (m, 4H, C*H*$_2$), 2.47 (m, 4H, C*H*$_2$), 1.73 (m, 4H, C*H*$_2$). Elemental analysis: Calcd. for C$_{60}$H$_{50}$Cl$_4$N$_6$O$_2$Ru$_2$Zn: C, 55.59; H, 3.89; N 6.48. Found: C, 56.44; H 4.09; N 6.56. ESI-MS, m/z, 952.9 [M – [Ru(PhPrOH)Cl$_2$] – Cl]$^{+1}$. UV/vis (DMSO), λ, nm (ε, $M^{-1}.cm^{-1}$): 482 (21700), 521 (46900), 559 (253400), 600 (108700), 626 (37900). FT-IR (ATR, solid, cm^{-1}): ν; br s (3580-3150), s (3012), s (2917), s (1591).

8.2 Preparation of human synovial cells

RA synoviocytes were isolated from fresh synovial biopsies obtained from four RA patients undergoing finger arthroplasty. All patients fulfilled the 1987 American Rheumatism Association criteria for RA [160]. The mean age of the patients was 67 ± 5 years (range 60–72 years). The mean disease duration was 8.7 ± 2.3 years. At the time of surgery, the disease activity score (DAS 28) was greater than 3.2. These activities were approved by local institutional review boards, and all subjects gave written informed consent. Synovia were

minced and digested with 1.5 mg/mL collagenase-dispase for 3-4 h at 37 °C as previously reported [161]. After centrifugation, cells were resuspended in DMEM supplemented with 10 % FCS, 4.5 g/L D-glucose, 25 mM Hepes, 100 U/mL penicillin, and 100 μg/mL streptomycin (Gibco BRL) in a humidified atmosphere containing 5 % (v/v) CO_2 at 37 °C. After 48 h, nonadherent cells were removed. Adherent cells (macrophage-like and FLS) were cultured in complete medium, and, at confluence, cells were trypsinized and only the FLS were passed. These cells were used between passages 4 and 8, when they morphologically resembled FLS after an indirect immunofluorescence study (see Culture of human RA FLS). RA FLS were cultured 45–60 days before experimentation. This delay allowed for the elimination of all possible interactions resulting from any preoperative treatment (with nonsteroidal anti-inflammatory drugs, analgesics, disease-modifying antirheumatic drugs, or steroids).

8.3 Culture of human RA FLS and treatment

Between passages 4 and 8, RA FLS were trypsinized. Cell count and survival rate were determined, and cells were plated in culture plates or flasks (Falcon, Oxnard, CA, USA). Survival rate, measured by trypan blue dye exclusion [162] at the start and the end of culture, was always greater than 95 %. FLS (1.10^5) from RA patients were used for an indirect immunofluorescence study [163]. The following monoclonal antibodies were used: 5B5 (anti-prolyl hydroxylase) for fibroblasts at a 1/50 dilution (Dako, Burlingame, CA, USA), JC/70A (anti-CD31), for endothelial cells at 1/50 (Dako), and RMO52 (anti-CD14) for macrophages at 1/50 (Immunotech). The negative control was a mouse antibody of the same isotype (Immunotech). Incubations were performed at room temperature for 30 min. Binding of monoclonal antibodies was visualized using fluorescein (DTAF)-conjugated goat anti-mouse antibody (Immunotech) at 1/50 dilution.

8.4 Culture of SW982 sarcoma synovicytes

One the other hand, SW982 sarcoma synovial cells were provided by the American Type Culture Collection (ATCC—LGC Standards) and culture in RPMI medium (supplemented with 10 % FCS, 4.5 g/L D-glucose, 25 mM Hepes, 100 U/mL penicillin, and 100 μg/mL streptomycin).

8.5 Antiproliferative assays

All described *in vitro* experiments were carried out under aseptic conditions. 3-(4,5-Dimethylthiazol-2-yl)-2,5-diphenyltetrazolium bromide (MTT) and L-glutamine were

purchased from Sigma-Aldrich. Dimethyl sulfoxide (DMSO) for *in vitro* assays was bought from Acros Organics. RA FLS cells were collected in fresh DMEM culture medium by trypsinization. Approximately 700,000 cells were poured in 10 ml of medium and softly homogenized. 100 µl of this solution were added per well in a 96-well plate (7000 cells per well) and the cells were incubated for 24 h at 37 °C in the presence of 5 % CO_2. Then, 100 µL of the PS solution in increasing concentration were dispensed per row in the plate and incubated 24 h in the same conditions. The compounds were dissolved in DMSO (1 mM) just before use and then added in the culture medium in the desired concentrations. The concentration of DMSO in the cell medium was never exceeding 0.05 %. After incubation, the medium was changed carefully with 100 µL of complete medium (without red phenol). Subsequently, irradiation was performed using a red-light source, CureLight®, PhotoCure ASA at 630 nm for 30 min (dose 72 J/cm^2). After the irradiation, the 96-well plate was incubated 18 h. After that, 10 µl of a MTT solution (5 g/l) was added and the 96-well plate was put again inside the incubator for 4 h. Then, the media was removed and 200 µl of DMSO added in each well, followed by stirring the plate softly for 3 min. Absorbance after the MTT assay was carried out at 540 nm by a Dynex Triad Multi Mode Microplate Reader (Dynex Technologies). The assays were executed in triplicate. Cytotoxicity evaluation in the dark was carried out by repeating the same protocol without irradiation. The SW982 synovial sarcoma cell were treated as the same way. The maximum concentration used in SW982 of DMSO was 0.1 %.

8.6 Protein extraction and Western-Blot analysis

For total protein extraction, RA FLS were washed in PBS, and the total cell pool was centrifuged at 200 G for 5 min at 4 °C and homogenized in RIPA lysis buffer (50 mM HEPES, pH 7.5, 150 mM NaCl, 1 % sodium deoxycholate, 1 % NP-40, 0.1 % SDS, and 20 mg/mL of aprotinin) containing protease inhibitors (CompleteTM Mini, Roche Di-agnostics) according to the manufacturer's instructions. Proteins (60 µg) were separated by electrophoresis on 10% SDS–PAGE gels and transferred to polyvinylidene fluoride (PVDF) membranes (Amersham Pharmacia Biotech, Saclay, France), which were then probed with a COX-2 human primary antibody (Cayman Chemical, Bertin Pharma, Montigny le Bretonneux, France). After incubation with a secondary antibody (Dako France S.A.S., Trappes, France), blots were developed using the ECL Plus Western Blotting Detection System (Amersham Pharmacia Biotech) and G: BOX system (Syngene, Ozyme, Saint Quentin en Yvelines, France). Membranes were then reblotted with human anti-β-actin (Sigma-Aldrich, Saint Quentin Fallavier, France) used as a loading control.

8.7 Assay of COX-2 activity and IL-1β production

RA FLS were maintained in DMEM supplemented with 10% (v/v) FCS, 4.5 g/l D-glucose, 100 U/mL penicillin and 100 μg/mL streptomycin. The cells were grown in a humidified incubator at 37 °C in the presence of 5 % CO_2. Then, 2.10^6 RA FLS cells were seeded in a 25 cm^2 flask and incubated during 24 h. Then, the volume of the PS solution to reach the IC_{50} values was added, and the cells incubated for 24 h. The medium was removed and replaced by medium without red phenol, like previously. Then, cells were irradiated at the same conditions, and expressed in the MTT assays and incubated 18 h. The non-irradiated cells were kept in the incubator. After this, LPS (1 μg/ml) was added to the medium of irradiated and non-irradiated cells, and the cells were incubated for an additional 4 h. Cells were trypsinized and culture medium supernatant isolated. The PGE_2 and IL-1β levels were quantified in culture media supernatants from treated and control cells by enzyme immunoassay using an ELISA Kit (Cayman Chemical and Thermo Fisher Scientific, respectively). The results were expressed by the average of three independent experiments.

8.8 Statistical analysis

All quantitative results were expressed as the mean ± 3 standard deviations (SEM) of separate experiments using Excel (Microsoft Office, Version 2019). Statistical significance was evaluated by the two-tailed unpaired Student's t-test, P-value < 0.001 (***).

CHAPTER 9 – REFERENCES

1. Dougherty, T. J., Gomer, C. J., Henderson, B. W., Jori, G., Kessel, D., Korbelik, M., Moan, J. and Peng, Q. Photodynamic therapy. *J. Natl. Cancer Inst*. **1998**, 90, 889–905.

2. Kwiatkowski, S., Knap, B., Przystupski, D., Saczko, J., Kędzierska, E., Knap-Czop, K., Kotlińska J., Michel O., Kotowski K. and Kulbacka, J. Photodynamic therapy–mechanisms, photosensitizers and combinations. *Biomed. Pharmacother*. **2018**, 106, 1098-1107.

3. Castano, A. P., Demidova, T. N. and Hamblin, M. R. Mechanisms in photodynamic therapy: part one—photosensitizers, photochemistry and cellular localization. *Photodiagnosis Photodyn. Ther*. **2004**, 1, 279-293.

4. Van Straten, D., Mashayekhi, V., De Bruijn, H. S., Oliveira, S. and Robinson, D. J. Oncologic photodynamic therapy: basic principles, current clinical status and future directions. *Cancers*. **2017**, 9, 19.

5. Dolmans, D. E., Fukumura, D. and Jain, R. K. Photodynamic therapy for cancer. *Nat. Rev. Cancer*. **2003**, 3, 380-387.

6. Dougherty, T. J., Kaufman, J. E., Goldfarb, A., Weishaupt, K. R., Boyle, D. and Mittleman, A. Photoradiation therapy for the treatment of malignant tumors. *Cancer Res*. **1978**, 38, 2628-2635.

7. Yano, T. and Wang, K. K. Photodynamic therapy for gastrointestinal cancer. *Photochem. Photobiol*. **2020**, 96, 517-523.

8. Hwang, H. S., Shin, H., Han, J. and Na, K. Combination of photodynamic therapy (PDT) and anti-tumor immunity in cancer therapy. *J. Pharm. Investig*. **2018**, 48, 143-151.

9. Bouramtane, S., Bretin, L., Pinon, A., Leger, D., Liagre, B., Richard, L., Brégier, F., Sol, V. and Chaleix, V. Porphyrin-xylan-coated silica nanoparticles for anticancer photodynamic therapy. *Carbohydr. Polym*. **2019**, 213, 168-175.

10. Gold, M. H. Acne and PDT: new techniques with lasers and light sources. *Lasers Med. Sci*. **2007**, 22, 67-72.

11. Wiegell, S. R. and Wulf, H. C. Photodynamic therapy of acne vulgaris using 5-aminolevulinic acid versus methyl aminolevulinate. *J.Am. Acad. Dermatol*. **2006**, 54, 647-651.

12. Choi, Y. M., Adelzadeh, L. and Wu, J. J. Photodynamic therapy for psoriasis. *J. Dermatol. Treat*. **2015**, 26, 202-207.

13. Otsuji, T., Sho, K., Tsumura, A., Koike, N., Nishimura, T. and Takahashi, K. Three-year results of a modified photodynamic therapy procedure (Ironing PDT) for age-related macular degeneration patients with large lesions. *Clin. Ophthalmol*. **2016**, 10, 431.

14. Jia, Q., Song, Q., Li, P. and Huang, W. Rejuvenated photodynamic therapy for bacterial infections. *Adv. Healthc. Mater*. **2019**, 8, 1900608.

15. Sarna, T. and Swartz, H. A. The physical properties of melanins. *The pigmentary system: physiology and pathophysiology*. **2006**, 311-341.

16. Hale, G. M. and Querry, M. R. Optical constants of water in the 200-nm to 200-μm wavelength region. *Appl. Opt*. **1973**, 12, 555-563.

17. McInnes, I.B.; Schett, G. The pathogenesis of rheumatoid arthritis. *N. Engl. J. Med*. **2011**, 365, 2205–2219.

18. Majithia, V. and Geraci, S. A. Rheumatoid arthritis: diagnosis and management. *Am. J. Med.* **2007**, 120, 936-939.

19. Scherer, H. U., Häupl, T. and Burmester, G. R. The etiology of rheumatoid arthritis. *J. Autoimmun*. **2020**, 110, 102400.

20. Symmons, D. P., Bankhead, C. R., Harrison, B. J., Brennan, P., Silman, A. J., Barrett, E. M. and Scott, D. G. Blood transfusion, smoking, and obesity as risk factors for the development of rheumatoid arthritis. Results from a primary care-based incident case-control study in Norfolk, England. *Arthritis Rheum*. **1997**, 40, 1955-1961.

21. Croia, C., Bursi, R., Sutera, D., Petrelli, F., Alunno, A. and Puxeddu, I. One year in review 2019: Pathogenesis of rheumatoid arthritis. *Clin. Exp. Rheumatol*. **2019**, 37, 347–357.

22. Deane, K. D. and Holers, V. M. The natural history of rheumatoid arthritis. *Clin. Ther*. **2019**, 41, 1256-1269.

23. Smolen, J. S., Aletaha, D. and McInnes, I. B. Rheumatoid arthritis. *Lancet*. **2016**, 388, 2023–2038.

24. Aletaha, D. and Smolen, J. S. Diagnosis and management of rheumatoid arthritis: A review. *JAMA*. **2018**, 320, 1360-1372.

25. Silvagni, E., Di Battista, M., Bonifacio, A. F., Zucchi, D., Governato, G. and Scirè, C. A. One year in review 2019: Novelties in the treatment of rheumatoid arthritis. *Clin. Exp. Rheumatol*. **2019**, 37, 519-534.

26. Seymour, H. E., Worsley, A., Smith, J. M. and Thomas, S. H. L. Anti-TNF agents for rheumatoid arthritis. *Br. J. Clin. Pharmacol*. **2001**, 51, 201-208.

27. Kremer, J. M., Bloom, B. J., Breedveld, F. C., Coombs, J. H., Fletcher, M. P., Gruben, D., Krishnaswami, S., Burgos-Vargas, R., Wilkinson, B., Zerbini, C. A. F. and Zwillich, S. H. The safety and efficacy of a JAK inhibitor in patients with active rheumatoid arthritis: Results of a double-blind, placebo-controlled phase IIa trial of three dosage levels of CP-690,550 versus placebo. *Arthritis Rheum*. **2009**, 60, 1895-1905.

28. Smolen, J. S., Landewé, R. B., Bijlsma, J. W., Burmester, G. R., Dougados, M., Kerschbaumer, A., McInnes, I. B., Sepriano, A., van Vollenhoven, R. F. and de Wit, M. EULAR recommendations for the management of rheumatoid arthritis with synthetic and biological disease-modifying antirheumatic drugs: 2019 update. *Ann. Rheum. Dis*. **2020**, 79, 685–699.

29. Smolen, J. S., van der Heijde, D., Machold, K. P., Aletaha, D., Landewé, R. Proposal for a new nomenclature of disease-modifying antirheumatic drugs. Ann. Rheum. Dis. 2014, 73, 3-5

30. Buch, M.H. Defining refractory rheumatoid arthritis *Ann. Rheum. Dis.* **2018**, 77, 966-969.

31. Nagy G., Roodenrijs N. M. T., Welsing P. M. J., *et al.* EULAR definition of difficult-to-treat rheumatoid arthritis *Ann. Rheum. Dis.* **2021**, 80, 31-35.

32. Gallardo-Villagrán, M., Leger, D. Y., Liagre, B. and Therrien, B. Photosensitizers used in the photodynamic therapy of rheumatoid arthritis. *Int. J. Mol. Sci*. **2019**, 20, 3339.

33. Zenkevich, E., Sagun, E., Knyukshto, V., Shulga, A., Mironov, A., Efremova, O. and Kassem, M. Photophysical and photochemical properties of potential porphyrin and chlorin photosensitizers for PDT. J. of Photochem. Photobiol. B, Biol. **1996**, 33, 171-180.

34. Ethirajan, M., Chen, Y., Joshi, P. and Pandey, R. K. The role of porphyrin chemistry in tumor imaging and photodynamic therapy. *Chem. Soc. Rev*. **2011**, 40, 340-362.

35. Yang, M., Cao, S., Sun, X., Su, H., Li, H., Liu, G. and Wu, F. Self-assembled naphthalimide conjugated porphyrin nanomaterials with D–A structure for PDT/PTT synergistic therapy. *Bioconjug. Chem*. **2019**, 31, 663-672.

36. Ratkay, L. G., Chowdhary, R. K., Neyndorff, H. C., Tonzetich, J., Waterfield, J. D. and Levy, J. G. Photodynamic therapy; a comparison with other immunomodulatory treatments of adjuvant-enhanced arthritis in MRL-lpr mice. *Clin. Exp. Immunol*. **1994**, 95, 373-377.

37. Chowdhary, R. K., Ratkay, L. G., Canaan, A.J., Waterfield, J. D., Richter, A. M. and Levy, J. G. Uptake of Verteporfin® by articular tissues following systemic and intra-articular administration. *Biopharm. Drug Dispos*. **1998**, 19, 395–400.

38. Trauner, K. B., Gandour-Edwards, R., Bamberg, M., Shortkro, S., Sledge, C. and Hasan, T. Photodynamic synovectomy using benzoporphyrin derivative in an antigen-induced arthritis model for rheumatoid arthritis. *Photochem. Photobiol*. **1998**, 67, 133–139.

39. Hendrich, C., Hüttmann, G., Vispo-Seara, J. L., Houserek, S. and Siebert, W. E. Experimental photodynamic laser therapy for rheumatoid arthritis with a second generation photosensitizer. Knee Surg. *Sports Traumatol. Arthrosc*. **2000**, 8, 190–194.

40. Trauner, K., Gandour-Edwards, R., Bamberg, M., Nishioka, N. S., Flotte, T., Autry, S. and Hasan, T. Influence of light delivery on photodynamic synovectomy in an antigen-induced arthritis model for rheumatoid arthritis. *Lasers Surg. Med*. **1998**, 22, 147-156.

41. Hendrich, C., Diddens, H., Nosir, H. and Siebert, W. E. Treatment of Rheumatoid Arthritis using Photodynamic Therapy? *Proc. SPIE Int. Soc. Opt. Eng*. **1995**, 2371, 592–595.

42. Hendrich, C., Hüttmann, G., Lehnert, C., Diddens, H. and Siebert, W.E. Photodynamic laser therapy for rheumatoid arthritis cell culture studies and animal experiments. *Knee Surg. Sports Traumatol. Arthrosc*. **1997**, 5, 58–63.

43. Leeper, F. J. The biosynthesis of porphyrins, chlorophylls, and vitamin B12. *Nat. Prod. Rep.* **1989**, 6, 171–203.

44. Layer, G., Reichelt, J., Jahn, D., Heinz, D. W. Structure and function of enzymes in heme biosynthesis. *Protein Sci*. **2010**, 19, 1137–1161.

45. Kirdaite, G., Lange, N., Busso, N., Van Den Bergh, H., Kucera, P. and So, A. Protoporphyrin IX photodynamic therapy for synovitis. *Arthritis Rheum*. **2002**, 46, 1371–1378.

46. Bagdonas, S., Kirdaite, G., Streckyte, G., Graziene, V., Leonaviciene, L., Bradunaite, R., Venalis, A. and Rotomskis, R. Spectroscopic study of ALA-induced endogenous porphyrins in arthritic knee tissues: Targeting rheumatoid arthritis PDT. *Photochem. Photobiol. Sci*. **2005**, 4, 497–502.

47. Dietze, A., Engesæter, B. and Berg, K. Transgene delivery and gelonin cytotoxicity enhanced by photochemical internalization in fibroblast-like synoviocytes (FLS) from rheumatoid arthritis patients. *Photochem. Photobiol. Sci.* **2005**, 4, 341–347.

48. Miyazawa, S., Nishida, K., Komiyama, T., Nakae, Y., Takeda, K., Yorimitsu, M., Kitamura, A., Kunisada, T., Ohtsuka, A. and Inoue, H. Novel transdermal photodynamic therapy using ATX-S10Na(II) induces apoptosis of synovial fibroblasts and ameliorates collagen antibody-induced arthritis in mice. *Rheumatol. Int*. **2006**, 26, 717–725.

49. Torikai, E., Kageyama, Y., Kohno, E., Hirano, T., Koide, Y., Terakawa, S. and Nagano, A. Photodynamic therapy using talaporfin sodium for synovial membrane from rheumatoid arthritis patients and collagen-induced arthritis rats. *Clin. Rheumatol*. **2008**, 27, 751–761.

50. Hansch, A., Frey, O., Gajda, M., Susanna, G., Boettcher, J., Bräuer, R. and Kaiser, W. A. Photodynamic treatment as a novel approach in the therapy of arthritic joints. *Lasers Surg. Med*. **2008**, 40, 265–272.

51. Gabriel, D., Lange, N., Chobaz-Peclat, V., Zuluaga, M. F., Gurny, R., Van Den Bergh, H. and Busso, N. Thrombin-sensitive dual fluorescence imaging and therapeutic agent for

detection and treatment of synovial inflammation in murine rheumatoid arthritis. *J. Control. Release.* **2012**, 163, 178–186.

52. Hendrich, C. and Siebert, W. E. Photodynamic therapy for rheumatoid arthritis? *Lasers Surg. Med.* **1997**, 21, 359–364.

53. Neupane, J., Ghimire, S., Shakya, S., Chaudhary, L. and Shrivastava, V.P. Effect of light emitting diodes in the photodynamic therapy of rheumatoid arthritis. *Photodiagn. Photodyn. Ther.* **2010**, 7, 44–49.

54. García, I., Ballesta, S., Gilaberte, Y., Rezusta, A. and Pascual, Á. Antimicrobial photodynamic activity of hypericin against methicillin-susceptible and resistant Staphylococcus aureus biofilms. *Future Microbiol.* **2015**, 10, 347–356.

55. Karioti, A. and Bilia, A. R. Hypericins as Potential Leads for New Therapeutics. *Int. J. Mol. Sci.* **2010**, 11, 562–594.

56. Zhang, K., Gao, S., Guo, J., Ni, G., Chen, Z., Li, F., Zhu, X., Wen, Y. and Guo, Y. Hypericin-photodynamic therapy inhibits proliferation and induces apoptosis in human rheumatoid arthritis fibroblast-like synoviocytes cell line MH7A. *Iran. J. Basic Med. Sci.* **2018**, 21, 130–137.

57. Schmitt, F., Lagopoulos, L., Käuper, P., Rossi, N., Busso, N., Barge, J., Wagnières, G., Laue, C., Wandrey, C. and Juillerat-Jeanneret, L. Chitosan-based nanogels for selective delivery of photosensitizers to macrophages and improved retention in and therapy of articular joints. *J. Control. Release.* **2010**, 144, 242–250.

58. Zhao, C., Rehman, F. U., Jiang, H., Selke, M., Wang, X. and Liu, C. Y. Titanium dioxide-tetra sulphonatophenyl porphyrin nanocomposites for target cellular bio-imaging and treatment of rheumatoid arthritis. *Sci. China Chem.* **2016**, 59, 637–642.

59. Rehman, F. U., Zhao, C., Wu, C., Li, X., Jiang, H., Selke, M., Wang, X. Synergy and translation of allogenic bone marrow stem cells after photodynamic treatment of rheumatoid arthritis with tetra sulfonatophenyl porphyrin and TiO_2 nanowhiskers. *Nano Res.* **2016**, 9, 3305–3321.

60. Tang, Q., Cui, J., Tian, Z., Sun, J., Wang, Z., Chang, S. and Zhu, S. Oxygen and indocyanine green loaded phase-transition nanoparticle-mediated photo-sonodynamic cytotoxic effects on rheumatoid arthritis fibroblast-like synoviocytes. *Int. J. Nanomed.* **2017**, 12, 381–393.

61. Lu, Y., Li, L., Lin, Z., Wang, L., Lin, L., Li, M., Zhang, Y., Yin, Q., Li, Q. and Xia, H. A new treatment modality for rheumatoid arthritis: combined photothermal and photodynamic therapy using $Cu_{7.2}S_4$ nanoparticles. *Adv. Healthc. Mater.* **2018**, 7, 1–11.

62. H. Yan, Süss-Fink, G., Neels A. and Stoeckli-Evans, H. *J. Chem. Soc. Dalton Trans*. **1997**, 22, 4345–4350.

63. Zelonka, R. A. and Baird, M. Benzene complexes of ruthenium (II). *Can. J. Chem*. **1972**, 50, 3063-3072.

64. Severin, K. Supramolecular chemistry with organometallic half-sandwich complexes. *Chem. Comm.* **2006**, 37, 3859-3867.

65. Piotrowski, H., Polborn, K., Hilt, G. and Severin, K. A self-assembled metallomacrocyclic ionophore with high affinity and selectivity for Li+ and Na+. *J. Am. Chem. Soc*. **2001**, 123, 2699-2700.

66. Annen, P., Schildberg, S. and Sheldrick, W. S. (η^5-Pentamethylcyclopentadienyl) iridium (III) complexes of purine nucleobases and nucleotides: a comparison with (η^6-arene) ruthenium (II) and (η^5-pentamethylcyclopentadienyl) rhodium (III) species. *Inorganica Chim. Acta*. **2000,** 307, 115-124.

67. Furrer, M. A., Schmitt, F., Wiederkehr, M., Juillerat-Jeanneret, L. and Therrien, B. Cellular delivery of pyrenyl-arene ruthenium complexes by a water-soluble arene ruthenium metalla-cage. *Dalton Trans*. **2012**, 41, 7201-7211.

68. Barry, N. P., Zava, O., Wu, W., Zhao, J. and Therrien, B. Encapsulation of hydrophobic pyrenylcycloplatinate complexes within a water-soluble arene ruthenium metallacage. *Inorg. Chem. Comm.* **2012**, 18, 25-28.

69. Pitto-Barry, A., Zava, O., Dyson, P. J., Deschenaux, R. and Therrien, B. Enhancement of cytotoxicity by combining pyrenyl-dendrimers and arene ruthenium metallacages. Inorganic Chemistry. **2012**, 51, 7119-7124.

70. Zhao, Y., Zhang, L., Li, X., Shi, Y., Ding, R., Teng, M. and Stang, P. J. Self-assembled ruthenium (II) metallacycles and metallacages with imidazole-based ligands and their in vitro anticancer activity. *Proc. Natl. Acad. Sci*. **2019**, 116, 4090-4098.

71. Sepehrpour, H., Fu, W., Sun, Y. and Stang, P. J. (2019). Biomedically relevant self-assembled metallacycles and metallacages. *J. Am. Chem. Soc*. **2019**, 141, 14005-14020.

72. Gallardo-Villagrán, M., Paulus, L., Charissoux, J.-L., Sutour, S., Vergne-Salle, P., Leger, D. Y., Liagre, B. and Therrien, B. Evaluation of ruthenium-based assemblies as carriers of photosensitizers to treat rheumatoid arthritis by photodynamic therapy. *Pharmaceutics*. **2021**, 13, 2104.

73. Schmitt, F., Freudenreich, J., Barry, N. P., Juillerat-Jeanneret, L., Süss-Fink, G., Therrien, B. Organometallic cages as vehicles for intracellular release of photosensitizers. *J. Am. Chem. Soc*. **2012**, 134, 754–757.

74. Barry, N. P. E., Zava, O., Dyson, P.J. and Therrien, B. Excellent Correlation between Drug Release and Portal Size in Metalla-Cage Drug-Delivery Systems. *Chem. Eur. J*. **2011**, 17, 9669–9677.

75. Kamkaew, A., Lim, S. H., Lee, H. B., Kiew, L. V., Chung, L.Y. and Burgess, K. BODIPY dyes in photodynamic therapy. *Chem. Soc. Rev*. **2013**, 42, 77–88.

76. Yang, B., Chen, Y. and Shi, J. Reactive oxygen species (ROS)-based nanomedicine. *Chem. Rev*. **2019**, 119, 4881-4985.

77. Agostinis, P., Berg, K., Cengel, K. A., Foster, T. H., Girotti, A.W., Gollnick, S. O., Hahn, S. M., Hamblin, M. R., Juzeniene, A., Kessel, D., *et al*. Photodynamic therapy of cancer: An update. *CA Cancer, J. Clin*. **2011**, 61, 250–281.

78. Afaneh, A. T. and Schreckenbach, G. Fluorescence enhancement/quenching based on metal orbital control: computational studies of a 6-thienyllumazine-based mercury sensor. *J Physi Chem A*. **2015**, 119, 8106-8116.

79. Lutton, J. D., Abraham, N. G., Drummond, G. S., Levere, R. D. and Kappas, A. Zinc porphyrins: Potent inhibitors of hematopoieses in animal and human bone marrow. *Proc. Natl. Acad. Sci*. **1997**, 94, 1432–1436.

80. Yang, G., Nguyen, X., Ou, J., Rekulapelli, P., Stevenson, D. K. and Dennery, P.A. Unique effects of zinc protoporphyrin on HO-1 induction and apoptosis. *Am. J. Hematol*. **2001**, 97, 1306–1313.

81. Bartok, B. and Firestein, G.S. Fibroblast-like synoviocytes: Key effector cells in rheumatoid arthritis. *Immunol. Rev*. **2010**, 233, 233–255.

82. Park, C., Moon, D. O., Choi, I. W., Choi, B. T., Nam, T. J., Rhu, C. H., Kwon, T. K., Lee, W. H., Kim, G. Y. and Choi, Y. H. Curcumin induces apoptosis and inhibits prostaglandin E2 production in synovial fibroblasts of patients with rheumatoid arthritis. *Int. J. Mol. Med*. **2007**, 20, 365–372.

83. Nasry, W. H. S., Rodriguez-Lecompte, J. C. and Martin, C. K. Role of COX-2/PGE2 mediated inflammation in oral squamous cell carcinoma. *Cancers*. **2018**, 10, 348.

84. Sung, M. S., Lee, E. G., Jeon, H. S., Chae, H. J., Park, S. J, Lee, Y. C. and Yoo, W. H. Quercetin inhibits IL-1β-induced proliferation and production of MMPs, COX-2, and PGE2 by rheumatoid synovial fibroblast. Inflammation. **2012**, 35, 1585–1594.3.

85. Agostinis, P., Breyssens, H., Buytaert, E. and Hendrickx, N. Regulatory pathways in photodynamic therapy induced apoptosis. *Photochem. Photobiol. Sci*. **2004**, 3, 721–729.

86. Downey, G. P., Gumbay, R. S., Doherty, D. E., LaBrecque, J. F., Henson, J. E., Henson, P. M. and Worthen, G. S. Enhancement of pulmonary inflammation by PGE2: Evidence for a vasodilator effect. *J. Appl. Physiol*. **1988**, 64, 728–741.

87. Fidanzi-Dugas, C., Liagre, B., Chemin, G., Perraud, A., Carrion, C., Couquet, C. Y., Granet, R., Sol, V. and Léger, D. Y. Analysis of the in vitro and in vivo effects of photodynamic therapy on prostate cancer by using new photosensitizers, protoporphyrin IX-polyamine derivatives. Biochim. Biophys. *Acta Gen. Subj*. **2017**, 1861, 1676–1690.

88. Luna, M., Wong, S., Ferrario, A. and Gomer, C. J. Cyclooxygenase-2 Expression Induced by Photofrin Photodynamic Therapy Involves the p38 MAPK Pathway. *Photochem. Photobiol*. **2008**, 84, 509–514.

89. Rayar, A. M., Lagarde, N., Martin, F., Blanchard, F., Liagre, B., Ferroud, C., Zagury, J. F., Montes, M. and Veitía, M. S. I. New selective cyclooxygenase-2 inhibitors from cyclocoumarol: Synthesis, characterization, biological evaluation and molecular modeling. *Eur. J. Med. Chem*. 2018, 146, 577–587.

90. Hendrickx, N., Volanti, C., Moens, U., Seternes, O. M., De Witte, P., Vandenheede, J. R., Piette, J. and Agostinis, P. Up-regulation of cyclooxygenase-2 and apoptosis resistance by p38 MAPK in hypericin-mediated photodynamic therapy of human cancer cells. *J. Biol. Chem*. **2003**, 278, 52231–52239.

91. Ferrario, A., Von Tiehl, K., Wong, S., Luna, M. and Gomer, C. J. Cyclooxygenase-2 inhibitor treatment enhances photodynamic therapy-mediated tumor response. *Cancer Res*. **2002**, 62, 3956–3961.

92. Williams, C. S., Mann, M. and DuBois, R. N. The role of cyclooxygenases in inflammation, cancer, and development. *Oncogene*. **1999**, 18, 7908-7916.

93. van Dalen, S. C. M., Blom, A. B., Slöetjes, A. W., Helsen, M. M. A., Roth, J., Vogl, T., van de Loo, F. A., Koenders, M. I., van der Kraan, P. M., van den Berg, W. B., *et al.* Interleukin-1 is not involved in synovial inflammation and cartilage destruction in collagenase-induced osteoarthritis. *Osteoarthr. Cartil*. **2017**, 25, 385–396.

94. Nasi, S., Ea, H. K., So, A. and Busso, N. Revisiting the role of interleukin-1 pathway in osteoarthritis: Interleukin-1α and-1β, and NLRP3 inflammasome are not involved in the pathological features of the murine menisectomy model of osteoarthritis. *Front. Pharmacol*. **2017**, 8, 282.

95. Shimomura, K., Kanamoto, T., Kita, K., Akamine, Y., Nakamura, N., Mae, T., Yoshikawa, H. and Nakata, K. Cyclic compressive loading on 3D tissue of human synovial fibroblasts

upregulates prostaglandin E2 via COX-2 production without IL-1β and TNF-α. *Bone Jt. Res*. **2014**, 3, 280–288.

96. Barry, N. P. E., Zava, O., Dyson, P. J. and Therrien, B. Synthesis, Characterization and Anticancer Activity of Porphyrin-Containing Organometallic Cubes. *Aust. J. Chem*. **2010**, 63, 1529-1537.

97. Moriwaki, S. I., Misawa, J., Yoshinari, Y., Yamada, I., Takigawa, M. and Tokura, Y. Analysis of photosensitivity in Japanese cancer-bearing patients receiving photodynamic therapy with porfimer sodium (PhotofrinTM). *Photodermatol. Photoimmunol. Photomed*. **2001**, 17, 241-243.

98. Usuda, J., Kato, H., Okunaka, T., Furukawa, K., Tsutsui, H., Yamada, K.,Suga, Y., Honda, H., Nagatsuka, Y., Ohira, T., Tsuboi, M. and Hirano, T. Photodynamic therapy (PDT) for lung cancers. J. Thorac. Oncol. **2006**, 1, 489-493.

99. Jing, C., Wang, R., Ou, H., Li, A., An, Y., Guo, S. and Shi, L. Axial modification inhibited H-aggregation of phthalocyanines in polymeric micelles for enhanced PDT efficacy. *Chem. Comm*. **2018**, 54, 3985-3988.

100. Tuncel, S., Dumoulin, F., Gailer, J., Sooriyaarachchi, M., Atilla, D., Durmuş, M., Bouchu, D., Savoie, H., W. Boyle, W. R. and Ahsen, V. A set of highly water-soluble tetraethyleneglycol-substituted Zn (II) phthalocyanines: synthesis, photochemical and photophysical properties, interaction with plasma proteins and in vitro phototoxicity. *Dalton Trans*. **2011**, 40, 4067-4079.

101. Jiang, X., Zhou, Z., Yang, H., Shan, C., Yu, H., Wojtas, L., Zhang, M., Mao, Z., Ming Wang, M. and Stang, P. J. Self-assembly of porphyrin-containing metalla-assemblies and cancer photodynamic therapy. *Inorg. Chem*. **2020**, 59, 7380-7388.

102. Volchkov, V. V., Ivanov, V. L. and Uzhinov, B. M. Induced intersystem crossing at the fluorescence quenching of laser dye 7-amino-1, 3-naphthalenedisulfonic acid by paramagnetic metal ions. *J. Fluoresc*. **2010**, 20, 299-303.

103. Ng, K. K. and Zheng, G. Molecular interactions in organic nanoparticles for phototheranostic applications. *Chem. Rev*. **2015**, 115, 11012-11042.

104. Hevekerl, H., Spielmann, T., Chmyrov, A. and Widengren, J. Forster resonance energy transfer beyond 10 nm: exploiting the triplet state kinetics of organic fluorophores. *J. Phys. Chem. B.* **2011**, 115, 13360-13370.

105. Barry, N. P., Austeri, M., Lacour, J. and Therrien, B. Highly efficient NMR enantiodiscrimination of chiral octanuclear metalla-boxes in polar solvent. *Organometallics*. **2009**, 28, 4894-4897.

106. Oldacre, A. N., Crawley, M. R., Friedman, A. E. and Cook, T. R. Tuning the Activity of Heterogeneous Cofacial Cobalt Porphyrins for Oxygen Reduction Electrocatalysis through Self-Assembly. *Chem. Eur. J.* **2018**, 24, 10984-10987.

107. Han, Y. F., Lin, Y. J., Weng, L. H., Berke, H. and Jin, G. X. Stepwise formation of "organometallic boxes" with half-sandwich Ir, Rh and Ru fragments. *Chem. Comm.* **2008**, 3, 350-352.

108. Barry, N. P. and Therrien, B. Host-guest chemistry in the hexanuclear (arene) ruthenium metalla-prismatic cage [Ru_6 (*p*-cymene)$_6$(tpt)$_2$(dhnq)$_3$]$^{6+}$. *Eur. J. Inorg. Chem.* **2009**, 31, 4695-4700.

109. Newton, R., Kuitert, L. M., Bergmann, M., Adcock, I. M. and Barnes, P. J. Evidence for involvement of NF-κB in the transcriptional control of COX-2 gene expression by IL-1β. *Biochem. Biophys. Res. Comm.* **1997**, 237, 28-32.

110. Dos Santos, A. F., De Almeida, D. R. Q., Terra, L. F., Baptista, M. S. and Labriola, L. Photodynamic therapy in cancer treatment-an update review. *J. Cancer Metastasis Treat.* **2019**, 5, 25.

111. Zhang, L., Ji, Z., Zhang, J. and Yang, S. Photodynamic therapy enhances skin cancer chemotherapy effects through autophagy regulation. *Photodiagnosis Photodyn. Ther.* **2019**, 28, 159-165.

112. Hilerowicz, Y., Friedman, O., Zur, E., Ziv, R., Koren, A., Salameh, F., Mehrabi, J. N. and Artzi, O. Thermomechanical ablation-assisted photodynamic therapy for the treatment of acne vulgaris. A retrospective chart review of 30 patients. *Lasers Surg. Med.* **2020**, 52, 966-970.

113. Ding, H. L., Wang, X. L., Wang, H. W. and Huang, Z. Successful treatment of refractory facial acne using repeat short-cycle ALA-PDT: Case study. *Photodiagnosis Photodyn. Ther.* **2011**, 8, 343-346.

114. Ruiz-Moreno, J. M., Montero, J. A. and Barile, S. Triamcinolone and PDT to treat exudative age-related macular degeneration and submacular hemorrhage. *Eur. J. Ophthalmol.* **2006**, 16, 426-434.

115. Montero, J. A., Ruiz-Moreno, J. M. and Fernandez-Muñoz, M. Intravitreal bevacizumab to treat choroidal neovascularization following photodynamic therapy in central serous choroidopathy. *Eur. J. Ophthalmol.* **2011**, 21, 503-505.

116. Maisch, T., Szeimies, R. M., Jori, G. and Abels, C. Antibacterial photodynamic therapy in dermatology. *Photochem. Photobiol. Sci.* **2004**, 3, 907-917.

117. Maldonado-Carmona, N., Ouk, T. S., Calvete, M. J., Pereira, M. M., Villandier, N. and Leroy-Lhez, S. Conjugating biomaterials with photosensitizers: Advances and perspectives for photodynamic antimicrobial chemotherapy. *Photochem. Photobiol. Sci*. **2020**, 19, 445-461.

118. Kusuzaki, K., Murata, H., Matsubara, T., Miyazaki, S., Shintani, K., Seto, M., Matsumine, A., Hosol, A., Sugimoto, T. and Uchida, A. Clinical outcome of a novel photodynamic therapy technique using acridine orange for synovial sarcomas. *Photochem. Photobiol*. **2005**, 81, 705-710.

119. Takeda, K., Kunisada, T., Miyazawa, S., Nakae, Y. and Ozaki, T. Photodynamic Therapy with ATX-S10· Na (II) Inhibits Synovial Sarcoma Cell Growth. *Clin. Orthop. Relat. Res*. **2008**, 466, 1726-1733.

120. Dorst, D. N., Rijpkema, M., Buitinga, M., Walgreen, B., Helsen, M., Brennan and E., Koenders, M. I. Targeting of fibroblast activation protein in rheumatoid arthritis patients: imaging and ex vivo photodynamic therapy. *Rheumatology*. **2021**, keab664.

121. Siegel, H. J., Sessions, W., Casillas Jr, M. A., Said-Al-Naief, N., Lander, P. H. and Lopez-Ben, R. Synovial sarcoma: clinicopathologic features, treatment, and prognosis. *Orthopedics*. **2007**, 30, 1020.

122. Cadman, N. L., Soule, E. H. and Kelly, P. J. Synovial sarcoma. An analysis of 134 tumors. *Cancers*. **1965**, 18, 613-627.

123. Bergovec, M., Smerdelj, M., Bacan, F., Seiwerth, S., Herceg, D. and Prutki, M. Intraarticular synovial sarcoma of the knee rising from a lateral meniscus–a case report. *Orthop Traumatol. Surg. Res*. **2018**, 104, 227-230.

124. Kampe, C. E., Rosen, G., Eilber, F., Eckardt, J., Lowenbraun, S., Foster, J., Forscher, C. and Selch, M. Synovial sarcoma. A study of intensive chemotherapy in 14 patients with localized disease. *Cancer*. **1993**, 72, 2161-2169.

125. Gunaydin, G., Gedik, M. E. and Ayan, S. Photodynamic therapy - Current limitations and novel approaches. *Front. Chem*. **2021**, 9, 400.

126. Lucky, S. S., Soo, K. C. and Zhang, Y. Nanoparticles in photodynamic therapy. *Chem. Rev*. **2015**,115, 1990-2042.

127. Jiang, Z., Shao, J., Yang, T., Wang, J. and Jia, L. Pharmaceutical development, composition and quantitative analysis of phthalocyanine as the photosensitizer for cancer photodynamic therapy. *J. Pharm. Biomed. Anal*. **2014**, 87, 98-104.

128. Huang, H., Yu, B., Zhang, P., Huang, J., Chen, Y., Gasser, G., Ji, L. and Chao, H. Highly charged ruthenium (II) polypyridyl complexes as lysosome-localized photosensitizers for two-photon photodynamic therapy. *Angew. Chem. Int. Ed*. **2015**, 54, 14049-14052.

129. Dubuc, C., Langlois, R., Bénard, F., Cauchon, N., Klarskov, K., Tone, P. and van Lier, J. E. Targeting gastrin-releasing peptide receptors of prostate cancer cells for photodynamic therapy with a phthalocyanine–bombesin conjugate. *Bioorg. Med. Chem. Lett*. **2008**, 18, 2424-2427.

130. Liang, G., Wang, L., Yang, Z., Koon, H., Mak, N., Chang, C. K. and Xu, B. Using enzymatic reactions to enhance the photodynamic therapy effect of porphyrin dityrosine phosphates. *Chem. Comm*. **2006**, 48, 5021-5023.

131. Patra, M., Joshi, T., Pierroz, V., Ingram, K., Kaiser, M., Ferrari, S., Spingler, B., Keiser, J. and Gasser, G. DMSO-Mediated Ligand Dissociation: Renaissance for Biological Activity of N-Heterocyclic-[Ru(η6-arene)Cl2] Drug Candidates. *Chem. Eur. J*. **2013**, 19, 14768-14772.

132. Hockel, M. and Vaupel, P. Tumor hypoxia: definitions and current clinical, biologic, and molecular aspects. *J. Natl. Cancer Inst*. **2001**, 93, 266-276.

133. Vaupel, P., Mayer, A. and Höckel, M. Tumor hypoxia and malignant progression. *Methods Enzymol*. **2004**, 381, 335-354.

134. Maier, A., Tomaselli, F., Anegg, U., Rehak, P., Fell, B., Luznik, S., Pinter, H., Smolle-Jüttner, F. M. Combined photodynamic therapy and hyperbaric oxygenation in carcinoma of the esophagus and the esophago-gastric junction. *Eur. J. Cardiothorac. Surg*. **2000**, 18, 649-655.

135. Bonnett, R., Djelal, B. D., and Nguyen, A. Physical and chemical studies related to the development of m-THPC (FOSCAN®) for the photodynamic therapy (PDT) of tumours. *J. Porphyr. Phthaloc*. **2001**, *5*, 652-661.

136. Kaspler, P., Lazic, S., Forward, S., Arenas, Y., Mandel, A. and Lilge, L. A ruthenium (ii) based photosensitizer and transferrin complexes enhance photo-physical properties, cell uptake, and photodynamic therapy safety and efficacy. *Photochem. Photobiol. Sci*. **2016**, 15, 481-495.

137. Lv, Z., Wei, H., Li, Q., Su, X., Liu, S., Zhang, K. Y., Lv, W., Zhao, Q., Li, X. and Huang, W. Achieving efficient photodynamic therapy under both normoxia and hypoxia using cyclometalated Ru (ii) photosensitizer through type I photochemical process. *Chem. Sci*. **2018**, 9, 502-512.

138. Yano, T., Hishida, S., Nakai, M. and Nakabayashi, Y. Anticancer activity of heterodinuclear ruthenium (II)–platinum (II) complexes as photochemotherapeutic agents. *Inorganica Chim. Acta*. **2017**, 454, 162-170.

139. Lei, W., Zhou, Q., Jiang, G., Zhang, B. and Wang, X. Photodynamic inactivation of Escherichia coli by Ru (II) complexes. *Photochem. Photobiol. Sci*. **2011**, 10, 887-890.

140. Huang, H., Zhang, P., Yu, B., Jin, C., Ji, L. and Chao, H. Synthesis, characterization and biological evaluation of mixed-ligand ruthenium (II) complexes for photodynamic therapy. *Dalton Trans*. **2015**, 44, 17335-17345.

141. Schmitt, F., Govindaswamy, P., Süss-Fink, G., Ang, W. H., Dyson, P. J., Juillerat-Jeanneret, L. and Therrien, B. Synthesis, characterization and biological evaluation of mixed-ligand ruthenium (II) complexes for photodynamic therapy. *J. Med. Chem*. **2008**, 51, 1811-1816.

142. Therrien, B., and Furrer, J. The biological side of water-soluble arene ruthenium assemblies. *Adv. Chem. Eng*. **2014**, 2014, 1-20.

143. Bogoeva, V., Siksjø, M., Sæterbø, K. G., Melø, T. B., Bjørkøy, A., Lindgren, M. and Gederaas, O. A. Ruthenium porphyrin-induced photodamage in bladder cancer cells. *Photodiagn. Photodyn. Ther*. **2016**, 14, 9-17.

144. Čubrilo, J., Hartenbach, I., Schleid, T. and Winter, R. F. Z. Tethering versus Non-Coordination of Hydroxy and Methoxy Side Chains in Arene Half Sandwich Dichloro Ruthenium Complexes. *Anorg. Allg. Chem*. **2006**, 632, 400-408.

145. Govindaswamy, P., Süss-Fink, G. and Therrien, B. Self-Assembled Chloro-Bridged (Arene) ruthenium Metallo-Prisms: Synthesis and Molecular Structure of Cationic Complexes of the Type $[Ru_6(\eta^6\text{-arene})_6(\mu^3\text{-tpt-}\kappa N)_2(\mu\text{-Cl})_6]^{6+}$ (tpt=2,4,6-tris(pyridinyl)-1,3,5-triazine). *Organometallics*. **2007**, 26, 915-924.

146. Stringer, T., Therrien, B., Hendricks, D. T., Guzgay, H. and Smith, G. S. Mono-and dinuclear (η6-arene) ruthenium (II) benzaldehyde thiosemicarbazone complexes: Synthesis, characterization and cytotoxicity. *Inorg. Chem. Commun*. **2011**, 14, 956-960.

147. Gupta, G., Yap, G. P., Therrien, B. and Rao, K. M. Study of novel η5-cyclopentadienyl and η6-arene platinum group metal complexes containing a N4-type ligand and their structural characterization. *Polyhedron*. **2009**, 28, 844-850.

148. Kota, T. P. and Kollipara, M. R. Synthesis and structural study of platinum group metal complexes containing pyrimidine bridged pyrazolyl-pyridine ligand and η^5 and η^6–cyclic hydrocarbons. *J. Chem. Sci*. **2014**, 126, 1143-1151.

149. Gomes, A. C., Mello, A. L., Ribeiro, M. G., Garcia, D. G., Da Fonseca, C. O., Salazar, M. D. A., Schönthal, A. H. and Quirico-Santos, T. Perillyl alcohol, a pleiotropic natural compound suitable for brain tumor therapy, targets free radicals. *Arch. Immunol. Ther. Exp*. **2017**, 65, 285-297.

150. Mroz, P., Bhaumik, J., Dogutan, D. K., Aly, Z., Kamal, Z., Khalid, L., Kee, H. L., Bocian, D. F., Holten, D., Lindsey, J. S. and Hamblin, M. R. Imidazole metalloporphyrins as

photosensitizers for photodynamic therapy: role of molecular charge, central metal and hydroxyl radical production. *Cancer lett*. **2009**, 282, 63-76.

151. Jones, H. J., Vernon, D. I., and Brown, S. B. Photodynamic therapy effect of m-THPC (Foscan®) in vivo: correlation with pharmacokinetics. *Br. J. Cancer*. **2003**, 89, 398-404.

152. Meier, D., Botter, S. M., Campanile, C., Robl, B., Gräfe, S., Pellegrini, G., Born, W. and Fuchs, B. Foscan and foslip based photodynamic therapy in osteosarcoma in vitro and in intratibial mouse models. *Int. J. Cancer*. **2017**, 140, 1680-1692.

153. Senge, M. O. and Brandt, J. C. Temoporfin (Foscan®, 5, 10, 15, 20-tetra (m-hydroxyphenyl) chlorin) - a second-generation photosensitizer. *Photochem. Photobiol*. **2011**, 87, 1240-1296.

154. Barry, N. P., Edafe, F. and Therrien, B. Anticancer activity of tetracationic arene ruthenium metalla-cycles. *Dalton Trans*. **2011**, *40*, 7172-7180.

155. Xu, F., Zhu, X. H., Shen, Q., Lu, J. and Li, J. Q. Catalytic cyclotrimerization of arylnitriles using the novel samarium (II) complexes as catalysts. *Chin. J. Chem*. **2002**, *20*, 1334–1339.

156. Amoroso, A. J., Thompson, A. M. C., Maher, J. P., McCleverty, J. A. and Ward, M. D. Di-, tri-, and tetranucleating pyridyl ligands which Facilitate multicenter magnetic exchange between paramagnetic molybdenum centers. *Inorg. Chem*. **1995**, *34*, 4828–4835.

157. Wang, L., Tao, X. T., Yang, J. X., Yu, W. T., Ren, Y., Xin, Q., Liu, Z. and Jiang, M. H. Synthesis, structure and two-photon absorption properties of a new multi-branched compound, 1, 2, 4, 5-tetrakis (4-pyridylvinyl) benzene. *J. Solid State Chem*. **2004**, *177*, 4293–4299.

158. Freudenreich, J., Dalvit, C., Süss-Fink, G. and Therrien, B. Encapsulation of photosensitizers in hexa-and octanuclear organometallic cages: Synthesis and characterization of carceplex and host–guest systems in solution. *Organometallics*. **2013**, 32, 3018–3033.

159. Dogutan, D. K., Ptaszek, M. and Lindsey, J. S. Direct synthesis of magnesium porphine via 1-formyldipyrromethane. *J. Org. Chem*. **2007**, 72, 5008–5011.

160. Arnett, F. C., Edworthy, S. M., Bloch, D. A., Mcshane, D. J., Fries, J. F., Cooper, N. S., Healey, L. A., Kaplan, S. R., Liang, M. H., Luthra, H. S., Medsger, T. A., Mitchell, D. M., Neustadt, D. H., Pinals, R. S., Schaller, J. G., Sharp, J. T., Wilder, R. L. and Hunder, G. G. The American Rheumatism Association 1987 revised criteria for the classification of rheumatoid arthritis. *Arthritis Rheumatol*. **1988**, 31, 315-324.

161. Liagre, B., Vergne-Salle, P., Corbiere, C., Charissoux, J. L. and Beneytout, J. L. Diosgenin, a plant steroid, induces apoptosis in human rheumatoid arthritis synoviocytes with cyclooxygenase-2 overexpression. *Arthritis Res. Ther*. **2004**, 6, 1-11.

162. Glant, T. T., Jacobs, J. J., Molnár, G., Shanbhag, A. S., Valyon, M. and Galante, J. O. Bone resorption activity of particulate-stimulated macrophages. *J. Bone Miner. Res*. **1993**, 8, 1071-1079.

163. Bonnet, C., Bertin, P., Cook-Moreau, J., Chable-Rabinovitch, H., Treves, R. and Rigaud, M. Lipoxygenase products and expression of 5-lipoxygenase and 5-lipoxygenase-activating protein in human cultured synovial cells. *Prostaglandins*. **1995**, 50, 127-135.

Abbreviations

COX-2 - cyclooxygenase-2

DMSO - dimethyl sulfoxide

FLS - fibroblast-like synoviocyte

HOMO - highest occupied molecular orbital

IL - interleukin

LUMO - lowest unoccupied molecular orbital

MTT - 3-(4,5-Dimethylthiazol-2-yl)-2,5-diphenyltetrazolium bromide

PDT - photodynamic therapy

PGE_2 - prostaglandin E_2

PI - phototoxic index

PS - photosensitizer

r.t. - room temperature

RA - rheumatoid arthritis

ROS - radical oxygen species

TPyP - tetra(4-pyridyl)porphine

List of publications

- Gallardo-Villagrán, M., Leger, D. Y., Liagre, B. and Therrien, B. Photosensitizers used in the photodynamic therapy of rheumatoid arthritis. *Int. J. Mol. Sci.* **2019**, 20, 3339.

- Gallardo-Villagran, M., Paulus, Champavier, Y., Leger, D. Y., Therrien, B. and Liagre, B. Combination of tetrapyridylporphyrins and arene ruthenium (II) complexes to treat synovial sarcoma by photodynamic therapy. *J. Porphyr. Phthalocyanines.* **2021**, A-I.

- Gallardo-Villagrán, M., Paulus, L., Charissoux, J. L., Sutour, S., Vergne-Salle, P., Leger, D. Y., Liagre, B. and Therrien, B. Evaluation of ruthenium-based assemblies as carriers of photosensitizers to treat rheumatoid arthritis by photodynamic therapy. *Pharmaceutics.* **2021**,13, 2104.

- Ruthenium-based assemblies incorporating tetrapyridylporphyrin panels: A photosensitizers delivery strategy for the treatment of rheumatoid arthritis by photodynamic therapy. *In preparation.*

- Toxicity of dimethyl sulfoxide in human fibroblast-like synoviocyte. *In preparation.*

ANNEX

(Published versions of papers from the thesis project)

Review

Photosensitizers Used in the Photodynamic Therapy of Rheumatoid Arthritis

Manuel Gallardo-Villagrán [1,2] [iD]**, David Yannick Leger** [1,]*****, Bertrand Liagre** [1,]***** [iD] **and Bruno Therrien** [2,]***** [iD]

[1] Laboratoire PEIRENE, Faculté de Pharmacie, Université de Limoges, EA 7500, F-87025 Limoges, France
[2] Institut de Chimie, Université de Neuchâtel, Avenue de Bellevaux 51, CH-2000 Neuchâtel, Switzerland
***** Correspondence: david.leger@unilim.fr (D.Y.L.); bertrand.liagre@unilim.fr (B.L.); bruno.therrien@unine.ch (B.T.)

check for updates

Abstract: Photodynamic Therapy (PDT) has become one of the most promising treatment against autoimmune diseases, such as rheumatoid arthritis (RA), as well as in the treatment of different types of cancer, since it is a non-invasive method and easy to carry out. The three main ingredients of PDT are light irradiation, oxygen, and a photosensitizer (PS). Light irradiation depends on the type of molecule or compound to be used as a PS. The concentration of O_2 fluctuates according to the medium where the target tissue is located and over time, although it is known that it is possible to provide oxygenated species to the treated area through the PS itself. Finally, each PS has its own characteristics, the efficacy of which depends on multiple factors, such as solubility, administration technique, retention time, stability, excitation wavelength, biocompatibility, and clearance, among others. Therefore, it is essential to have a thorough knowledge of the disease to select the best PS for a specific target, such as RA. In this review we will present the PSs used in the last three decades to treat RA under PDT protocol, as well as insights on the relevant strategies.

Keywords: photodynamic therapy; rheumatoid arthritis; photosensitizers; porphyrins; tetrapyrroles; nanoparticles

1. Background

1.1. Photodynamic Therapy Principle

Some compounds are known to absorb the energy they receive from light to reach higher excited states. This energy can be transferred to other substances or molecules, thus allowing the excited compound to return to its initial state of minimal energy [1]. Photodynamic therapy (PDT) is based on this principle, in which designed photoactive chemical compounds, known as photosensitizers (PSs), are injected into tissues and then irradiated at a certain wavelength to reach an excited energy level. The absorbed energy can then be transferred directly to neighboring molecules, such as O_2, giving rise to singlet oxygen, which in turn gives rise to radical oxygen species (ROS). This phenomenon is associated with the type II mechanism (Figure 1). The type I mechanism involves the transmission of the PS energy to a substrate or biomolecule, and, from this intermediate, the energy is forwarded to oxygen, giving rise again to ROS. In both cases, ROS induce cell death by apoptosis or necrosis, thus making PDT interesting for the treatment of several diseases [2–7].
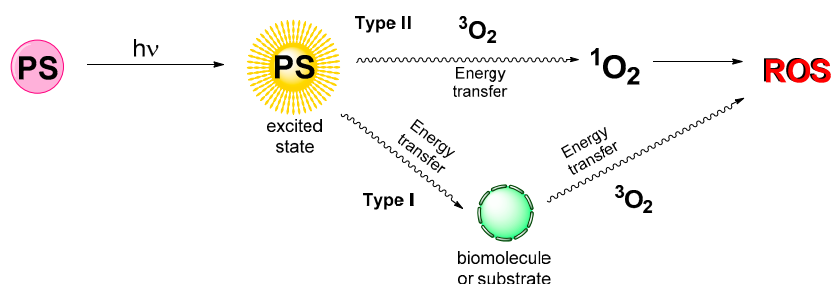
Figure 1. Standard Photodynamic Therapy (PDT) process involving a photosensitizer (PS), oxygen, and light.

1.2. Rheumatoid Arthritis

Rheumatoid arthritis (RA) is a chronic inflammatory autoimmune disease that can affect multiple organ systems. It is considered a disease of the joints, attacking mainly the wrists and the metacarpophalangeal and proximal interphalangeal joints of the hands. RA is characterized by synovial inflammation and hyperplasia, autoantibody production (particularly to rheumatoid factor and citrullinated peptide), and cartilage and bone destruction [8]. The etiology of RA remains mainly unknown, but the clinical features of RA seems to be the consequence of interactions between environmental factors, including smoking, diet, obesity, infections and microbiota, as well as genetic predisposition (histocompatibility complex, cytokines, chemokines, and growth factor genes) to autoimmune responses [9,10].

Many of the newly developed treatments and drugs for RA have focused on inducing the cell death of fibroblast-like synoviocytes (FLS) by reducing and stopping their proliferation. Studies suggest that this proliferation is linked to the activation of certain intracellular signaling pathways [8,11]. Such inflammation, if not treated in time, leads to the appearance of hyper-vascularization and damage to cartilage and bones by erosion, which causes joint pain and reduced mobility. Since standard treatments against RA, such as synovectomy, are invasive, destructive, and involve long rehabilitation periods, in recent decades, less invasive treatments have been explored [12–14].

To date, the current treatment strategy is to initiate aggressive therapy by applying antirheumatic drugs (DMARDs) and to escalate the therapy, guided by an assessment of the disease's activity [12]. DMARDs reduce the rate of erosive changes and, therefore, have the potential to alter the disease's course by preventing irreversible damage. However, conventional and biologic disease modifying therapies sometimes fail or produce only partial responses and, consequently, clinical remission is rarely achieved.

In this context, alternative or complementary therapies could be of interest. PDT is a new therapy that could improve the well-being of patients and increase the possibility of clinical remission. Therefore, PDT treatment, regardless of the photosensitizer used, aims to induce cell death in cells involved in inflammation and hyperplasia in the joint. In combination with standard treatments, PDT would enhance the control of cartilage and bone destruction in the treated joint. Consequently, the constant development of new photosensitizers, and the improvement of cell targeting, could, in the future, allow the use of PDT in the initiation of RA treatment. The effectiveness of PDT in the treatment of RA depends on multiple factors, most of them being directly related to the type of PS used. Solubility, retention time, excitation wavelength, elimination, transport, and cytotoxicity are some of the factors to consider when choosing a PS for PDT.

Therefore, in this review, we want to gather all the compounds used as a PS in the treatment of RA by PDT. An emphasis on the factors influencing the efficiency of the PS is given, to illustrate the advantages and limitations of each of them. Overall, we want to provide to researchers in the fields of PDT and RA an overview of the actual state of the art, as well as new avenues for designing the next generation of photosensitizers for the treatment of RA by photodynamic therapy.

2. Photosensitizers Used to Treat Rheumatoid Arthritis

2.1. First Generation of Photosensitizers

Undoubtedly, the first and the most studied PS to treat RA by PDT is benzoporphyrin monoacid ring A (BPD-MA) [15], a tetrapyrrole derivative with alkyl, methanoate, and carboxylic groups at its periphery (Figure 2). In 1994, Ratkay and co-workers demonstrated the efficacy of using a PS to ameliorate the symptoms associated with RA [16]. In this pioneering study, BPD-MA was administered by intravenous injection (5% dextrose in water), in doses of 0.5 mg/kg body weight, in Murphy Roths Large (MRL)-lpr mice treated with Freund's complete adjuvant (FCA) to enhance RA. After an incubation period, the animals were irradiated under red light (λ = 690 nm) at an 80 J/cm^3 trans-cutaneous light dose (LiD) of the whole body at day 0, 10, and 20 of a 30 day treatment. The result of this PDT protocol was compared to those of the three clinically used treatments at the time, indomethacin, cyclosporin A, and 3 Gy sub-lethal whole body irradiation (WBI). The outcome showed that the effectiveness of the PDT treatment was comparable to those obtained with conventional treatments, with no apparent side effects.
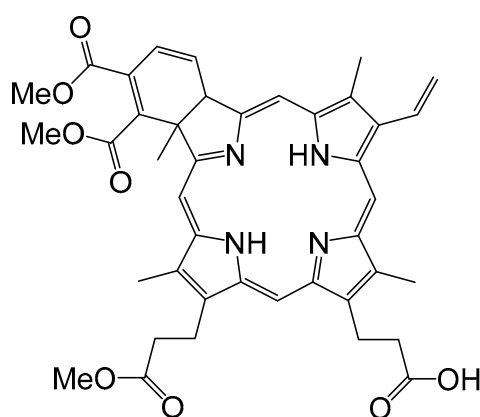
Figure 2. Molecular structure of benzoporphyrin monoacid ring A (BPD-MA).

In the conventional treatments, undesirable side effects occur, such as an increase of proteinuria in the case of indomethacin, or the aggravation of arthritis when low doses of cyclosporin A and WBI are applied. On the other hand, after administration of BPD-MA and light irradiation, only positive responses of the symptoms of RA were observed, including a reduction of pannus formation, a reduction of cartilage and bone destruction, the maintenance of normal survival rate, and no lymph-proliferation or proteinuria [16]. The absence of side effects is probably related to the fast captured of BPD-MA by synovial tissues and the relatively short retention time of the compound, two prerequisites for reducing side effects related to the PS, and especially skin photosensitivity [17]. Moreover, with an excitation wavelength at 690 nm, excellent light penetration in the tissues was obtained, thus making trans-cutaneous irradiation possible. This initial study confirmed the potential of PDT to treat RA.

A few years later, the same research group extended their investigation on BPD-MA by comparing intra-articular and intravenous administration, as well as intra-articular and trans-cutaneous irradiation [18]. The results found for the different administrations of the drug and the different techniques used for light irradiation were remarkable. Intravenous administration resulted in a rapid uptake of BPD-MA in the vascularized tissue, like the synovium, muscles, and skin, and a very low or negligible uptake in cartilages and tendons. The clearance of the drug in the synovium was very fast, which is why a rapid exposure to light is essential for an effective treatment. On the other hand, when intra-articular administration was applied, high uptake and slower clearance were observed, which allowed subjects to maintain a greater control of the concentration of the drug in the joint, in addition to a greater flexibility in the delay between injection and irradiation. The better uptake

associated with intra-articular administration ensures that the drug reaches the target tissues, thus making trans-cutaneous irradiation safer and as efficient as the intra-articular irradiation. Moreover, additional studies showed that trans-cutaneous irradiation of skin and muscles containing a small amount of BPD-MA did not cause damage and still reduced the inflammation of the joint [19].

The same year, Trauner et al. published a similar study on BPD-MA and the results were complementary to the previous one [20]. In this specific study, more data concerning the uptake of BPD-MA in tissues were compiled. The concentration peak in the synovium was reached after 15 min (intravenous injection of 2 mg/kg), and after 3 h, the concentration was 0.35 µg/g of tissue, which is within the therapeutic range (0.01–0.50 µg/g of tissue) [21]. A similar concentration was found in the muscles 3 h after intravenous administration, with no muscle necrosis being observed in rabbits after four weeks following treatment. The concentration in the skin after 3 h was 0.137 µg/g of tissue, which forced the animal to be protected from sunlight after treatment for at least 24 h. In blood serum, the concentration of BPD-MA was 89 µg/g. However, it drastically decreased within 5 min. No uptake was observed in the meniscus, bones, and tendons, and only a small uptake was seen in the cartilage, but no necrosis was observed, possibly as a consequence of the low concentration of oxygen in such tissues. In these experiments, 20 min of intra-articular irradiation was performed, corresponding to an LiD of 100 J/cm^2. This irradiation technique allowed a spatial control of the irradiated region, thus providing a selective destruction of the inflamed synovium without affecting the rest of the surrounding tissues.

The chemical structures of PSs are diverse, and, accordingly, the biological behavior of tetrapyrrole-based photosensitizers can be quite different from one to the other. For instance, some of the first hematoporphyrins used for photodynamic treatments, such as the hematoporphyrin Photofrin (whose structure is a mixture of oligomers and will be discussed later) showed a slow immunosuppressive effect [22], giving rise to long periods of photosensitivity in the skin after treatment, which limits the possibility of repeated treatments. In addition, the wavelength necessary to activate Photofrin (630–635 nm) did not show much depth, which invalidates the application of light by trans-cutaneous irradiation. In contrast, the so called second generation of PSs, like the aforementioned BPD-MA or other porphyrins such as tetra(4-carboxyphenyl)porphyrin, have a well-defined structure and a shorter retention time. Within approximately 72 h, 99% of the BPD-MA dose vanished from the patient's body, and, as described before, the wavelength necessary to activate the BPD-MA is usually 690 nm, which shows a deeper light penetration.

A subsequent study by Hendrich et al. focused on treatments with BPD-MA [23], using intra-articular irradiation with a cylindrical light diffuser (photodynamic laser therapy, 690 nm) after an intravenously injection of 2 mg/kg of the derived hematoporphyrin. Two different light doses were applied, 180 J and 470 J. Complete necrosis was observed in 67% of the joints of the treated rabbits at 470 J, whereas with the lower dose, 60% of the treated animals showed necrotic tissues. In both cases, cartilage, tendons, menisci, and ligaments were unaffected. The administration of the drug without subsequent irradiation did not have a therapeutic effect in the joints after 1 week, nor did the irradiation at 470 J alone without BPD-MA. This new study showed that the cytotoxic effect of PDT depends predominantly on the light dose applied to the patient, at least in the case of BPD-MA.

Overall, these multiple studies on BPD-MA emphasize the difficulty of determining the optimal conditions in PDT, as several factors (PS, administration, type of irradiation, wavelength, and injection-time-delay) play a crucial role in the results. Therefore, taking a systems biology approach is an elegant method to rapidly screen various factors without having to run hundreds of experiments [24].

Photofrin is one of the most successful PSs in PDT [25–30], despite some drawbacks and having a poorly defined structure (Figure 3). Photofrin belongs to the first generation of PSs, and because it is food and drug administration (FDA) approved to treat cancers (esophageal cancer, non-small cell lung cancer, gastric cancer, bladder cancer, and cervical cancer), it is not surprising that photofrin has been tested as a PS to treat RA.
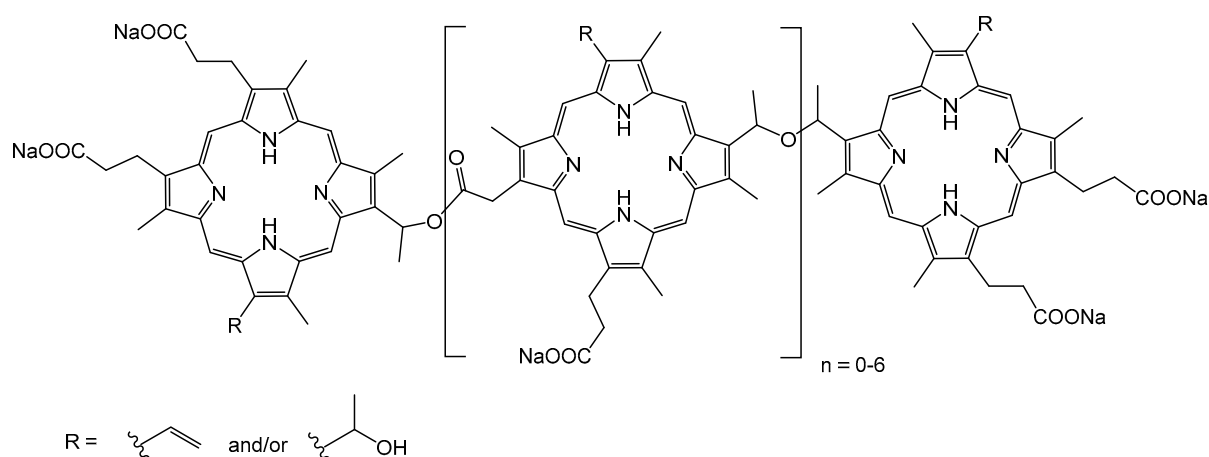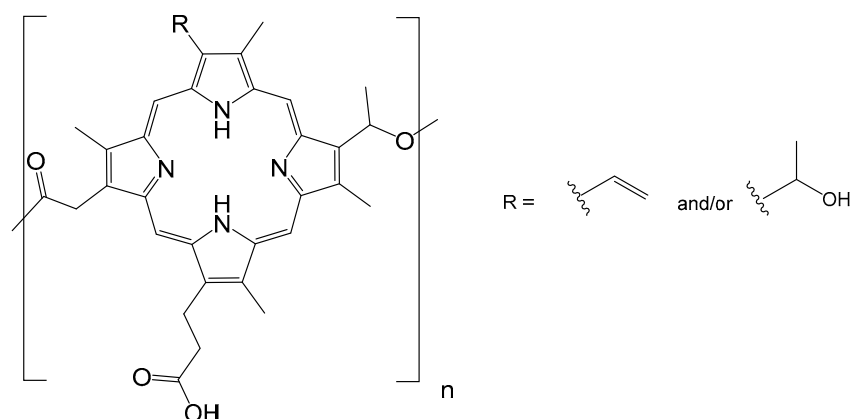
Figure 3. Structure of Photofrin [31].

In parallel to their study on BPD-MA, Trauner and co-workers evaluated the use of Photofrin as a PS in PDT to treat RA in New Zealand white rabbits with antigen-induced arthritis [32]. The study was divided into three parts: the distribution of Photofrin in the body, the evaluation of PDT by bare cleaved fiber irradiation, and the evaluation of PDT by diffusion tip fiber irradiation. Regarding distribution and accumulation, 2 mg/kg of PS were injected intravenously into the rabbit. The maximum peak in the synovium was observed at 48 h after injection, where the concentration reached 3.32 μg/g, which is within the therapeutic window. In addition, they found one-third of the concentration in the skin, a concentration that requires protection of the skin from sunlight for at least a month. Regarding the mode of activation, the results of the PDT were discordant. The irradiation dose was provided for 20 min at 630 nm, with an intensity of 100 J/cm^2. When a bare clear fiber was used, only 17% of the treated rabbits showed synovial necrosis two weeks after treatment. In contrast, when a diffusion tip fiber was used, 43% of the animals presented synovial necrosis after two weeks and 38% after four weeks. The authors assume that this lack of uniformity could be due to several reasons, such as the low control over the orientation and homogeneity of the light that generates the bare clear fiber or the non-uniform distribution of the PS. However, they emphasize that only the synovial tissue suffered necrosis; no necrosis was observed in the cartilage or other adjacent tissues. In addition, the authors mentioned that the treatment causes additional inflammation in the joint, although the inflammation disappeared within a week after treatment.

The next compound from the first generation of PSs evaluated as PDT agents against RA was Photosan-3 (Figure 4). This analogue to Photofrin is commonly used in PDT to treat cancer (human glioma, squamous carcinoma, gynecological cancers, head and neck cancers, and pancreatic cancers) [33–36]. Interestingly, for this in vitro study with Photosan-3, cells from human synovial fibroblasts, the most abundant cells in swollen synovial tissues [37], were cultured and tested for the first time under a PDT protocol [38]. More precisely, in a petri dish cultured with human synovial fibroblast cells, Photosan-3 was added at different concentrations. Then, visible light ($\lambda = 630$ nm) was applied for 2 h, which corresponded to a light dose of 2 J/cm^2. Cell survival was determined 24 h after exposure to light. The results showed a different cytotoxicity depending on the concentration of the PS. Complete phototoxicity was achieved at a concentration of 10 μg/mL of PS. Control experiments (only light exposure without Photosan-3 and Photosan-3 without application of light) showed no cellular effect from the light and low cellular cytotoxicity of the PS.

Following this in vitro study, two years later, the same research group performed in vivo experiments with Photosan-3 to treat rabbits with immunoglobin-G-induced arthritis [39]. Intravenous and intra-articular administration of drugs, followed by laser irradiation at 630 nm, were the conditions used. The results showed a complete destruction of the swollen synovial membrane and no changes in

menisci, ligaments, and cartilage, confirming the applicability of this treatment in vivo. Moreover, this study highlighted the efficacy of this treatment in small joints by photodynamic laser therapy.


Figure 4. Monomeric structure of Photosan-3.

2.2. Second Generation of Photosensitizers

Protoporphyrin IX (PpIX) is certainly the most common tetrapyrrole found in nature [40]. It forms the skeleton of the heme in organic compounds, which is of vital importance in cellular metabolism, acting also as a gas transporter and as a catalyst for metabolic reactions, among other functions. This tetrapyrrole has been widely used in PDT treatments against cancers [40], as well as in other autoimmune diseases, such as RA. In nature, the precursor of PpIX is 5-aminolevulinic acid (ALA), as illustrated in Scheme 1 [41,42]. It has been demonstrated that the formation of PpIX from 5-aminolevulinic acid (ALA) is much higher in neoplastic tissues than in normal tissues [43]. In addition, lipophilic ALA derivatives, such as 5-aminolevulinic acid hexyl ester (h-ALA), increase the formation of PpIX in cells [44]. Based on these two premises, So et al. carried out a study where they examined the formation, accumulation and cytotoxicity of PpIX in vivo (synovial tissue of mice with induced RA) and in vitro (human cells from patients with RA) [45].

The protocol of the in vivo study involved an intra-articular injection (30 μL of an 8 mM solution of h-ALA) in the infected joints, followed by trans-cutaneous irradiation at 635 nm, 3 h post-injection. The accumulation of the PS was analyzed by fluorescence microscopy. Accumulation and formation of PpIX were only observed in the animals with RA, not in healthy animals. They also incubated human synovial tissues with h-ALA and studied the conversion to PpIX, observing an accumulation of PpIX in different cellular organelles, especially in the synovial lining layer, vascular endothelium, and macrophages. In both cases, cell necrosis was higher in the tissues where the accumulation of PpIX was maximal. A light dose of 5 J/cm^2 was necessary to obtain significant results, namely a reduction of inflammation and damage to the cartilage. However, when the light dose was reduced to 2 J/cm^2, no significant effects were observed.

Distribution and accumulation of PpIX after the administration of ALA has also been studied on rabbits with rheumatoid mono-arthritis induced in one joint (keeping the other joint untouched) [46]. Administration of ALA was carried out both intravenously and intra-articularly, and then the joints were analyzed by fluorescence to determine the accumulation of PpIX during the first 5 h post-injection. The study showed a greater accumulation of porphyrin in the tissue of the inflamed joint—twice as much as healthy joints. The maximum peak of accumulation of PpIX occurred between 2–3 h after the injection of ALA. It should be noted that traces of porphyrins were detected even before the addition of ALA. This residual fluorescence was associated with naturally occurring PS. The accumulation of porphyrins was not restricted only to the infected joints, since fluorescence was also detected in the belly and back of the treated animals. A post-mortem analysis of the animals revealed that in the synovial tissue of the inflamed joint, a high concentration of PpIX was obtained, while only traces

of porphyrin were detected in the skin, tendons, and cartilage. Moreover, PpIX was not detected in healthy joints, except in cartilage (one third of the cartilage of the infected joint). Surprisingly, the porphyrin detected in the cartilage was not PpIX, whose absorbance band is different. Localization in the cartilage suggests a more hydrophilic porphyrin. This result may be due to the fact that the greater solubility of hydrophilic porphyrins facilitates clearance from the synovium, which is not the case with cartilage. Otherwise, no significant differences between the results obtained by intra-articular and intravenous injection were observed.
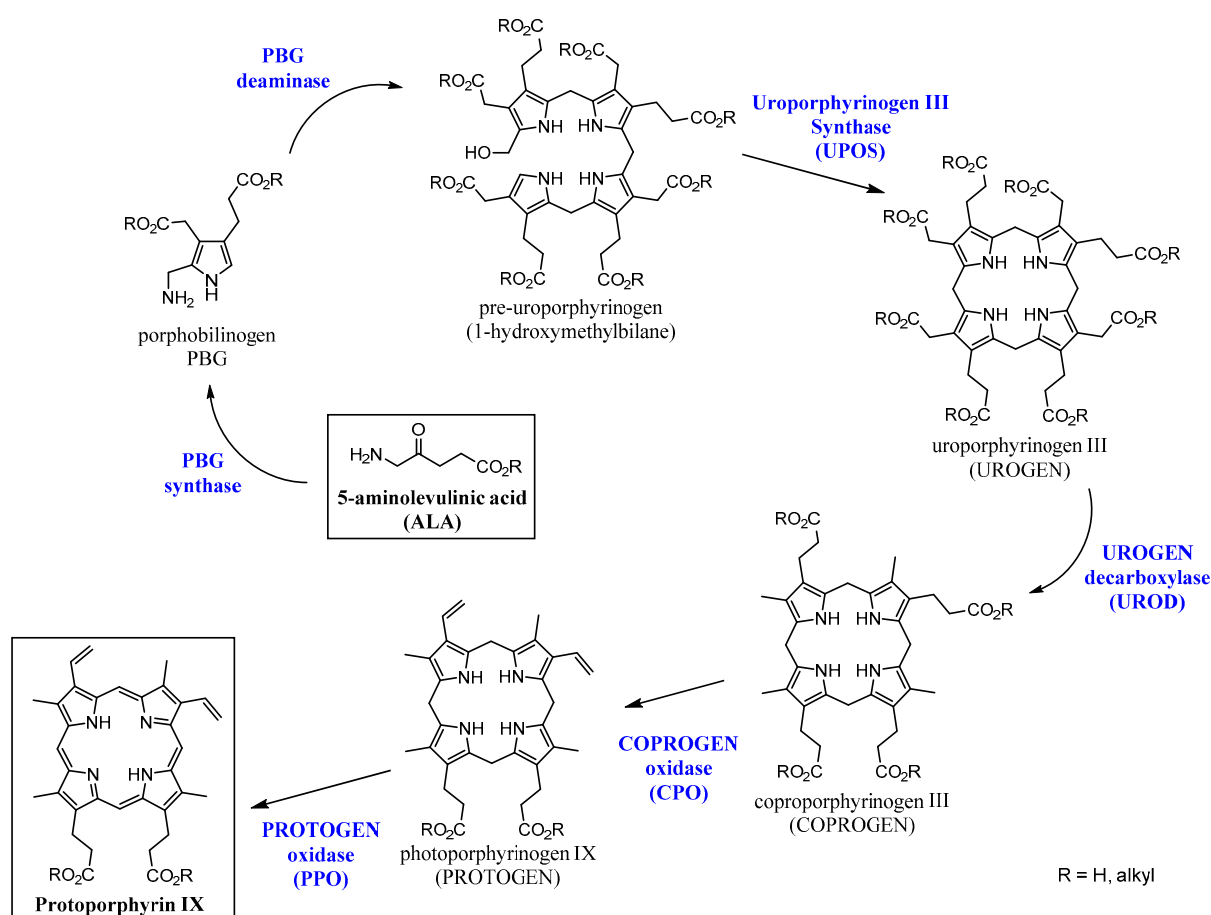

Scheme 1. Intracellular synthesis of Protoporphyrin IX (PpIX) from 5-aminolevulinic acid [41,42].

With the aim of finding a less invasive, simpler, and safer treatment against RA, Nishida et al. investigated the use of [Na][ATX-S10] as a PS in PDT [47]. This compound consisted of a sodium salt whose organic part was constituted by a tetrapyrrole frame (Figure 5). This hydrophilic salt was completely eliminated from the body in less than 48 h, thereby reducing the patient's photosensitization. In addition, it may be possible to use trans-cutaneous irradiation, since the excitation of this PS is performed at 670 nm, so it is more penetrating than those of the first generation of PSs. The study was conducted in vitro in human RA fibroblast-like synoviocytes (FLS) and in vivo in mice with induced RA. With respect to FLS cells, a large number of apoptotic cells were observed after administration of [Na][ATX-S10] and irradiation. The effectiveness of the treatment depended mainly on the concentration of the PS and the dose of irradiation. These in vitro assays showed that the PS accumulates predominantly in lysosomes. For the in vivo study, again, it was observed that the effectiveness of the treatment depends on the concentration of the PS and the dose of irradiation. In both cases, the affinity of [Na][ATX-S10] was demonstrated by an accumulation in the target tissue. In vivo, a dose of 10 mg/kg of [Na][ATX-S10] and irradiation at 670 nm of 10 J/cm^2 three hours after intravenous administration of the drug were necessary to achieve significant phototoxicity.
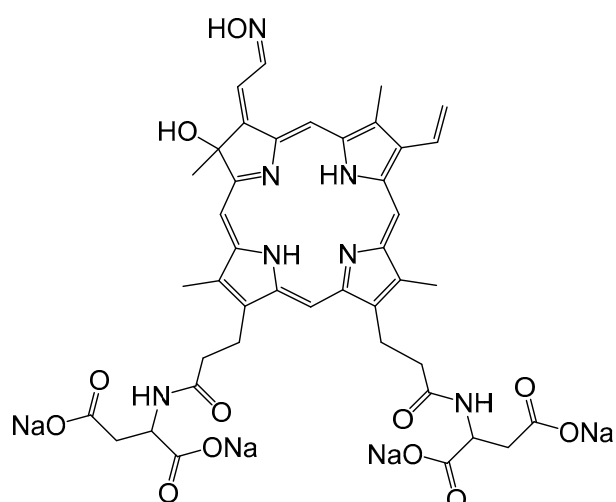
Figure 5. Molecular structure of [Na][ATX-S10].

Another porphyrin sodium salt, already used in PDT for the treatment of cancer, is Talaporfin sodium, whose structure is presented in Figure 6. In 2008, Talaporfin sodium was used as a PS in PDT against RA [48]. The study was carried out in vitro and in vivo, assessing, under different conditions, both the PS localization and the cytotoxic effect. The intracellular localization of Talaporfin sodium after administration in FLS cells showed accumulation in lysosomes. The activity of dehydrogenase in mitochondria (MTT assay, MTT = 3-(4,5-dimethylthiazol-2-yl)-2,5-diphenyltetrazolium bromide) was also determined to assess cell viability. The PS was added in amounts of 0–100 μg/mL, and after 4 h the culture was washed. Frontal irradiation at 664 nm at different energies (0, 2.5, 5, 10, and 20 J/cm^2) was then performed. After 24 h, an MTT assay was carried out. The study found a clear phototoxicity dependence between the PS concentration and the irradiation dose. When a concentration of 25 μg/mL and an irradiation of 10 J/cm^2 were applied, 50% inhibition was obtained. Likewise, when 50 μg/mL and 5 J/cm^2 were used, 50% inhibition of cell viability was observed. However, with the highest concentration (50 μg/mL) and the strongest irradiation dose (10 J/cm^2), the inhibition reached 80%.
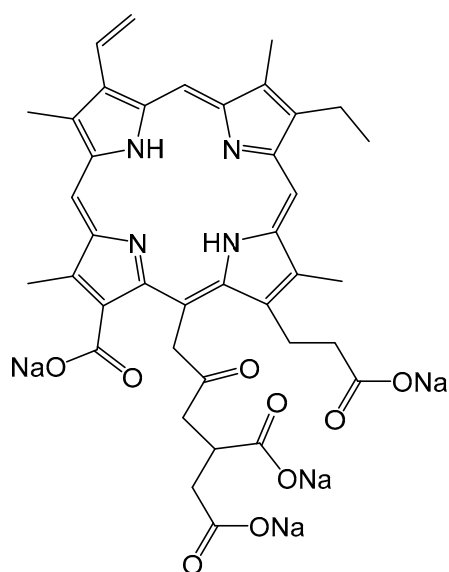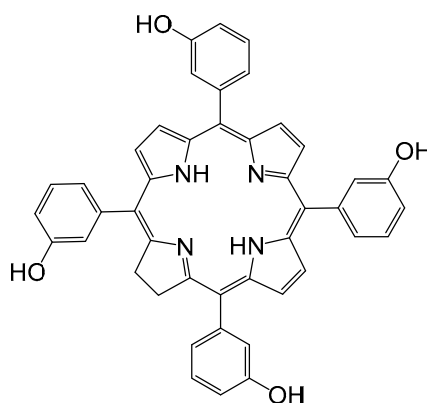

Figure 6. Molecular structure of Talaporfin sodium.

Similarly, the activity of Talaporfin sodium on human RA synovial membranes implanted in the back of mice with severe combined immunodeficiency (SCID) was evaluated [48]. Mice were

divided into two groups: One of them receiving a static dose of irradiation (30 J/cm^2) and variable concentrations of PS (0, 0.01, 0.1, and 1 mg/mL), while the other group received 0.1 mg/mL of the PS and various irradiation doses (0, 3, 10, 30, 50 J/cm^2). It was found that the toxicity is directly related to the PS concentration and the irradiation dose, which was higher when these variables were higher in both groups. In these experiments, the best phototoxicity was achieved when combining the strongest light dose (50 J/cm^2) and the highest concentration (1 mg/mL).

A further set of experiments involving Talaporfin sodium was carried out in rats with induced RA, in which 0.3 mL of PS solution at a concentration of 1 mg/mL was injected intra-articularly into the knee. Subsequently, the PS concentration in the synovial membrane, skin, cartilage, and muscle was determined after 1, 4, 8, 24, and 48 h post-injection. The concentration of Talaporfin sodium in the synovial membrane tended to be higher than in the rest of the tissues, being 50 times higher than in cartilage, skin, and muscles at 4 h after intra-articular injection. Therefore, it was established that the best time for light activation was 4 h after the administration of the PS solution. The outcome of the therapy was controlled after 24 h and after 56 days, using different intra-articular irradiation doses and concentrations of PS. After 24 h, necrosis was observed throughout the thickness of the synovial membrane around the irradiated area, with the proportion of damaged area, depending on the concentration of the PS and the dose of irradiation used. The higher the PS concentration and the radiation dose, the greater the necrosis was in the tissue. The same result was obtained 56 days after treatment—direct dependence on the concentration of PS and the irradiation. The histological analysis showed the synovial membrane without inflammation, smooth cartilage, and no bone destruction.

Sometimes it is advisable to prolong the distribution and accumulation of PS in the target tissues, in order to be able to perform multiple light activations without having to re-inject the PS into the patient. This idea was followed by Hansch et al., using a PEGylated-liposomal form of Temoporfin (meso-tetra(hydroxyphenyl)chlorin, or m-THPC) [49]. The structure of the tetrapyrrole alone is described in Figure 7. In this particular case, the alcohol groups of the m-THPC were used to attach PEG chains, and the term PEGylated refers to the binding of the polyethylene glycol function (H-[OCH$_2$CH$_2$]$_n$-OH) to a molecule. Such insertion modifies the retention time of the PEG-conjugated-drugs in patients—to some extent, mimicking a continuous intravenous administration.

**Figure 7.** Molecular structure of meso-tetra(hydroxyphenyl)chlorin, Temoporfin (m-THPC).

Indeed, interesting results were obtained when intravenous administrations in mice with induced RA of m-THPC in its native form, m-THPC in the liposomal form, and m-THPC in the PEGylated-liposomal form at the same concentrations (0.1, 0.05, 0.01, and 0.005 mg/kg), were performed [49]. The native m-THPC and the liposomal m-THPC did not show good distribution in arthritic joints. The authors suggested that this was probably due to the fact that the native form of m-THPC is not soluble enough in water and ends up accumulating in the endothelial cells, while the liposomal form is rapidly eliminated from the bloodstream, accumulating instead in the liver and the spleen. However, the PEGylated-liposomal m-THPC possesses optimal solubility, thus preferentially

accumulating in swelling joints. Comparing the joints with RA to those without inflammation, there was a clear tendency of the PS to accumulate in infected joints, with the maximum peak being reached 12 h after intravenous injections. Local irradiation was performed on the knees with an energy of 5 J/cm^2 (652 nm, 25 s). The most effective dose was at a concentration of 0.01 mg/kg. A higher dose (0.1 mg/kg) did not show a significant reduction in the symptoms of RA, possibly because a higher dose induces an inflammatory response. At a lower concentration (0.005 mg/kg), no significant effect after light irradiation was observed. Moreover, no damage to the cartilage was observed, probably due to the absence of blood vessels, which hindered distribution of the PS in this tissue. Photosensitivity was observed for 96 h after injection. The prolonged retention time of the PS in its PEGylated-liposomal form allowed a second irradiation 24 h after the first one without needing to provide a new injection.

The ability of porphyrins to accumulate in lysosomal and endosomal membranes can be exploited to inhibit or enhance intracellular signaling pathways. In combination with other drugs, a complementary or synergetic effect can be obtained. This strategy was applied by Dietze et al. in 2005, combining Gelonin and meso-tetraphenylporphyrin sulfonate (TPPS$_{2a}$) to optimize PDT treatments against RA [50]. Occasionally, cells can survive the partial destruction of lysosomes, thus reducing the effectiveness of PDT [51]. Gelonin is a ribosome inactivating protein toxin, which cancels the protein synthesis of extra-nuclear organisms through the activity of its rRNA glycosidase. However, the toxicity of Gelonin at a cellular level remains low, as it has difficulty to reach the cellular cytosol where it performs its inhibitory function [52]. Therefore, destruction of lysosomal or endosomal membranes upon activation of a PS can facilitate the uptake of Gelonin to the cytosol, thus increasing its cytotoxicity effect (Figure 8). Indeed, the efficacy of this combination has been proven [52,53], and the technique is generally called photochemical internalization. A biological study showed that Gelonin has no effect on cells (T-cells, B-cells, macrophages, and human RA FLS) when it is delivered alone. In contrast, in combination with TPPS$_{2a}$ and upon irradiation (435 nm), the effectiveness of the treatment is considerably multiplied. Cells with higher endocytic activity (FLS) are the most affected by the combination Gelonin-TPPS$_{2a}$-irradiation, thus confirming the potential of a combined therapy involving PDT.

Pheophorbide A, a product derived from the degradation of chlorophyll, has been used in the clinic as an imaging and anticancer agent [54–59]. Consequently, the ability of Pheophorbide A to treat RA has been evaluated [60]. The photoactivity of Pheophorbide A alone and of a modified lysine polymeric Pheophorbide A derivative (T-PS, Figure 9) were studied under different conditions. The goal of the project was to synthesize a photosensitizing agent with two functions: visualization–localization of the PS and phototoxicity. Local irradiation with a wavelength of 665 nm at a fluency rate of 50 mW/cm^2 (laser diode) was applied on synovial tissues. This was carried out on a murine collagen-induced arthritis model, which showed comparable characteristics to those found in human RA patients. The drug was administrated by intravenous injection. The maximum concentration of the PS was reached after 5 h post-injection, whereas the maximum accumulation of T-PS was observed after 24 h. In the healthy joints, the concentration of drugs was minimal in the case of T-PS. Clearly, the polymeric form improves the accumulation and retention time of Pheophorbide A in RA joints. The intensity of the fluorescence and the cytotoxic effect were linearly related to the dose of T-PS and the irradiation, while for Pheophorbide A alone, a linear relationship was not observed. Only animals injected with T-PS and irradiated showed histological changes. On the other hand, no effect was observed in the tissues of animals who did not receive the PS or who received the PS but were not irradiated. However, vascular damage and hemorrhages appeared in the treated areas but disappeared completely three weeks later. In addition, inflammation was observed in the irradiated areas just after the treatment. However, this can be potentially attenuated by the concomitant use of anti-inflammatories drugs.
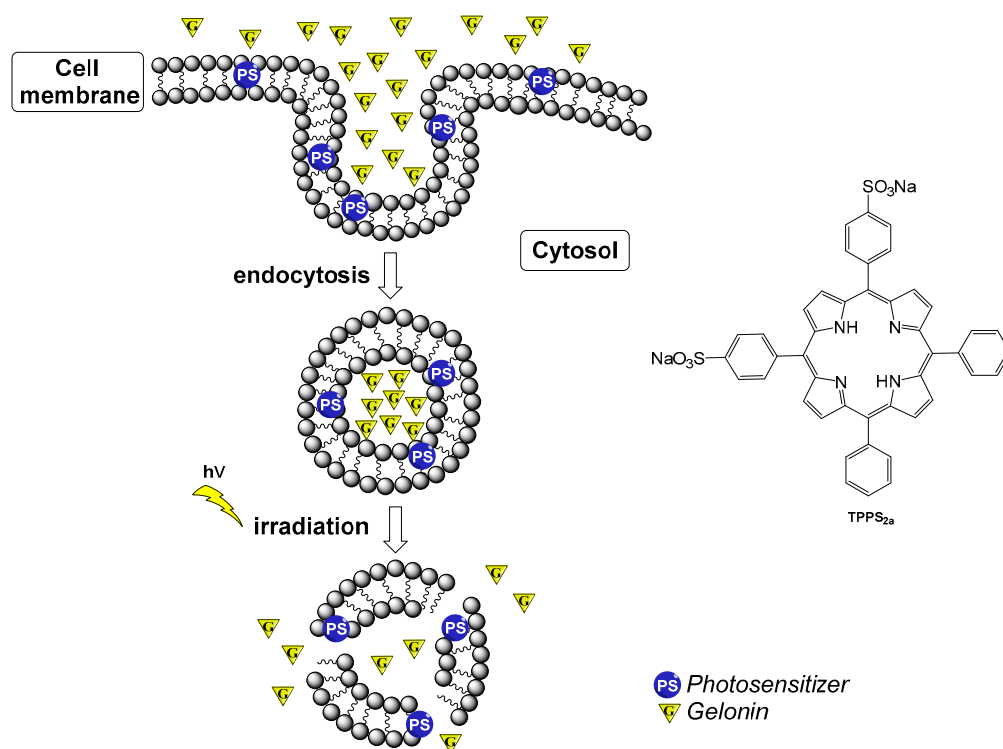
Figure 8. Simplified representation of the photochemical internalization (PCI) of Gelonin using PDT [52,53].
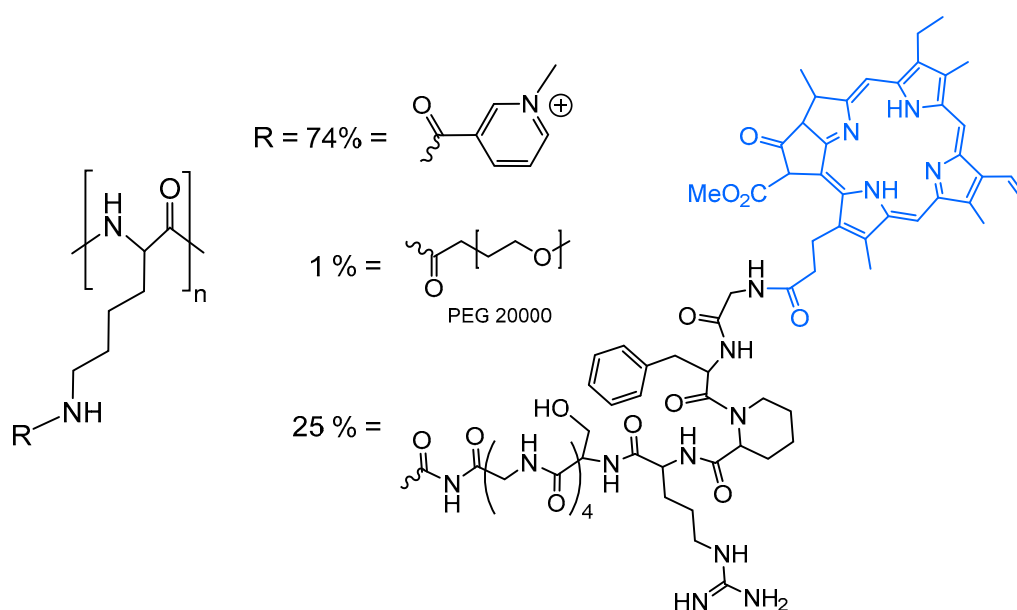

Figure 9. Pheophorbide A (blue) linked to a modified lysine polymer [60].

2.3. Other Photosensitizers

Porphyrins and their tetrapyrrole analogues remain the most common photosensitizers used to treat RA by PDT. However, other organic molecules can be envisaged. This was demonstrated by Hendrich and co-workers [61]. In this study, they have followed the same in vitro procedure as the one they used with Photosan-3 [38]. They tested four different substances on FLS cells: chloroquine, methotrexate, piroxicam, and sodium morrhuate, irradiating them at 351 nm with 1 J/cm^2 pulse/minute. Chloroquine is a well-known anti-malarial drug [62], while methotrexate is a derivative of folic acid

used in cancer therapies as an abortive agent, as well as in the treatment of RA [63]. Piroxicam is an anti-inflammatory drug for osteoarthritis and for autoimmune diseases, such as RA [64,65]. Finally, sodium morrhuate was used at the beginning of the 20th century as a drug against tuberculosis and more recently as a sclerosing and fibrosing agent [66]. The structures of these four organic molecules are presented in Figure 10.
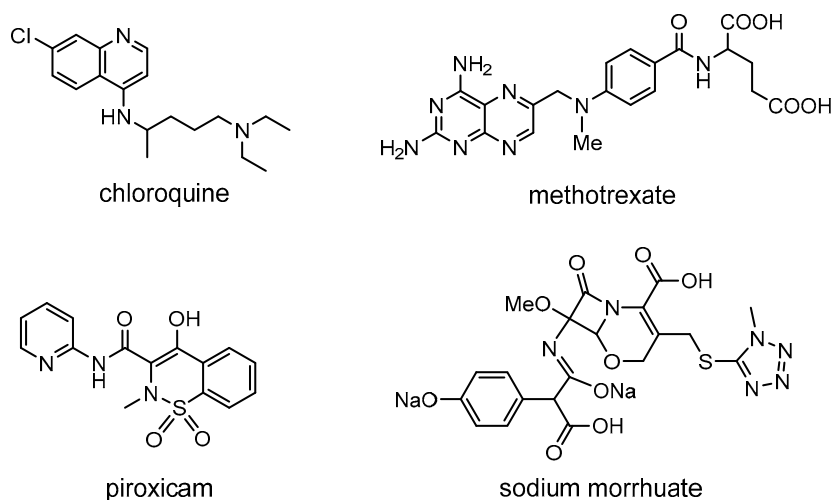
**Figure 10.** Molecular structures of four drugs tested as PSs to treat RA by PDT.

Under a PDT protocol, piroxicam and sodium morrhuate show no effect on FLS cells. On the other hand, chloroquine and methotrexate present a phototoxicity 20 times greater than the sum of the activity of the PS (cytotoxicity), and with a separate irradiation, thus suggesting a synergetic effect [61]. If the irradiation occurs prior to the administration of the drug, a simple additive effect is observed.

Later on, methotrexate was re-evaluated as a PS in a study focusing on the effectiveness of using light-emitting diodes (LEDs) in PDT. LEDs possess interesting characteristics, such as being thermally non-destructive, cheap, available, easy to operate, and small. Therefore, LEDs can be considered a "low cost" light source for PDT [67]. To demonstrate the effectiveness of LEDs, different colors were tested: white, yellow, red, and infrared (IR). Methotrexate was injected into the muscles and skin of goats and chickens. The effectiveness of the treatment was determined by counting lymphocytes in the blood, which could be correlated to light penetration and PDT treatment efficacy. The results showed that the yellow light was the least penetrating, followed by the white light. Red light showed a greater penetration, like the IR, but with a scattering effect. Therefore, the IR LED was selected as the most suitable for further experiments on blood from RA patients. The blood samples were exposed to 24 h of IR LED irradiation after the addition of the PS, and the lymphocytes were counted at the beginning of, and during, a 5 day period after irradiation. Progressive lymphocyte reduction occurred during the first 5 days, and the phototoxicity effect lasted for about a week. Control experiments without irradiation and without PS did not show changes in the number of lymphocytes. However, the use of PS only or IR light alone also caused a reduction in the number of lymphocytes (higher in the first case) but to a lesser extent than when LEDs and methotrexate were used together. The same treatment was carried out in the blood of patients without RA, showing the same cytotoxic effect in lymphocytes, although to a lesser extent.

Hypericin is a naphthoadiantrone derivative of vegetable origin (Figure 11), which was once used as an antidepressant and antimicrobial agent [68,69] and also as an anticancer agent [70–76]. Hypericin was tested as a PS in PDT on human RA FLS (MH7A cells) (irradiation at 593 nm and a LiD of 1.5 J/cm^2) [77]. The concentration of PS varied from 0 to 4 μM. The in vitro experiments, evaluated by MTT assays, showed how hypericin through PDT increases the ROS production, leading to the apoptosis and death of MH7A cells. The result of the therapy improves as the PS concentration

increases. Mechanism studies suggest that the therapy provokes morphological changes in MH7A cells (shrinkage and cytoplasmic vacuolation), thus inhibiting their proliferation. By itself, hypericin slightly reduces cell proliferation, but its performance improves significantly when it is irradiated at its excitation wavelength.
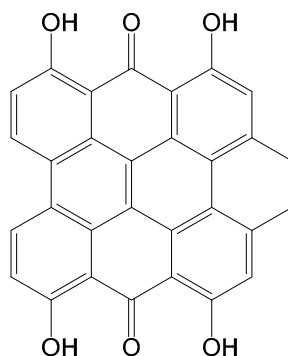
Figure 11. The molecular structure of hypericin.

2.4. Encapsulation of Photosensitizers

It is possible to increase the accumulation and retention time of PS in target tissues by encapsulating them in nanogel or nano-particles. Juillerat-Jeanneret et al. proposed to use chitosan-based nanogels to transport PS [78], in order to increase the retention time and accumulation of the PS in inflamed tissues. Intra-articular administration and local laser irradiation were used in this study. In vitro (human THP-1 macrophages and murine RAW 264.7 macrophages) and in vivo (mice with antigen-induced arthritis) tests were performed. Three different PSs (Figure 12) were encapsulated in the chitosan-based nanogel: Tetra(4-sulfonatophenyl)porphine (TSPP), tetra(4-carboxyphenyl)chlorin (TPCC), and Chlorin e6 (Ce6). The PS-nanogels require an anionic form of the PS (carboxyl and sulfonate groups) to be able to be retained in the core of the positively charged particle.
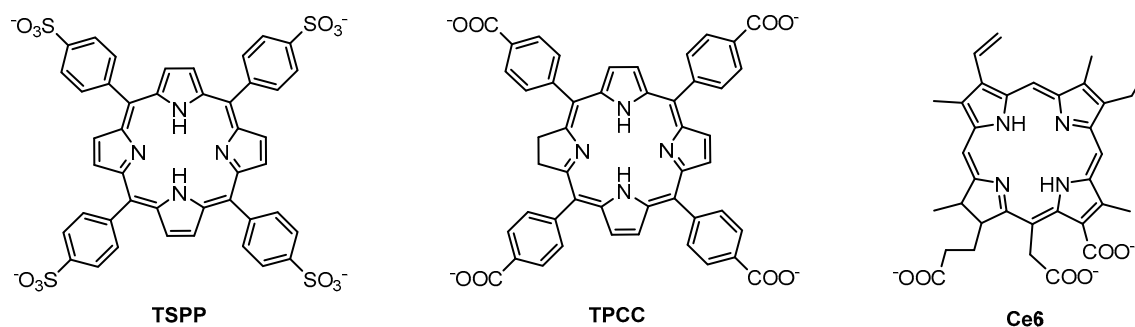

Figure 12. Molecular structure of encapsulated anionic PS in chitosan-based nanogel [78].

PDT was carried out with irradiation at 652 nm using a laser diode, which, according to the time of exposure, corresponded to doses of 0.5–15 J/cm^2. In the in vitro study, cell viability was controlled by MTT assays, while in the in vivo study, the level of serum amyloid A (SAA) in the blood, which is a protein secreted during the inflammation and used for the diagnosis of RA in humans, was quantified. First, the in vitro toxicity of the PS-nanogel derivatives was determined without irradiation. Only the Ce6-nanogel showed a degree of toxicity in the absence of light at a concentration higher than 20% (v/v). The other two did not show toxicity in murine RAW 264.7 macrophages or in human THP-1 macrophages. The maximum concentrations were observed after 3 h (RAW 264.7) and 4 h (THP-1), respectively. Regarding the PDT effect in the RAW macrophages, 50% cell mortality (LD$_{50}$) was observed at doses of 0.5 J/cm^2 with Ce6, 2 J/cm^2 with TPCC, and 12 J/cm^2 with TSPP, using a concentration of 17% (v/v) of PS-nanogels. On the other hand, in THP-1 macrophages, LD$_{50}$

was observed with a dose of 2 J/cm^2 with Ce6. Fluorescence microscopy in vivo showed that the PS-nanogels were retained for a longer period in the infected knees of the mice than the PS alone. In addition, the nanogels were retained for a longer period in joints with RA than in healthy joints. In vitro, it was observed that the PS-nanogels were located in the cytoplasm of cells, as well as in cellular organelles, not in the nucleus. Measurements of SAA in blood (8 days after irradiation) showed that at doses of 25 J/cm^2, the level of proteins was reduced to amounts comparable to those observed in local treatments with corticoids (methylprednisolone). Finally, the production of ROS by PS-nanogels was estimated, resulting in quantities close to those produced by the PS alone.

The sodium salt of indocyanine green (ICG) has been used as an indicator in certain diagnostics, such as cardiology or angiography, thanks to its fluorescent features, solubility in water, and rapid elimination (Figure 13). In addition, when ICG is irradiated at a certain wavelength, like porphyrin derivatives, it is capable of producing ROS in the presence of oxygen. Recently, this ability has been tested to treat RA by studying its photo-capacity to induce apoptosis in human FLS [79]. ICG was encapsulated within a biodegradable/biocompatible globular polymer (poly [DL-lactide-*co*-glycolic acid], PLGA) together with the oxygen carrier perfluoro-*n*-pentane (PFP), forming a complexed mixture (OI-NP). PDT was applied together with sonodynamic therapy, whose function was to break the polymeric structure to release ICG and PFP into the cell. This study shows that cellular uptake in the case of OI-NP tripled the concentration of ICG. Moreover, without PFP (I-NP) cellular concentration remained higher (more than double) than with ICG alone. MTT assays showed a cell viability of 75% with ICG, 35% with I-NP, and 25% with OI-NP. The authors suggested that this result may be due to the greater stability of ICG when it is encapsulated in the polymer. The apoptosis induced after photo-sonodynamic treatment was doubled when using I-NP compared to ICG alone, and tripled when using OI-NP, but with no significant statistical differences.
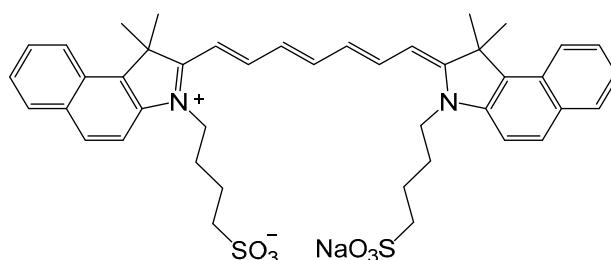
Figure 13. Molecular structure of Indocyanine Green.

Recently, Wand, Liu et al. proposed the use of nanoparticles to eliminate some of the drawbacks and improve the effectiveness of porphyrin derivatives in PDT [80]. In this study, they used TiO$_2$ nanoparticles containing molecules of tetra(4-sulfonatophenyl)porphine (TSPP). This porphyrin is generally not selective and poorly biocompatible [81]. They showed how the TSPP-TiO$_2$ tandem can reduce these drawbacks. The study was conducted in human RA FLS and in murines with the same pathology. Fluorescence studies showed that TSPP-TiO$_2$ accumulates effectively in human RA FLS and very ineffectively in healthy cells. MTT assays showed a lower toxicity of TSPP-TiO$_2$ compared to TSPP alone. They suggested that this could be a consequence of the slow interaction of the TSPP with the tissue when it is retained in the TiO$_2$ nanoparticles. These observations suggest fewer side effects in the treatment, since the PS is slowly released mainly in the target tissues, which will reduce the damage to healthy tissues.

Wang et al. extended the use of the TSPP-TiO$_2$ on bone marrow stromal cells [82]. These cells are associated with the palliation of different adverse effects and have been used as regulators in some autoimmune diseases, although their exact role remains under investigation. One result, among others, showed a significant decrease in the biomarkers tumor necrosis factor (TNF)-α and interleukin-17 (IL-17), both being indicative of an increase in RA symptoms. These results confirm the potential of using nanoparticles in the treatment of RA.

Nanoparticles composed of Cu-S with anchored L-cysteine molecules have been used in PDT against RA. $Cu_{7.2}S_4$ nanoparticles were tested as PSs in combined PDT and photothermal treatment of RA [83]. The study was carried out in vitro on mouse fibroblast cells and in vivo on a collagen induced arthritis murine model. Both biological studies involved near-infrared (NIR) irradiation, and, in vivo, an intra-articular injection was performed. In vitro, the NIR irradiation of the cells in the presence of $Cu_{7.2}S_4$ nanoparticles increased the temperature to 51 °C, while in the absence of nanoparticles, the temperature remained at 32 °C. In addition, ROS production increases in the presence of Cu-S nanoparticles with NIR irradiation. Similarly, in vivo tests showed an increased temperature in the joints during the treatment. Inflammation and redness of the irradiated area (observed when using saline solution) were not observed with the Cu-S nanoparticles. After the treatment, the infected joints showed an appearance similar to that of healthy joints. Bone density and cartilage were unaffected. In addition, the level of pro-inflammatory proteins was reduced, while the level of anti-inflammatory proteins was higher in specimens who did not receive the $Cu_{7.2}S_4$ nanoparticles.

2.5. Summary

As emphasized in Table 1, using PDT to treat RA implicates several variables, which makes it difficult to find a winning combination. The selection of the PS is important, but the modality of treatment (activation wavelength, irradiation mode, and type of administration) can also greatly influence the outcome. PDT is not like other treatments, where the dose and the administration are the two main factors to consider. In PDT, activation of the PS at the right time and at the right place is crucial. Therefore, optimization of PDT remains a difficult task. Nevertheless, in recent years, new modalities in PDT have emerged, such as the use of nanoparticles [84], nanoporous photo-sensitizing hydrogels [85], and organometallic complexes [86,87], thereby offering new perspectives on PDT.

Table 1. A list of PSs tested as PDT agents against rheumatoid arthritis (RA), including some modalities of treatment. ND = not determined, NA = not applicable. FCA, Freund's complete adjuvant. FLS, fibroblast-like synoviocytes. ICG, indocyanine green. MRL-lpr, Murphy Roths Large lymphoproliferation NZW, New Zealand White. TPCC, tetra(4-carboxyphenyl)chlorin. $TPPS_{2A}$, meso-tetraphenylporphyrin disulfonate with two sulfonate groups on adjacent phenyl rings. TSPP, tetra(4-sulfonatophenyl)porphine.

PS	Activation Wavelength (nm)	Type of Administration	Irradiation Mode	Target/Model	Ref.
[Na][ATX-S10]	670	intravenous	trans-cutaneous	FLS/mice	[44]
BPD-MA	690	intravenous	trans-cutaneous	MRL-lpr mice (FCA)	[14]
BPD-MA	690	intravenous	intra-anticular	rabbit	[18]
BPD-MA lyposomal	690	intravenous/intra-articular	trans-cutaneous/intra-articular	NZW rabbit (FCA)	[16]
Ce6	652	intra-articular	intra-anticular	human THP-1 and murine RAW 264.7 macrophages/mice	[76]
Chloroquine	351	NA	ND	FLS	[58]
$Cu_{7.2}S_4$ nanoparticles	808	intra-articular	trans-cutaneous	FLS/murine	[80]
Hypericin	593	NA	ND	FLS	[75]
ICG	780	NA	ND	FLS	[65]
Methotrexate	450, 550, 590, 660, and 850	intra-articular	trans-cutaneous	goat/chicken	[64]
Methotrexate	351	NA	ND	FLS	[58]
m-THPC	652	intravenous	trans-cutaneous	mice	[46]
Pheophorbide A (T-PS)	665	intravenous	trans-cutaneous	murine	[57]
Photofrin	630	intravenous	intra-anticular	NZW rabbit	[29]
Photosan-3	630	intravenous/intra-articular	intra-anticular	FLS/rabbit	[34,36]
Piroxicam	351	NA	ND	FLS	[58]
PpIX	635	intra-articular	trans-cutaneous	FLS/mice	[42]
PpIX	635	intra-articular	trans-cutaneous	rabbit	[43]
Sodium morrhuate	351	NA	ND	FLS	[58]
Talaporfin	664	intra-articular	intra-articular	FLS/mice/rat	[45]
TPCC	652	intra-articular	intra-articular	human THP-1 and murine RAW 264.7 macrophages/mice	[76]
$TPPS_{2A}$	435	NA	ND	FLS	[47]
TSPP	652	intra-articular	intra-articular	human THP-1 and murine RAW 264.7 macrophages/mice	[76]
$TSPP$-TiO_2 nanoparticle	490	NA	ND	FLS/bone marrow stromal cells	[77,79]
$TSPP$-TiO_2 nanoparticle	500–550	intravenous	trans-cutaneous	murine	[77]

3. Conclusions

At the moment, alternatives to rheumatoid arthritis (RA) treatment, such as synovectomy, are invasive, destructive, and involve elaborate techniques that require long periods of rehabilitation. Moreover, these treatments cannot cure the disease but only treat the symptoms. Therefore, photodynamic therapy (PDT) treatments are quite encouraging as they offer endless possibilities, without the drawbacks of the current treatments. As illustrated in this review, to find a successful treatment for rheumatoid arthritis by photodynamic therapy, it is not only mandatory to use an excellent photosensitizer, but also to find the best possible conditions (administration, localization, formulation, irradiation, or injection-time-delay). Consequently, the main challenge for researchers in the fields of photodynamic therapy and rheumatoid arthritis is to pinpoint the best combination. The overview provided here should help researchers to design new combinations and bring the treatment of rheumatoid arthritis by photodynamic therapy to the clinic.

Author Contributions: Conceptualization, D.Y.L., B.L., and B.T.; Writing the original draft, M.G.-V., D.Y.L., B.L., and B.T.; Figures and Schemes, M.G.-V.; References, M.G.-V., D.Y.L. and B.L.; Editing, B.T.

Conflicts of Interest: The authors declare no conflict of interest.

Abbreviations

BPD-MA	benzoporphyrin derivative monoacid ring a
Ce6	Chlorin e6
DMARDs	disease-modifying antirheumatic drugs
FCA	Freund's complete adjuvant
FDA	food and drug administration
FLS	fibroblast-like synoviocytes
ICG	indocyanine green
IL-17	interleukin-17
IR	infrared
LiD	light dose
LD$_{50}$	50% of cell mortality after light activation
LED	light-emitting diode
lpr	lymphoproliferation
MRL	Murphy Roths Large
m-THPC	meso-tetra(hydroxyphenyl)chlorin
MTT	3-(4,5-dimethythiazol-2-yl)-2,5-diphenyl tetrazolium bromide
NA	not applicable
ND	not determined
NIR	near infrared
NZW	New Zealand white
PDT	photodynamic therapy
PEG	polyethylene glycol
PFP	perfluoro-n-pentane
PLGA	poly(DL-lactide-*co*-glycolic acid)
PpIX	protoporphyrin IX
PS	photosensitizer
RA	rheumatoid arthritis
ROS	radical oxygen species
SAA	serum amyloid A
SCID	severe combined immunodeficiency
TNF	tumor necrosis factor
THPC	tetra(hydroxyphenyl)chlorin
TPCC	tetra(4-carboxyphenyl)chlorin
TPPS$_{2a}$	meso-tetraphenylporphyrin disulfonate with two sulfonate groups on adjacent phenyl rings
TSPP	tetra(4-sulfonatophenyl)porphine
WBI	whole body irradiation

References

1.   Stacey, O.J.; Pope, S.J.A. New avenues in the design and potential application of metal complexes for photodynamic therapy. *RSC Adv.* **2013**, *3*, 25550–25564. [CrossRef]

2. Dolmans, D.E.J.G.J.; Fukumura, D.; Jain, R.K. Photodynamic Therapy for Cancer. *Nat. Rev. Cancer* **2003**, *3*, 380–387. [CrossRef] [PubMed]

3. Robertson, C.A.; Evans, D.H.; Abrahamse, H. Photodynamic therapy (PDT): A short review on cellular mechanisms and cancer research applications for PDT. *J. Photochem. Photobiol. B Biol.* **2009**, *96*, 1–8. [CrossRef] [PubMed]

4. Brown, S.B.; Brown, E.A.; Walker, I. The present and future role of photodynamic therapy in cancer treatment. *Lancet* **2004**, *5*, 497–508. [CrossRef]

5. Shi, X.; Zhang, C.Y.; Gao, J.; Wang, Z. Recent advances in photodynamic therapy for cancer and infectious diseases. *Wiley Interdiscip. Rev. Nanomed. Nanobiotechnol.* **2019**, e1560. [CrossRef] [PubMed]

6. Aniogo, E.C.; George, B.P.A.; Abrahamse, H. The role of photodynamic therapy on multidrug resistant breast cancer. *Cancer Cell Int.* **2019**, *19*, 91. [CrossRef] [PubMed]

7. Hwang, H.S.; Shin, H.; Han, J.; Na, K. Combination of photodynamic therapy (PDT) and anti-tumor immunity in cancer therapy. *J. Pharm. Investig.* **2018**, *48*, 143–151. [CrossRef] [PubMed]

8. McInnes, I.B.; Schett, G. The pathogenesis of rheumatoid arthritis. *N. Engl. J. Med.* **2011**, *365*, 2205–2219. [CrossRef] [PubMed]

9. Croia, C.; Bursi, R.; Sutera, D.; Petrelli, F.; Alunno, A.; Puxeddu, I. One year in review 2019: Pathogenesis of rheumatoid arthritis. *Clin. Exp. Rheumatol.* **2019**, *37*, 347–357.

10. Deane, K.D.; Holers, V.M. The Natural History of Rheumatoid Arthritis. *Clin. Ther.* **2019**, in press. [CrossRef]

11. Aletaha, D.; Smolen, J.S. Diagnosis and management of rheumatoid arthritis: A review. *JAMA* **2018**, *320*, 1360–1372. [CrossRef] [PubMed]

12. Silvagni, E.; Di Battista, M.; Bonifacio, A.F.; Zucchi, D.; Governato, G.; Scirè, C.A. One year in review 2019: Novelties in the treatment of rheumatoid arthritis. *Clin. Exp. Rheumatol.* **2019**, *37*, 519–534. [PubMed]

13. Seymour, H.E.; Worsley, A.; Smith, J.M.; Thomas, S.H.L. Anti-TNF agents for rheumatoid arthritis. *Br. J. Clin. Pharmacol.* **2001**, *51*, 201–208. [CrossRef] [PubMed]

14. Kremer, J.M.; Bloom, B.J.; Breedveld, F.C.; Coombs, J.H.; Fletcher, M.P.; Gruben, D.; Krishnaswami, S.; Burgos-Vargas, R.; Wilkinson, B.; Zerbini, C.A.F.; et al. The safety and efficacy of a JAK inhibitor in patients with active rheumatoid arthritis: Results of a double-blind, placebo-controlled phase IIa trial of three dosage levels of CP-690,550 versus placebo. *Arthritis Rheum.* **2009**, *60*, 1895–1905. [CrossRef] [PubMed]

15. Allison, B.A.; Pritchard, P.H.; Richter, A.M.; Levy, J.G. The plasma distribution of benzoporphyrin derivative and the effects of plasma lipoproteins on its biodistribution. *Photochem. Photobiol.* **1990**, *52*, 501–507. [CrossRef] [PubMed]

16. Ratkay, L.G.; Chowdhary, R.K.; Neyndorff, H.C.; Tonzetich, J.; Waterfield, J.D.; Levy, J.G. Photodynamic therapy; a comparison with other immunomodulatory treatments of adjuvant-enhanced arthritis in MRL-lpr mice. *J. Clin. Exp. Immunol.* **1994**, *95*, 373–377. [CrossRef] [PubMed]

17. Richter, A.M.; Jam, A.K.; Canaan, A.J.; Meadows, H.; Levy, J.G. Skin photosensitivity as a model in photodynamic therapy. *Proc. SPIE Int. Soc. Opt. Eng.* **1996**, *2625*, 194–205. [CrossRef]

18. Chowdhary, R.K.; Ratkay, L.G.; Canaan, A.J.; Waterfield, J.D.; Richter, A.M.; Levy, J.G. Uptake of Verteporfin® by articular tissues following systemic and intra-articular administration. *Biopharm. Drug Dispos.* **1998**, *19*, 395–400. [CrossRef]

19. Chowdhary, R.K.; Neyndorff, H.C.; Waterfield, J.D.; Levy, J.G.; Keystone, E.C.; Iamaroon, A.; Ratkay, L.G.; Richter, A.M. Amelioration of antigen-induced arthritis in rabbits by induction of apoptosis of inflammatory-cells with local application of transdermal photodynamic therapy. *Arthritis Rheum.* **1998**, *41*, 525–534. [CrossRef]

20. Trauner, K.B.; Gandour-Edwards, R.; Bamberg, M.; Shortkroff, S.; Sledge, C.; Hasan, T. Photodynamic Synovectomy Using Benzoporphyrin Derivative in an Antigen-induced Arthritis Model for Rheumatoid Arthritis. *Photochem. Photobiol.* **1998**, *67*, 133–139. [CrossRef]

21. Richter, A.M.; Kelly, B.; Chow, J.; Liu, D.J.; Towers, G.H.; Dolphin, D.; Levy, J.G. Preliminary studies on a more effective phototoxic agent than hematoporphyrin. *J. Natl. Cancer Inst.* **1987**, *79*, 1327–1332. [PubMed]

22. Waterfield, J.D.; Fairhurst, M.; Waterfield, E.M.; Norbury, K.C. Evaluation of the immunotoxicity of benzoporphyrin derivative (BPD-MA) in mice. *Immunopharmacol. Immunotoxicol.* **1997**, *19*, 89–103. [CrossRef] [PubMed]

23. Hendrich, C.; Hüttmann, G.; Vispo-Seara, J.L.; Houserek, S.; Siebert, W.E. Experimental photodynamic laser therapy for rheumatoid arthritis with a second generation photosensitizer. *Knee Surg. Sports Traumatol. Arthrosc.* **2000**, *8*, 190–194. [CrossRef] [PubMed]

24. Pernot, M.; Bastogne, T.; Barry, N.P.E.; Therrien, B.; Koellensperger, G.; Hann, S.; Reshetov, V.; Barberi-Heyob, M. Systems biology approach for in vivo photodynamic therapy optimization of ruthenium-porphyrin compounds. *J. Photochem. Photobiol. B Biol.* **2012**, *117*, 80–89. [CrossRef] [PubMed]

25. Jalili, A.; Makowski, M.; Świtaj, T.; Nowis, D.; Wilczyński, G.M.; Wilczek, E.; Chorąży-Massalska, M.; Radzikowska, A.; Maśliński, W.; Biały, Ł.; et al. Effective photoimmunotherapy of murine colon carcinoma induced by the combination of photodynamic therapy and dendritic cells. *Clin. Cancer Res.* **2004**, *10*, 4498–4508. [CrossRef] [PubMed]

26. Peng, Q.; Warloe, T.; Moan, J.; Godal, A.; Apricena, F.; Giercksky, K.E.; Nesland, J.M. Antitumor effect of 5-aminolevulinic acid-mediated photodynamic therapy can be enhanced by the use of a low dose of photofrin in human tumor xenografts. *Cancer Res.* **2001**, *61*, 5824–5832. [PubMed]

27. Firczuk, M.; Gabrysiak, M.; Barankiewicz, J.; Domagala, A.; Nowis, D.; Kujawa, M.; Jankowska-Steifer, E.; Wachowska, M.; Glodkowska-Mrowka, E.; Korsak, B.; et al. GRP78-targeting subtilase cytotoxin sensitizes cancer cells to photodynamic therapy. *Cell Death Dis.* **2013**, *4*, e741. [CrossRef] [PubMed]

28. Schuitmaker, J.J.; Baas, P.; van Leengoed, H.L.L.M.; van der Meulen, F.W.; Star, W.M.; van Zandwijk, N. Photodynamic therapy: A promising new modality for the treatment of cancer. *J. Photochem. Photobiol. B Biol.* **1996**, *34*, 3–12. [CrossRef]

29. Sutedja, T.; Baas, P.; Stewart, F.; van Zandwijk, N. A pilot study of photodynamic therapy in patients with inoperable non-small cell lung cancer. *Eur. J. Cancer* **1992**, *28*, 1370–1373. [CrossRef]

30. Nseyo, U.O.; DeHaven, J.; Dougherty, T.J.; Potter, W.R.; Merrill, D.L.; Lundahl, S.L.; Lamm, D.L. Photodynamic Therapy (PDT) in the Treatment of Patients with Resistant Superficial Bladder Cancer: A Long Term Experience. *J. Clin. Laser Med. Surg.* **1998**, *16*, 61–68. [CrossRef]

31. Abdel Gaber, S.A. Photodynamic Diagnosis and Therapy for Oral Potentially Malignant Disorders and Cancers. In *Development of Oral Cancer: Risk Factors and Prevention Strategies*; Al Moustafa, A.-E., Ed.; Springer: Cham, Switzerland, 2017; Chapter 10; pp. 147–175. [CrossRef]

32. Trauner, K.; Gandour-Edwards, R.; Bamberg, M.; Nishioka, N.S.; Flotte, T.; Autry, S.; Hasan, T. Influence of light delivery on photodynamic synovectomy in an antigen- induced arthritis model for rheumatoid arthritis. *Lasers Surg. Med.* **1998**, *22*, 147–156. [CrossRef]

33. Koren, H.; Alth, G. Photodynamic therapy in gynaecologic cancer. *J. Photochem. Photobiol. B Biol.* **1996**, *36*, 189–191. [CrossRef]

34. Feyh, J. Photodynamic treatment for cancers of the head and neck. *J. Photochem. Photobiol. B Biol.* **1996**, *36*, 175–177. [CrossRef]

35. Gupta, S.; Dwarakanath, B.S.; Muralidhar, K.; Jain, V. Cellular uptake, localization and photodynamic effects of haematoporphyrin derivative in human glioma and squamous carcinoma cell lines. *J. Photochem. Photobiol. B Biol.* **2003**, *69*, 107–120. [CrossRef]

36. Yu, Z.; Li, H.; Zhang, L.-M.; Zhu, Z.; Yang, L. Enhancement of phototoxicity against human pancreatic cancer cells with photosensitizer-encapsulated amphiphilic sodium alginate derivative nanoparticles. *Int. J. Pharm.* **2014**, *473*, 501–509. [CrossRef]

37. Burmester, G.R.; Locher, P.; Koch, B.; Winchester, R.J.; Dimitriu-Bona, A.; Kalden, J.R.; Mohr, W. The tissue architecture of synovial membranes in inflammatory and non-inflammatory joint diseases. *Rheumatol. Int.* **1983**, *3*, 173–181. [CrossRef]

38. Hendrich, C.; Diddens, H.; Nosir, H.; Siebert, W.E. Treatment of Rheumatoid Arthritis using Photodynamic Therapy? *Proc. SPIE Int. Soc. Opt. Eng.* **1995**, *2371*, 592–595. [CrossRef]

39. Hendrich, C.; Hüttmann, G.; Lehnert, C.; Diddens, H.; Siebert, W.E. Photodynamic laser therapy for rheumatoid arthritis cell culture studies and animal experiments. *Knee Surg. Sports Traumatol. Arthrosc.* **1997**, *5*, 58–63. [CrossRef]

40. Fidanzi-Dugas, C.; Liagre, B.; Chemin, G.; Perraud, A.; Carrion, C.; Couquet, C.-Y.; Granet, R.; Sol, V.; Léger, D.Y. Analysis of the in vitro and in vivo effects of photodynamic therapy on prostate cancer by using new photosensitizers, protoporphyrin IX-polyamine derivatives. *Biochim. Biophys. Acta Gen. Subj.* **2017**, *1861*, 1676–1690. [CrossRef]

41. Leeper, F.J. The biosynthesis of porphyrins, chlorophylls, and vitamin B12. *Nat. Prod. Rep.* **1989**, *6*, 171–203. [CrossRef]

42. Layer, G.; Reichelt, J.; Jahn, D.; Heinz, D.W. Structure and function of enzymes in heme biosynthesis. *Protein Sci.* **2010**, *19*, 1137–1161. [CrossRef] [PubMed]

43. Shulman, D.G.; Golub, A.L.; Marcus, S.L.; Carroll, R.L.; Sobel, R.S.; Lundahl, S. Photodynamic Therapy (PDT) and Photodiagnosis (PD) Using Endogenous Photosensitization Induced by 5-Aminolevulinic Acid (ALA): Current Clinical and Development Status. *J. Clin. Laser Med. Surg.* **1996**, *14*, 59–66. [CrossRef]

44. Uehlinger, P.; Zellweger, M.; Wagnières, G.; Juillerat-Jeanneret, L.; Van Den Bergh, H.; Lange, N. 5-Aminolevulinic acid and its derivatives: Physical chemical properties and protoporphyrin IX formation in cultured cells. *J. Photochem. Photobiol. B Biol.* **2000**, *54*, 72–80. [CrossRef]

45. Kirdaite, G.; Lange, N.; Busso, N.; Van Den Bergh, H.; Kucera, P.; So, A. Protoporphyrin IX photodynamic therapy for synovitis. *Arthritis Rheum.* **2002**, *46*, 1371–1378. [CrossRef] [PubMed]

46. Bagdonas, S.; Kirdaite, G.; Streckyte, G.; Graziene, V.; Leonaviciene, L.; Bradunaite, R.; Venalis, A.; Rotomskis, R. Spectroscopic study of ALA-induced endogenous porphyrins in arthritic knee tissues: Targeting rheumatoid arthritis PDT. *Photochem. Photobiol. Sci.* **2005**, *4*, 497–502. [CrossRef] [PubMed]

47. Miyazawa, S.; Nishida, K.; Komiyama, T.; Nakae, Y.; Takeda, K.; Yorimitsu, M.; Kitamura, A.; Kunisada, T.; Ohtsuka, A.; Inoue, H. Novel transdermal photodynamic therapy using ATX-S10·Na(II) induces apoptosis of synovial fibroblasts and ameliorates collagen antibody-induced arthritis in mice. *Rheumatol. Int.* **2006**, *26*, 717–725. [CrossRef] [PubMed]

48. Torikai, E.; Kageyama, Y.; Kohno, E.; Hirano, T.; Koide, Y.; Terakawa, S.; Nagano, A. Photodynamic therapy using talaporfin sodium for synovial membrane from rheumatoid arthritis patients and collagen-induced arthritis rats. *Clin. Rheumatol.* **2008**, *27*, 751–761. [CrossRef]

49. Hansch, A.; Frey, O.; Gajda, M.; Susanna, G.; Boettcher, J.; Bräuer, R.; Kaiser, W.A. Photodynamic treatment as a novel approach in the therapy of arthritic joints. *Lasers Surg. Med.* **2008**, *40*, 265–272. [CrossRef]

50. Dietze, A.; Engesæter, B.; Berg, K. Transgene delivery and gelonin cytotoxicity enhanced by photochemical internalization in fibroblast-like synoviocytes (FLS) from rheumatoid arthritis patients. *Photochem. Photobiol. Sci.* **2005**, *4*, 341–347. [CrossRef]

51. Berg, K.; Moan, J. Lysosomes as photochemical targets. *Int. J. Cancer* **1994**, *59*, 814–822. [CrossRef]

52. Selbo, P.K.; Weyergang, A.; Høgset, A.; Norum, O.J.; Berstad, M.B.; Vikdal, M.; Berg, K. Photochemical internalization provides time- and space-controlled endolysosomal escape of therapeutic molecules. *J. Control. Release* **2010**, *148*, 2–12. [CrossRef] [PubMed]

53. Berg, K.; Selbo, P.K.; Prasmickaite, L.; Tjelle, T.E.; Sandvig, K.; Moan, J.; Gaudernack, G.; Fodstad, Ø.; Kjølsrud, S.; Anholt, H.; et al. Photochemical internalization: A novel technology for delivery of macromolecules into cytosol. *Cancer Res.* **1999**, *59*, 1180–1183. [PubMed]

54. Keller, P.; Sowinska, M.; Tassetti, V.; Heisel, F.; Hajri, A.; Evrard, S.; Miehe, J.A.; Marescaux, J.; Aprahamian, M. Photodynamic imaging of a rat pancreatic cancer with pheophorbide a. *Photochem. Photobiol.* **1996**, *63*, 860–867. [CrossRef] [PubMed]

55. Xu, D.D.; Xu, C.B.; Lam, H.M.; Wong, F.-L.; Leung, A.W.N.; Leong, M.M.L.; Cho, W.C.S.; Hoeven, R.; Lv, Q.; Rong, R. Proteomic analysis reveals that pheophorbide a-mediated photodynamic treatment inhibits prostate cancer growth by hampering GDP-GTP exchange of ras-family proteins. *Photodiagn. Photodyn. Ther.* **2018**, *23*, 35–39. [CrossRef] [PubMed]

56. Gheewala, T.; Skwor, T.; Munirathinam, G. Photodynamic therapy using pheophorbide and 670nm LEDs exhibits anti-cancer effects in-vitro in androgen dependent prostate cancer. *Photodiagn. Photodyn. Ther.* **2018**, *21*, 130–137. [CrossRef] [PubMed]

57. Moon, S.; Kim, D.K.; Kim, J. Apoptosis-related microRNA-145-5p enhances the effects of pheophorbide a-based photodynamic therapy in oral cancer. *Oncotarget* **2017**, *8*, 35184–35192. [CrossRef] [PubMed]

58. Zhang, C.; Zhang, J.; Shi, G.; Song, H.; Shi, S.; Zhang, X.; Huang, P.; Wang, Z.; Wang, W.; Wang, C.; et al. A Light Responsive Nanoparticle-Based Delivery System Using Pheophorbide a Graft Polyethylenimine for Dendritic Cell-Based Cancer Immunotherapy. *Mol. Pharm.* **2017**, *14*, 1760–1770. [CrossRef]

59. You, H.; Yoon, H.-E.; Jeong, P.-H.; Ko, H.; Yoon, J.-H.; Kim, Y.-C. Pheophorbide-a conjugates with cancer-targeting moieties for targeted photodynamic cancer therapy. *Bioorg. Med. Chem.* **2015**, *23*, 1453–1462. [CrossRef]

60. Gabriel, D.; Lange, N.; Chobaz-Peclat, V.; Zuluaga, M.F.; Gurny, R.; Van Den Bergh, H.; Busso, N. Thrombin-sensitive dual fluorescence imaging and therapeutic agent for detection and treatment of synovial inflammation in murine rheumatoid arthritis. *J. Control. Release* **2012**, *163*, 178–186. [CrossRef]

61. Hendrich, C.; Siebert, W.E. Photodynamic therapy for rheumatoid arthritis? *Lasers Surg. Med.* **1997**, *21*, 359–364. [CrossRef]

62. Loeb, F.; Clark, W.M.; Coatney, G.R.; Coggeshall, L.T.; Dieuaide, F.R.; Dochez, A.R.; Hakansson, E.G.; Marshall, E.K., Jr.; Marvel, C.S.; et al. Activity of a new antimalarial agent, chloroquine (SN 7618): Statement approved by the Board for coordination of malarial studies. *JAMA* **1946**, *130*, 1069–1070. [CrossRef]

63. Vergne, P.; Liagre, B.; Bertin, P.; Cook-Moreau, J.; Treves, R.; Beneytout, J.L.; Rigaud, M. Methotrexate and cyclooxygenase metabolism in cultured human rheumatoid synoviocytes. *J. Rheumatol.* **1998**, *25*, 433–440. [PubMed]

64. Biemond, P.; Swaak, A.J.G.; Penders, J.M.A.; Beindorff, C.M.; Koster, J.F. Superoxide production by polymorphonuclear leucocytes in rheumatoid arthritis and osteoarthritis: In vivo inhibition by the antirheumatic drug piroxicam due to interference with the activation of the NADPH-oxidase. *Ann. Rheum. Dis.* **1986**, *45*, 249–255. [CrossRef] [PubMed]

65. Brogden, R.N.; Heel, R.C.; Speight, T.M.; Avery, G.S. Piroxicam. A reappraisal of its pharmacology and therapeutic efficacy. *Drugs* **1984**, *28*, 292–323. [CrossRef] [PubMed]

66. Abu Dayyeh, B.K.; Jirapinyo, P.; Weitzner, Z.; Barker, C.; Flicker, M.S.; Lautz, D.B.; Thompson, C.C. Endoscopic sclerotherapy for the treatment of weight regain after Roux-en-Y gastric bypass: Outcomes, complications, and predictors of response in 575 procedures. *Gastrointest. Endosc.* **2012**, *76*, 275–282. [CrossRef] [PubMed]

67. Neupane, J.; Ghimire, S.; Shakya, S.; Chaudhary, L.; Shrivastava, V.P. Effect of light emitting diodes in the photodynamic therapy of rheumatoid arthritis. *Photodiagn. Photodyn. Ther.* **2010**, *7*, 44–49. [CrossRef] [PubMed]

68. Butterweck, V.; Petereit, F.; Winterhoff, H.; Nahrstedtl, A. Solubilized Hypericin and Pseudohypericin from Hypericum perforatum Exert Antidepressant Activity in the Forced Swimming Test. *Planta Med.* **1998**, *64*, 291–294. [CrossRef]

69. García, I.; Ballesta, S.; Gilaberte, Y.; Rezusta, A.; Pascual, Á. Antimicrobial photodynamic activity of hypericin against methicillin-susceptible and resistant Staphylococcus aureus biofilms. *Future Microbiol.* **2015**, *10*, 347–356. [CrossRef]

70. Assefa, Z.; Vantieghem, A.; Declercq, W.; Vandenabeele, P.; Vandenheede, J.R.; Merlevede, W.; de Witte, P.; Agostinis, P. The activation of the c-Jun N-terminal kinase and p38 mitogen-activated protein kinase signaling pathways protects HeLa cells from apoptosis following photodynamic therapy with hypericin. *J. Biol. Chem.* **1999**, *274*, 8788–8796. [CrossRef]

71. Vantieghem, A.; Xu, Y.; Declercq, W.; Vandenabeele, P.; Denecker, G.; Vandenheede, J.R.; Merlevede, W.; De Witte, P.A.; Agostinis, P. Different Pathways Mediate Cytochrome *c* Release After Photodynamic Therapy with Hypericin. *Photochem. Photobiol.* **2001**, *74*, 133–142. [CrossRef]

72. Hendrickx, N.; Volanti, C.; Moens, U.; Seternes, O.M.; de Witte, P.; Vandenheede, J.R.; Piette, J.; Agostinis, P. Up-regulation of cyclooxygenase-2 and apoptosis resistance by p38 MAPK in hypericin-mediated photodynamic therapy of human cancer cells. *J. Biol. Chem.* **2003**, *278*, 52231–52239. [CrossRef] [PubMed]

73. Mikeš, J.; Kovaľ, J.; Jendželovský, R.; Sačková, V.; Uhrinová, I.; Kello, M.; Kuliková, L.; Fedoročko, P. The role of p53 in the efficiency of photodynamic therapy with hypericin and subsequent long-term survival of colon cancer cells. *Photochem. Photobiol. Sci.* **2009**, *8*, 1558–1567. [CrossRef] [PubMed]

74. Ferenc, P.; Solár, P.; Kleban, J.; Mikeš, J.; Fedoročko, P. Down-regulation of Bcl-2 and Akt induced by combination of photoactivated hypericin and genistein in human breast cancer cells. *J. Photochem. Photobiol. B Biol.* **2010**, *98*, 25–34. [CrossRef] [PubMed]

75. Kovaľ, J.; Mikeš, J.; Jendželovský, R.; Kello, M.; Solár, P.; Fedoročko, P. Degradation of HER2 Receptor Through Hypericin-mediated Photodynamic Therapy. *Photochem. Photobiol.* **2010**, *86*, 200–205. [CrossRef] [PubMed]

76. Karioti, A.; Bilia, A.R. Hypericins as Potential Leads for New Therapeutics. *Int. J. Mol. Sci.* **2010**, *11*, 562–594. [CrossRef] [PubMed]

77. Zhang, K.; Gao, S.; Guo, J.; Ni, G.; Chen, Z.; Li, F.; Zhu, X.; Wen, Y.; Guo, Y. Hypericin-photodynamic therapy inhibits proliferation and induces apoptosis in human rheumatoid arthritis fibroblast-like synoviocytes cell line MH7A. *Iran. J. Basic Med. Sci.* **2018**, *21*, 130–137. [CrossRef]

78. Schmitt, F.; Lagopoulos, L.; Käuper, P.; Rossi, N.; Busso, N.; Barge, J.; Wagnières, G.; Laue, C.; Wandrey, C.; Juillerat-Jeanneret, L. Chitosan-based nanogels for selective delivery of photosensitizers to macrophages and improved retention in and therapy of articular joints. *J. Control. Release* **2010**, *144*, 242–250. [CrossRef]

79. Tang, Q.; Cui, J.; Tian, Z.; Sun, J.; Wang, Z.; Chang, S.; Zhu, S. Oxygen and indocyanine green loaded phase-transition nanoparticle-mediated photo-sonodynamic cytotoxic effects on rheumatoid arthritis fibroblast-like synoviocytes. *Int. J. Nanomed.* **2017**, *12*, 381–393. [CrossRef]

80. Zhao, C.; Rehman, F.U.; Jiang, H.; Selke, M.; Wang, X.; Liu, C.Y. Titanium dioxide-tetra sulphonatophenyl porphyrin nanocomposites for target cellular bio-imaging and treatment of rheumatoid arthritis. *Sci. China Chem.* **2016**, *59*, 637–642. [CrossRef]

81. Dougherty, T.J.; Gomer, C.J.; Henderson, B.W.; Jori, G.; Kessel, D.; Korbelik, M.; Moan, J.; Peng, Q. Photodynamic therapy. *J. Natl. Cancer Inst.* **1998**, *90*, 889–905. [CrossRef]

82. Rehman, F.U.; Zhao, C.; Wu, C.; Li, X.; Jiang, H.; Selke, M.; Wang, X. Synergy and translation of allogenic bone marrow stem cells after photodynamic treatment of rheumatoid arthritis with tetra sulfonatophenyl porphyrin and TiO$_2$ nanowhiskers. *Nano Res.* **2016**, *9*, 3305–3321. [CrossRef]

83. Lu, Y.; Li, L.; Lin, Z.; Wang, L.; Lin, L.; Li, M.; Zhang, Y.; Yin, Q.; Li, Q.; Xia, H. A New Treatment Modality for Rheumatoid Arthritis: Combined Photothermal and Photodynamic Therapy Using Cu$_{7.2}$S$_4$ Nanoparticles. *Adv. Healthc. Mater.* **2018**, *7*, 1–11. [CrossRef] [PubMed]

84. Alexeree, S.M.; Sliem, M.A.; El-Balshy, R.M.; Amin, R.M.; Harith, M.A. Exploiting biosynthetic gold nanoparticles for improving the aqueous solubility of metal-free phthalocyanine as biocompatible PDT agent. *Mater. Sci. Eng. C* **2017**, *76*, 727–734. [CrossRef] [PubMed]

85. Karimi, A.R.; Khodadadi, A.; Hadizadeh, M. A nanoporous photosensitizing hydrogel based on chitosan cross-linked by zinc phthalocyanine: An injectable and pH-stimuli responsive system for effective cancer therapy. *RSC Adv.* **2016**, *6*, 91445–91452. [CrossRef]

86. Tian, N.; Sun, W.; Guo, X.; Lu, J.; Li, C.; Hou, Y.; Wang, X.; Zhou, Q. Mitochondria targeted and NADH triggered photodynamic activity of chloromethyl modified Ru(II) complexes under hypoxic conditions. *Chem. Commun.* **2019**, *55*, 2676–2679. [CrossRef] [PubMed]

87. Schmitt, F.; Freudenreich, J.; Barry, N.P.; Juillerat-Jeanneret, L.; Süss-Fink, G.; Therrien, B. Organometallic cages as vehicles for intracellular release of photosensitizers. *J. Am. Chem. Soc.* **2012**, *134*, 754–757. [CrossRef] [PubMed]
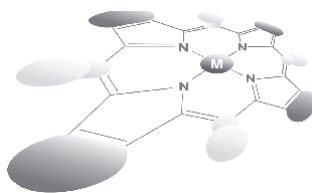
Combination of tetrapyridylporphyrins and arene ruthenium(II) complexes to treat synovial sarcoma by photodynamic therapy

Manuel Gallardo-Villagrán[a,c], Lucie, Yves Champavier[a,b], David Yannick Leger[a]*, Bruno Therrien[c]* and Bertrand Liagre[a]*

[a] *Laboratoire PEIRENE, Faculté de Pharmacie, Université de Limoges, EA 7500, F-87025 Limoges, France*

[b] *BISCEm, NMR platform, Centre de Biologie et de Recherche en Santé (CBRS), Limoges, France*

[c] *Institut de Chimie, Université de Neuchâtel, Avenue de Bellevaux 51, CH-2000 Neuchâtel, Switzerland*

ABSTRACT: Four tetrapyridylporphyrin and four dipyridylporphyrin arene ruthenium complexes have been synthesized and characterized. In these complexes, the porphyrin core is either metal-free or occupied by zinc, and the arene ligand of the arene ruthenium units are either the standard methyl-isopropyl-benzene (*p*-cymene) or the less common phenylpropanol (PhPrOH) derivative. The porphyrin derivatives are coordinated to four arene ruthenium units or only two, in accordance with the number of pyridyl substituents at the periphery of the porphyrins, 5,10,15,20-tetra(4-pyridyl)-21H,23H-porphine (TPyP) and 5,15-diphenyl-10,20-di(pyridin-4-yl)porphyrin (DPhDpyP). All eight complexes were evaluated as anticancer agents on synovial sarcoma cells, in the presence and absence of light, suggesting that both the arene ligand and the porphyrin core substituent can play a crucial role in fine-tuning the photodynamic activity of such organometallic photosensitizers.

KEYWORDS: photodynamic therapy, porphyrins, arene ruthenium, synovial sarcoma.

INTRODUCTION

Could we cure cancer with light? The answer is yes we could, using photodynamic therapy (PDT). However, light must go hand in hand with oxygen and a chemical compound that acts as an intermediary between the other two. The energy from light can be absorbed and reused or transferred by substances that we know as photoactive compounds, chromophores or photosensitizers (PS). These substances reach a higher energy excited state as a consequence of their interaction with photons. During relaxation, the PS can interact with other molecules or substrates to transmit the absorbed energy. This is the principle on which PDT is based (Fig. 1). In PDT, the PS is irradiated at a certain wavelength (λ), reaching an excited singlet state. During relaxation to ground state, the PS can go through an intermediate excited triplet state and interact with O_2 (Fig. 2). This interaction can produce singlet oxygen ($^1O_2$) that in turn can give rise to radical oxygen species (ROS) [1–4]. The key to PDT is ROS production, since it could lead to oxidative stress and consequently to cell death [5, 6]. Moreover, ROS are tremendously reactive, so their lifetime lasts only a few nanoseconds [2, 7], which makes the cell death process specifically located to the irradiated area. For these reasons, PDT is considered non-invasive, and its use is increasingly widespread in the fight against cancer and other diseases.

Throughout recent decades, PDT has been one of the most fast-growing treatments against skin cancer [8, 9], acne [10, 11] and other skin diseases [12, 13]. The FDA have already approved the use of PDT in multiple pathologies like actinic keratosis, advanced cutaneous T-cell lymphoma, Barrett's esophagus, basal cell skin cancer, esophageal cancer, non-small cell lung cancer

*Correspondence to: David Yannick Leger, email: david.leger@unilim.fr and Bertand Liagre, email: bertrand.liagre@unilim.fr
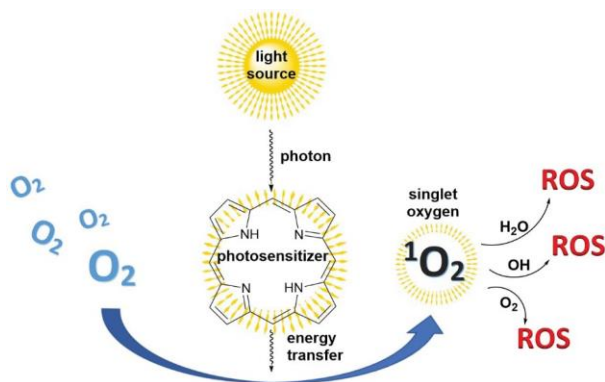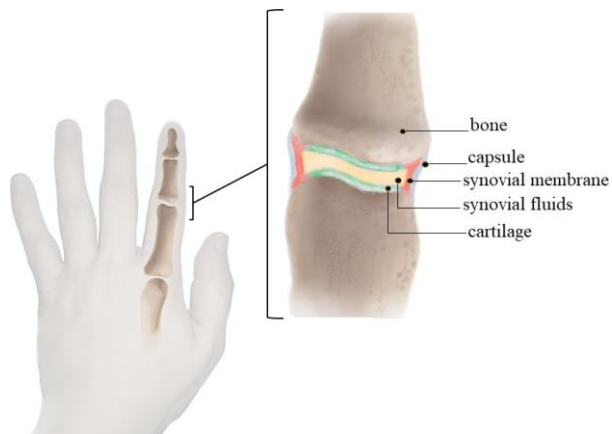
Fig. 1. Basic outline of the principles of PDT. The photosensitizer is excited by an external light source, transfers its energy to O_2, which is transformed into singlet oxygen, giving rise to reactive oxygen species (ROS).

**Fig. 3.** Representation of the synovial tissue that connects the bones in the joints (only major tissues are represented).

Fig. 2. Upon excitation to a triplet state, an electron can return directly to the ground state (fluorescence) or go through an intermediate triplet state (phosphorescence), where it can interact with O_2.

and squamous cell skin cancer. Furthermore, other types of cancer and more pathologies such as synovial sarcoma [14, 15], rheumatoid arthritis [16], bacterial infections [17, 18], are also under PDT investigations.

Synovial sarcoma is the fourth most common type of soft tissue cancer [19], representing approximately 10% of such cancers. It usually occurs in the surrounding area of large joints such as the synovial membrane, tendons, bursae or joint capsules. It is more common in men than women and in ages between 15 to 40 years old [20]. However, it is usually diagnosed late due to its slow progression, its benign appearance and the fact that it is often mistaken with pain due to trauma. The causes that give rise to this type of cancer are not yet fully understood [14]. The actual treatment involves invasive

surgery where tumoral tissues are removed [21]. Often, this is followed by radiotherapy and/or chemotherapy [22]. Evidently, this treatment entails a significant loss of soft tissue that can involve loss of mobility or add rigidity to the joint (Fig. 3). Therefore, minimizing the impact on healthy tissue can help to preserve better mobility in the joint and this is why PDT could play an important role, thanks to its minimal invasiveness and high precision.

However, PDT can likewise have some limitations, as a low solubility of PS, low concentration of oxygen in the target tissue or photosensitivity of the skin after treatment [23]. Many chromophores used in PDT show low solubility in biological media. This could lead to increase doses of PS to ensure optimal concentration in the target tissue, thus by increasing the dose of PS, side effects such as skin photosensitivity can appear. On the other hand, skin photosensitivity after PDT can be resolved using PS that require very low concentrations to be effective, in addition to the fact that the PSs can be totally inactive in the absence of light. A solution to increase solubility without increasing the dose is encapsulation of the PS in nanoparticles [24], coordination to peptides [25] or entrapment in lysosomes [26]. Also, it is possible to increase the solubility by designing PSs that incorporate hydrophilic substituents like sulfonate ($-SO_3H$) [27] or phosphonate ($-PO(OR)_2$) [28]. One more common solution is to use a solvent (other than water) in which the PS is soluble. However, it is necessary to take into account the toxicity of that solvent and the stability of the PS in this media, since some of these solvents are potential ligands and could degrade a drug before activation [29]. The inactivation or photoprotection of PS is another solution to limit photosensitivity. In this approach, the PS is transported in physiological medium and released selectively when necessary, thus reducing side effects [30–32].

Regarding the lack of oxygen, the accelerated growth of cancer cells generally leads to decreasing concentrations of O_2 [33, 34], which reduces the probability of giving rise to ROS. To resolve this inconvenience, it is
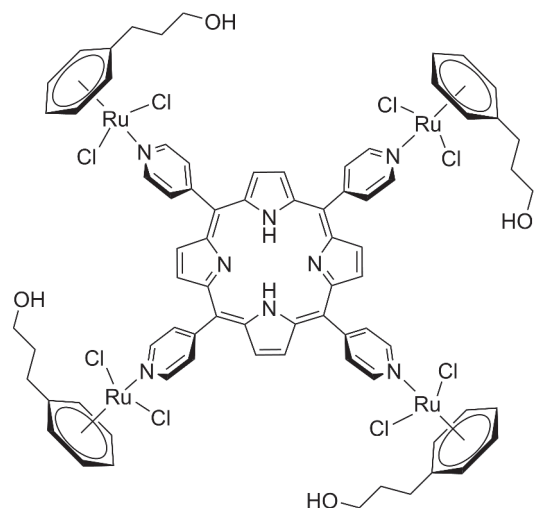
Fig. 4. Structure of a functionalized tetrapyridylporphyrin arene ruthenium complex.

possible to oxygenate the tumor tissue by hyperbaric oxygen therapy (HBO$_2$), prior to PDT [35].

Taking these aspects into account, we decided to design new PSs that increase the efficacy of PDT in synovial sarcoma based on the chromophore 5,10,15,20-tetra-(4-pyridyl)-21H,23H-porphine (TPyP). The TPyP is insoluble in water and poorly soluble in biological media. However, by coordination of arene ruthenium units to the pyridine substituents of TPyP (Fig. 4), solubility can be increased significantly. Moreover, these ruthenium complexes include arene ligands that have hydroxide groups (OH), that can potentially contribute to the presence of oxygen species, which can give rise to more ^{1}O$_2$ and ultimately increase ROS production [36].

The use of ruthenium organometallic complexes is not new to PDT, since it has been in use for years. The major reason behind that choice of metal is its oxidation state stability, being almost unreactive to air, water and O$_2$, unlike other metal-based compounds [37–43]. In addition, ruthenium has a high coordination number (6) and great facility to coordinate with ligands of complexed structures [37]. The arene ruthenium complexes could also improve the solubility in biological media [44]. Finally, ruthenium is less toxic than other metals such as platinum, a metal extensively used in metal-based drugs [45, 46].

In the present work, we show the synthesis and characterization of eight arene ruthenium complexes with tetrapyridylporphyrin or dipyridylporphyrin photosensitizers as a central ligand. For comparison, other derivatives incorporating different arene ligands, having two or four pyridyl groups, and with or without a metal in the core of the porphyrin have been synthesized and characterized. All new complexes were evaluated *in vitro*, in the presence and absence of light on synovial sarcoma cells.

RESULTS AND DISCUSSION

Synthesis and characterization of photosensitizers

The synthesis of these PSs is carried out by a one step reaction (Scheme 1). The dinuclear arene ruthenium dimers (**d1** or **d2**), synthesized as reported in the literature [47, 48], are mixed and reacted with the corresponding porphyrin (Scheme 1). Dimer **d1** is widely used [49–52] since the publication in 1972 by Zelonka and Baird [47], while the dimer **d2** is a more recent analogue and its reactivity remains unexplored [48].
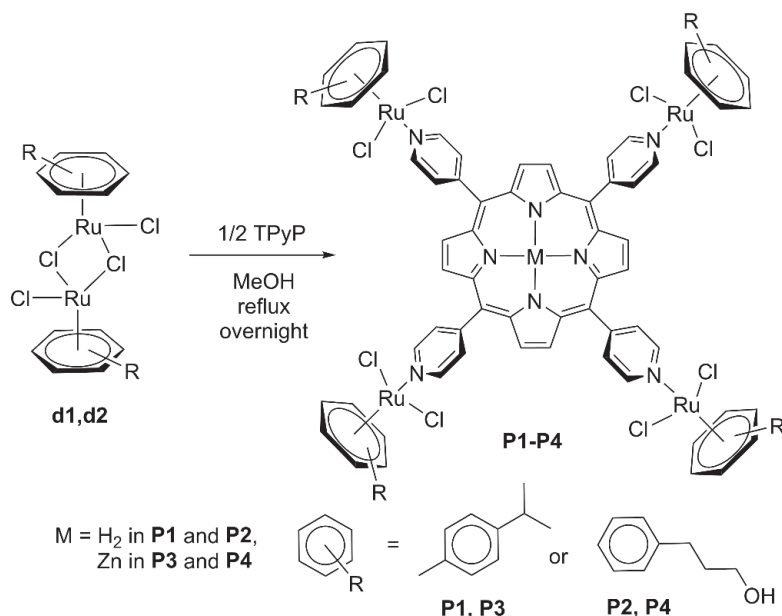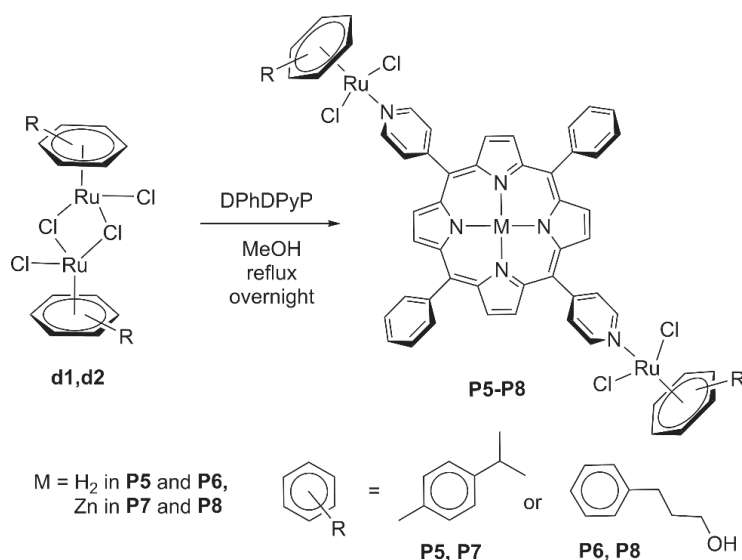

Scheme 1. Reactions of dimers **d1** or **d2** with TPyP or Zn-TPyP to form photosensitizers **P1**-**P4**.

As illustrated in Scheme 1, the reaction involves the breakage of the dimer into two monomers prior to the coordination of the porphyrin through a Ru–N(Py) bond. The reaction is carried out at reflux in methanol for at least 8 hr with a 2:1 molar ratio. Then, the suspension is filtered off and washed repeatedly with Et$_2$O, to obtain the desired tetranuclear complexes **P1**-**P4**. We had already reported the synthesis of **P1** ([Ru$_4$(*p*-cymene)$_4$(TPyP)Cl$_8$]) [53]. However, new derivatives (with TPyP and Zn-TPyP) involving the dimer **d2**, giving rise to the photosensitizer **P2** ([Ru$_4$(PhPrOH)$_4$(TPyP)Cl$_8$]) and **P4** ([Ru$_4$(PhPrOH)$_4$(Zn-TPyP)Cl$_8$], and with dimer **d1** to give rise to **P3** ([Ru$_4$(*p*-cymene)$_4$(Zn-TPyP)Cl$_8$]), have been also synthesized following the same methodology (see 'Experimental'). All compounds remain stable and unaltered at 4 °C for at least six months in the solid state. These compounds have acceptable solubility in DMSO and low solubility in other common solvents such as water, dichloromethane, chloroform, benzene, acetonitrile, acetone and ethanol. It should be noted that **P2** easily precipitates after minutes in DMSO. The recommended concentration of DMSO for *in vitro* tests is usually around 0.5%, although it depends on the cell line and the experimental conditions. According to the literature, 1% DMSO does not lead to toxicity in human myeloid leukemia and epithelia cancer [54]. On the other hand, in MDA-MB-231, MCF-7 and VNBRCA1 cell lines it is not recommended to use more than 0.6% of DMSO [55]. The maximum concentration used in our study has been 0.25% DMSO in the highest concentration of PS tested (5 μM). We have not observed any deleterious effect on synovial sarcoma cells that could be attributed to the presence of DMSO.

Similarly, we synthesized and characterized four new derivatives, which are based on 5,15-diphenyl-10,20-di(pyridin-4-yl)porphyrin (DPhDpyP), giving rise to the corresponding photosensitizers **P5**-**P8** (Scheme 2). We have decided to explore the synthesis with this new porphyrin to study the influence of the number of ruthenium complexes coordinated to the porphyrin in terms of its efficacy in PDT, as well as the influence of the presence of phenyl groups in the porphyrinic unit. The experimental conditions are the same as those mentioned for TPyP but a 1:1 molar ratio is needed. Dimers **d1** and **d2** give rise to the photosensitizers **P5** ([Ru$_2$(p-cymene)$_2$(DPhPyP)Cl$_4$]) and **P6** ([Ru$_2$(PhPrOH)$_2$(DPhPyP)Cl$_4$]) respectively, while **P7** ([Ru$_2$(p-cymene)$_2$(Zn-DPhPyP)Cl$_4$]) and **P8** ([Ru$_2$(PhPrOH)$_2$(Zn-DPhPyP)Cl$_4$]) are synthesized from the Zn-porphyrin analogue, with **d1** and **d2** respectively. The yields are a bit lower than those observed with TPyP, between 51–67%. Like **P1**-**P4**, compounds **P5**-**P8** are soluble in DMSO. They also remain unaltered at 4 °C for at least 6 months in the solid state. All compounds are stable in DMSO for at least 1 hr. After that, new signals can be seen in the ^{1}H-NMR spectrum (< 1%), which can be attributed to the decomposition or transformation of the compound by ligand exchange with DMSO [29].

### *In vitro* evaluation in synovial sarcoma cells

The photocytotoxicity (after irradiation) and cytotoxicity in the dark of photosensitizers **P1**-**P8** were evaluated *in vitro* on SW982 synovial sarcoma cells. A red-light lamp (λ = 630 nm) was used for irradiation (dose = 40 mW/cm^2 for 30 min). We decided to use red light because it is the only visible radiation that can pass through the skin and tissues of the synovial area of the joints. Blue radiation penetrates the skin for approximately 1 mm, green for about 2.5 mm, yellow not more than 4 mm, and red can penetrate as much as 5 mm before being fully absorbed [56]. The thickness of the human skin varies depending on the location between 0,5 - 4 mm, so to adapt our study to the future least invasive conditions possible, that is, transcutaneous PDT (without incision), irradiation with red light was the most appropriate.

Cell viability was analyzed by MTT assays for both, irradiated and non-irradiated cells. The results are shown in Table 1. The irradiated cells curve was fitted to the second order polynomial and from the resulting equation the IC$_{50}$ (inhibitory concentration at 50% viability) was calculated (Fig. 5). All PSs showed good photocytotoxic activity after irradiation and no significant toxicity in the dark. The synthesized PSs present three structural variations. One of them is the arene ligand, which is *p*-cymene or phenylpropanol. Interestingly, the four PSs with PhPrOH (**P2**, **P4**, **P6** and **P8**) as the arene improve the result when compared to their *p*-cymene analogues (**P1**, **P3**, **P5** and **P7**) (Table 1). The higher activity might be attributed to the presence of OH groups, which can help to increase the production of ROS after irradiation, either by direct interaction with another excited PS

Scheme 2. Synthesis of photosensitizers **P5**-**P8** from dimers **d1** and **d2**.

Table 1. Results of MTT assays in synovial sarcoma cells after PDT. Graphic representations are shown in the supporting information (Fig. S48-S55). Irradiation 24 hr after addition of PS, λ = 630 nm, 40 mW/cm^2 for 30 min irradiation. IC$_{50}$ was calculated fitting the curve to the second-degree polynomial $\pm$ 3 sigma deviation. The maximum concentration tested was 5 μM.

PS	Arene	Porphyrin	IC$_{50}$ (μM) light	IC$_{50}$ (μM) dark
P1	*p*-cymene	TPyP	0.170 $\pm$ 0.008	> 5
P2	C$_6$H$_5$PrOH	TPyP	0.060 $\pm$ 0.012	> 5
P3	*p*-cymene	Zn-TPyP	0.341 $\pm$ 0.008	1.092 $\pm$ 0.004
P4	C$_6$H$_5$PrOH	Zn-TPyP	0.256 $\pm$ 0.010	0.729 $\pm$ 0.005
P5	*p*-cymene	DPhDPyP	0.307 $\pm$ 0.014	> 5
P6	C$_6$H$_5$PrOH	DPhDPyP	0.212 $\pm$ 0.008	2.341 $\pm$ 0.005
P7	*p*-cymene	Zn-DPhDPyP	0.387 $\pm$ 0.010	1.096 $\pm$ 0.003
P8	C$_6$H$_5$PrOH	Zn-DPhDPyP	0.312 $\pm$ 0.010	0.689 $\pm$ 0.007
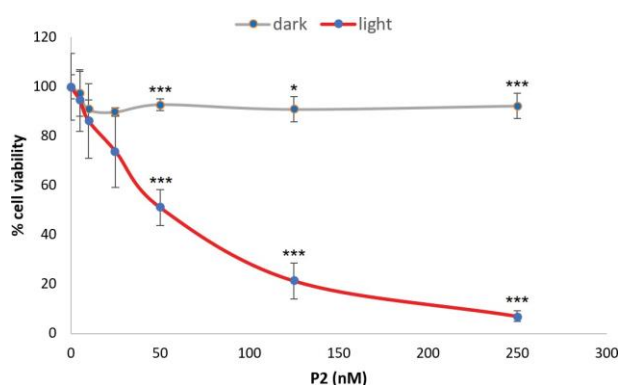
Fig. 5. Data obtained in the MTT assays in SW982 synovial sarcoma using **P2** as PS. Irradiation 24 hr after addition of **P2** (630 nm, 40 mW/cm^2, 30 min irradiation). Two-tailed Student's t-test significance, $P < 0.05$ (*), $P < 0.01$ (**) and $P < 0.001$ (***).

molecules or with other reactive species. Alcohols have been reported as an initial product in the production of ROS by metabolism [57]. In addition, porphyrins with phenol groups have proven their efficacy in PDT [58], as is the case of 5,10,15,20-tetra(*m*-hydroxyphenyl)chlorin (FOSCAN) [59–61]. Therefore, introduction of aliphatic alcohol at the periphery of a photosensitizer appears to be beneficial in our systems, increasing the PDT efficacy.

Another structural difference in **P1**-**P8** is the presence or absence of zinc in the center of the porphyrin. According to the results (Table 1), the presence of zinc worsens PDT efficacy. In all cases, the metal-free derivative shows a higher activity than its zinc analogue. One possible cause could be the fluorescence quantum yield ($\emptyset_F$). For instance, the photosensitizer **P1** shows a quantum yield lower than **P3** ($\emptyset_F{}^{P1}$ (%) = 3.0 and $\emptyset_F{}^{P3}$ (%) = 4.9) and the toxicity in the dark of the first was higher. Fluorescence is a consequence of the energetic decay from the excited state of the PS to the minimum energy state. Therefore, high $\emptyset_F$ suggests that much of the energy in the singlet excited state of the PS returns to the ground state without passing through the triplet excited state, generating more fluorescence but leaving behind less energy in the triplet state to interact with O$_2$ and to give rise to ROS [62]. Zinc is responsible for this increased fluorescence. The fluorescence emission of PS containing zinc as a metal center is higher than the metal-free analogue (Fig. 6). This can also be understood from the point of view of the HOMO and LUMO orbitals. When the chromophore is excited, an electron rises from the highest energy occupied orbital (HOMO) to the lowest energy unoccupied orbital (LUMO). In the case that there is no metal center in the porphyrin, the electron vacancy that remains in the HOMO orbital can be filled by the lone pair electrons of the N in the tetrapyrrole unit. Then, the excited electron in the LUMO orbital will have more difficulties to return back to the HOMO orbital during relaxation, favoring intersystem crossing (see Fig. 2). On the other hand, if the porphyrin has a metal center coordinated to the N atoms of the tetrapyrrole through their lone pair electrons, the vacancy left in the HOMO orbital is not filled and the excited electron can return from the LUMO orbital easily, thus favoring fluorescence [63]. This may
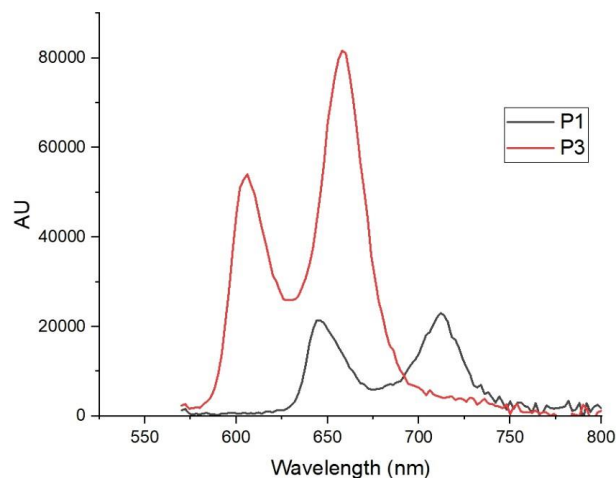
Fig. 6. Fluorescence spectrum of **P1** and **P3** (10 nM in DMSO).

explain why all our zinc-free PSs have a better IC$_{50}$ under light than their analogs with zinc.

The last structural difference in our PSs is the presence of two (DPhDPyP) or four (TPyP) pyridyl substituents on the PS and as a consequence, the presence of two or four coordinated arene ruthenium units. All PSs with DPhDPyP showed a reduced PDT effect than their tetranuclear counterparts. The reason may be due to the fact that PSs with DPhDPyP only have two coordinated ruthenium arenes, instead of the four presented in PSs with TPyP. Ru (II) arenes have been reported as solubility improvers in biological media for organic compounds [45], thus potentially increasing the uptake. Finally, it is worth noting the absence or very low toxicity of the compounds without metal (**P1**-**P4**) even at the highest concentration tested. While, Zn compounds (**P5**-**P6**) show some toxicity in the dark (Table 1). Similar results have been reported with zinc porphyrins, pointing to the metal as the cause for the cell growth decay [64, 65].

CONCLUSIONS

We report the synthesis and characterization of eight arene ruthenium porphyrin photosensitizers with great potential to treat synovial sarcoma by PDT. The photosensitizer **P2** showed the best light/dark photocytotoxicity ratio (0.06 μM/5 μM), being around two orders of magnitude. We have demonstrated that the presence of zinc (II) in the core of the photosensitizers have a double negative effect, increasing toxicity and reducing PDT efficacy. On the other hand, we have shown how alkyl alcohols on the arene ligands can improve the PDT effect in SW982 sarcoma cells. These results encourage us to continue studying these compounds and their potential in PDT, such as intracellular localization, PDT effect in another type of cancers, as well as performing an *in vivo* study.

EXPERIMENTAL

General

Compounds **d1**, **d2** and **P1** were prepared as described in the literature [47, 48, 42]. Methanol, ethanol, diethyl ether, CDCl$_3$ and (CD$_3$)$_2$SO were acquired from Sigma-Aldrich and used as received. NMR spectra were recorded on a Bruker Avance III HD 500 MHz, Avance III HD 400 MHz or a DRX 400 MHz spectrometers. The ^{1}H and ^{13}C resonances of the deuterated solvents were used as the internal reference. Ruthenium(III) chloride hydrate, 1-isopropyl-4-methylcyclohexa-1,4-diene, 5,10,15,20-tetra(4-pyridyl)-21*H*,23*H*-porphine and zinc 5,10,15,20-tetra(4-pyridyl)-21*H*,23*H*-porphine were acquired from Sigma-Aldrich, 3-(cyclohexa-1,4-dien-1-yl)propan-1-ol from Fisher Scientific and 5,15-diphenyl-10,20-di(pyridin-4-yl)porphyrin and zinc 5,15-diphenyl-10,20-di(pyridin-

4-yl)porphyrin from Porphychem. We carried out all the *in vitro* tests and manipulations under an aseptic atmosphere and constant sterilization conditions. SW982 sarcoma synovial cells were provided by the American Type Culture Collection (ATCC—LGC Standards). Cells were grown in DMEM medium supplemented with 10% fetal bovine serum, 1% L-glutamine and 100 U/ml penicillin and 100 μg/ml streptomycin (Gibco BRL, Cergy-Pontoise, France). 3-(4,5-Dimethylthiazol-2-yl)-2,5-diphenyltetrazolium bromide (MTT) and L-glutamine were acquired from Sigma-Aldrich. Dimethyl sulfoxide (DMSO) was bought in Acros Organics. The PSs (**P1**-**P8**) were dissolved at 1 mM concentration in DMSO just before use, then diluted in complete medium to the needed concentration and immediately preceding to use. The concentration of DMSO in the cell medium was in all cases lower than 0.1%. Cell irradiation was carried out using a red-light source, CureLight®, PhotoCure ASA, at 630 nm, and dose 40 mW/cm^2 for 30 min. Absorbance after MTT assay was measured at 540 nm by Dynex Triad Multi Mode Microplate Reader, Dynex Technologies. UV-vis spectrums were carried out in SI Analytics model UvLine 9400 (Xenon lamp) spectrophotometer, 1.5 mL polystyrene cuvettes (wavelength range 280–800 nm) and diluting the PS in DMSO (10 nM). Fluorescence spectrums were measured (550–800 nm) on a FLS980 spectrometer from Edinburgh Instruments, using 5,10,15,20-tetraphenylporphin as reference in toluene, while the PSs were dissolved 10 nM in DMSO. IR spectrums were performed on a Frontier PerkinElmer spectrometer (600 – 400 cm^{-1}). Spectra are shown in the Supporting Information (Fig. S1-S47).

Photocytotoxicity evaluation by MTT assays

First, trypsinization and counting of SW982 synovial sarcoma cells were carried out. Homogeneous solutions were prepared in 10 mL of culture medium with 700,000 cells. In a 96-well plate, 100 μL of the solution (7000 cells per well) were poured and the cells were incubated for 24 hr (37 °C and 5% CO$_2$). After that, 100 μL of PS solution in increasing concentration were poured per row in the plate and subsequent incubation 24 hr in the same conditions previously described. The PSs were dissolved in DMSO just before use and then added to culture medium in the desired concentrations. We have decided to use DMSO since it is the only solvent in which all PSs showed acceptable solubility, to keep the same experimental conditions. After incubation the medium was removed carefully and poured 100 μL of complete medium without red phenol per well. Then, the activation of PS by irradiation is carried out with red light (λ = 630 nm) is then carried out, applying 40 mW/cm^2 for 30 min. The lamp is put at 12 cm above of the plate in vertical position. After the irradiation the 96-well plate was put in the incubator during 18 hr. After this time, we added 10 μL of MTT solution (5 g/L) and the plate was put

again inside the incubator during 4 hr. Then, the media is removed and added 200 μL of DMSO per well, stirring the plate gently (to avoid splashing between wells) for 3 min until homogenized. Finally, the absorbance is measured at 550 nm. This whole process is repeated in triplicate. Cytotoxicity measurements in the absence of light are carried out by repeating this entire protocol except the irradiation dose. The results obtained in the photocytotoxicity tests are expressed graphically as the mean ± three standard deviations. Statistical significance was calculated using the Student's t-test where $P < 0.05$, < 0.01 and < 0.001 is expressed as *, ** and *** respectively.

Synthesis of P2. In a 100 mL round bottom flask, a solution containing 60.0 mg (0,098 mml) of **d2** and 30.1 mg (0,049 mmol) of TPyP in 30 mL of MeOH, is prepared. The solution is refluxed for 12 hr, then cooled to room temperature. The solution is filtered off and the resulting brown solid is washed with Et_2O (5 × 10 mL).

P2. Yield 86% (78 mg). ^{1}H NMR (DMSO-d$_6$, 25 °C, 500 MHz): δ 9.08 (m, 8H, CH_{py}), 8.92 (br s, 8H, CH_{porph}), 8,28 (m, 8H, CH_{py}), 5.98 (m, 8H, m-CH_{ar}), 5.76 (overlapping doublets, 8H, o-CH_{ar}), 5.75 (overlapping triplets, 4H, p-CH_{ar}), 4.59 (s, 4H, OH), 3.45 (m, 8H, CH_2), 2.47 (m, 8H, CH_2), 1.73 (m, 8H, CH_2), -3.06 (s, 2H, NH). ^{13}C NMR (DMSO-d6, 25 °C, 125 MHz): δ 142.06 (C_{py}), 128.16 (C_{py}), 128.10 (C_{porph}), 125.46 (C_{py}), 107.83 ($C_{propanol}$), 88.79 (m-C_{ar}), 84.80 (o-C_{ar}), 82.91 (p-C_{ar}), 59.89 (CH_2), 32.04 (CH_2), 29.42 (CH_2). UV/vis (DMSO), λ, nm (ε, $M^{-1}.cm^{-1}$): 445 (262300), 523 (197400), 588 (152500), 638 (125300). FT-IR (ATR, solid, cm^{-1}): ν; br s (3700-3200), s (3108), s (2916), s (2824), s (1614), s (1418).

The synthesis of **P3** and **P4** utilize the same protocol and molar ratio as in **P2**, but using the corresponding dimer (**d1**, **d2**) and porphyrin. **P5-P8** are synthesize in the same manner but using a molar ratio of 1:1 (dimer:porphyrin) (**DPhDPyP** or **Zn-DPhDPyP**).

P3. Yield 81% (234 mg). ^{1}H NMR (DMSO-d6, 25 °C, 400 MHz): δ 9.03 (d, $^3J_{HH}$ = 5.55 Hz, 8H, CH_{py}), 8.85 (s, 8H, CH_{porph}), 8,23 (d, $^3J_{HH}$ = 5.72 Hz, 8H, CH_{py}), 5.83 (d, $^3J_{HH}$ = 6.14 Hz, 8H, CH_{ar}), 5.78 (d, $^3J_{HH}$ = 6.15 Hz, 8H, CH_{ar}), 2.84 (m, $^3J_{HH}$ = 6.91 Hz, 4H, CH $_{iPr}$), 4.58 (bs, 4H, OH), 2.09 (s, 12H, CH_3), 1.20 (m, $^3J_{HH}$ = 5.55 Hz, 24H, CH_3 $_{iPr}$). ^{13}C NMR (DMSO-d6, 25 °C, 101 MHz): δ 149.12 (C_{ar}), 148.50 (C_{py}), 132.48 (C_{porph}), 129.72 (C_{py}), 118.57 (C_{py}), 106.83 (C_{porph}), 100.56 (C_{ar}), 86.83 (CH_{ar}), 85.99 (CH_{ar}), 30.44 (CH $_{iPr}$), 21.97 (CH_3 $_{iPr}$), 18.34 (CH_3). Elemental analysis: Calcd. for $C_{80}H_{80}Cl_8N_8O_4Ru_4Zn$ + 4 H_2O: C, 48.56; H, 4.48; N 5.66. Found: C, 48.46; H, 4.63; N, 5.90. UV/vis (DMSO), λ, nm (ε, $M^{-1}.cm^{-1}$): 472 (59400), 518 (138300), 558 (55000), 599 (53300). FT-IR (ATR, solid, cm^{-1}): ν; br s (3600-3250), s (3091), s (2944), s (2881), s (1609).

P4. Yield 88% (82 mg). ^{1}H NMR (DMSO-d6, 25 °C, 400 MHz): δ 9.02 (br s, 8H, CH_{py}), 8.65 (br s, 8H, CH_{porph}), 8,22 (br s, 8H, CH_{py}), 5.98 (m, 8H, m-CH_{ar}), 5.75 (overlapping doublet, 8H, o-CH_{ar}), 5.73 (overlapping triplet,

4H, p-CH_{ar}), 4.58 (br s, 4H, OH), 3.45 (m, 8H, CH_2), 2.48 (m, 8H, CH_2), 1.73 (m, 8H, CH_2). ^{13}C NMR (DMSO-d6, 25 °C, 101 MHz): δ 149.11 (C_{ar}), 148.47 (C_{py}), 132.48 (C_{porph}), 129.72 (C_{py}), 108.44 ($C_{propanol}$), 89.40 (m-C_{ar}), 85.33 (o-C_{ar}), 83.43 (p-C_{ar}), 60.46 (CH_2), 32.64 (CH_2), 30.00 (CH_2). Elemental analysis: Calcd. for $C_{76}H_{72}Cl_8$-$N_8O_4Ru_4Zn$: C, 47.67; H, 3.79; N 5.85. Found: C, 47.67; H 3.79; N 6.09. ESI-MS, m/z, 954.8 [M – [Ru(PhPrOH)-$Cl_2]_3$ – Cl]$^{+1}$. UV/vis (DMSO), λ, nm (ε, $M^{-1}.cm^{-1}$): 522 (95300), 561 (45200), 598 (49800). FT-IR (ATR, solid, cm^{-1}): ν; br s (3500-3200), s (3067), s (2910), s (2881), s (1619), s (1408).

P5. Yield 51% (51 mg). ^{1}H NMR (CDCl$_3$, 25 °C, 400 MHz): δ 9.47 (m, 4H, CH_{py}), 8.87 (m, 10H, CH_{Ph}), 8.21 (m, 8H, CH_{porph} and CH_{py}), 7.78 (br s, 4H, CH_{porph}), 5.69 (d, $^3J_{HH}$ = 5.72 Hz, 4H, CH_{ar}), 5.47 (d, $^3J_{HH}$ = 5.48 Hz, 4H, CH_{ar}), 3.20 (m, 2H, CH $_{iPr}$), 2.23 (s, 6H, CH_3), 1.47 (d, $^3J_{HH}$ = 6.86 Hz, 12H, CH_3 $_{iPr}$), -2.81 (s, 1H, NH), -2.87 (s, 1H, NH). ^{13}C NMR (CDCl$_3$, 25 °C, 101 MHz): δ 153.04 (C_{py}), 141.76 (C_{ph}), 134.54 (C_{py}), 130.20 (C_{ph}), 127.97 (C_{py}), 126.77 (C_{porph}), 121.55 (C_{porph}), 120.93 (C_{porph}), 83.23 (CH_{ar}), 82.55 (CH_{ar}), 30.92 (CH $_{iPr}$), 22.50 (CH_3 $_{iPr}$), 18.42 (CH_3). Elemental analysis: Calcd. for $C_{62}H_{56}Cl_4N_6Ru_2$: C, 60.99; H, 4.59; N 6.84. Found: C, 62.76; H 4.81; N 7.09. UV/vis (DMSO), λ, nm (ε, M^{-1}.cm^{-1}): 513 (143500), 549 (319100), 590 (134400), 648 (29000). FT-IR (ATR, solid, cm^{-1}): ν; br s (3550-3400), s (3080), s (2968), s (1638), s (1491).

P6. Yield 61% (60 mg). ^{1}H NMR (CDCl$_3$, 25 °C, 400 MHz): δ 9.50 (d, $^3J_{HH}$ = 5.96 Hz, 4H, CH_{py}), 8.89 (m, 10H, CH_{Ph}), 8.23 (m, 8H, CH_{porph} and CH_{py}), 7.80 (m, 4H, CH_{porph}), 5.93 (t, $^3J_{HH}$ = 5.64 Hz, 4H, m-CH_{ar}), 5.81 (t,

$^3J_{HH}$ = 5.58 Hz, 2H, p-CH_{ar}), 5.62 (d, $^3J_{HH}$ = 5.72 Hz, 4H, o-CH_{ar}), 3.88 (q, $^3J_{HH}$ = 5.83 Hz, 4H, CH_2), 2.84 (t, $^3J_{HH}$ = 7.71 Hz, 4H, CH_2), 2.07 (m, 4H, CH_2), 1.69 (overlapping multiplet, 2H, OH), -2.80 (s, 2H, NH). Elemental analysis: Calcd. for $C_{60}H_{52}Cl_4N_6O_2Ru_2$: C, 58.45; H, 4.25; N 6.82. Found: C, 59.85; H 4.56; N 6.88. UV/vis (DMSO), λ, nm (ε, $M^{-1}.cm^{-1}$): 509 (43400), 550 (154700), 589 (48200), 648 (4000). FT-IR (ATR, solid, cm^{-1}): ν; br s (3600-3200), s (3102), s (2892), s (1641).

P7. Yield 54% (68 mg). ^{1}H NMR (DMSO-d6, 25 °C, 400 MHz): δ 9.00 (m, 4H, CH_{py}), 8.82 (m, 10H, CH_{Ph}), 8.20 (m, 8H, CH_{porph} and CH_{py}), 7.81 (m, 4H, CH_{porph}), 5.83 (d, $^3J_{HH}$ = 5.39 Hz, 4H, CH_{ar}), 5.78 (d, $^3J_{HH}$ = 6.18 Hz, 4H, CH_{ar}), 2.84 (m, 2H, CH $_{iPr}$), 2.09 (s, 6H, CH_3), 1.20 (d, $^3J_{HH}$ = 6.94 Hz, 12H, CH_3 $_{iPr}$). Elemental analysis: Calcd. for $C_{62}H_{54}Cl_4N_6Ru_2Zn$: C, 57.62; H, 4.21; N 6.50. Found: C, 58.51; H 4.32; N 6.59. ESI-MS, m/z, 950.9 [M – [Ru(p-cymene)Cl$_2$] – Cl]$^{+1}$, 680.8 [Zn-DPhDPyP + H]$^{+1}$. UV/vis (DMSO), λ, nm (ε, $M^{-1}.cm^{-1}$): 493 (55600), 524 (99900), 562 (349500), 600 (221100), 626 (81300) (. FT-IR (ATR, solid, cm^{-1}): ν; br s (3650-3200), s (3080), s (2988), s (1639).

P8. Yield 67% (84 mg). ^{1}H NMR (DMSO-d6, 25 °C, 400 MHz): δ 9.01 (m, 4H, CH_{py}), 8.82 (m, 10H, CH_{Ph}), 8.20 (m, 8H, CH_{porph} and CH_{py}), 7.82 (m, 4H, CH_{porph}),

5.99 (m, 4H, *m*-CH_{ar}), 5.75 (m, 6H, *p*-CH_{ar} and *o*-CH_{ar}), 4.59 (m, 2H, OH), 3.46 (m, 4H, CH_2), 2.47 (m, 4H, CH_2), 1.73 (m, 4H, CH_2). Elemental analysis: Calcd. for C$_{60}$H$_{50}$Cl$_4$N$_6$O$_2$Ru$_2$Zn: C, 55.59; H, 3.89; N 6.48. Found: C, 56.44; H 4.09; N 6.56. ESI-MS, m/z, 952.9 [M − [Ru(PhPrOH)Cl$_2$] − Cl]$^{+1}$. UV/vis (DMSO), λ, nm (ε, M^{-1}.cm^{-1}): 482 (21700), 521 (46900), 559 (253400), 600 (108700), 626 (37900). FT-IR (ATR, solid, cm^{-1}): ν; br s (3580-3150), s (3012), s (2917), s (1591).

Acknowledgments

Supporting information

Additional photosensitizer results are given in the supplementary material. This material is available free of charge *via* the Internet at http://www.worldscientific.com/doi/suppl/10.1142/S1088424622020011

REFERENCES

1. Dougherty TJ, Gomer CJ, Henderson BW, Jori G, Kessel D, Korbelik MJ and Peng Q. *J. Natl Cancer Inst.* 1998; **90**: 889–905.

2. Dolmans DE., Fukumura D and Jain RK. *Nat. Rev. Cancer*. 2003; **3**: 380–387.

3. De Silva P, Saad MA, Thomsen HC, Bano S, Ashraf S and Hasan T. *J Porphyrins Phthalocyanines*. 2020; **24**: 1320–1360.

4. Vargas-Zúñiga GI, Kim HS, Li M, Sessler JL and Kim JS. *J Porphyrins Phthalocyanines*. 2021; **25**: 773–793.

5. Mroz P, Yaroslavsky A, Kharkwal GB and Hamblin MR. *Cancers*. 2011; **3**: 2516–2539.

6. Buytaert E, Dewaele M and Agostinis P. *BBA-Rev Cancer*. 2007; **1776**: 86–107.

7. Simon HU, Haj-Yehia A and Levi-Schaffer F. *Apoptosis*. 2000; **5**: 415–418.

8. Dos Santos AF, De Almeida DRQ, Terra LF, Baptista MS and Labriola, L. *J Cancer Metastasis Treat*. 2019; **5**: 25.

9. Zhang L, Ji Z, Zhang J and Yang S. *Photodiagnosis Photodyn Ther*. 2019; **28**: 159–165.

10. Hilerowicz Y, Friedman O, Zur E, Ziv R, Koren A, Salameh F, Mehrabi JN and Artzi O. *Lasers Surg Med*. 2020; **52**: 966–970.

11. Ding HL, Wang XL, Wang HW and Huang Z. *Photodiagnosis Photodyn Ther*. 2011; **8**: 343–346.

12. Ruiz-Moreno JM, Montero JA and Barile S. *Eur. J. Ophthalmol*. 2006; **16**: 426–434.

13. Montero JA, Ruiz-Moreno JM and Fernandez-Muñoz M. *Eur J Ophthalmol*. 2011; **21**: 503–505.

14. Kusuzaki K, Murata H, Matsubara T, Miyazaki S, Shintani K, Seto M, Matsumine A, Hosol A, Sugimoto T and Uchida A. *Photochem Photobiol*. 2005; **81**: 705–710.

15. Takeda K, Kunisada T, Miyazawa S, Nakae Y and Ozaki T. Clinical orthopaedics and related research. 2008; **466**: 1726–1733.

16. Gallardo-Villagrán M, Leger DY, Liagre B, Therrien B. *Int J Mol Sci*. 2019; **20**: 3339.

17. Maisch T, Szeimies RM, Jori G and Abels C. *Photochem. Photobiol. Sci*. 2004; **3**: 907–917.

18. Maldonado-Carmona N, Ouk TS, Calvete MJ, Pereira MM, Villandier N and Leroy-Lhez S. *Photochem. Photobiol. Sci*. 2020; **19**: 445–461.

19. Siegel, H. J., Sessions, W., Casillas Jr, M. A., Said-Al-Naief, N., Lander, P. H. and Lopez-Ben, R. *Orthopedics*. 2007; **30**: 1020.

20. Cadman NL, Soule EH and Kelly PJ. 1965; **18**: 613–627.

21. Bergovec M, Smerdelj M, Bacan F, Seiwerth S, Herceg D and Prutki M. *Orthop Traumatol Surg Res.* 2018; **104**: 227–230.

22. Kampe CE, Rosen G, Eilber F, Eckardt J, Lowenbraun S, Foster J, Forscher C and Selch M. *Cancer*. 1993; **72**: 2161–2169.

23. Gunaydin G, Gedik ME and Ayan S. *Front Chem*. 2021; **9**: 400.

24. Lucky SS, Soo KC and Zhang Y. *Chem Rev*. 2015; **115**: 1990–2042.

25. Jiang Z, Shao J, Yang T, Wang J and Jia L. *J Pharm Biomed Anal*. 2014; **87**: 98–104.

26. Huang H, Yu B, Zhang P, Huang J, Chen Y, Gasser G, Ji L and Chao H. *Angew Chem Int Ed*. 2015; **54**: 14049–14052.

27. Dubuc C, Langlois R, Bénard F, Cauchon N, Klarskov K, Tone P and van Lier JE. *Bioorg Med Chem Lett*. 2008; **18**: 2424–2427.

28. Liang G, Wang L, Yang Z, Koon H, Mak N, Chang CK and Xu B. *Chem Comm*. 2006; **48**: 5021–5023.

29. Patra M, Joshi T, Pierroz V, Ingram K, Kaiser M, Ferrari S, Spingler B, Keiser J and Gasser G. *Chem Eur J*. 2013; **19**: 14768–14772.

30. Roy I, Bobbala S, Young RM, Beldjoudi Y, Nguyen MT, Cetin MM, Cooper JA, Allen S, Anamimoghadam O, Scott EA, Wasielewski MR and Stoddart JF. *J Am Chem Soc*. 2019; **141**: 12296–12304.

31. Leonidova A, Anstaett P, Pierroz V, Mari C, Spingler B, Ferrari S and Gasser G. *Inorg Chem*. 2015; **54**: 9740–9748.

32. Leonidova A, Mari C, Aebersold C and Gasser G. *Organometallics*. 2016; **35**: 851–854.

33. Hockel M and Vaupel P. *J Natl Cancer Inst*. 2001; **93**: 266–276.

34. Vaupel P, Mayer A and Höckel M. *Methods Enzymol*. 2004; **381**: 335–354.

35. Maier A, Tomaselli F, Anegg U, Rehak P, Fell B, Luznik S, Pinter H and Smolle-Jüttner FM. *Eur J Cardiothorac Surg*. 2000; **18**: 649–655.

36. Bonnett R, Djelal BD and Nguyen A. *J Porphyrins Phthalocyanines*. 2001; **5**: 652–661.

37. Kaspler P, Lazic S, Forward S, Arenas Y, Mandel A and Lilge L. *Photochem Photobiol Sci*. 2016; **15**: 481–495.

38. Lv Z, Wei H, Li Q, Su X, Liu S, Zhang KY, Lv W, Zhao Q, Li X and Huang W. *Chem Sci*. 2018; **9**: 502–512.

39. Yano T, Hishida S, Nakai M and Nakabayashi Y. *Inorganica Chim Acta*. 2017; **454**: 162–170.

40. Lei W, Zhou Q, Jiang G, Zhang B and Wang X. *Photochem Photobiol Sci*. 2011; **10**: 887–890.

41. Huang H, Zhang P, Yu B, Jin C, Ji L and Chao H. *Dalton Trans*. 2015; **44**: 17335–17345.

42. Schmitt F, Govindaswamy P, Süss-Fink G, Ang WH, Dyson PJ, Juillerat-Jeanneret L and Therrien B. *J Med Chem*. 2008; **51**: 1811–1816.

43. Schmitt F, Freudenreich J, Barry NP, Juillerat-Jeanneret L, Süss-Fink G and Therrien B. *J Am Chem Soc*. 2012; **134**: 754–757.

44. Therrien B and Furrer J. *Adv Chem Eng*. 2014; **2014**: 1–20.

45. Yano T, Hishida S, Nakai M and Nakabayashi Y. *Inorganica Chim Acta*. 2017; **454**: 162–170.

46. Bogoeva V, Siksjø M, Sæterbø KG, Melø TB, Bjørkøy A, Lindgren M and Gederaas OA. *Photodiagn Photodyn Ther*. 2016; **14**: 9–17.

47. Zelonka RA and Baird M. *Can J Chem*. 1972; **50**: 3063–3072.

48. Čubrilo J, Hartenbach I, Schleid T and Winter RF. *Z Anorg Allg Chem*. 2006; **632**: 400–408.

49. Govindaswamy P, Süss-Fink G and Therrien B. *Organometallics*. 2007; **26**: 915–924.

50. Stringer T, Therrien B, Hendricks DT, Guzgay H and Smith GS. *Inorg Chem Commun*. 2011; **14**: 956–960.

51. Gupta G, Yap GP, Therrien B and Rao KM. *Polyhedron*. 2009; **28**: 844–850.

52. Kota TP and Kollipara MR. *J Chem Sci*. 2014; **126**: 1143–1151.

53. Schmitt F, Govindaswamy P, Süss-Fink G, Ang WH, Dyson PJ, Juillerat-Jeanneret L and Therrien B. *J Med Chem*. 2008; **51**: 1811–1816.

54. Villarroel A, Duff A and Hu T. *FASEB J*. 2020; **34**: 1–1.

55. Nguyen ST, Nguyen HTL and Truong KD. *Biomed Res Ther*. 2020; **7**: 3855–3859.

56. Clement M, Daniel G and Trelles M. *J Cosmet Laser Ther*. 2005; **7**: 177–189.

57. Gomes AC, Mello AL, Ribeiro MG, Garcia DG, Da Fonseca CO, Salazar MDA, Schönthal AH and Quirico-Santos T. *Arch Immunol Ther Exp*. 2017; **65**: 285–297.

58. Mroz P, Bhaumik J, Dogutan DK, Aly Z, Kamal Z, Khalid L, Kee HL, Bocian DF, Holten D, Lindsey JS and Hamblin MR. *Cancer lett*. 2009; **282**: 63–76.

59. Jones HJ, Vernon DI and Brown SB. *Br J Cancer*. 2003; **89**: 398–404.

60. Meier D, Botter SM, Campanile C, Robl B, Gräfe S, Pellegrini G, Born W and Fuchs B. *Int J Cancer*. 2017; **140**: 1680–1692.

61. Senge MO and Brandt JC. *Photochem Photobiol*. 2011; **87**: 1240–1296.

62. Kamkaew A, Lim SH, Lee HB, Kiew LV, Chung LY and Burgess K. *Chem Soc Rev*. 2013; **42**: 77–88.

63. Afaneh AT and Schreckenbach G. *Am J Phys Chem*. 2015; **119**: 8106–8116.

64. Lutton JD, Abraham NG, Drummond GS, Levere RD and Kappas A. *Proc Natl Acad Sci*. 1997, **94**: 1432–1436.

65. Yang G, Nguyen X, Ou J, Rekulapelli P, Stevenson DK and Dennery PA. *Am J Hematol*. 2001; **97**: 1306–1313.

Evaluation of Ruthenium-Based Assemblies as Carriers of Photosensitizers to Treat Rheumatoid Arthritis by Photodynamic Therapy

Manuel Gallardo-Villagrán [1,2], Lucie Paulus [2], Jean-Louis Charissoux [3], Sylvain Sutour [4], Pascale Vergne-Salle [5], David Yannick Leger [2], Bertrand Liagre [2,*,†] and Bruno Therrien [1,*,†]

1   Institut de Chimie, Université de Neuchâtel, Avenue de Bellevaux 51, CH-2000 Neuchâtel, Switzerland; manuel.gallardo@unine.ch
2   Laboratoire PEIRENE EA 7500, Faculté de Pharmacie, Université de Limoges, 87025 Limoges, France; lucie.paulus@etu.unilim.fr (L.P.); david.leger@unilim.fr (D.Y.L.)
3   Service d'Orthopédie-Traumatologie, CHRU Dupuytren, 2 Avenue Martin Luther King, CEDEX, 87042 Limoges, France; jlouis.charissoux@chu-limoges.fr
4   Neuchâtel Platform for Analytical Chemistry (NPAC), University of Neuchâtel, Avenue de Bellevaux 51, CH-2000 Neuchâtel, Switzerland; sylvain.sutour@unine.ch
5   Service de Rhumatologie, CHRU Dupuytren 2, 16 rue Bernard Descottes, CEDEX, 87042 Limoges, France; pascale.vergne-salle@chu-limoges.fr
*   Correspondence: bertrand.liagre@unilim.fr (B.L.); bruno.therrien@unine.ch (B.T.)
†   These authors contributed equally to the work.

Abstract: For the first time, ruthenium-based assemblies have been used as carriers for photosensitizers in the treatment of rheumatoid arthritis by photodynamic therapy (PDT). These metallacages are totally soluble in physiological media and can transport photosensitizers (PS) in their cavity. After an incubation period, the PS is released in the cytoplasm and irradiation can take place. This strategy allows photosensitizers with low or null solubility in biological media to be evaluated as PDT agents in rheumatoid arthritis. The systems in which 21*H*,23*H*-porphine and 29*H*,31*H*-phthalocyanine are encapsulated show excellent photocytotoxicity and no toxicity in the dark. On the other hand, systems in which metalated derivatives such as Mg(II)-porphine and Zn(II)-phthalocyanine are used show good photocytotoxicity, but to a lesser extent than the previous two. Furthermore, the presence of Zn(II)-phthalocyanine significantly increases the toxicity of the system. Overall, fifteen different host–guest systems have been evaluated, and based on the results obtained, they show high potential for treating rheumatoid arthritis by PDT.

Keywords: rheumatoid arthritis; photodynamic therapy; drug delivery; host–guest system; COX-2; photosensitizer; arene ruthenium complexes

1. Introduction

Rheumatoid arthritis (RA) is a chronic inflammatory autoimmune joint disease, leading to cartilage and bone damage, and finally disability. Occasionally, RA is complicated with extra-articular manifestations, particularly pulmonary involvement, and is associated with cardiovascular comorbidities [1]. The prevalence is 0.3% to 1%, and is 2–3 times higher in women than in men [2].

In recent years, it has become evident that RA arises based on both genetic and epigenetic components, but also has an environmental component, such as cigarette smoke, dust exposure, and particularly the effect of the microbiome [3]. Abnormalities in the cellular and humoral immune response lead to the occurrence of autoantibodies, detected many months or years before the clinical disease is apparent. These autoantibodies are rheumatoid factors (directed against the Fc fragment of immunoglobulins) and anti-citrullinated protein antibodies (ACPA) [4,5].

In RA, the synovial lining, which normally is comprised of 1–3 cell layers, becomes remarkably thickened. This is due to an invasion of macrophage-like cells and the proliferation of resident synovial fibroblasts. The degree of synovial hyperplasia correlates with the severity of cartilage erosion, resulting in inflammatory pannus formation that attaches to, and invades, joint cartilage, while osteoclast activation leads to parallel bone destruction [6]. The interaction between synovial resident cells and cells of the innate and adaptative immune system leads to the production of many pro-inflammatory cytokines (TNF-α, interleukine-1 (IL-1), IL-6), proteolytic enzymes, and inflammatory molecules [1].

Treatment algorithms involve measuring disease activity with composite indices and applying a treatment-to-target strategy, with disease modifying antirheumatic drugs (DMARDs) to maintain stringent remission or at least low disease activity and reduce articular destruction and disability [7]. There are two major classes of DMARDs, namely synthetic (sDMARDs) and biological (bDMARDs) [8].

Despite all of the advances made over the last two decades, and given that remission or at least low disease activity are the current therapeutic goals for RA patients, a significant proportion of patients still do not reach this target. There is a need for new treatments or local treatments to control some resistant synovitis.

In recent years, promising results have been achieved using non-invasive treatments such as anti-tumor necrosis factor drugs [9], Janus kinase inhibitors [10], and photodynamic therapy (PDT) [11]. The latter involves a photoactive compound, termed the photosensitizer (PS), which is excited by suitable light radiation. Subsequently, the excitation energy gives rise to radical oxygen species (ROS) from oxygen present in the medium [12,13]. ROS show a high cytotoxicity, but also a short lifetime and reduced radius of action [14], so it is possible to treat the inflamed zone without affecting the surrounding tissue, avoiding damage to healthy structures. Accordingly, PDT could be an effective solution for cases of RA with refractory synovitis and failure of local steroid injection.

Since the late 1990s, PDT began to demonstrate its potential as a less invasive treatment for RA. Trauner and colleagues [15] reported the in vivo efficacy of this technique in rabbits with an antigen-induced arthritis model, using benzoporphyrin derivative monoacid ring A (one of the first-generation PSs) and intra-articular irradiation. Later, with the new generation PSs, in vivo results remained promising, such as the use of ATX-S10.Na (II) in collagen antibody-induced arthritis in mice [16]. Recently, it has been reported that the combined use of photothermal therapy and PDT using $Cu_{7.2}S_4$ nanoparticles under NIR laser in mice, improves anti-inflammatory effects and reduces cartilage and bone damage [17].

The simplicity of the technique makes PDT an ideal treatment to alleviate the pain or disability caused by RA. Unfortunately, even considering the enormous potential of PDT, conventional PSs often have some drawbacks mainly related to their chemical and structural features, as well as undesirable side effects in some cases, such as light hypersensitivity [18]. Most recent studies have focused on solving the poor solubility of PSs in biological media using soluble carriers [19] such as nanoparticles or by adding a soluble functional group in the PS structure [20]. We believe that it may be possible to solve the poor water solubility of PSs using another approach: ruthenium-based carriers (Figure 1). These organometallic complexes are soluble in biological media and have an inner cavity in which a PS can be lodged. Such metallacages have already been tested in vitro on cancer cells, demonstrating their potential in cells [21,22].

For the first time, we showed that such carriers can be used as PDT agents in fibroblast-like synoviocyte cells (FLS) from RA patients. We also demonstrated that commercially available PSs (Figure 2), namely 21*H*,23*H*-porphine (**G1**), Mg(II)-porphine (**G2**), 29*H*,31*H*-phthalocyanine (**G3**), and zinc(II)-phthalocyanine (**G4**), can be encapsulated in the cavity of the metallacages and, after being released, become effective PSs against RA. We have hosted these basic PSs in different ruthenium-based assemblies, showing the importance of the carrier in delivering the PS. The in vitro evaluation of these PS-metallacages in

human RA FLS cells is promising. The anti-proliferative assays are excellent, providing new avenues for the treatment of RA by PDT.
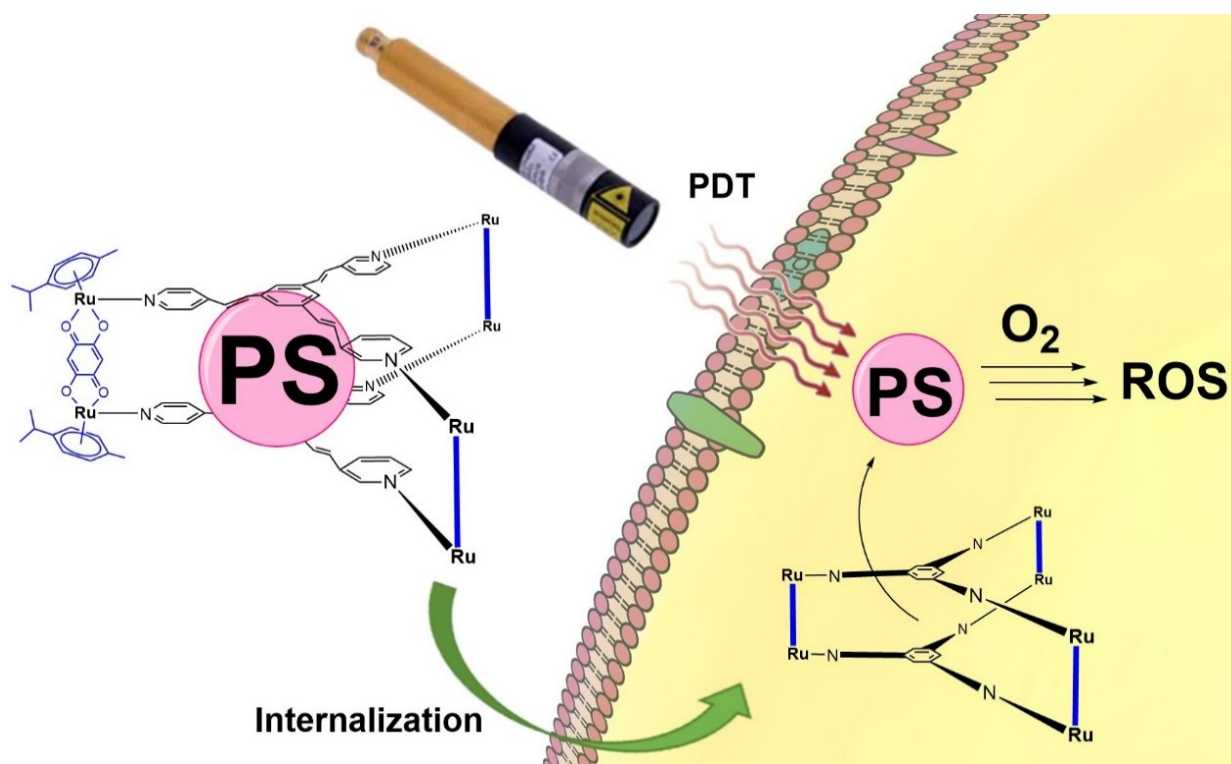
Figure 1. Typical ruthenium-based assemblies used as PS carrier for cellular internalization and subsequent activation of PS by irradiation, giving rise to ROS.
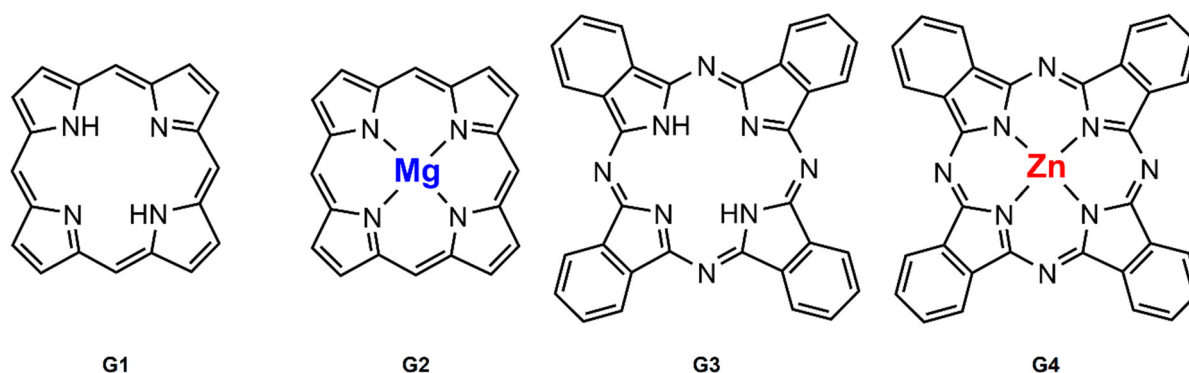
Figure 2. Photosensitizers used in this work. From left to right, 21H,23H-porphine (**G1**), Mg(II)-porphine (**G2**), 29H,31H-phthalocyanine (**G3**) and Zn(II)-phthalocyanine (**G4**).

2. Materials and Methods

2.1. Synthesis of Compounds

Despite the fact that the hosts **M1**-**M6** (Figure 3) and the guests **G1**-**G4** are known, several host–guest systems are new, except for **G1**⊂**M2**, **G1**⊂**M3**, **G2**⊂**M1**, **G2**⊂**M4**, and **G2**⊂**M6**. The complexes [Ru$_2$(p-cymene)$_2$(2,5-dioxydo-1,4-benzoquinonato)Cl$_2$], [Ru$_2$(p-cymene)$_2$(5,8-dioxydo-1,4-naphthoquinonato)Cl$_2$], [Ru$_2$(p-cymene)$_2$(6,11-dioxydo-5,12-naphthacenedionato)Cl$_2$] [23], and the ligands 2,4,6-tris(pyridin-4-yl)-1,3,5-triazine [24], 1,3,5-tris{2-(pyridin-4-yl)vinyl} benzene [25], and 1,2,4,5-tetrakis{2-(pyridine-4-yl)vinyl} benzene [26] were prepared following reported methods. The metallacages **M1** and **M4** with **G1** inside [21], **M4** with **G3** and **G4**, **M5** and **M6** with **G1**, **G3**, and **G4** [27] were

synthesized according to the literature. The photosensitizers **G1** and **G2** were synthesized as reported in the literature [28], while **G3** and **G4** were bought from Sigma-Aldrich. Dichloromethane, diethyl ether, methanol, d_3-acetonitrile, and d_6-DMSO were purchased from Sigma-Aldrich and used as received. NMR spectra were measured on a Bruker Avance Neo Ascend 600 MHz spectrometer. The acquired spectra were processed using the Mnova NMR software package (v.14.2.0, MestReLab Research, Santiago de Compostela, Spain). The ^{1}H and ^{13}C resonances of the deuterated solvents were used as internal references. The following abbreviations are used for describing the signals in the NMR spectra: s (singlet), d (doublet), m (multiplet), br (broad), q (quaternary). All described in vitro experiments were carried out under aseptic conditions. 3-(4,5-Dimethylthiazol-2-yl)-2,5-diphenyltetrazolium bromide (MTT) and L-glutamine were purchased from Sigma-Aldrich (St. Louis, MO, USA). Dimethyl sulfoxide (DMSO) was bought from Acros Organics (Geel, Belgium). All solvents, reagents, and products described above were used without prior treatments or purifications. IR spectra of the compounds were performed on a Frontier Perkin Elmer spectrometer (600–4000 cm^{-1}), Thermo Fisher Scientific, Waltham, MA, USA. Fluorescence spectra were performed on a FLS980 spectrometer from Edinburgh instruments (550–800 nm) using 5,10,15,20-tetraphenylporphin (TPP) as an internal reference in toluene and the compounds were dissolved in DMSO (10 nM concentration). UV-vis spectra were acquired on a SI Analytics model UvLine 9400 (Xenon lamp) spectrophotometer, using 1.5 mL polystyrene cuvettes (wavelength range 280–800 nm) and diluting the compounds in DMSO (10 μM and 10 nM).

Synthesis of G1⊂M2. In a 250 mL round bottom flask, 50.0 mg (0.069 mmol) of [Ru$_2$(p-cymene)$_2$(5,8-dioxydo-1,4-naphthoquinonato)Cl$_2$] and 35.5 mg (0.138 mmol) of AgCF$_3$SO$_3$ were dissolved in 20 mL of MeOH and stirred for 2 h at room temperature. Next, silver chloride was filtered off. To the remaining solution, 14.6 mg (0.046 mmol) of 2,4,6-tri(pyridin-4-yl)-1,3,5-triazine and 7.1 mg (0.023 mmol) of **G1** were added, and the solution was refluxed and stirred for 18 h. The solvent was then removed at reduced pressure, and the resulting oily, dark green solid was dissolved in 20 mL of CH$_2$Cl$_2$. The solution was concentrated to approximately 3 mL, and 5 mL of Et$_2$O was added dropwise. The resulting precipitate was filtered and dried under vacuum. Yield 52% (45 mg). ^{1}H NMR (CD$_3$CN, 25 °C, 600 MHz): δ 9.17 (d, $^3J_{HH}$ = 6.0 Hz, 12H, CH_{naphce}), 8.44 (d, $^3J_{HH}$ = 4.1 Hz, 12H, CH_{naphce}), 8.24 (d, $^3J_{HH}$ = 6.3 Hz, 12H, CH_{py}), 8.00 (s, 4H, CH_{porphine}), 6.89 (s, 8H, CH_{porphine}), 5.91 (d, $^3J_{HH}$ = 6.4 Hz, 12H, CH_{py}), 5.87 (d, $^3J_{HH}$ = 5.9 Hz, 12H, CH_{cym}), 5.57 (d, $^3J_{HH}$ = 5.8 Hz, 12H, CH_{cym}), 2.95 (m, 6H, CH_{iPr}), 1.97 (overlapped singlet, 18H, CH_3), 1.32 (d, $^3J_{HH}$ = 7.0 Hz, 36H, CH$_{3\text{ iPr}}$). ^{13}C NMR (CD$_3$CN, 25 °C, 150 MHz): δ 170.4 (*C*-O), 164.3 (C_q), 152.1 (CH$_{\text{py}}$), 140.7 (C_q), 134.6 (CH$_{\text{naphce}}$), 130.1 (CH$_{\text{porph}}$), 128.4 (CH$_{\text{naphce}}$), 122.8 (C_q), 122.3 (CH$_{\text{py}}$), 120.7 (C_q), 107.9 (C_q), 104.4 (C_{cym}), 103.3 (CH$_{\text{porph}}$), 100.3 (C_{cym}), 84.9 (CH$_{\text{cym}}$), 83.0 (CH$_{\text{cym}}$), 31.0 (CH$_{\text{iPr}}$), 22.0 (CH$_{3\text{ iPr}}$), 17.3 (CH$_3$). ESI-MS, m/z, 1120 [**M2**+**G1**-3OTf]$^{3+}$. UV/vis (DMSO), λ, nm (ε, M^{-1}·cm^{-1}): 454 (132400), 488 (117700), 567 (54300), 648 (62900). FT-IR (ATR, solid, cm^{-1}): ν; br s (3700–3100), s (2995), s (1524), s (1516). Spectra in Supplementary Materials (Figures S1–S9).

Synthesis of G1⊂M3. In a 250 mL round bottom flask, 50.0 mg (0.060 mmol) of [Ru$_2$(p-cymene)$_2$(6,11-dioxydo-5,12-naphthacenedionato)Cl$_2$] and 31.0 mg (0.120 mmol) of AgCF$_3$SO$_3$ were dissolved in 20 mL of MeOH and stirred for 2 h at room temperature. Next, silver chloride was filtered off. To the remaining solution, 12.5 mg (0.040 mmol) of 2,4,6-tri(pyridine-4-yl)-1,3,5-triazine and 6.2 mg (0.020 mmol) of **G1** were added, and the solution was refluxed and stirred for 18 h. The solvent was then removed at reduced pressure, and the resulting oily, dark green solid was dissolved in 20 mL of CH$_2$Cl$_2$. The solution was concentrated to approximately 3 mL, and 5 mL of Et$_2$O was added dropwise. The resulting precipitate was filtered and dried under vacuum. Yield 76% (62 mg). ^{1}H NMR (CD$_3$CN, 25 °C, 600 MHz): δ 8.68 (s, 4H, CH_{porphine}), 8.21 (d, $^3J_{HH}$ = 6.3 Hz, 12H, CH_{py}), 7.92 (s, 12H, CH_{naph}), 7.71 (s, 8H, CH_{porphine}), 6.12 (d, $^3J_{HH}$ = 5.7 Hz, 12H, CH_{py}), 5.68 (d, $^3J_{HH}$ = 5.8 Hz, 12H, CH_{cym}), 5.43 (d, $^3J_{HH}$ = 5.9 Hz, 12H, CH_{cym}), 2.84 (m, $^3J_{HH}$ = 6.8 Hz, 6H, CH_{iPr}), 1.99 (s, 18H, CH_3), 1.33 (d, $^3J_{HH}$ = 6.9 Hz, 36H, CH$_{3\text{ iPr}}$). ^{13}C NMR

(CD$_3$CN, 25 °C, 150 MHz): δ 171.9 (*C*-O), 164.5 (*C*$_q$), 152.3 (*C*H$_{py}$), 140.9 (*C*$_q$), 138.9 (*C*H$_{naph}$), 130.9 (*C*H$_{porph}$), 124.9 (*C*$_q$), 122.8 (*C*H$_{py}$), 122.5 (*C*H$_{py}$), 120.7 (*C*$_q$), 112.5 (*C*$_q$), 104.4 (*C*$_{cym}$), 103.9 (*C*H$_{porph}$), 100.3 (*C*$_{cym}$), 85.0 (*C*H$_{cym}$), 83.7 (*C*H$_{cym}$), 31.0 (*C*H$_{iPr}$), 21.9 (*C*H$_{3\ iPr}$), 16.8 (*C*H$_3$). UV/vis (DMSO), λ, nm (ε, M^{-1}·cm^{-1}): 489 (53700), 573 (40200), 623 (62900). FT-IR (ATR, solid, cm^{-1}): ν; br s (3700–3100), br s (3092), s (2992), s (2915), s (1531), s (1502). Spectra in Supplementary Materials (Figures S10–S17).
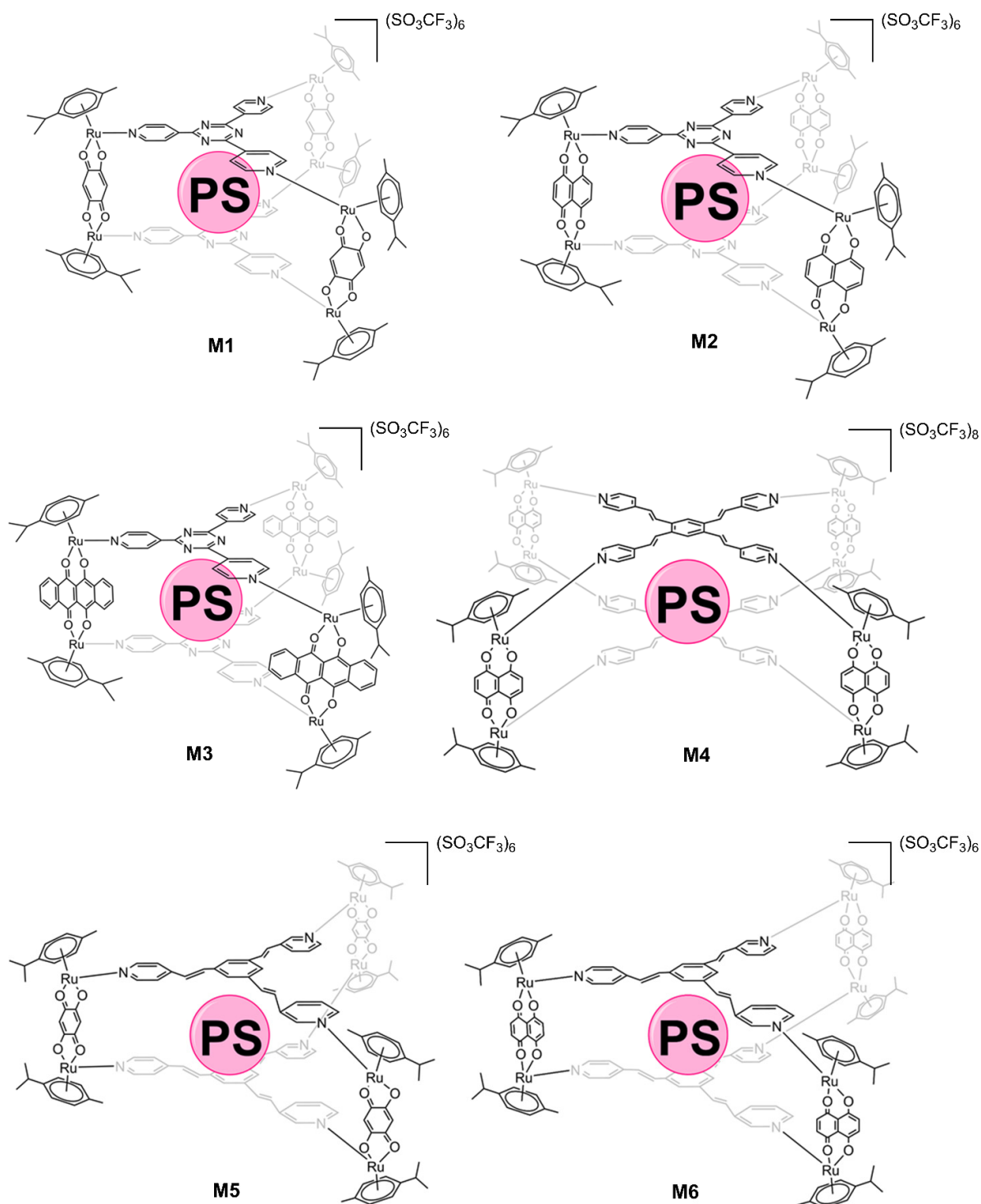
Figure 3. Structures of ruthenium(II) metallacages used in this work. The photosensitizer is represented by a sphere (PS), 21*H*,23*H*-porphine (**G1**) was inserted in **M1**–**M6**, Mg(II)-porphine (**G2**) in **M1**, **M4,** and **M6**, 29*H*,31*H*-phthalocyanine (**G3**) and Zn(II)-phthalocyanine (**G4**) in **M4**–**M6**.

Synthesis of G2⊂M1. In a 250 mL round bottom flask, 50 mg (0.074 mmol) of [Ru$_2$(*p*-cymene)$_2$(2,5-dioxydo-1,4-benzoquinonato)Cl$_2$] and 37.8 (0.148 mmol) mg of AgCF$_3$SO$_3$ were dissolved in 20 mL of MeOH and stirred for 2 h at room temperature. Next, silver chloride was filtered off. To the remaining solution, 15.4 mg (0.049 mmol) of 2,4,6-tri(pyridin-4-yl)-1,3,5-triazine and 8.1 mg (0.025 mmol) of **G2** were added, and the solution was refluxed and stirred for 18 h. The solvent was then removed at reduced pressure, and the resulting oily, dark green solid was dissolved in 20 mL of CH$_2$Cl$_2$. The solution was concentrated to approximately 3 mL, and 5 mL of Et$_2$O was added dropwise. The resulting precipitate was filtered and dried under vacuum. Yield 64% (59 mg). ^{1}H NMR (DMSO-d6, 25 °C, 600 MHz): δ 10.42 (s, 4H, C*H*$_{\text{Mg-porphine}}$), 9.61 (s, 8H, C*H*$_{\text{Mg-porphine}}$), 8.57 (m, 24H, C*H*$_{\text{py}}$), 5.62 (d, $^3J_{HH}$ = 6.1 Hz, 12H, C*H*$_{\text{cym}}$), 5.98 (d, $^3J_{HH}$ = 6.1 Hz, 12H, C*H*$_{\text{cym}}$), 5.91 (s, 6H, C*H*$_{\text{bz}}$), 2.82 (m, 6H, C*H*$_{\text{iPr}}$), 2.08 (s, 18H, C*H*$_3$), 1.28 (d, $^3J_{HH}$ = 6.9 Hz, 36H, CH$_{3\,\text{iPr}}$). ^{13}C NMR (DMSO-d6, 25 °C, 150 MHz): δ 184.1 (*C*-O), 169.4 (*C*$_q$), 154.5 (*C*H$_{\text{py}}$), 149.3 (*C*$_q$), 144.6 (*C*$_q$), 132.7 (*C*H$_{\text{Mg-porphine}}$), 129.2 (*C*$_q$), 126.5 (*C*$_q$), 124.8 (*C*H$_{\text{py}}$), 122.2 (*C*$_q$), 120.0 (*C*$_q$), 105.9 (*C*H$_{\text{Mg-porphine}}$), 103.8 (*C*$_{\text{cym}}$), 101.8 (*C*H$_{\text{bz}}$), 99.7 (*C*$_{\text{cym}}$), 84.1 (*C*H$_{\text{cym}}$), 81.9 (*C*H$_{\text{cym}}$), 31.1 (*C*H$_{\text{iPr}}$), 22.4 (*C*H$_{3\,\text{iPr}}$), 17.9 (*C*H$_3$). Elemental analysis: Calcd. For C$_{140}$H$_{126}$F$_{18}$MgN$_{16}$O$_{30}$Ru$_6$S$_6$ + 6H$_2$O: C, 44.42; H, 3.67; N, 5.92. Found: C, 45.23; H, 4.08; N, 6.09. ESI-MS, m/z, 770 [**M1**+**G2**-4OTf]$^{4+}$. UV/vis (DMSO), λ, nm (ε, M^{-1}·cm^{-1}): 500 (140700), 535 (130400). FT-IR (ATR, solid, cm^{-1}): ν; s (3093), s (2977), s (2911), s (2804), s (1508). Spectra in Supplementary Materials (Figures S18–S26).

Synthesis of G2⊂M4. In a 250 mL round bottom flask, 50 mg (0.069 mmol) of [Ru$_2$(*p*-cymene)$_2$(5,8-dioxydo-1,4-naphthoquinonato)Cl$_2$] and 35.5 mg (0.138 mmol) of AgCF$_3$SO$_3$ were dissolved in 20 mL of MeOH and stirred for 2 h at room temperature. Next, silver chloride was filtered off. To the remaining solution, 16.81 mg (0.034 mmol) of 1,2,4,5-tetrakis{2-(pyridine-4-yl)vinyl} benzene and 5.7 mg (0.017 mmol) of **G2** were added, and the solution was refluxed and stirred for 18 h. The solvent was then removed at reduced pressure, and the resulting oily, dark green solid was dissolved in 20 mL of CH$_2$Cl$_2$. The solution was concentrated to approximately 3 mL, and 5 mL of Et$_2$O was added dropwise. The resulting precipitate was filtered and dried under vacuum. Yield 59% (52 mg). ^{1}H NMR (CD$_3$CN, 25 °C, 600 MHz): δ 10.02 (s, 4H, C*H*$_{\text{Mg-porphine}}$), 9.13 (s, 8H, C*H*$_{\text{Mg-porphine}}$), 8.18 (d, $^3J_{HH}$ = 5.1 Hz, 16H, C*H*$_{\text{py}}$), 7.49 (d, $^3J_{HH}$ = 15.1 Hz, 8H, C*H*=C), 7.20 (m, 40H, C*H*$_{\text{naph}}$, C*H*$_{\text{py}}$, C*H*=C), 6.90 (s, 4H, C*H*$_{\text{ar}}$), 5.60 (d, $^3J_{HH}$ = 4.46 Hz, 16H, C*H*$_{\text{cym}}$), 5.41 (d, $^3J_{HH}$ = 3.1 Hz, 16H, C*H*$_{\text{cym}}$), 2.76 (m, $^3J_{HH}$ = 6.9 Hz, 8H, C*H*$_{\text{iPr}}$), 2.03 (overlapped singlet, 24H, C*H*$_3$), 1.25 (d, $^3J_{HH}$ = 6.9 Hz, 48H, CH$_{3\,\text{iPr}}$). ^{13}C NMR (CD$_3$CN, 25 °C, 150 MHz): δ 171.4 (*C*-O), 152.3 (*C*H$_{\text{py}}$), 149.9 (*C*$_q$), 147.7 (*C*$_q$), 138.1 (*C*H$_{\text{py}}$), 128.6 (*C*H=C), 127.6 (*C*H=C), 123.6 (*C*H$_{\text{naph}}$), 122.8 (*C*$_q$), 112.1 (*C*$_q$), 104.1 (*C*$_{\text{cym}}$), 99.7 (*C*$_{\text{cym}}$), 84.7 (*C*H$_{\text{cym}}$), 83.7 (*C*H$_{\text{cym}}$), 31.0 (*C*H$_{\text{iPr}}$), 21.9 (*C*H$_{3\,\text{iPr}}$), 16.9 (*C*H$_3$). ESI-MS, m/z, 880 [**M4**+**G2**-5OTf]$^{5+}$. UV/vis (DMSO), λ, nm (ε, M^{-1}·cm^{-1}): 536 (137900), 572 (80300), 610 (64600). FT-IR (ATR, solid, cm^{-1}): ν; s (3089), s (2947), s (2911), s (2861), s (1619), (1554). Spectra in Supplementary Materials (Figures S27–S35).

Synthesis of G2⊂M6. In a 250 mL round bottom flask, 50 mg (0.069 mmol) of [Ru$_2$(*p*-cymene)$_2$(5,8-dioxydo-1,4-naphthoquinonato)Cl$_2$] and 35.5 mg (0.138) of AgCF$_3$SO$_3$ were dissolved in 20 mL of MeOH and stirred for 2 h at room temperature. Next, silver chloride was filtered off. To the remaining solution, 17.8 mg (0.046 mmol) of panel ligand 1,3,5-tris{2-(pyridin-4-yl)vinyl}benzene and 7.6 mg (0.023 mmol) of **G2** were added, and the solution was refluxed and stirred for 18 h. The solvent was then removed at reduced pressure, and the resulting oily, dark green solid was dissolved in 20 mL of CH$_2$Cl$_2$. The solution was concentrated to approximately 3 mL, and 5 mL of Et$_2$O was added dropwise. The resulting precipitate was filtered and dried under vacuum. Yield 61% (56 mg). ^{1}H NMR (CD$_3$CN, 25 °C, 600 MHz): δ 10.29 (s, 4H, C*H*$_{\text{Mg-porphine}}$), 9.41 (s, 8H, C*H*$_{\text{Mg-porphine}}$), 8.57 (d, $^3J_{HH}$ = 5.7 Hz, 12H, C*H*$_{\text{py}}$), 7.50 (s, 6H, C*H*$_{\text{ar}}$), 7.33 (d, $^3J_{HH}$ = 5.7 Hz, 12H, C*H*$_{\text{py}}$), 7.26 (s, 12H, C*H*$_{\text{naph}}$), 7.22 (overlapped doublet, 6H, C*H*=C), 6.98 (d, $^3J_{HH}$ = 16.1 Hz, 6H, C*H*=C), 5.69 (d, $^3J_{HH}$ = 5.9 Hz, 12H, C*H*$_{\text{cym}}$), 5.48 (d, $^3J_{HH}$ = 4.2 Hz, 12H, C*H*$_{\text{cym}}$), 2.84

(m, $^3J_{HH}$ = 7.0 Hz, 6H, CH_{iPr}), 2.10 (s, 18H, CH_3), 1.33 (d, $^3J_{HH}$ = 7.0 Hz, 36H, CH$_{3\ iPr}$). ^{13}C NMR (CD$_3$CN, 25 °C, 150 MHz): δ 171.3 (*C*-O), 152.3 (CH$_{py}$), 147.9 (C$_q$), 138.0 (CH$_{py}$), 137.0 (CH$_{naph}$), 135.1 (CH$_{naph}$), 132.5 (CH$_{Mg-Porphine}$), 127.4 (CH=C), 125.2 (CH=C), 123.1 (CH$_{ar}$), 120.6 (C$_q$), 112.0 (C$_q$), 105.9 (CH$_{Mg-porphine}$), 104.0 (C$_{cym}$), 99.7 (C$_{cym}$), 84.6 (CH$_{cym}$), 83.5 (CH$_{cym}$), 31.0 (CH$_{iPr}$), 21.9 (CH$_{3\ iPr}$), 16.9 (CH$_3$). Elemental analysis: Calcd. For C$_{170}$H$_{150}$F$_{18}$MgN$_{10}$O$_{30}$Ru$_6$S$_6$ + 6CH$_2$Cl$_2$: C, 46.49; H, 3.62; N, 3.06. Found: C, 45.47; H, 3.51; N, 3.88. ESI-MS, m/z, 1177 [**M6**+**G2**-3OTf]$^{3+}$. UV/vis (DMSO), λ, nm (ε, M^{-1}·cm^{-1}): 446 (150800), 536 (110500), 573 (53500), 610 (47100). FT-IR (ATR, solid, cm-1): ν; s (3101), s (2979), s (2914), s (1604), s (1522). Spectra in Supplementary Materials (Figures S36–S43).

2.2. Preparation of Human Synovial Cells

RA synoviocytes were isolated from fresh synovial biopsies obtained from four RA patients undergoing finger arthroplasty. All patients fulfilled the 1987 American Rheumatism Association criteria for RA [29]. The mean age of the patients was 67.4 ± 3.2 years (range 53–81 years). The mean disease duration was 8.7 ± 2.3 years. At the time of surgery, the disease activity score (DAS 28) was greater than 3.2. These activities were approved by local institutional review boards, and all subjects gave written informed consent. Synovia were minced and digested with 1.5 mg/mL collagenase-dispase for 3–4 h at 37 °C as previously described [30]. After centrifugation, cells were resuspended in DMEM supplemented with 10% FCS, 4.5 g/L D-glucose, 25 mM Hepes, 100 U/mL penicillin, and 100 μg/mL streptomycin (Gibco BRL) in a humidified atmosphere containing 5% (*v/v*) CO$_2$ at 37 °C. After 48 h, nonadherent cells were removed. Adherent cells (macrophage-like and FLS) were cultured in complete medium, and, at confluence, cells were trypsinized and only the FLS were passed. These cells were used between passages 4 and 8, when they morphologically resembled FLS after an indirect immunofluorescence study (see Culture of human RA FLS). RA FLS were cultured 45–60 days before experimentation. This delay allowed for the elimination of all possible interactions resulting from any preoperative treatment (with nonsteroidal anti-inflammatory drugs, analgesics, disease-modifying antirheumatic drugs, or steroids).

2.3. Culture of Human RA FLS and Treatment

Between passages 4 and 8, RA FLS were trypsinized. Cell count and viability were determined, and cells were plated in culture plates or flasks (Falcon, Oxnard, CA, USA). Viability, measured by trypan blue dye exclusion [31] at the start and the end of culture, was always greater than 95%. FLS (10^5) from RA patients were used for an indirect immunofluorescence study [32]. The following monoclonal antibodies were used: 5B5 (anti-prolyl hydroxylase) for fibroblasts at a 1/50 dilution (Dako, Burlingame, CA, USA), JC/70A (anti-CD31), for endothelial cells at 1/50 (Dako), and RMO52 (anti-CD14) for macrophages at 1/50 (Immunotech). The negative control was a mouse antibody of the same isotype (Immunotech). Incubations were performed at room temperature for 30 min. Binding of monoclonal antibodies was visualized using fluorescein (DTAF)-conjugated goat anti-mouse antibody (Immunotech) at a 1/50 dilution.

2.4. Antiproliferative Assays

RA FLS cells were trypsinized in fresh DMEM culture medium. Homogeneous solutions were prepared in 10 mL of medium with 700,000 cells. In a 96-well plate, 100 μL of the solution (7000 cells per well) was poured and the cells were incubated for 24 h at 37 °C and 5% CO$_2$. Subsequently, 100 μL of PS solution in increasing concentration was poured per row in the plate and incubated for 24 h in the same conditions. The compounds were dissolved in DMSO (1 mM) just before use and then added to the culture medium in the desired concentrations. The concentration of DMSO in the cell medium was never more than 0.05%. After incubation, the medium was removed and 100 μL of complete medium without red phenol was added per well. At that point, irradiation was carried out using a red-light source, CureLight®, PhotoCure ASA at 630 nm, at a dose of 40 mW/cm^2 for

30 min. After the irradiation, the wells plates were put in the incubator for 18 h. After this time, 10 μL of MTT solution (5 g/L) was added and the plates were again placed inside the incubator for 4 h. Next, the media was removed and 200 μL of DMSO was added per well, stirring the plate softly for 3 min. Absorbance after the MTT assay was measured at 540 nm by a Dynex Triad Multi Mode Microplate Reader, Dynex Technologies. The assays were executed in triplicate. Cytotoxicity evaluations in the dark were carried out by repeating this entire protocol without the irradiation dose. $\cdot cm^{-1}$

2.5. Protein Extraction and Western-Blot Analysis

For total protein extraction, RA FLS were washed in PBS, and the total cell pool was centrifuged at 200 g for 5 min at 4 °C and homogenized in RIPA lysis buffer (50 mM HEPES, pH 7.5, 150 mM NaCl, 1% sodium deoxycholate, 1% NP-40, 0.1% SDS, and 20 mg/mL of aprotinin) containing protease inhibitors (CompleteTM Mini, Roche Diagnostics) according to the manufacturer's instructions. Proteins (60 μg) were separated by electrophoresis on 10% SDS–PAGE gels and transferred to polyvinylidene fluoride (PVDF) membranes (Amersham Pharmacia Biotech, Saclay, France), which were then probed with a COX-2 human primary antibody (Cayman Chemical, Bertin Pharma, Montigny le Bretonneux, France). After incubation with a secondary antibody (Dako France S.A.S., Trappes, France), blots were developed using the ECL Plus Western Blotting Detection System (Amersham Pharmacia Biotech) and G: BOX system (Syngene, Ozyme, Saint Quentin en Yvelines, France). Membranes were then reblotted with human anti-β-actin (Sigma-Aldrich, Saint Quentin Fallavier, France) used as a loading control.

2.6. Assay of COX-2 Activity

RA FLS were maintained in DMEM supplemented with 10% (*v/v*) FCS, 4.5 g/L D-glucose, 100 U/mL penicillin, and 100 μg/mL streptomycin. The cells were grown in a humidified incubator at 37 °C and 5% CO_2. Next, 2.10^6 RA FLS cells were seeded in a 25 cm^2 flask and incubated for 24 h. Then, the IC_{50} of each PS was added and the cells were incubated for 24 h. The medium was removed and a medium without red phenol was added. Immediately, cells were irradiated under the same conditions expressed in the MTT assays and incubated for 18 h. The non-irradiated cells were kept in the incubator. After this, LPS (1 μg/mL) was added to the medium of both irradiated and non-irradiated cells, and the cells were incubated for 4 h. Cells were trypsinized and the culture medium supernatant was isolated. The PGE_2 levels were quantified in the culture media supernatants from treated and control cells by enzyme immunoassay using an ELISA Kit (Cayman Chemical) [33]. The results were expressed as the average of three independent experiments.

2.7. Assay of IL-1β Production

The IL-1β levels were quantified in the culture media supernatants, isolated by the same protocol described for PGE_2, from treated and control cells by ELISA Kit (Thermo Fisher Scientific). The results were expressed as the average of three independent experiments.

2.8. Statistical Analysis

All quantitative results are expressed as the mean ± 3 standard deviations (SEM) of separate experiments using Excel (Microsoft Office, Version 2019). Statistical significance was evaluated by the two-tailed unpaired Student's *t*-test, *p*-value < 0.001 (***).

3. Results and Discussion

3.1. Phototoxicity Tests

Although it is the first time that these PS–metallacage systems have been tested to treat RA using PDT, two of the fifteen systems described here (Figure 3) have already been tested in cancer (HeLa, Me300, A2780, A2780cisR, and A549) [21]. Specifically, the prismatic metallacage **M1** and the cubic **M4**, both with **G1** in their internal cavity. In

cancer cells, a total absence of cytotoxicity was demonstrated prior to cell internalization. Once inside the cells, the PS is released from the cage and can be irradiated giving rise to photocytotoxicity. Two mechanisms have been suggested to explain the releasing of the PS from the metallacage: (i) from a partial or total rupture of the cage; or (ii) through an aperture [21,22]. Furthermore, intracellular ruthenium contents [22] and fluorescence studies [21] have confirmed the ability of these metallacages to cross cell membranes. Fluorescence studies also reveal that, once inside the cell and after the PS leaves the cavity of the metallacage, both are positioned in different cellular areas, which did not include the nucleus.

In this work, we wanted to demonstrate the efficacy and potential of these systems in another pathology, RA, looking for a treatment that is fairly non-invasive. In addition, we have synthesized cages with structural variations to evaluate how the different elements of the metallacage influence its PDT effect (Figure 3). Moreover, we have evaluated new PSs, such as **G2**, **G3,** and **G4**, in addition to **G1** which have been evaluated to treat RA by PDT.

First, these metallacages can be differentiated by their two main elements: the panel ligand and the dinuclear ruthenium clips. The panel ligand is a flat organic compound with three or four pyridine substituents, which give rise to prismatic or cubic cages, respectively. In this work, we used 2,4,6-tri(pyridin-4-yl)-1,3,5-triazine, 1,3,5-tris{2-(pyridin-4-yl)vinyl}benzene, or 1,2,4,5-tetrakis{2-(pyridine-4-yl)vinyl} benzene. Dinuclear arene ruthenium(II) complexes are the edges of the cage, whose two metal atoms are linked by 2,5-dioxydo-1,4-benzoquinonato, 5,8-dioxydo-1,4-naphthoquinonato, or 6,11-dioxydo-5,12-naphthacenedionato ligands (Figure 3).

The results of the photocytotoxicity tests after PDT in RA FLS were excellent (Table 1). MTT assays showed 50% inhibition concentrations (IC_{50}) lower than those seen in cancer cells [21]. The latter was to be expected, since RA FLS are primary cells and their growth is not accelerated, unlike cancer cells. As we anticipated, the structural variation in the cages gave rise to significant differences in the PDT effect.

Table 1. Results of the MTT assays. Irradiation after 24 h of incubation with G $\subset$ M, λ = 630 nm, 40 mW/cm^2 for 30 min. IC_{50} values were calculated fitting the curve to a second degree polynomial ± 3 sigma deviations. The maximum concentration tested was 1.5 μM. Quantum yield (Φ_F) was calculated using TPP as an internal standard in DMSO at 25 °C.

Entry	G $\subset$ M	IC_{50} (nM) Light	IC_{50} (nM) Dark	ΦF (%)
1	**G1 $\subset$ M1**	211.7 ± 5.8	>1500	-
2	**G1 $\subset$ M2**	95.0 ± 5.9	>1500	-
3	**G1 $\subset$ M3**	53.6 ± 4.3	>1500	-
4	**G1 $\subset$ M4**	48.1 ± 9.7	>1500	-
5	**G1 $\subset$ M5**	35.4 ± 4.7	>1500	0.8
6	**G1 $\subset$ M6**	31.7 ± 6.6	>1500	1.1
7	**G2 $\subset$ M1**	302.6 ± 5.2	>1500	-
8	**G2 $\subset$ M4**	100.7 ± 5.8	>1500	-
9	**G2 $\subset$ M6**	91.8 ± 8.3	>1500	2.0
10	**G3 $\subset$ M4**	>1500	>1500	-
11	**G3 $\subset$ M5**	53.4 ± 4.5	>1500	0.11
12	**G3 $\subset$ M6**	47.4 ± 6.3	>1500	-
13	**G4 $\subset$ M4**	>1500	>1500	-
14	**G4 $\subset$ M5**	66.0 ± 2.6	103.8 ± 2.9	1.6
15	**G4 $\subset$ M6**	64.4 ± 4.4	163.8 ± 17.1	-

First, we have observed that when the size of the panel ligand is bigger, the photocytotoxicity is higher. For example, the structures of cages **M2**, **M4,** and **M6** differ only by the panel ligand, 2,4,6-tri(pyridin-4-yl)-1,3,5-triazine, 1,3,5-tris{2-(pyridin-4-yl)vinyl}benzene, and 1,2,4,5-tetrakis{2-(pyridine-4-yl)vinyl} benzene, respectively. When the IC_{50} values obtained with porphine as the PS are compared (entries 2, 4, and 6 in Table 1), we observed that cage **M2**, with the smallest panel, needed a higher concentration than **M4** and **M6**

(triple when compared to **M6**). This difference becomes more evident if we compare cage **M1** and **M5**, which have panels 2,4,6-tri(pyridin-4-yl)-1,3,5-triazine and 1,3,5-tris{2-(pyridin-4-yl)vinyl}benzene, respectively. With **G1** as the PS, the IC$_{50}$ of **M1** is six times higher than that observed in **M5** (entries 1 and 5 in Table 1). This coincides with what has been reported in cancer cells [21]. A larger panel gives rise to larger apertures that facilitate the release of the PS once inside the cell, producing more ROS and, subsequently, more photocytotoxicity. This result is consistent with the other three PSs tested (Table 1).

The second of the structural elements of the cages that we can modify, the dinuclear ruthenium clip, also showed significant differences, as we expected. When the volume of the ruthenium complex is bulkier, we observed that the IC$_{50}$ is lower, which translates into a better PDT effect. For instance, cages **M1**, **M2**, and **M3** contain the same panel ligand and differ only in the dinuclear ruthenium "edges", being 2,5-dioxydo-1,4-benzoquinonato, 5,8-dioxydo-1,4-naphthoquinonato, and 6,11-dioxydo-5,12-naphthacenedionato respectively. With **G1** as the PS, the result obtained with **M3** was four times lower than the IC$_{50}$ obtained in **M1** (entries 1 and 3 in Table 1), while the IC$_{50}$ of **M2** (entry 2 in Table 1) shows an intermediate value. These results are consistent with the structure of the metallacages, which suggest the release of the PS through an aperture [22]. Indeed, when the metallacage is smaller, the host–guest system is stabilized, making it difficult for the PS to escape, which translates into lower ROS production and a lower PDT effect. The same result, although in a lesser proportion, is observed with the other PSs tested (Table 1).

Finally, the four PSs tested have shown significant differences. First, it is worth noting the presence or absence of a metal in the center of the tetrapyrrole. In all cases, using the same cage, the PSs without a metal showed a better PDT effect (Table 1). The cause of this result is directly related to fluorescence [34]. When the PS is irradiated, part of the energy is absorbed and the PS reaches the excited singlet state. The PS can then return to the minimum energy state by releasing that energy, producing fluorescence, or the energy can pass through an intermediate excited triplet state. From this last state, the PS can return to the ground state, giving rise to phosphorescence, or interact with O$_2$ to give rise to singlet oxygen and, in turn, ROS [12,13]. Therefore, since the derivate with Zn and Mg give rise to higher fluorescence (Figure 4), lower ROS production would be expected than their equivalents without metal. This corroborates the obtained results, that is, the presence of Mg or Zn favor fluorescence and therefore reduce ROS production and PDT efficiency. Calculating the quantum yields (Table 1), we observed the same result as expected, that is, higher quantum yield equates to less of a PDT effect.
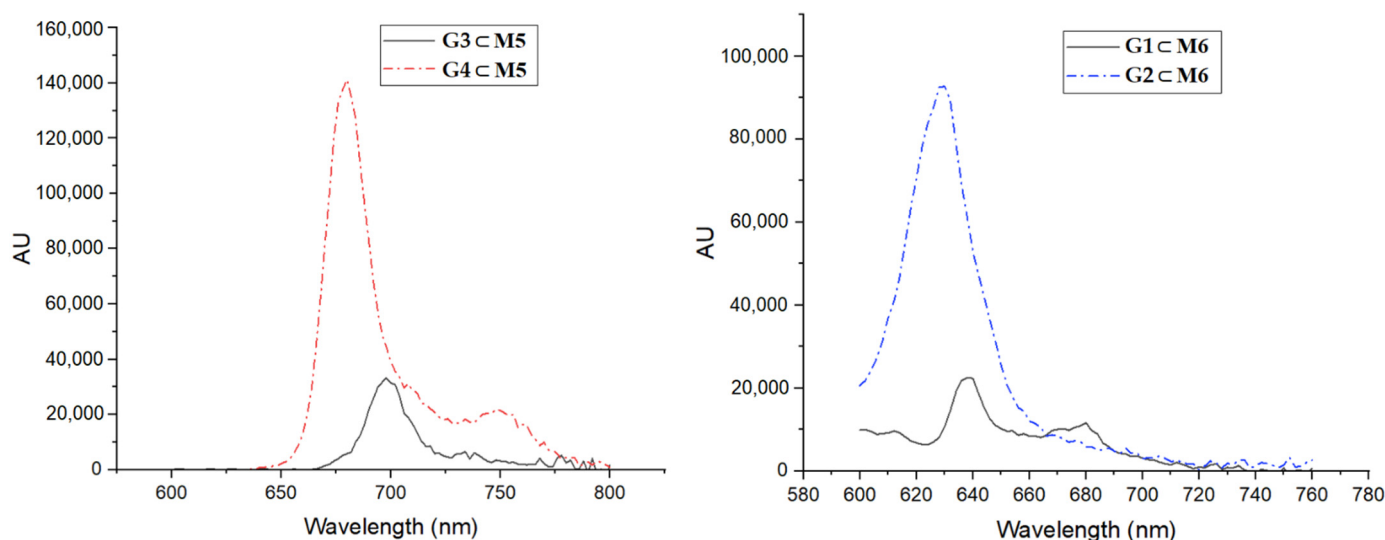
Figure 4. Emission spectra of **M5** with **G3** or **G4** (**left**) and **M6** with **G1** or **G2** (**right**), in DMSO at 25 °C (10 nM concentration).

Regarding the differences between porphine (**G1**) and phthalocyanine (**G3**), the results show that **G1** works better as a PS than **G3** when carried in the same metallacage (Table 1). However, the IC_{50} for **G3** is still excellent, with both showing great potential as PSs. Surprisingly, one of the results was unexpected. When **G3** or **G4** is transported by the cubic metallacage (**M4**), no effect on RA FLS is observed (Table 1), even at the highest concentration tested. This also suggests a stronger binding affinity between the host and the guest, thus supporting that the PS is released through an aperture, rather than having a breakage of the metallacage [22].

Another excellent result is the total absence of cytotoxicity in the dark for all compounds, except for those with **G4** in their cavity, which show dark toxicity (Figure 5). Therefore, this result suggests that **G4** is not a good PS, although it is something we could have anticipated since other zinc tetrapyrrole derivatives have already been reported to show toxicity in the dark [35,36]. Another intriguing result comes from the metallated photosensitizers (**G3** and **G4**) encapsulated in the 1,2,4,5-tetrakis{2-(pyridine-4-yl)vinyl} benzene derivative (**M4**) (entries 10 and 13, Table 1). In both systems (**G3**⊂**M4** and **G4**⊂**M4**), no phototoxicity and no toxicity is observed, suggesting the absence of a photo-response from the photosensitizers in these particular cases. When compared to the other **G**⊂**M** systems, the most plausible explanation is that the presence of Mg or Zn in the core of the PS generates a stronger interaction between the host and the guest, thus shielding the PS and blocking their release.
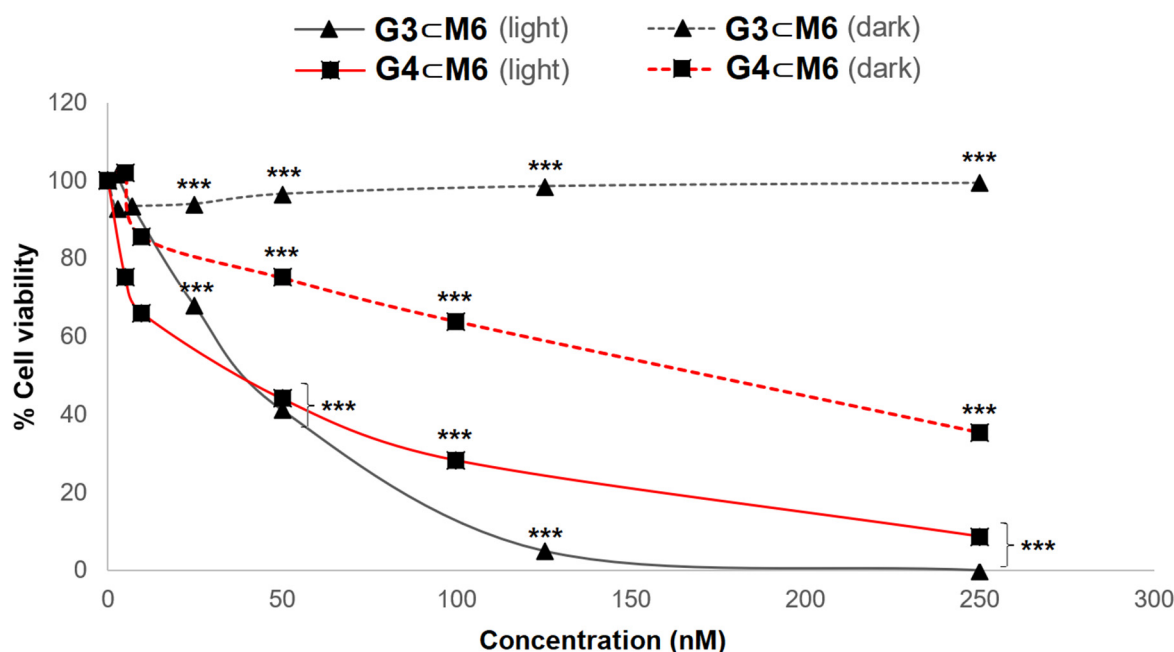

Figure 5. MTT assays of **G3**⊂**M6** (black) and **G4**⊂**M6** (red), in the dark (dashed line) and after irradiation (solid line). Statistical significance determined by the two-tailed unpaired Student's *t*-test, *p*-value < 0.001 (***).

3.2. Inflammatory Evaluation

The synovial membrane encapsulates the joint, providing structural support, lubricating the tissues, and providing nutrients to the cartilage. FLS are part of the inner lining layer of the synovial membrane. One of the main functions of FLS is the production of cytokines [37]. One of the cytokines involved in the inflammatory response is the interleukin (IL) family. IL-1 can express cyclooxygenase-2 (COX-2), an enzyme that acts as a catalyst in the production of prostaglandin E_2 (PGE_2) from arachidonic acid [38–41]. PGE_2 causes vasodilation in the synovial tissue, leading to inflammation in the area [42]. To evaluate in RA FLS the in vitro inflammatory activity after PDT, we decided to measure the production of PGE_2 and IL-1β in the supernatant, in addition to the expression of COX-2 in both the irradiated and non-irradiated treated cells.

The determination of COX-2 expression reveals that treated RA FLS with our systems by PDT generates an overexpression of this enzyme (Figure 6), when the cells were irradiated. This result was expected, since multiple examples of COX-2 overexpression after PDT have been reported. For instance, other porphyrin-based PSs such as PpIX-polyamine [43] or Photofrin [44] increased COX-2 expression. Additionally, this not only happens with PSs based on porphyrins, but also with other PSs used in PDT [45,46]. It should be noted that most of the systems with a lower IC_{50} (Table 1) show less intensity in the COX-2 expression band (Figure 6). For instance, the compounds that obtained the lowest IC_{50}, entries 4, 5, 6, 11, and 12 (Table 1), showed a COX-2 band with the lowest intensity.
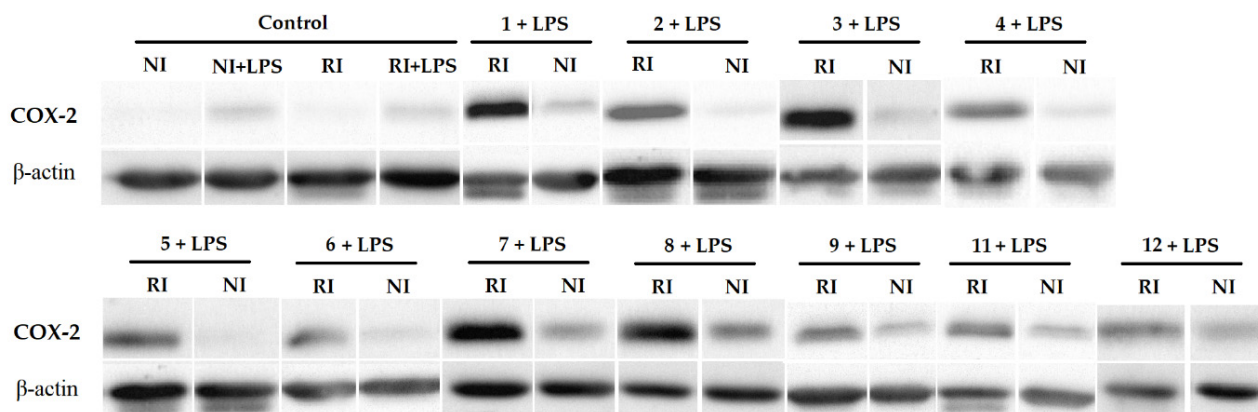
Figure 6. Effects of the systems tested on COX-2 expression after PDT. The numbers correspond to the entries in Table 1. Cells (2×10^6) were cultured in DMEM medium (FBS 10%, L-glutamine 1%, penicillin 100 U/mL, Streptomycin 100 μg/mL) for 24 h and treated with the corresponding system **G⊂M**. After 24 h, the medium was replaced by a DMEM medium without red phenol, and then irradiated (RI) or not (NI) by 630 nm irradiation (40 mW/cm^2, 30 min). After 18 h, LPS (1 μg/mL) was added to the medium to stimulate the expression of COX-2, and 4 h later the trypsination was carried out. COX-2 expression was determined by Western Blot and β-actin was used as a protein loading control. All experiments were done in triplicate.

As expected, an overexpression of COX-2 generates a greater production of PGE$_2$ [43], which may lead to an increase in inflammation. That is what we see in the results obtained in the determination of PGE$_2$ (Table 2). As with COX-2, it can be seen that when the IC_{50} is lower, the production of PGE$_2$ is also lower, which again points out that reducing the required concentration of PS could reduce the adverse effects of PDT. However, it is possible to minimize the expression of COX-2 and, consequently, the production of PGE$_2$ by using a COX-2 inhibitor, such as NS-398 during PDT treatment [43,47].

On the other hand, IL-1β is known to be a pro-inflammatory cytokine that leads to the expression of COX-2, among other functions [48]. Since our experiments showed an overexpression of COX-2 and the production of PGE$_2$, we anticipated the presence of this cytokine as a response to the PDT treatment. Unexpectedly, the determination of IL-1β indicates that its presence after PDT is insignificant (Table 2). It is even below the standard of lower concentration and their values were not significantly different from the control samples. This indicates that, in vitro, when RA FLS are treated with our systems by PDT, IL-1β is not generating more COX-2 than what is already present in the cells, so it is not involved in the detected overexpression. However, also in synovial tissues, other cases have been reported in which IL-1β was not involved in the overexpression of COX-2 [49–51], indicating that other cytokines like IL-6 or IL-8 were responsible [51].

Table 2. PGE$_2$ and IL-1β results. The assays were performed using the protocol provided by the ELISA kit in triplicate. The data were treated as explained in this protocol. The cells tested were treated by PDT with each of the indicated compounds as described in the experimental section. The control sample was treated exactly as the cells tested, that is, 18 h after the irradiation dose, 1 µg/mL of LPS was added to the medium and the cells were incubated for 4 h, then trypsinized and the cells and supernatant were isolated. The results are expressed by the average of three independent experiments. After testing the photocytotoxic activity, we chose the systems with the greatest potential to be used in PDT against RA and evaluated their inflammatory activity. Of these fifteen systems, we obviously ruled out those that did not work (cubic cage **M4** + phthalocyanines) and the systems that generated toxicity in the dark.

Entry	G ⊂ M	PGE$_2$ (pg/mL)	IL-1β (pg/mL)
Ctrl	-	286.6 ± 0.1	1.8 ± 0.7
1	**G1 ⊂ M1**	460.8 ± 4.3	2.3 ± 1.2
2	**G1 ⊂ M2**	471.2 ± 3.4	1.9 ± 1.0
3	**G1 ⊂ M3**	445.1 ± 4.7	2.8 ± 0.1
4	**G1 ⊂ M4**	378.3 ± 14.2	3.2 ± 0.4
5	**G1 ⊂ M5**	407.4 ± 14.5	2.1 ± 0.2
6	**G1 ⊂ M6**	439.2 ± 10.1	1.6 ± 0.1
7	**G2 ⊂ M1**	476.8 ± 3.4	1.9 ± 0.6
8	**G2 ⊂ M4**	473.6 ± 7.5	1.4 ± 0.2
9	**G2 ⊂ M6**	430.6 ± 1.4	2.2 ± 0.2
10	**G3 ⊂ M5**	368.2 ± 26.5	2.4 ± 0.4
11	**G3 ⊂ M6**	425.2 ± 2.7	0.1 ± 0.1

4. Conclusions

A series of photosensitizers (**G**) encapsulated in arene ruthenium metallacages (**M**) have been synthesized and characterized. The PDT effect of these host–guest systems (**G⊂M**) has been evaluated on fibroblast-like synoviocyte cells (FLS). With the exception of the zinc phthalocyanine derivatives (**G4⊂M5** and **G4⊂M6**), all **G⊂M** compounds show no toxicity in the dark at the highest concentration tested (1.5 µM). When under light, the most photoactive compounds appear to be those with the largest cavity and the smallest guest, suggesting that the release of the photosensitizers from the host occurs without any breakage of the metallacage. However, when **G4** is encapsulated in the metallacages built with 1,3,5-tris{2-(pyridin-4-yl)vinyl} benzene panels (**M5** and **M6**), the difference between phototoxicity and toxicity is limited. On the other hand, when the metallated photosensitizers (**G3** and **G4**) are encapsulated in the 1,2,4,5-tetrakis{2-(pyridine-4-yl)vinyl} benzene derivative (**M4**), no phototoxicity is observed, suggesting a strong interaction between the host and guest, which shields the photosensitizer. Nevertheless, in all systems, PDT gives rise to the overexpression of COX-2 and PGE$_2$. However, we have also observed that when a lower concentration of the drug is used, this overexpression is significantly reduced. Surprisingly, IL-1β does not seem to be involved in this COX-2 overexpression, despite being previously reported. This indicates that other cytokines are responsible for this overexpression of COX-2. With a few exceptions, all systems show encouraging results, and further in vitro investigations should be performed and other host–guest systems evaluated in order to validate our strategy; however, we think our results show an interesting method for the treatment of RA by PDT. This work, added to those already reported in the last three decades, both in vitro and in vivo, show the inherent potential that PDT could have in the treatment of RA.

of **G1⊂M2**, Figure S8: UV-vis absorbance spectrum of **G1⊂M2** (10 μM in DMSO), Figure S9: ATR FT-IR spectrum of **G1⊂M2**, Figure S10: 1H NMR spectrum of **G1⊂M3** in CD$_3$CN at 25 °C, Figure S11: ^{13}C NMR spectrum of **G1⊂M3** in CD$_3$CN at 25 °C, Figure S12: ^{1}H-^{1}H COSY NMR spectrum of **G1⊂M3** in CD$_3$CN at 25 °C, Figure S13: DOSY NMR spectrum of **G1⊂M3** in CD$_3$CN at 25 °C, Figure S14: ^{1}H-^{13}C HSQC NMR spectrum of **G1⊂M3** in CD$_3$CN at 25 °C, Figure S15: ^{1}H-^{13}C HMQC NMR spectrum of **G1⊂M3** in CD$_3$CN at 25 °C, Figure S16: UV-vis absorbance spectrum of **G1⊂M3** (10 μM in DMSO), Figure S17: ATR FT-IR spectrum spectrum of **G1⊂M3**, Figure S18: ^{1}H NMR spectrum of **G2⊂M1** in DMSO-d$_6$ at 25 °C, Figure S19: ^{13}C NMR spectrum of **G2⊂M1** in DMSO-d$_6$ at 25 °C, Figure S20: ^{1}H-^{1}H COSY NMR spectrum of **G2⊂M1** in DMSO-d$_6$ at 25 °C, Figure S21: DOSY NMR spectrum of **G2⊂M1** in DMSO-d$_6$ at 25 °C, Figure S22: ^{1}H-^{13}C HSQC NMR spectrum of **G2⊂M1** in DMSO-d$_6$ at 25 °C, Figure S23: ^{1}H-^{13}C HMQC NMR spectrum of **G2⊂M1** in DMSO-d$_6$ at 25 °C, Figure S24: ESI-MS spectrum of **G2⊂M1**, Figure S25: UV-vis absorbance spectrum of **G2⊂M1** (10 μM in DMSO), Figure S26: ATR FT-IR spectrum spectrum of **G2⊂M1**, Figure S27: ^{1}H NMR spectrum of **G2⊂M4** in CD$_3$CN at 25 °C, Figure S28: ^{13}C NMR spectrum of **G2⊂M4** in CD$_3$CN at 25 °C, Figure S29: ^{1}H-^{1}H COSY NMR spectrum of **G2⊂M4** in CD$_3$CN at 25 °C, Figure S30: DOSY NMR spectrum of **G2⊂M4** in CD$_3$CN at 25 °C, Figure S31: ^{1}H-^{13}C HSQC NMR spectrum of **G2⊂M4** in CD$_3$CN at 25 °C, Figure S32: ^{1}H-^{13}C HMQC NMR spectrum of **G2⊂M4** in CD$_3$CN at 25 °C, Figure S33: ESI-MS spectrum of **G2⊂M4**, Figure S34: UV-vis absorbance spectrum of **G2⊂M4** (10 μM in DMSO), Figure S35: ATR FT-IR spectrum spectrum of **G2⊂M4**, Figure S36: ^{1}H NMR spectrum of **G2⊂M6** in CD$_3$CN at 25 °C, Figure S37: ^{13}C NMR spectrum of **G2⊂M6** in CD$_3$CN at 25 °C, Figure S38: ^{1}H-^{1}H COSY NMR spectrum of **G2⊂M6** in CD$_3$CN at 25 °C, Figure S39: ^{1}H-^{13}C HSQC NMR spectrum of **G2⊂M6** in CD$_3$CN at 25 °C, Figure S40: ^{1}H-^{13}C HMQC NMR spectrum of **G2⊂M6** in CD$_3$CN at 25 °C, Figure S41: ESI-MS spectrum of **G2⊂M6**, Figure S42: UV-vis absorbance spectrum of **G2⊂M6** (10 μM in DMSO), Figure S43: ATR FT-IR spectrum spectrum of **G2⊂M6**.

References

1. Smolen, J.S.; Aletaha, D.; McInnes, I.B. Rheumatoid arthritis. *Lancet* **2016**, *388*, 2023–2038. [CrossRef]
2. Roux, C.H.; Saraux, A.; Le Bihan, E.; Fardellone, P.; Guggenbuhl, P.; Fautrel, B.; Masson, C.; Chary-Valckenaere, I.; Cantagrel, A.; Juvin, R.; et al. Rheumatoid arthritis and spondyloarthropathies: Geographical variations in prevalence in France. *J. Rheumatol.* **2007**, *34*, 117–122.
3. Scherer, H.U.; Häupl, T.; Burmester, G.R. The etiology of rheumatoid arthritis. *J. Autoimmun.* **2020**, *110*, 102400. [CrossRef] [PubMed]
4. Kerkman, P.F.; Fabre, E.; van der Voort, E.I.; Zaldumbide, A.; Rombouts, Y.; Rispens, T.; Wolbink, G.; Hoeben, R.C.; Spits, H.; Baeten, D.L.; et al. Identification and characterization of citrullinated antigen-specific B cells in peripheral blood of patients with rheumatoid arthritis. *Ann. Rheum. Dis.* **2016**, *75*, 1170–1176. [CrossRef] [PubMed]
5. Aletaha, D.; Alasti, F.; Smolen, J.S. Rheumatoid factor, not antibodies against citrullinated proteins, is associated with baseline disease activity in rheumatoid arthritis clinical trials. *Arthritis Res. Ther.* **2015**, *17*, 229. [CrossRef]
6. McInnes, I.B.; Schett, G. The pathogenesis of rheumatoid arthritis. *N. Engl. J. Med.* **2011**, *365*, 2205–2219. [CrossRef]

7. Smolen, J.S.; Landewé, R.B.; Bijlsma, J.W.; Burmester, G.R.; Dougados, M.; Kerschbaumer, A.; McInnes, I.B.; Sepriano, A.; van Vollenhoven, R.F.; de Wit, M.; et al. EULAR recommendations for the management of rheumatoid arthritis with synthetic and biological disease-modifying antirheumatic drugs: 2019 update. *Ann. Rheum. Dis.* **2020**, *79*, 685–699. [CrossRef]

8. Smolen, J.S.; van der Heijde, D.; Machold, K.P.; Aletaha, D.; Landewé, R. Proposal for a new nomenclature of disease-modifying antirheumatic drugs. *Ann. Rheum. Dis.* **2014**, *73*, 3–5. [CrossRef]

9. Ma, X.; Xu, S. TNF inhibitor therapy for rheumatoid arthritis. *Biomed. Rep.* **2013**, *1*, 177–184. [CrossRef]

10. Dowty, M.E.; Lin, T.H.; Jesson, M.I.; Hegen, M.; Martin, D.A.; Katkade, V.; Menon, S.; Telliez, J.B. Janus kinase inhibitors for the treatment of rheumatoid arthritis demonstrate similar profiles of in vitro cytokine receptor inhibition. *Pharmacol. Res. Perspect.* **2019**, *7*, e00537. [CrossRef]

11. Gallardo-Villagrán, M.; Leger, D.Y.; Liagre, B.; Therrien, B. Photosensitizers used in the photodynamic therapy of rheumatoid arthritis. *Int. J. Mol. Sci.* **2019**, *20*, 3339. [CrossRef]

12. Dougherty, T.J.; Gomer, C.J.; Henderson, B.W.; Jori, G.; Kessel, D.; Korbelik, M.; Moan, J.; Peng, Q. Photodynamic therapy. *J. Natl. Cancer Inst.* **1998**, *90*, 889–905. [CrossRef]

13. Agostinis, P.; Berg, K.; Cengel, K.A.; Foster, T.H.; Girotti, A.W.; Gollnick, S.O.; Hahn, S.M.; Hamblin, M.R.; Juzeniene, A.; Kessel, D.; et al. Photodynamic therapy of cancer: An update. *CA Cancer. J. Clin.* **2011**, *61*, 250–281. [CrossRef]

14. Hopper, C. Photodynamic therapy: A clinical reality in the treatment of cancer. *Lancet Oncol.* **2000**, *1*, 212–219. [CrossRef]

15. Trauner, K.B.; Gandour-Edwards, R.; Bamberg, M.; Shortkroff, S.; Sledge, C.; Hasan, T. Photodynamic synovectomy using benzoporphyrin derivative in an antigen-induced arthritis model for rheumatoid arthritis. *Photochem. Photobiol.* **1998**, *67*, 133–139. [CrossRef]

16. Miyazawa, S.; Nishida, K.; Komiyama, T.; Nakae, Y.; Takeda, K.; Yorimitsu, M.; Kitamura, A.; Kunisada, T.; Ohtsuka, A.; Inoue, H. Novel transdermal photodynamic therapy using ATX-S10· Na (II) induces apoptosis of synovial fibroblasts and ameliorates collagen antibody-induced arthritis in mice. *Rheumatol. Int.* **2006**, *26*, 717. [CrossRef] [PubMed]

17. Lu, Y.; Li, L.; Lin, Z.; Wang, L.; Lin, L.; Li, M.; Zhang, Y.; Yin, Q.; Li, Q.; Xia, H. A new treatment modality for rheumatoid arthritis: Combined photothermal and photodynamic therapy using Cu7. 2S4 nanoparticles. *Adv. Healthc. Mater.* **2018**, *7*, 1800013. [CrossRef] [PubMed]

18. Koderhold, G.; Jindra, R.; Koren, H.; Alth, G.; Schenk, G. Experiences of photodynamic therapy in dermatology. *J. Photochem. Photobiol. Biol.* **1996**, *36*, 221–223. [CrossRef]

19. Búzová, D.; Kasák, P.; Miškovský, P.; Jancura, D. Solubilization of poorly soluble photosensitizer hypericin by polymeric micelles and polyethylene glycol. *Gen. Physiol. Biophys.* **2013**, *32*, 201–208. [CrossRef] [PubMed]

20. Yang, X.; Bai, J.; Qian, Y. The investigation of unique water-soluble heptamethine cyanine dye for use as NIR photosensitizer in photodynamic therapy of cancer cells. *Spectrochim. Acta A* **2020**, *228*, 117702. [CrossRef]

21. Schmitt, F.; Freudenreich, J.; Barry, N.P.; Juillerat-Jeanneret, L.; Süss-Fink, G.; Therrien, B. Organometallic cages as vehicles for intracellular release of photosensitizers. *J. Am. Chem. Soc.* **2012**, *134*, 754–757. [CrossRef]

22. Barry, N.P.E.; Zava, O.; Dyson, P.J.; Therrien, B. Excellent Correlation between Drug Release and Portal Size in Metalla-Cage Drug-Delivery Systems. *Chem. Eur. J.* **2011**, *17*, 9669–9677. [CrossRef] [PubMed]

23. Barry, N.P.; Edafe, F.; Therrien, B. Anticancer activity of tetracationic arene ruthenium metalla-cycles. *Dalton Trans.* **2011**, *40*, 7172–7180. [CrossRef]

24. Xu, F.; Zhu, X.H.; Shen, Q.; Lu, J.; Li, J.Q. Catalytic cyclotrimerization of arylnitriles using the novel samarium (II) complexes as catalysts. *Chin. J. Chem.* **2002**, *20*, 1334–1339. [CrossRef]

25. Amoroso, A.J.; Thompson, A.M.C.; Maher, J.P.; McCleverty, J.A.; Ward, M.D. Di-, tri-, and tetranucleating pyridyl ligands which Facilitate multicenter magnetic exchange between paramagnetic molybdenum centers. *Inorg. Chem.* **1995**, *34*, 4828–4835. [CrossRef]

26. Wang, L.; Tao, X.T.; Yang, J.X.; Yu, W.T.; Ren, Y.; Xin, Q.; Liu, Z.; Jiang, M.H. Synthesis, structure and two-photon absorption properties of a new multi-branched compound, 1, 2, 4, 5-tetrakis (4-pyridylvinyl) benzene. *J. Solid State Chem.* **2004**, *177*, 4293–4299. [CrossRef]

27. Freudenreich, J.; Dalvit, C.; Süss-Fink, G.; Therrien, B. Encapsulation of photosensitizers in hexa-and octanuclear organometallic cages: Synthesis and characterization of carceplex and host–guest systems in solution. *Organometallics* **2013**, *32*, 3018–3033. [CrossRef]

28. Dogutan, D.K.; Ptaszek, M.; Lindsey, J.S. Direct synthesis of magnesium porphine via 1-formyldipyrromethane. *J. Org. Chem.* **2007**, *72*, 5008–5011. [CrossRef] [PubMed]

29. Arnett, F.C.; Edworthy, S.M.; Bloch, D.A.; Mcshane, D.J.; Fries, J.F.; Cooper, N.S.; Healey, L.A.; Kaplan, S.R.; Liang, M.H.; Luthra, H.S.; et al. The American Rheumatism Association 1987 revised criteria for the classification of rheumatoid arthritis. *Arthritis Rheumatol.* **1988**, *31*, 315–324. [CrossRef]

30. Liagre, B.; Vergne-Salle, P.; Corbiere, C.; Charissoux, J.L.; Beneytout, J.L. Diosgenin, a plant steroid, induces apoptosis in human rheumatoid arthritis synoviocytes with cyclooxygenase-2 overexpression. *Arthritis Res. Ther.* **2004**, *6*, R373. [CrossRef]

31. Glant, T.T.; Jacobs, J.J.; Molnár, G.; Shanbhag, A.S.; Valyon, M.; Galante, J.O. Bone resorption activity of particulate-stimulated macrophages. *J. Bone Miner. Res.* **1993**, *8*, 1071–1079. [CrossRef]

32. Bonnet, C.; Bertin, P.; Cook-Moreau, J.; Chable-Rabinovitch, H.; Treves, R.; Rigaud, M. Lipoxygenase products and expression of 5-lipoxygenase and 5-lipoxygenase-activating protein in human cultured synovial cells. *Prostaglandins* **1995**, *50*, 127–135. [CrossRef]

33. Semaan, J.; Pinon, A.; Rioux, B.; Hassan, L.; Limami, Y.; Pouget, C.; Fagnère, C.; Sol, V.; Diab-Assaf, M.; Simon, A.; et al. Resistance to 3-HTMC-induced apoptosis through activation of PI3K/Akt, MEK/ERK, and p38/COX-2/PGE2 pathways in human HT-29 and HCT116 colorectal cancer cells. *J. Cell. Biochem.* **2016**, *117*, 2875–2885. [CrossRef] [PubMed]

34. Kamkaew, A.; Lim, S.H.; Lee, H.B.; Kiew, L.V.; Chung, L.Y.; Burgess, K. BODIPY dyes in photodynamic therapy. *Chem. Soc. Rev.* **2013**, *42*, 77–88. [CrossRef] [PubMed]

35. Lutton, J.D.; Abraham, N.G.; Drummond, G.S.; Levere, R.D.; Kappas, A. Zinc porphyrins: Potent inhibitors of hematopoieses in animal and human bone marrow. *Proc. Natl. Acad. Sci. USA* **1997**, *94*, 1432–1436. [CrossRef]

36. Yang, G.; Nguyen, X.; Ou, J.; Rekulapelli, P.; Stevenson, D.K.; Dennery, P.A. Unique effects of zinc protoporphyrin on HO-1 induction and apoptosis. *Am. J. Hematol.* **2001**, *97*, 1306–1313. [CrossRef]

37. Bartok, B.; Firestein, G.S. Fibroblast-like synoviocytes: Key effector cells in rheumatoid arthritis. *Immunol. Rev.* **2010**, *233*, 233–255. [CrossRef]

38. Park, C.; Moon, D.O.; Choi, I.W.; Choi, B.T.; Nam, T.J.; Rhu, C.H.; Kwon, T.K.; Lee, W.H.; Kim, G.Y.; Choi, Y.H. Curcumin induces apoptosis and inhibits prostaglandin E2 production in synovial fibroblasts of patients with rheumatoid arthritis. *Int. J. Mol. Med.* **2007**, *20*, 365–372. [CrossRef]

39. Nasry, W.H.S.; Rodriguez-Lecompte, J.C.; Martin, C.K. Role of COX-2/PGE2 mediated inflammation in oral squamous cell carcinoma. *Cancers* **2018**, *10*, 348. [CrossRef]

40. Sung, M.S.; Lee, E.G.; Jeon, H.S.; Chae, H.J.; Park, S.J.; Lee, Y.C.; Yoo, W.H. Quercetin inhibits IL-1β-induced proliferation and production of MMPs, COX-2, and PGE2 by rheumatoid synovial fibroblast. *Inflammation* **2012**, *35*, 1585–1594.3. [CrossRef] [PubMed]

41. Agostinis, P.; Breyssens, H.; Buytaert, E.; Hendrickx, N. Regulatory pathways in photodynamic therapy induced apoptosis. *Photochem. Photobiol. Sci.* **2004**, *3*, 721–729. [CrossRef]

42. Downey, G.P.; Gumbay, R.S.; Doherty, D.E.; LaBrecque, J.F.; Henson, J.E.; Henson, P.M.; Worthen, G.S. Enhancement of pulmonary inflammation by PGE2: Evidence for a vasodilator effect. *J. Appl. Physiol.* **1988**, *64*, 728–741. [CrossRef] [PubMed]

43. Fidanzi-Dugas, C.; Liagre, B.; Chemin, G.; Perraud, A.; Carrion, C.; Couquet, C.Y.; Granet, R.; Sol, V.; Léger, D.Y. Analysis of the in vitro and in vivo effects of photodynamic therapy on prostate cancer by using new photosensitizers, protoporphyrin IX-polyamine derivatives. *Biochim. Biophys. Acta Gen. Subj.* **2017**, *1861*, 1676–1690. [CrossRef]

44. Luna, M.; Wong, S.; Ferrario, A.; Gomer, C.J. Cyclooxygenase-2 Expression Induced by Photofrin Photodynamic Therapy Involves the p38 MAPK Pathway. *Photochem. Photobiol.* **2008**, *84*, 509–514. [CrossRef] [PubMed]

45. Rayar, A.M.; Lagarde, N.; Martin, F.; Blanchard, F.; Liagre, B.; Ferroud, C.; Zagury, J.F.; Montes, M.; Veitía, M.S.I. New selective cyclooxygenase-2 inhibitors from cyclocoumarol: Synthesis, characterization, biological evaluation and molecular modeling. *Eur. J. Med. Chem.* **2018**, *146*, 577–587. [CrossRef]

46. Hendrickx, N.; Volanti, C.; Moens, U.; Seternes, O.M.; De Witte, P.; Vandenheede, J.R.; Piette, J.; Agostinis, P. Up-regulation of cyclooxygenase-2 and apoptosis resistance by p38 MAPK in hypericin-mediated photodynamic therapy of human cancer cells. *J. Biol. Chem.* **2003**, *278*, 52231–52239. [CrossRef] [PubMed]

47. Ferrario, A.; Von Tiehl, K.; Wong, S.; Luna, M.; Gomer, C.J. Cyclooxygenase-2 inhibitor treatment enhances photodynamic therapy-mediated tumor response. *Cancer Res.* **2002**, *62*, 3956–3961. [PubMed]

48. Williams, C.S.; Mann, M.; DuBois, R.N. The role of cyclooxygenases in inflammation, cancer, and development. *Oncogene* **1999**, *18*, 7908–7916. [CrossRef]

49. van Dalen, S.C.M.; Blom, A.B.; Slöetjes, A.W.; Helsen, M.M.A.; Roth, J.; Vogl, T.; van de Loo, F.A.; Koenders, M.I.; van der Kraan, P.M.; van den Berg, W.B.; et al. Interleukin-1 is not involved in synovial inflammation and cartilage destruction in collagenase-induced osteoarthritis. *Osteoarthr. Cartil.* **2017**, *25*, 385–396. [CrossRef]

50. Nasi, S.; Ea, H.K.; So, A.; Busso, N. Revisiting the role of interleukin-1 pathway in osteoarthritis: Interleukin-1α and-1β, and NLRP3 inflammasome are not involved in the pathological features of the murine menisectomy model of osteoarthritis. *Front. Pharmacol.* **2017**, *8*, 282. [CrossRef]

51. Shimomura, K.; Kanamoto, T.; Kita, K.; Akamine, Y.; Nakamura, N.; Mae, T.; Yoshikawa, H.; Nakata, K. Cyclic compressive loading on 3D tissue of human synovial fibroblasts upregulates prostaglandin E2 via COX-2 production without IL-1β and TNF-α. *Bone Jt. Res.* **2014**, *3*, 280–288. [CrossRef] [PubMed]